DEVELOPMENT OF MAGNETIC COMPONENTS FOR 1–10 MHZ DC/DC CONVERTERS

by

ANDREW FRANKLIN GOLDBERG

S.B., Massachusetts Institute of Technology
(1982)

S.M., Massachusetts Institute of Technology
(1985)

E.E., Massachusetts Institute of Technology
(1985)

Submitted to the Department of
Electrical Engineering and Computer Science
in Partial Fulfillment of the
Requirements for the Degree of

DOCTOR OF SCIENCE

at the

MASSACHUSETTS INSTITUTE OF TECHNOLOGY

September 1988

Signature of Author: ______________________
Department of Electrical Engineering and Computer Science
September 1, 1988

Certified by: ______________________
Prof. Martin F. Schlecht
Thesis Supervisor

Accepted by: ______________________
Prof. Arthur C. Smith
Chairman, Department Committee on Graduate Students

DEVELOPMENT OF MAGNETIC COMPONENTS FOR 1–10 MHZ DC/DC CONVERTERS

by

ANDREW FRANKLIN GOLDBERG

Submitted to the Department of
Electrical Engineering and Computer Science
on September 1, 1988 in partial fulfillment of the
requirements for the Degree of
Doctor of Science

ABSTRACT

Recent efforts to miniaturize one common type of power supply, the dc/dc converter, raise the internal switching frequency of the power circuit from the 20–200 kHz range to the 1–10 MHz range in an effort to reduce the size of the energy storage components that dominate the converter volume. Because of the difficulty of analyzing the power dissipation in the magnetic components, it has been unclear whether present designs represent the smallest components that can be achieved, or whether their size can be reduced further. This thesis, which is part of an MIT project to develop a miniaturized 10 MHz dc/dc converter, shows that by carefully analyzing copper and core loss, the physical size of the magnetic components can indeed be reduced significantly.

Both types of power dissipation, winding loss and core loss, are difficult to analyse. Above 1 MHz skin and proximity effects in the conductors greatly increase the copper loss and are difficult to analyse in closed form. Core loss predictions, unlike copper loss predictions, cannot be made from theory alone, but rather require measured data. Such data is generally unavailable for magnetic materials at these frequencies (1–10 MHz) and flux densities (above 50 G).

In order to make quantitative predictions of the copper loss, finite element analyses were employed. In order to make quantitative predictions of the core loss in the ferrite magnetic materials, whose permeability and loss vary greatly with flux density and frequency, a detailed measurement and analysis procedure was developed and used to measure the properties of eight commercially available nickel-zinc ferrites. The copper and core loss analyses were used to choose a core and winding geometry for the transformer of a prototype 10 MHz, 50 W dc/dc converter under development at MIT. The winding geometry discussed in this thesis, planar spirals on flexible printed circuit board, is much more amenable to economical mass production than the conventional technology of magnet wire and bobbins. The analyses were also used to derive a lumped parameter model of the transformer, and the model was verified by experimental measurements using a 6:1 transformer that was fabricated with planar spiral windings.

Even with a thorough understanding of the origins of power dissipation, careful design optimization is necessary in order to achieve the minimum size. The analytic models of copper and core loss were combined in a computer program that designed the transformer with the smallest footprint for a given energy storage, power dissipation, and frequency. This program was used both to produce a design for the transformer of the prototype MIT converter and to investigate the design tradeoffs. It was found that if the copper loss is not reduced by a strategy such as interleaving layers of primary and secondary, then the footprint area of the transformer can increase with increasing frequency, thereby negating one of the motivations for operating at high frequency. It was also found that the curve relating footprint area with the allowable power dissipation has a pronounced knee, so that constraining the power dissipation to be too low results in an unreasonably large transformer, while allowing the power dissipation to be unnecessarily large hardly buys any reduction in the transformer footprint.

Thesis Supervisor: Dr. Martin F. Schlecht
Title: Associate Professor of Electrical Engineering

ACKNOWLEDGEMENTS

I would like first to thank my thesis supervisor, Professor Martin F. Schlecht, for his guidance. I have learned a tremendous amount from Marty and am grateful for our many long discussions. I am also grateful for his patience and understanding.

I owe an immeasurable debt to Professor John G. Kassakian, who has guided me for almost a decade, supervising my undergraduate research, Bachelor's Thesis, and Master's Thesis, as well as actively participating in my doctoral work. I am grateful to him for the many opportunities he has given me, for our countless technical discussions, and for his wise personal advice.

I thank the other members of my thesis committee, Professors Jeffrey H. Lang and David J. Epstein, for the great care they took in reading and commenting on my thesis. I also thank my graduate adviser, Professor Richard D. Thornton, for his guidance, and Professor James R. Kirtley and Dr Stephen D. Umans for their technical advice.

I am very grateful to have studied electromagnetic field theory from Professor James R. Melcher.

I thank Digital Equipment Corporation, General Electric Corporate Research and Development, and Prime Computer for their financial support of this work. I thank Dr Ming Kuo of General Electric and Mr John Cross of Digital for their technical advice and assistance.

I thank the staff of the Barker Engineering Library, especially Mr Richard Hines, for their many data base searches and for hunting down ludicrously obscure technical journals.

I thank my pals Mr David Otten and Dr Leo Casey for their invariably excellent technical advice, and more importantly, for all the hours of enjoyably wasted time.

I thank my parents for their love and support.

Most of all I thank my beloved wife, Dina, for everything.

TABLE OF CONTENTS

Chapter 1

INTRODUCTION

While the physical size of digital and analog electronic circuits has been drastically reduced over the past twenty years, the size of their associated power supplies has been reduced at a much slower rate. As a result, the power supply represents an increasing proportion of the size and cost of electronic equipment.[1] Recent efforts to miniaturize one common type of power supply, the dc/dc converter, raise the internal switching frequency of the power circuit from the 100–200 kHz range to the 1–10 MHz range in an effort to reduce the size of the energy storage components that dominate the converter volume.

Because of the difficulty of analyzing the power dissipation in the magnetic components, it has been unclear whether present designs represent the smallest components that can be achieved, or whether their size can be reduced further. The difficulty of analysing both core and copper loss at high frequency has forced designers to make conservative designs with cores and windings that may be much larger than they need to be for a given power dissipation. In fact, one prominent member of the power electronics community has written that "...the magnetics design is the main bottleneck to the successful reduction of the overall converter size and weight," and suggests that, because of the limitations of the magnetic components, operation below 500 kHz might yield *smaller* converters than operation above 1 MHz.[2]

This thesis, which is part of an MIT project to develop a miniaturized 10 MHz dc/dc converter, investigates the issues involved in miniaturizing magnetic components for dc/dc converters, and employs both theoretical analyses and experimental measurements to develop appropriate designs.[3] The work presented in this thesis shows that with careful attention to both core and copper loss, increasing the switching frequency to 10 MHz does indeed reduce the size of the magnetic components.

---

[1] W. W. Burns, III and J. Kociecki, "Power Electronics in the Minicomputer Industry," *IEEE Proceedings*, **76**, 4 (1988), pp. 311–324.

[2] S. Ćuk, Z. Zhang, and L. A. Kajouke, "Low Profile, 50 W/in^3 Integrated Magnetics PWM Ćuk Converter," *Technical Papers of the Third International High Frequency Power Conversion Conference*, Intertec Communications, Ventura, California (1988), pp. 442–463.

[3] J. G. Kassakian, M. F. Schlecht, "High-Frequency High-Density Converters for Distributed Power Supply Systems," *IEEE Proceedings*, **76**, 4 (1988), pp. 362–376.

1.1 The Need for High Density Dc/Dc Converters

One of the most active areas of research in power electronics today is the development of very high power density dc/dc converters. Dc/dc converters are a basic type of power supply that transform power from one dc voltage and current level to another in order to match power sources with their loads. The new high density converters promise power densities of over 50 W/in^3, a ten-fold increase in power density over current technology.[4,5]

One application for these miniaturized converters is in equipment whose size and weight must be minimized, such as satellites and aircraft. These aerospace products are produced in low volume, and their performance and reliability take precedence over cost, especially for military applications.

Despite the sophistication of this new technology, these new converters are not limited to application in such specialized, low production volume applications. The converters are small enough to be fabricated by thick and thin film techniques, which permit their mass production and inclusion in high production volume products requiring inexpensive and standardized power supplies. Examples of such high volume products include mid-range and mainframe computers, telecommunications products, and automobiles.

In these products miniaturized power supplies would not just replace present-day equipment, but rather permit the use of a new distributed power supply architecture instead of today's centralized power supplies. In computers, for example, large currents must be bussed at low logic voltages from the centralized power supply to each logic card. In order to avoid ohmic drops in the distribution bus, large and expensive copper bars must be employed. A distributed power supply architecture, made possible by the availability of very high power density dc/dc converters, would greatly reduce the bus size by distributing power at a higher voltage and lower current than in a centralized power supply architecture. In the distributed architecture the conversion from the bus voltage (typically about 42 V in order to satisfy safety standards) to the logic supply voltage would be performed on each logic board. Since space on tightly packed logic boards is extremely valuable, the dc/dc converter that performs this voltage conversion must be as small as possible.

---

[4] Kassakian and Schlecht

[5] F. M. Magalhaes, F. T. Dickens, G. R. Westerman, and N. G. Ziesse, "'Zero-Voltage-Switched Resonant Half-Bridge High-Voltage Dc-Dc Converter," *Technical Papers of the Third International High Frequency Power Conversion Conference*, Intertec Communications, Ventura, California (1988), pp. 332–343.

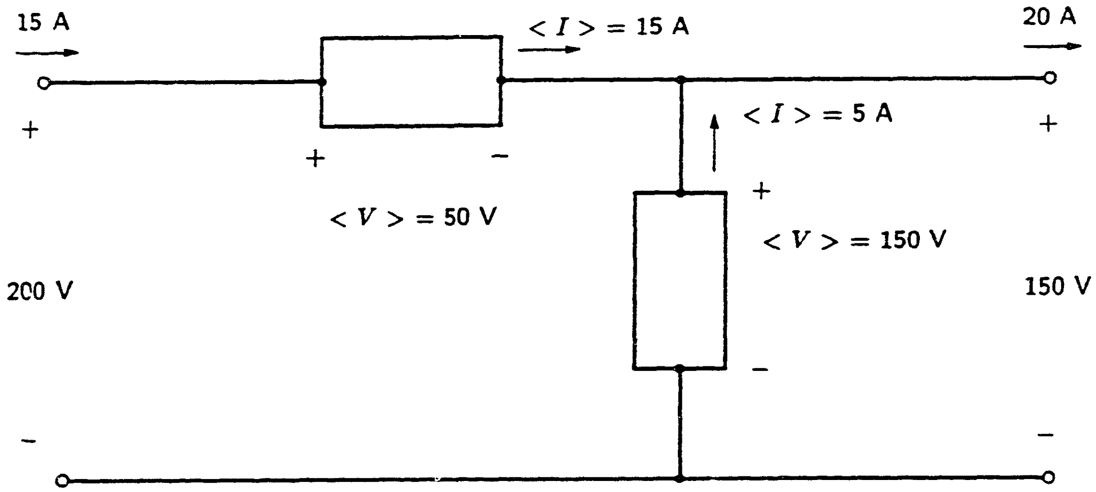

Fig. 1.1 Interfacing two dc systems. (Figure reproduced from *Principles of Power Electronics*).

1.2 Basic Attributes of the Dc/Dc Converter

This section describes the basic attributes of the conventional, low power density dc/dc converter, explains the role of the magnetic components, and discusses how increasing the internal switching frequency can decrease the volume of the magnetic components.[6]

A dc/dc converter is a two-port device which connects a power source that provides dc voltage and current to a load that requires its power at a different dc voltage and current. Figure 1.1 shows the basic configuration of such a two-port that connects a source that provides 200 V and 15 A and a load that requires 150 V at 20 A. The two-port must at least contain a series element to absorb the voltage difference, and a shunt element to balance the current difference. The series element is realized with an ideal switch that continously opens and closes at a fixed frequency. The required dc, or average, voltage across the switch (in this example 50 V) is achieved by choosing an appropriate ratio of its on-time to its off-time (in this example 0.75). This ratio is known as the *duty cycle*. Similarly, the shunt element is realized with an ideal switch that achieves the required dc, or average, current (in this example 5 A) by opening when the series switch is closed and by closing when the series switch is open. The waveforms of these switches are shown in Fig. 1.2.

Energy storage components must be added to the basic circuit of Fig. 1.1 in order

---

[6] J. G. Kassakian, M. F. Schlecht, and G. C. Verghese, *Principles of Power Electronics*, Addison-Wesley Publishing Co., Reading, Massachusetts (1989), chap. 6.

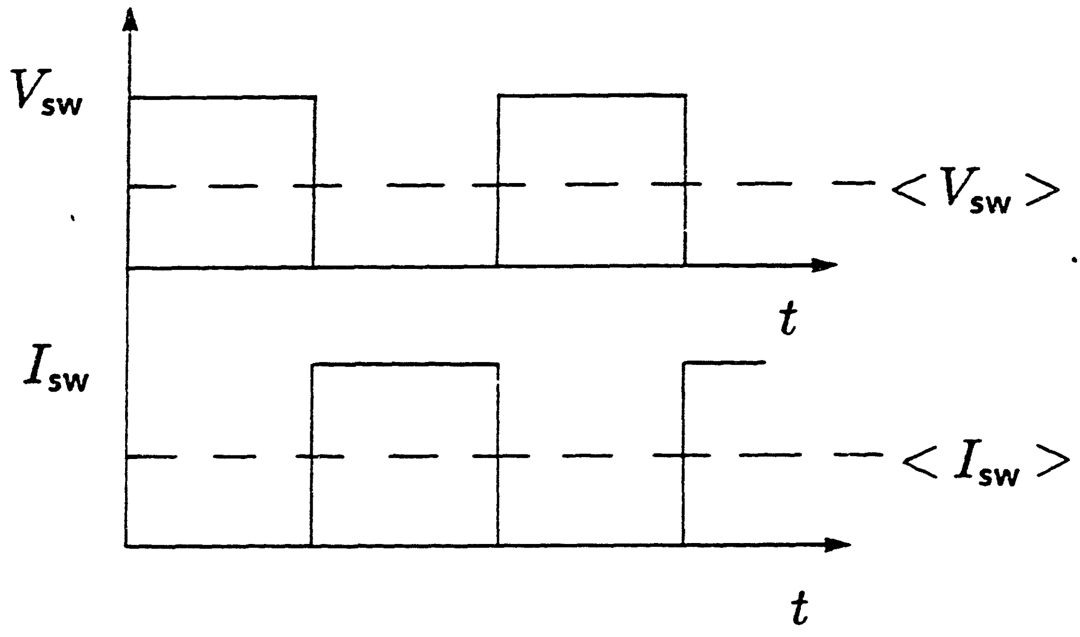

Fig. 1.2 Switch waveforms showing average values. (Figure reproduced from *Principles of Power Electronics*).

to filter the ac components of the switch waveforms, shown in Fig. 1.2, from the source and the load. These additional components are an inductor and capacitor, as shown in Fig. 1.3. These components would have to be infinitely large to remove completely the ac components from the input and output; minimum values for the inductor and the capacitor are determined by the acceptable ripple and the switching frequency.

The minimum value of the inductor can be determined by the following approach. The shunt switch conducts for a period $(1-d)/f$, where d is the duty cycle of the series switch and f is its frequency. During this conduction interval, the voltage across the inductor is $-V_{out}$, so that the current through the inductor will decrease by

$$\Delta I_{out} = -\int_0^{(1-d)/f} \frac{V_{out}}{L}\, dt \tag{1.1}$$

which, solved for the inductance, L, gives

$$L = \frac{V_{out}(1-d)}{\Delta I_{out} f} \tag{1.2}$$

Equation (1.2) shows that the value of the inductance required to give a current ripple with an amplitude of $\Delta I_{out}/2$ is inversely proportional to the switching frequency. Therefore, a higher switching frequency permits a smaller inductance and, assuming that less inductance

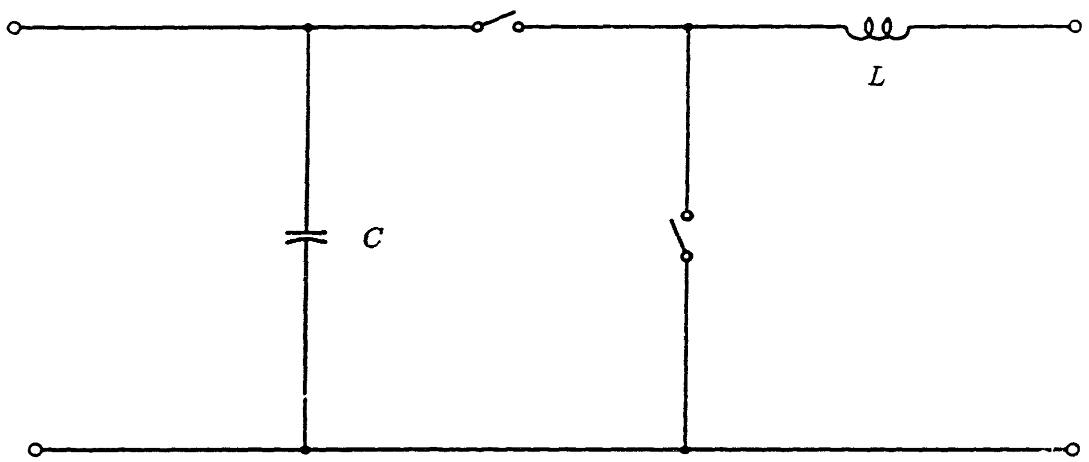

Fig. 1.3 Minimal topology for a dc/dc converter. (Figure reproduced from *Principles of Power Electronics*).

translates into a physically smaller component, a more compact converter. One of the major issues addressed in this thesis is whether the size of the magnetics still decreases as the switching frequency is pushed to 10 MHz.

The general conclusion that the size of the magnetic components decreases with increasing frequency for a given current ripple in this converter, known as the buck converter, also applies to the other commonly used conventional dc/dc converter topologies, such as the boost converter, the forward converter, and the flyback converter. A similar analysis can be performed on the capacitors to show that their size also decreases with frequency for a given voltage ripple.

1.3 The Impact of Parasitic Elements on High Frequency Converters

The new high density converters achieve their volume reduction through the use of switching frequencies above 1 MHz, frequencies which are much higher than those of conventional converters (typically 20–200 kHz). But as the switching frequency is raised above 1 MHz, parasitic energy storage elements, such as switch output capacitance and lead inductance, can cause ringing at transitions which overstress the semiconductor components and become an important source of dissipation. In addition, transformer leakage inductance can introduce load regulation, while transformer interwinding capacitance can introduce a common mode signal path. Both of these effects degrade circuit operation. For this reason, at high frequencies resonant circuit topologies, which seek to incorporate the parasitic energy storage elements in the normal operation of the circuit, are used instead.[7,8,9,10]

One representative resonant circuit is the resonant forward converter. This circuit, shown in Fig. 1.4, is used in the MIT miniaturized power supply project of which this thesis research is part.[11] The transformer in this circuit is the subject of detailed design studies that are presented in this thesis. This circuit uses the resonant tank formed by the switch's parasitic output capacitance, C_o, and the transformer's magnetizing inductance, L_m. As in the converter described in the last chapter, current flows through diode D_1 and power is delivered to the load when the switch, Q_1, is on. When Q_1 turns off, the energy stored in the magnetizing inductance of the transformer resonates first into the capacitance across the switch and then back into the magnetizing inductance. The circuit is switched near the tank's resonant frequency, so that $Q1$ is turned on again when the voltage across the switch and its parasitic capacitance is zero.

The resonant converter, like the conventional converter, requires less inductance at higher frequency, making possible the use of a smaller magnetic component. The dependence of the required value of magnetizing inductance on frequency is determined by its relationship to the characteristic impedance and the resonant frequency of the tank. The characteristic impedance, Z, is given by

$$Z = \sqrt{\frac{L_m}{C_o}} \tag{1.3}$$

and is roughly equal to the ratio of the peak voltage to the peak current in the tank. In order to keep the device stresses constant, this ratio should be held constant as the frequency is increased. The resonant frequency, f_r, is given by

$$f_r = \frac{1}{2\pi\sqrt{L_m C_o}} \tag{1.4}$$

---

[7] N. O. Sokal and A. D. Sokal, "Class E - A New Class of High Efficiency Tuned Single-Ended Switching Power Amplifiers," *Journal of Solid State Circuits*, **10**, 3 (1975), pp. 168–176.

[8] R. J. Gutmann, "Application of RF Circuit Design Principles to Distributed Power Converters," *IEEE Transactions on Industrial Electronics and Control Instrumentation*, **27**, 3 (1980), pp. 156–164.

[9] K. Liu and F. C. Lee, "Resonant Switches - A Unified Approach to Improve Performance of Switching Converters," *IEEE International Telecommunications Energy Conference Proceedings* (1984), pp. 334–341.

[10] M. F. Schlecht and L. F. Casey, "Comparison of the Square-Wave and Quasi-Resonant Topologies," *IEEE Applied Power Electronics Conference Record* (1987), pp. 124–134.

[11] Casey and Schlecht.

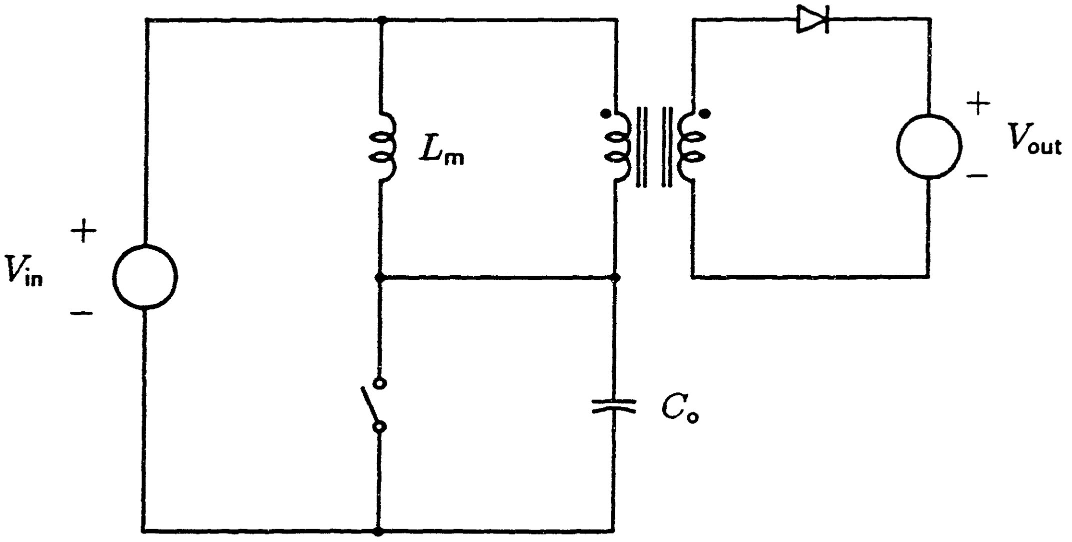

Fig. 1.4 Resonant forward converter.

and should be increased proportionately to the switching frequency in order to maintain the relative timing of the circuit waveforms. Solving (1.3) and (1.4) for L_m gives

$$L_m = \frac{Z}{2\pi f} \tag{1.5}$$

In other words, the inductor's impedance should be held constant. Thus, the required value of inductance in a resonant circuit is inversely proportional to frequency, as in the conventional switching converter.

1.4 The Challenges of Miniaturizing Magnetic Components

Although the use of higher switching frequencies has succeeded in reducing the size of the capacitors, excessive power dissipation in the magnetic components has so far limited their miniaturization. Copper loss is reduced by allocating more core window area for the copper windings, and core loss is reduced by reducing the flux density through making the core larger. As a result, the inductors and transformers currently used still dominate the converter volume and limit the presently achievable converter power density to about 30 W/in^3, substantially less than the 50 W/in^3 that is considered feasible.[12,13] One of

---

[12] L. F. Casey and M. F. Schlecht, "A High Frequency, Low Volume Point-of-Load Power Supply for Distributed Power Systems," *IEEE Power Electronics Specialists Conference Record,* June 1987, pp. 439–450.

[13] Magalhaes, et al.

the major obstacles to reducing the power dissipation in the magnetic components is the difficulty of analyzing the loss. Without an understanding of the origins of power dissipation, designers are forced to make conservative designs with core and winding geometries that are larger than they need to be for the dissipation that can be tolerated.

Both types of power dissipation, winding loss and core loss, are difficult to analyse. Above 1 MHz skin and proximity effects in the conductors greatly increase the copper loss, but these effects are difficult to analyse in closed form. Although qualitative arguments can be used to develop intuition, accurate computation of the copper loss may require the use of such computation-intensive numerical techniques as finite element analysis. Core loss predictions, unlike copper loss predictions, cannot be made from theory alone, but rather require measured data. Such data is generally unavailable for magnetic materials at these frequencies (1–10 MHz) and flux densities (above 50 G). This lack of data is due, at least in part, to the difficulty of making measurements and interpreting data in the 1–10 MHz range. Parasitic elements can cause large errors in the measurements. Nonuniform flux densities in the cores, together with field-dependent permeabilities, complicate the interpretation of the measured data. So not only must material properties be measured, but the measurement technique itself must be developed.

Even with a thorough understanding of the origins of power dissipation, careful design optimization is necessary in order to achieve the minimum size. The quantitative understandings of core and copper loss must both be used to design a component that has the required inductance and total dissipation in the minimum possible size. To accomplish this task is one of the most important challenges of this thesis.

Another challenge involves the fabrication of magnetic components. Since the characteristic frequency of the resonant circuits used in high frequency converters depends on the values of the energy storage elements, the parasitics that cannot be made negligible must be made highly reproducible. Unlike capacitors, which are sold ready to use, inductors and transformers must usually be assembled from core pieces and magnet wire. A conventional inductor or transformer is made by winding the magnet wire wound around a bobbin and then sliding the bobbin over a post of the magnetic core. These components, which are generally not made by a company specializing in magnetics, but rather put together by a power supply manufacturer, possess parasitic inductances and capacitances that can vary greatly between pieces. The successful development of magnetic components for high frequency resonant converters therefore requires designs and fabrication processes that permit economical manufacture to very close tolerances, in order to ensure consistent and small values for the parasitics. Thick and thin film fabrication techniques not only fulfill these requirements, but also are amenable to economical mass production, unlike wound bobbins which are difficult and expensive to produce.

1.5 Overview of Thesis

The goal of this thesis is the design of easily fabricated, compact magnetic components for the emerging generation of high density power supplies. These components should occupy the minimum circuit board area for a given energy storage and allowable power dissipation. This thesis approaches this goal in several stages.

First, studies are presented that investigate the impact of different core geometries on the copper loss. Although transformer design is the focus of these studies, inductor design is implicitly addressed by discussions of leakage and magnetizing fluxes. Based on considerations of copper loss and ease of fabrication, a core geometry is then selected for the transformer of the MIT prototype high power density converter and a lumped parameter model of this transformer is developed. Next, the magnetic material selection and core loss are discussed. Nickel-zinc ferrite was chosen as the magnetic material, based on considerations of permeability and core loss. A procedure was developed to experimentally measure the permeability and loss of nickel-zinc ferrites, and to model the dependence of these parameters on the magnetic field. The results of the copper and core loss analyses are incorporated in a computer program that uses sophisticated optimization algorithms to design transformers that provide the necessary energy storage and efficiency in the minimum possible size. A minimum area transformer design for the MIT prototype converter is presented. A transformer with planar spiral windings was then constructed and its properties experimentally measured in order to demonstrate the feasibility of fabricating planar spiral windings, to verify the copper and core loss analyses, and to validate the measurement procedure.

Chapter Two begins the thesis with a discussion of some basic issues of magnetic design, such as whether to use magnetic material, and if so, whether the structure should be gapped.

Chapter Three continues with a survey of previously published work describing attempts to make miniature magnetic components. This survey covers the efforts of two engineering communities, signal processing and power electronics, and shows that none of the reported work is appropriate for 1–10 MHz converters.

Chapter Four addresses the design of the transformer. The planar spiral windings are discussed. The nature of the proximity effect problem is described and the success of different core geometries in reducing proximity effects and copper loss is investigated with the aid of finite element analysis, a computerized numerical technique.

Chapter Five presents a lumped parameter model for one of the transformers described in Chapter Four. An approximate formula is derived for each element of the model, which includes all important parasitics. The model is verified by comparison with finite element analyses.

Chapter Six considers the choice and analysis of magnetic materials. A survey of available materials is presented and the choice of nickel-zinc ferrites is explained. An experimental procedure for determining the functional dependence of permeability and loss of the ferrite on the applied field is described, and data for eight different types of Ni-Zn ferrite is presented.

Chapter Seven describes the design studies for a 7:1 transformer intended for the MIT prototype dc/dc converter. These studies combines the analyses of Chapter Four with the material property measurements of Chapter Six in order to perform computer-assisted studies of the design tradeoffs. This chapter discusses such issues as the variation of transformer size with excitation frequency, with total power dissipation, and with the interleaving of multiple winding layers. The tradeoffs between leakage inductance and interwinding capacitance are discussed. The chapter concludes with a design for a 10 MHz converter.

Chapter Eight presents experimental measurements of a representative transformer which was constructed. These measurements serve to validate both the design process and the instrumentation.

Chapter Nine presents the conclusions and directions for further work.

Chapter 2

THE USE OF MAGNETIC MATERIAL

Since all of the magnetic components that are discussed in this thesis use magnetic material, it should first be asked whether magnetic material is in fact appropriate for use at 1–10 MHz, or whether air cores should be used instead. This short chapter justifies the use of magnetic material and explains the importance of including an air gap in a structure that stores magnetic energy.

2.1 Magnetic Material vs. Air Core

One of the initial decisions that must be made in the design of any magnetic component is whether or not to use magnetic materials. One advantage that magnetic materials provide is flux guidance. In transformers this flux guidance allows a stronger coupling of primary to secondary than is possible with an air core, while in both inductors and transformers it greatly reduces stray fields that can induce eddy currents and disrupt circuit operation. But for the dc/dc converter application addressed by this thesis, the most important advantage of using magnetic materials is that for a given total power dissipation, a given inductance can be achieved in a smaller volume.

This section shows the decrease in size that could be achieved if the magnetic material were lossless, so that the only power dissipation would be ohmic loss in the copper windings. The next section discusses how in reality core loss in the magnetic material limits the size decrease that can be achieved and explains how the introduction of an air gap in the core trades off some of the increased inductance per unit volume for less core loss. In this thesis the component size will be characterized by the area, or *footprint*, that the component would occupy on a printed circuit board, and the component efficiency will be characterized by the ratio of the peak energy stored in the component to the average power dissipated. This ratio is equal to L/R, where L is the component's inductance, and R is the component's resistance. In addition to core loss, the use of magnetic material introduces other problems, such as the dependence of the inductance on the core permeability, which in turn depends on current, temperature, time, and sample. These problems can also be mitigated by the use of an air gap.

This section considers a simple toroidal inductor in order to review the basic arguments for using magnetic material. Consider an N turn toroid of inner radius r_i, outer radius r_o, and height h, as shown in Figs. 2.1 and 2.2 (Figure 2.2 is shown with a gap, which will be considered in the next section). The toroid has an ungapped core with a

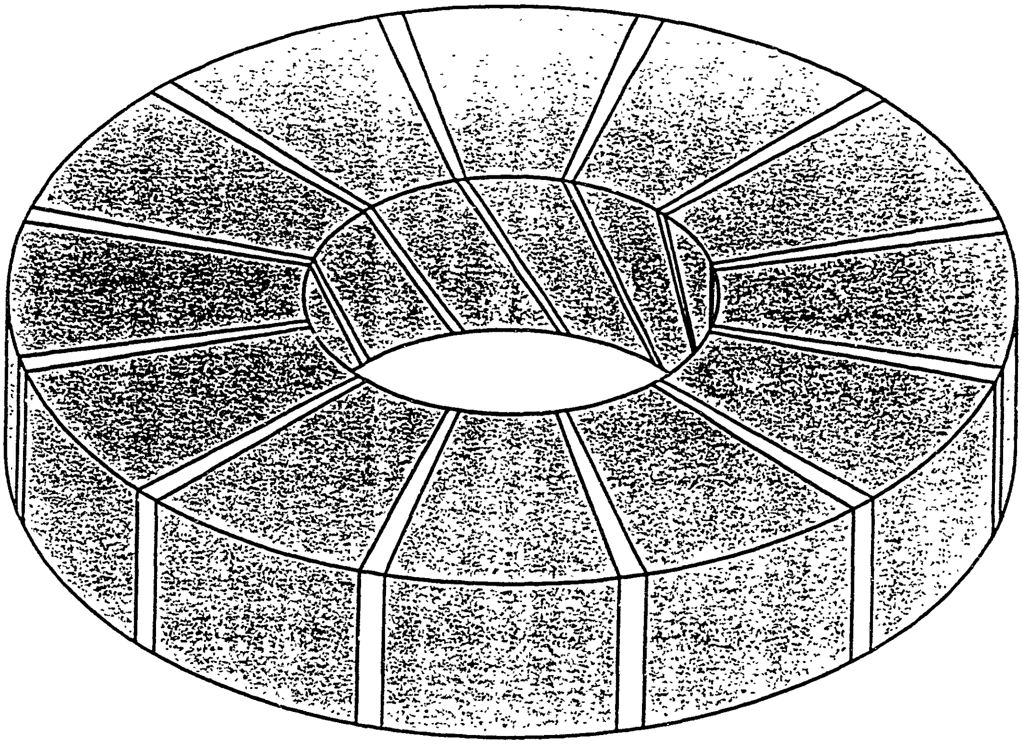

Fig. 2.1 Toroidal core with ribbon winding. Shading indicates winding.

permeability of μ. The winding is a ribbon whose average width is $\pi(r_o + r_i)/N$, so that the N turns fit side by side around the circumference of the toroid, as shown in Fig. 2.1. The ribbon is much thicker than a skin depth, so that for the purposes of computing the copper loss, the effective thickness of the ribbon is one skin depth, δ.[1] In a highly conductive material, such as copper, the skin depth is given by

$$\delta = \frac{1}{\sqrt{\pi f \mu_o \sigma}} \tag{2.1}$$

where σ is the conductivity of the copper.

In order to determine the dependence of the efficiency on the permeability and core size, it is necessary to compute L and R. The inductance is given approximately by

$$L = \frac{\mu N^2 A}{l} \tag{2.2}$$

where μ is the permeability of the core, N is the number of turns, A is the cross-sectional area of the toroid, and l is the mean magnetic path length of the toroid. This expression is

---

[1] S. Ramo, J. R. Whinnery, and T. Van Duzer, *Fields and Waves in Communication Electronics*, John Wiley and Sons, Inc., New York (1965), p. 288.

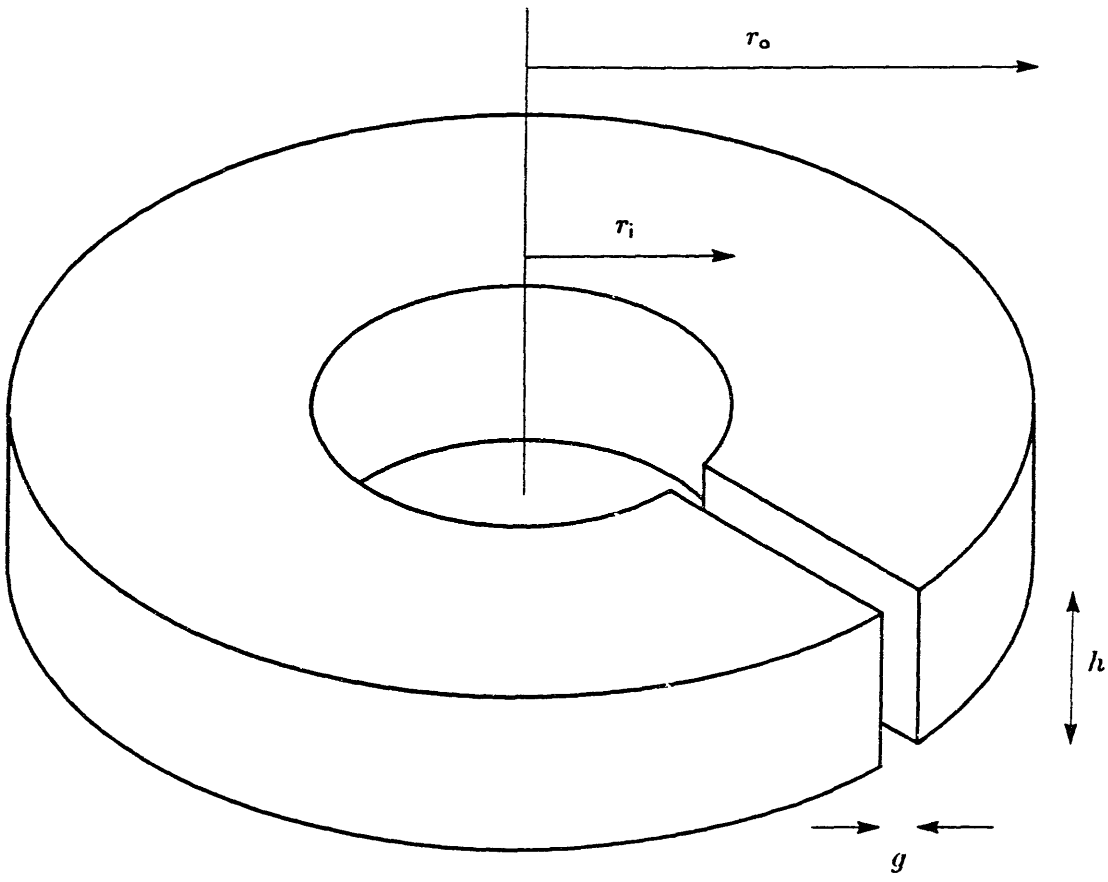

Fig. 2.2 Gapped toroidal core.

often written as

$$L = \frac{N^2}{\Re_c} \tag{2.3}$$

where $\Re_c$ is the reluctance of the core, given by $l/\mu A$. The cross-sectional area of the toroid is given by

$$A = h(r_o - r_i) \tag{2.4}$$

and the mean magnetic path is given by

$$l = 2\pi\left(\frac{r_o + r_i}{2}\right) \tag{2.5}$$

The inductance is therefore given by

$$L = \frac{\mu N^2 h}{\pi}\left(\frac{r_o - r_i}{r_o + r_i}\right) \tag{2.6}$$

The winding resistance is given approximately by

$$R = \frac{N l_w}{\sigma A_w} \tag{2.7}$$

where l_w is the length of each turn and A_w is the effective cross-sectional area of the ribbon winding. The length of each of the N turns is

$$l_w = 2(r_o - r_i + h) \tag{2.8}$$

The effective cross-sectional area of the ribbon winding is given by

$$A_w = \frac{2\pi}{N}\left(\frac{r_o + r_i}{2}\right)\delta \tag{2.9}$$

The resistance is therefore

$$R = \frac{2N^2}{\sigma\delta\pi}\frac{(r_o - r_i + h)}{(r_o + r_i)} \tag{2.10}$$

The L/R figure of merit can be computed using (2.4) and (2.10) as

$$\frac{L}{R} = \mu\sigma\delta h\left(\frac{r_o - r_i}{r_o - r_i + h}\right) \tag{2.11}$$

In order to consider the variation of the toroid's footprint, given by πr_o^2, with μ, it is necessary to assume some relationship between the toroid's dimensions. This analysis will simply assume that the aspect ratio of the core remains constant, so that

$$k_1 = \frac{h}{r_o - r_i}, \qquad k_2 = \frac{r_i}{r_o} \tag{2.12}$$

where k_1 and k_2 are constants. Equation (2.11) can be rewritten using (2.12) as

$$\frac{L}{R} = \frac{1}{2}\mu\sigma\delta r_o\left(\frac{k_1(1 - k_2)}{1 + k_1}\right) \tag{2.13}$$

This important result, (2.13), shows that if the efficiency is held constant (ignoring core loss), then the footprint, given by πr_o^2, is inversely proportional to μ^2. An air core would correspond to replacing μ in (2.13) with μ_o, so that replacing an air core with a permeable core would decrease the footprint by a factor of $(\mu_o/\mu)^2$.

2.2 Gapped Magnetic Material

Unfortunately, core loss can not be ignored. For a typical nickel-zinc ferrite operating at 10 MHz, about 20% of the energy stored in the core is lost each cycle. If the inductor must store an appreciable amount of energy, an ungapped core may be prohibitively lossy. In addition, the magnetic material introduces the problems of μ dependence and power loss mentioned above. The section considers the introduction of a small air gap into the core, which can ameliorate these problems.

If a small gap is introduced in the toroidal core, as shown by Fig. 2.2, and the core dimensions are changed so that the gapped and the ungapped cores both provide the same inductance, then the inductance of the gapped core is given by

$$L = \frac{N^2}{\dfrac{g'}{\mu_o A'} + \dfrac{l'}{\mu A'}} \tag{2.14}$$

where g' is the length of the gap. In (2.14) the dimension are given $'$ marks to emphasize that these dimensions are different from those of the ungapped core. Commonly, this expression is written as

$$L = \frac{N^2}{\Re_g' + \Re_c'} \tag{2.15}$$

where $\Re_g'$ is the reluctance of the gap, given by $g'/\mu_o A'$, and $\Re_c'$ is the reluctance of the magnetic material, given by $l'/\mu A'$.

The first point is that if $\Re_g' \gg \Re_c'$, then the inductance is essentially independent of the value of μ, and is given by

$$L = \frac{\mu_o N^2 A'}{g'} \tag{2.16}$$

Even if the reluctance of the magnetic material is not negligible, the dependence of the inductance on the permeability is still decreased.

The second point is that for a given inductance and current, introducing a gap reduces the energy stored in the magnetic material, thereby reducing the core loss. This analysis assumes that the core loss is roughly proportional to the energy stored in the core each cycle. The energy stored in the magnetic material of the ungapped core each cycle is given approximately by

$$W_{m,u} = \frac{1}{2\mu} B^2 V = \frac{1}{2\mu}\left[\frac{\mu N i}{l}\right]^2 lA = \frac{N^2 i^2}{\Re_c} \tag{2.17}$$

where V is the core volume and i is the exciting current. The energy stored in the gapped magnetic core is given by

$$W_{m,g} = \frac{1}{2\mu} B^2 V = \frac{1}{2\mu}\left[\frac{N i}{A'(\Re_c' + \Re_g')}\right]^2 lA = \frac{N^2 i^2 \Re_c'}{(\Re_c' + \Re_g')^2} \tag{2.18}$$

Since the inductances of the gapped and ungapped cores have been set equal in this analysis, comparison of (2.3) and (2.15) shows that

$$\Re_c = \Re_c' + \Re_g' \tag{2.19}$$

Equation (2.18) can therefore be rewritten as

$$W_{m,g} = \frac{N^2 i^2 \Re_c'}{\Re_c^2} \tag{2.20}$$

so that the ratio of core loss in the gapped core to core loss in the ungapped core, for a fixed inductance and current, is roughly given by

$$\frac{P_{c,g}}{P_{c,u}} = \frac{W_{m,g}}{W_{m,u}} = \frac{\Re_c'}{\Re_c} = \frac{l'/A'}{l/A} \tag{2.21}$$

which assumes that the permeability of the core is held constant. In other words, in order for the core loss to be less in the gapped structure than in the ungapped structure, so that $P_{c,g}/P_{c,u}$ is less than unity, the dimensions of the gapped core must be altered so that some of the energy is stored in the gap instead of the core. The impact of this conclusion on the toroidal core considered in this example can be seen by evaluating (l'/A') using (2.4), (2.5), and (2.12), giving

$$\frac{l'}{A'} = \frac{1}{r_o'}\left[\frac{\pi(1+k_2)}{k_1(1-k_2)^2}\right] \tag{2.22}$$

Equation (2.22) shows that in order to reduce l'/A' and reduce the core loss, r_o', and hence the footprint, must be allowed to increase. In other words, some of the decrease in footprint that the previous section showed could be gained by using magnetic material must be given up in order to reduce the core loss. A gapped core is still smaller than an air core, however. The decrease in footprint area that can actually be achieved by the use of magnetic material depends on the actual material, and on the core and winding geometry.

2.3 Conclusions

The results of this chapter show that for a given copper loss and neglecting core loss, the use of a magnetic core instead of an air core reduces an inductor's footprint by a factor of $(\mu_o/\mu)^2$. If the inductor has a substantial ac flux component, the core loss may necessitate the introduction of an air gap and limit the size reduction that the magnetic material would otherwise allow. Since copper loss and core loss both decrease as the inductor footprint is increased, the size reduction that can be achieved is limited primarily by the maximum total power dissipation that can be tolerated.

The analysis presented in this chapter is very approximate, and neglected such factors as proximity effects in the copper, which raise copper loss, and the greater than B^2 dependence of the core loss. A more accurate analysis must await the design studies of Chapter 7, which make use of the detailed copper and core loss analyses of Chapters 4, 5, and 6. Nevertheless, this chapter shows that gapped magnetic cores promise a higher L/R than air cores.

Chapter 3

PREVIOUS WORK

Efforts to make compact magnetic components have been driven by two different applications, signal processing and power electronics. This chapter briefly surveys the progress that has been made by these two communities. For the applications described in Chapter 7, the component should have an inductance between 1–10 μH. The circuit board area that the component requires, known as the *footprint*, should be less than 1.0 cm^2, while the height, determined by the spacing between circuit boards, should be less than about 1.0 cm. The ratio of the peak stored energy to the average energy dissipation per cycle, known as the Q, should be greater than about 60. This ratio is equal to $\omega L/R$.

3.1 Miniaturized Inductors for Signal Processing

The first efforts to miniaturize inductors for use in the 1–10 MHz range were intended for application to signal processing, primarily for use in tuned filters. While capacitors are easy to fabricate with semiconductor integrated circuit (IC) technology, inductors and transformers are much more difficult to realize. For this reason, small-signal inductance was achieved by devices that simulated a reactive impedance, such as active transistor circuits[1] and transit-time diodes.[2]

The first IC devices for actual magnetic energy storage were formed by the deposition of thin films (0.1 μm) of permalloy, a nickel-iron alloy, on a silicon substrate. The skin depth of permalloy at 1 MHz is about 2 μm, so that eddy current losses were negligible in the 0.1 μm films. In 1979 Soohoo proposed, but did not fabricate, a planar structure composed of a planar spiral of evaporated copper conductor embedded between two sputterred permalloy films.[3] A similar structure was fabricated in 1984 by Kawabe et al., in which a meander line, illustrated in Fig. 3.1, was used instead of a planar spiral.[4] Presumably

---

[1] S. Noguchi, "Solid State Inductor Using Hybrid IC and its Characteristics," *Proceedings of the Fourth International Symposium on Hybrid Microelectronics*, (1974), pp. 60–66.

[2] S. M. Sze, *Physics of Semiconductor Devices*, 2nd ed., John Wiley and Sons, Inc., New York (1981), pp. 579–585.

[3] R. F. Soohoo, "Magnetic Thin Film Inductors for Integrated Circuit Applications," *IEEE Transactions on Magnetics*, **15**, 6 (1979), pp. 1803–1805.

[4] K. Kawabe, H. Koyama, and K. Shirae, "Planar Inductor," *IEEE Transactions on Magnetics*, **20**, 5 (1984), pp. 1804–1806 (Page numbers are indeed close to those of previous reference).

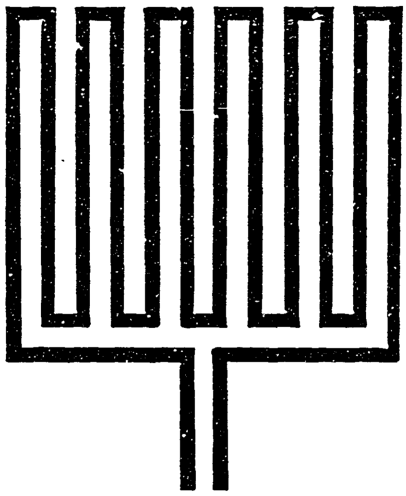

Fig. 3.1 Meander line.

the meander line, familiar from microwave devices, was substituted in order to avoid the difficulty of connecting the center of the planar spiral to the periphery of the device. While the device had a fairly large footprint of 1.4 cm^2, its height was only 20 μm. Unfortunately, this device functioned more as a resistor than an inductor. At 1 MHz the component had an inductance of 100 nH and a resistance of 10 Ω, for a Q of only 0.06. Despite further attempts at improving this approach, the authors were only able to increase the Q by a factor of two.[5,6]

The cloth inductor was an innovative device in which the windings were literally woven together with strands of amorphous magnetic metal, as shown in Fig. 3.2. [7, 8] For clarity, the structure can be approximated as many parallel solenoids, as shown in Fig. 3.3. Unfortunately, for reasons of fabrication, the threads of amorphous metal used

---

[5] O. Oshiro, H. Tsujimoto, and K. Shirae, "A Closed-type Planar Inductor," *IEEE Translation Journal on Magnetics in Japan*, **2**, 4 (1987), pp. 329–330.

[6] O. Oshiro, K. Kawabe, H. Tsujimoto, and K. Shirae, "A Wide Frequency Planar Inductor," *IEEE Translation Journal on Magnetics in Japan*, **2**, 4 (1987), pp. 331–332.

[7] H. Matsuki and K. Murakami, "A New Cloth Inductor Using Amorphous Fiber," *IEEE Transactions on Magnetics*, **21**, 5 (1985), pp. 1738–1740.

[8] H. Matsuki, K. Murakami, and T. Yamamoto, "Preparation and Characteristics of Cloth Inductor," *IEEE Translation Journal on Magnetics in Japan*, **2**, 4 (1987), pp. 324–326.

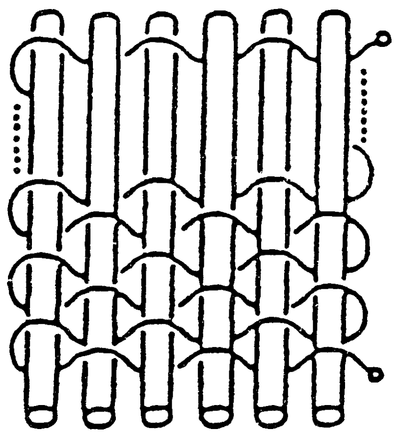

Fig. 3.2 Cloth inductor (Matsuki, Fig. 1a).

by Matsuki and Murakami in their original work had diameters of 80 μm, much larger than the material's skin depth at 1 MHz, 6 μm. For this reason the eddy current loss in the amorphous metal was severe. The cloth inductor they fabricated had an inductance of 80 μH at 1 MHz, but a resistance of 280 Ω, giving the very low Q of 1.8. The authors were able to improve this performance in later work by using threads with diameters of only 20 μm, producing an 8 μH inductor with a resistance of 2.5 Ω at 1 MHz.[9] The footprint of this inductor was only 0.1 cm^2, and the height only 4 mm. The Q of this new device was 20, an order of magnitude improvement over the original device. This loss, however, is still much too high for power applications, and the loss will only increase above 1 MHz, since the skin depth will decrease. The authors suggest that 1 MHz is the maximum usable frequency for the cloth inductor.

The most successful of the attempts to miniaturize inductors was the cylindrical chip inductor.[10] In this structure, shown in Fig. 3.4, a "barrel winding" is cofired inside a nickel-

---

[9] H. Matsuki, K. Murakami, and T. Yamamoto, "Performance of Miniaturized Magnetic Devices in Cloth Structure," *IEEE Transactions on Magnetics*, 22, 5 (1986), pp. 415–417.

[10] T. Hirai, Y. Hamazama, T. Ishida, T. Honda, T. Masumyama, "Cylindrical Chip Inductors," *International Journal of Hybrid Microelectronics*, 4, 2 (1981), pp. 96–99.

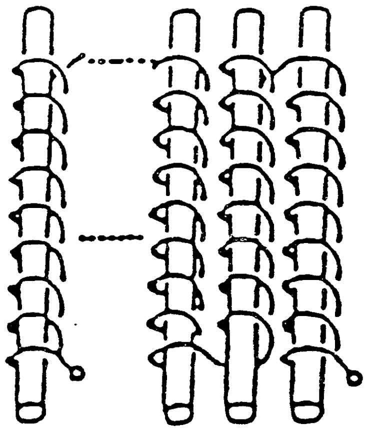

Fig. 3.3 Approximation to cloth inductor (Matsuki, Fig. 1b).

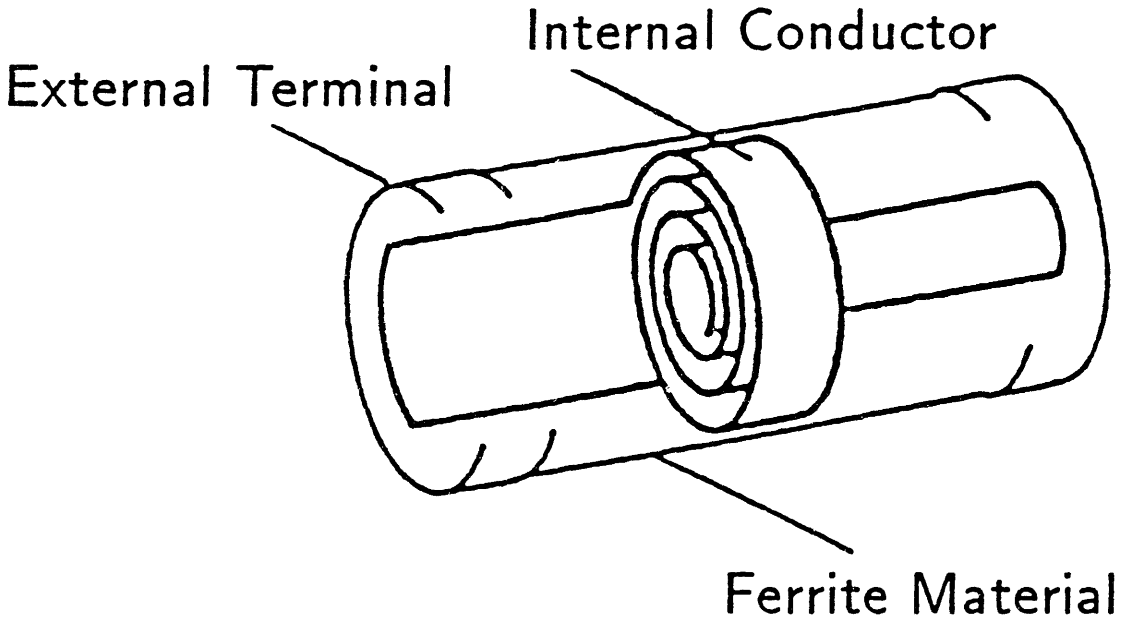

Fig. 3.4 Cylindrical chip inductor (Hirai, Fig. 3).

zinc ferrite. This device is essentially an ungapped pot core. Hirai et al. were able to fabricate an inductor that at 10 MHz displayed an inductance of 1.6 μH and a resistance of 2.1 Ω, for a Q of 48. Moreover, the footprint was only 0.13 cm^2 and the height only 2.2 mm.

While encouraging, this device is unsatisfactory for three reasons. First, the fabrication is difficult. The ferrite shrinks during cooling, which can cause defects. Moreover, the ferrite must be fired at temperatures between 900–1200°C. This precludes the use of copper windings, since copper would oxidize. Metals with lower conductivities must be used instead, such as silver (used by Hirai). The second problem is that in this structure proximity effects in the conductors have greatly increased the copper loss and reduced the Q. This problem will be described in great detail in Chapter 4, together with a discussion of structures that avoid the problem. The third problem is that the magnetic energy is stored in the magnetic material, instead of in an air gap. As explained in Chapter 2, at power flux levels the resulting core loss would greatly reduce the Q.

3.2 Miniaturized Transformers for Dc/Dc Converters

Power electronic applications have focussed on the development of miniaturized transformers, rather than inductors, since, as shown in Fig. 1.4, the inductances required in dc/dc converters can often be combined with the transformers. Published work to date reflects initial attempts to address some of the requirements of high frequency conversion.

One of the first power transformers to use printed circuit board windings was contained in the Analog Devices AD293/4, a 200 kHz hybrid flyback converter.[11] In this transformer the primary and secondary windings were planar spirals printed as multiple layers on an alumina substrate. The alumina in the center of the spirals was cut out and the windings were fitted around the center leg of a manganese-zinc ferrite E-core. Although the switching frequency was only 200 kHz, the transformer demonstrated that thick film techniques could greatly improve the manufacturability of the transformer windings. Five years later, a similar design was implemented for a 1 MHz resonant converter produced by Theta-J Corporation.[12] This very large transformer had a footprint of 10 cm^2 and a height of 1.8 cm.

In one of the earliest papers on megahertz range dc/dc converters, Gutmann suggested that above 1 MHz inductors might be formed simply from printed spirals, without magnetic material.[13] Such two-dimensional inductors were analyzed in detail by Rodriguez et al., who fabricated a 3 μH planar spiral inductor with a footprint of 4.9 cm^2, and measured its Q

---

[11] D. Bokil and W. Morong, "Thick-film Transformer Advances Hybrid Isolation Amplifier," *Electronics*, August 25, 1981, pp. 113–117.

[12] A. Estrov, "1–MHz Resonant Converter Power Transformer is Small, Efficient, Economical," *Power Conversion and Intelligent Motion*, August 1986, pp. 14–24.

[13] R. Gutmann, "Application of RF Circuit Design Principles to Distributed Power Converters," *IEEE Transactions on Industrial Electronics and Control Instrumentation*, **27**, 3 (1980), pp. 156–164.

as 38 between 1–10 MHz. Due to the large footprint and low Q, Rodriguez found that "...it is unlikely that such a structure will be adequate to store sufficient energy for power applications."[14]

Recent work has attempted to integrate the ferrite magnetic material into the thick film hybrid fabrication process. A 500 kHz thick film hybrid buck converter produced by Fuji Electrochemical Co. was fabricated on a nickel-zinc ferrite substrate, instead of the usual alumina substrate.[15] However, the windings of the buck converter's current source inductor were not printed with thick film. Instead, windings of ordinary magnet wire were wrapped around a notched tab of the substrate. This tab had a surface area of about 1,4 cm^2 and a thickness of 0.8 cm. Gradski fabricated a transformer whose windings were printed with multiple layers of thick film on a ferrite substrate for a 6 MHz resonant forward converter.[16] This design achieved a magnetizing inductance of 1.3 μH, but the resistance to the magnetizing current was too large, 2.5 Ω at 10 MHz, giving a Q at that frequency of only 33. The resistance, measured at an extremely low flux level, also does not reflect the additional core loss that would be present at power flux levels. The large resistance to the magnetizing current is in large part due to proximity effects in the conductors that occur because the windings are in the gap of this transformer. This effect will be discussed in more detail in Chapter 4. Gradski closed the magnetic circuit by covering the printed windings with half of a standard pot core. This pot core, the TDK RM5, has a footprint of 1.5 cm^2, and the core and substrate have a total height of about 1.6 mm. Both the footprint and height are too large. Efforts to print instead thick film ferrite layers on top of the windings, in the same fashion as insulating dielectric layers, were notably unsuccessful, due to the basic incompatibility of the thick film process with the high sintering temperatures of ferrite.[17]

Other transformer designs focussed on controlling parasitics that affect high frequency converter topologies, such as leakage inductance. For example, the dual forward converter

---

[14] R. Rodriguez, J. M. Dishman, F. T. Dickens, and E. W. Whelan, "Modeling of Two-Dimensional Spiral Inductors," *IEEE Transactions on Components, Hybrids, and Manufacturing Technology*, **3**, 4 (1980), pp. 535–541.

[15] N. Kato, S. Hirano, and M. Torii, "Ferrite Substrates for High-Frequency Switching Dc-To-Dc Converter Applications," *IEEE Transactions on Magnetics*, **21**, 5 (1985), pp. 1723–1725.

[16] P. M. Gradski and F. C. Lee, "Design of High-Frequency Hybrid Power Transformer," *IEEE Applied Power Electronics Conference Proceedings*, February 1988, pp. 319–326.

[17] P. A. Gradski, "High Frequency Magnetics," *Virginia Power Electronics Center Partnership '87* **2**, 1 (April 1987), pp. 3–6.

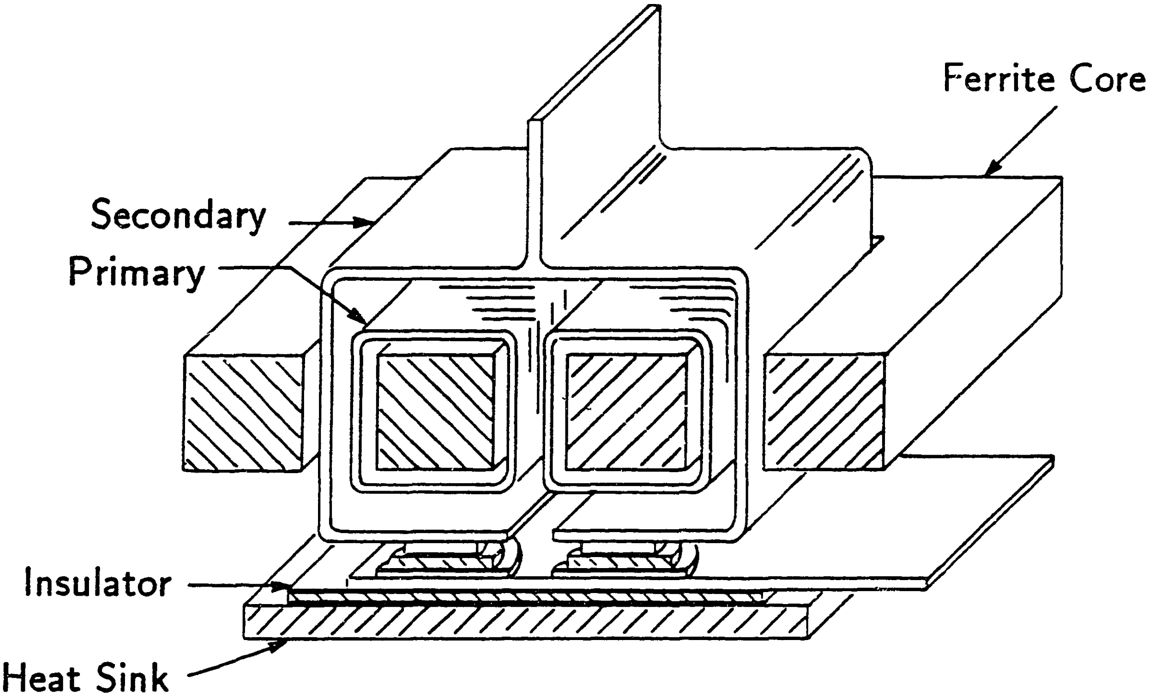

Fig. 3.5 Low leakage transformer incorporating output diodes into secondary (Carsten, Fig. 9).

cannot tolerate leakage inductance, since it delays the commutation of current from one output diode to the other. For that circuit Carsten designed the low leakage transformer of Fig. 3.5, which incorporates the output diodes into the secondary winding.[18]

Some resonant circuits, on the other hand, require a large leakage inductance that must function as part of a resonant tank. The transformer of Fig. 3.6 was used in the Vicor Corp. VI-200, a 1 MHz resonant converter.[19] This transformer achieved a very high leakage inductance by using a toroidal winding for the secondary.

3.3 Conclusions

The work reported to date has not produced magnetic components that meet the requirements of the new generation of high power dc/dc converters. The magnetic compo-

---

[18] B. Carsten and M. Chirea, "A Low Voltage Schottky for High Efficiency VLSI Power Supplies," *Official Proceedings of the Ninth International Power Conversion International Conference*, Intertec Communications, Ventura, California (1984), pp. 323–338.

[19] S. D. Cogger, "Dc-to-dc Converter Family Packs Power Into Tight Spots," *Electronic Design*, February 19, 1987, pp. 81–84.

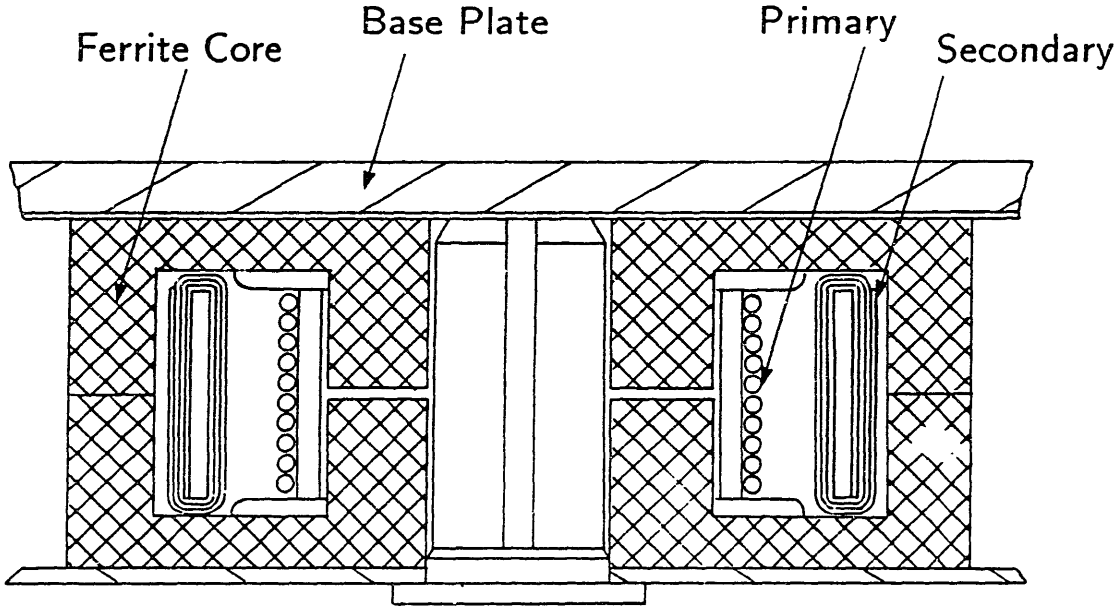

Fig. 3.6 High leakage transformer (Cogger, Fig. 2).

nents fabricated for signal processing applications are too lossy for power applications. The components designed for switching power converters were intended for application at 1 MHz and below and their designs cannot be easily extended for higher frequency operation. Their magnetic materials have been too lossy, their parasitics too large, and their windings have been subject to proximity effects and excessive copper loss. However, the Analog Devices and Theta-J transformers both demonstrated that the replacement of conventional magnet wire windings with thick film printed windings can greatly improve the manufacturability of magnetic components.

While the components described in this chapter represent important preliminary research, the work that produced them does not constitute an organized effort to identify the underlying limits to the miniaturization of these components and determine the levels of performance that can be achieved. This thesis attempts to address these issues and presents in Chapter 7 a design for a 10 MHz transformer with a footprint of 0.34 cm^2 and a height of 2.5 mm. The magnetizing inductance of this transformer is 1.33 μH, and the Q of the magnetizing inductance at the specified magnetizing current of 0.75 A is 71.

Chapter 4

DISCUSSION OF MAGNETIC COMPONENT GEOMETRY

The goal of this chapter is to choose a geometry for the magnetic component that stores a given amount of energy with the minimum copper loss. Several different geometries are examined and compared. The results of these studies are used in Chapter 7, which addresses the ultimate goal of designing transformers that have the minimum size for a given energy storage and power dissipation. As explained in the introduction, although this chapter considers transformers, since this is the component required for the MIT prototype converter, inductors are implicitly addressed by discussions of leakage and magnetizing fluxes. This chapter develops a transformer geometry, the slotted gapped transformer, that represents a reasonable compromise between low copper loss and fabrication complexity.

Careful design is required to minimize the total core and copper loss for a given transformer volume. For the core loss, the most difficult task is to understand its dependence on flux level, frequency, and dc bias. These issues of selection and characterization of the magnetic material will be addressed in Chapter 6. For the copper loss, the most difficult task is to understand the relationship between the current distribution and the transformer structure. Without an adequate understanding of this relationship, a structure that has an unexpectedly high copper loss due to skin and proximity effects might be designed. This chapter therefore focusses on the relationship between transformer structure and copper loss.

Unfortunately, the magnetic diffusion equation that describes the current distribution is difficult to solve for the transformer structures considered here. This thesis therefore develops qualitative understandings of the field and current distributions and employs finite element analyses to produce numerical solutions. The finite element method and software are briefly described.

The first structure considered is a simple sandwich transformer composed of a planar winding pressed between two plates of magnetic material, shown in Fig. 4.1. Although the sandwich structure is very simple to manufacture, the copper loss is greatly increased by circulating currents that are induced in each turn by the proximity of the magnetizing current in the other turns. The origin of these circulating currents, whose presence is known as the "proximity effect", is explained in detail, and a finite element analysis showing their distribution is presented.

In the sandwich transformer magnetic material surrounds a planar loop of conductor. Another way of constructing a simple magnetic circuit is for the conductor to surround a

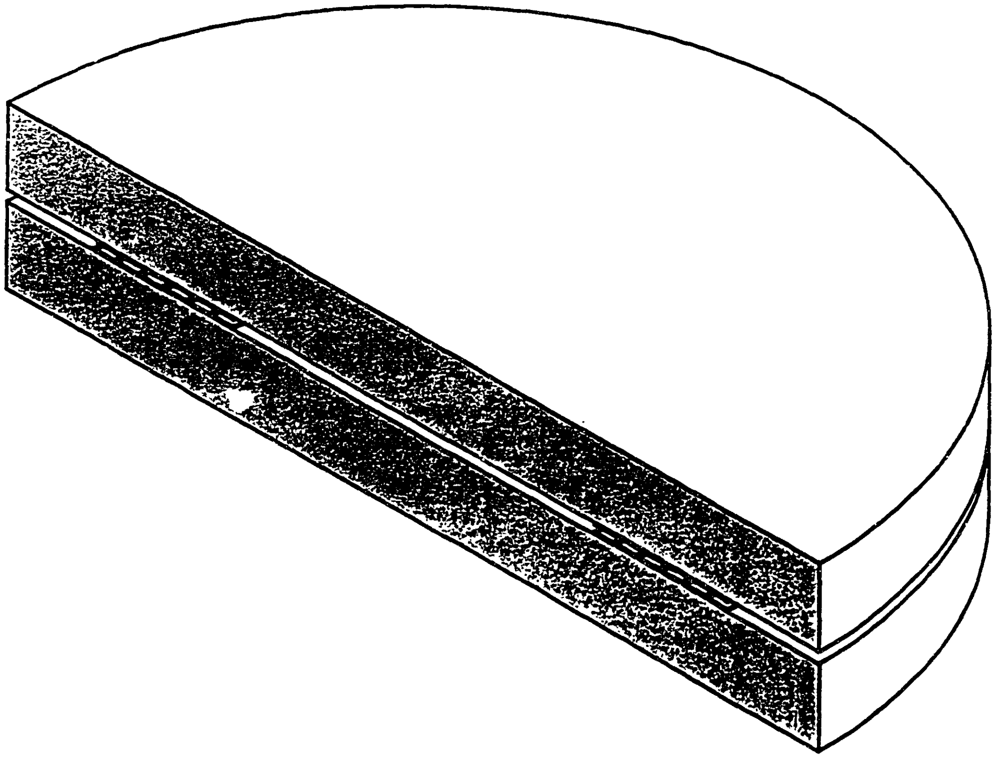

Fig. 4.1 Cutaway view of sandwich transformer with planar spiral winding.

planar loop of magnetic material, as in Fig. 2.1. If energy had to be stored in the structure, a gap could be added, as in Fig. 2.2. Instead of winding wire around the toroid, the windings could be composed of printed sections on the toroid's top and bottom surfaces that are connected by a piece of flexible printed circuit wrapped along the toroid's inner and outer edges. This complicated arrangement, pictured in Fig. 4.2, is necessary because printed circuits are essentially two dimensional, while the winding around the toroidal core is essentially three-dimensional. It is much simpler to make the sandwich transformer and structures like it, since they require essentially two-dimensional winding patterns. Toroidal structures will therefore not be considered here.

Since the sandwich transformer, while relatively easy to fabricate, has high copper losses, three alternative transformer structures are examined. Although these structures are more complicated to fabricate than the sandwich transformer since they require more complicated core shapes, their geometry serves to minimize the magnetizing current proximity effects and the resulting copper loss. These alternative structures are the cofired transformer of Fig. 4.3, the slotted gapped transformer of Fig. 4.4, and the slotted ungapped transformer of Fig. 4.5. The cofired transformer is formed by both eliminating the air gap

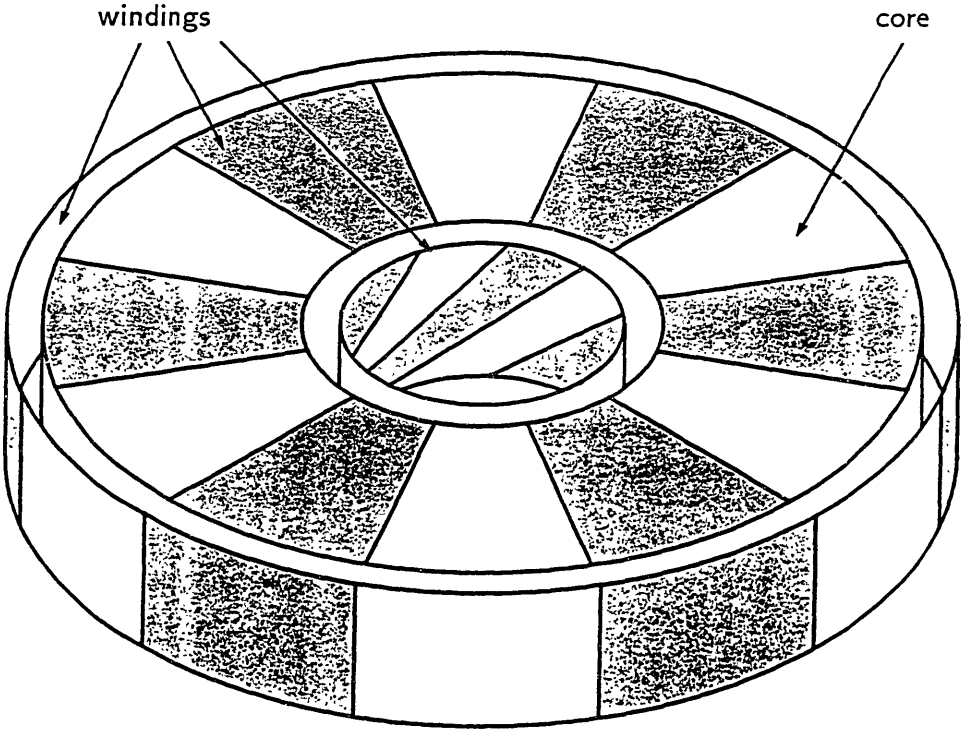

Fig. 4.2 Toroid with thick film windings on top and bottom and flexible printed circuit board connections at inner and outer edge.

and completely embedding the conductors in a lower permeability material, forming a ungapped structure. In the slotted gapped transformer the windings are recessed in a deep slot, forming a structure similar to a pot core. The slotted ungapped transformer is formed by eliminating the gap in the slotted gapped transformer and using a lower permeability material in order to maintain the same reluctance.

For each structure, finite element analyses were used to determine the magnetic field distribution and the effective ac resistance of the windings to the magnetizing current. Studies are presented that examine the dependence of the copper loss on the transformer dimensions in order to understand the tradeoff between increased transformer size and decreased copper loss.

These studies, which seek to minimize the copper loss when only the magnetizing current is present, are incomplete, since the copper loss in a transformer depends on the total current in the windings. This current is the sum of the magnetizing current, the load current, and any currents due to interwinding capacitances. This analysis neglects such currents,

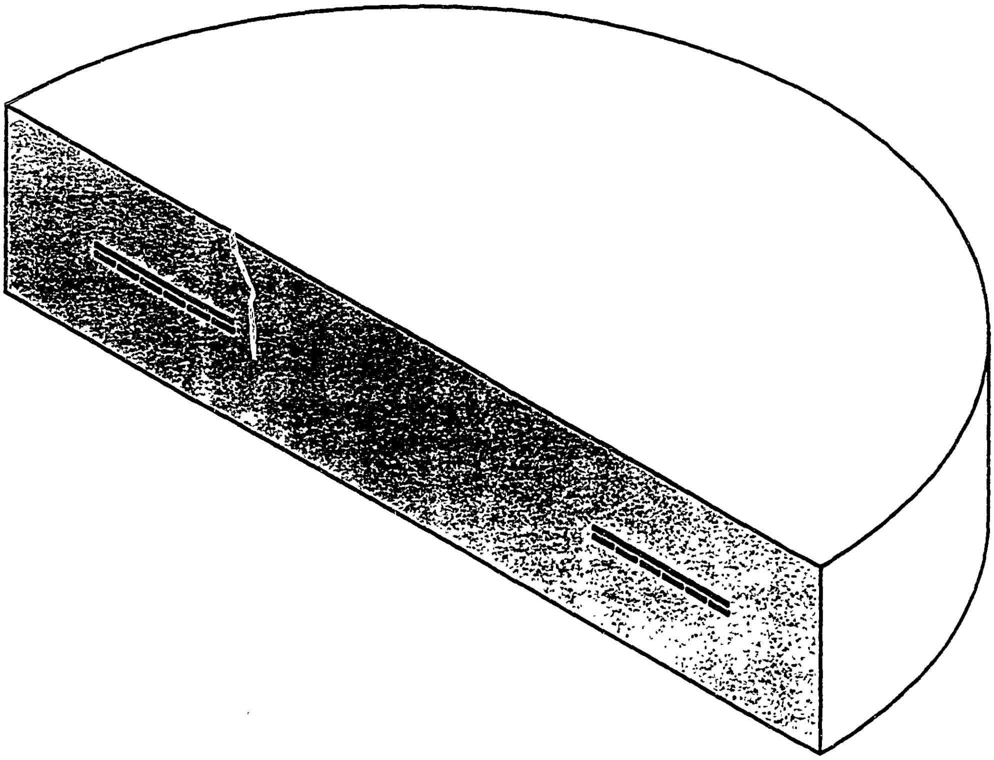

Fig. 4.3 Cutaway view of cofired transformer with planar spiral winding.

which are shown in the next chapter to be small. The two significant components of the current, the load current and the magnetizing current, may be distributed very differently in the conductors. The loss associated with a particular design therefore depends very strongly on the relative magnitudes of the magnetizing and load currents. In order to prevent the results presented here from depending on specific values of magnetizing and load current, the different transformer designs were evaluated by comparing the dissipations that would have resulted if only the magnetizing current were present. This chapter will show that the load current would have the same distribution in each structure that was investigated. Since computing the copper loss due to the magnetizing and load currents separately does not necessarily give the correct value for the total copper loss, the analysis assumes that a reduction in the magnetizing current proximity effect is beneficial. This assumption is reasonable for a gapped transformer, since the magnetizing current is generally substantial.

Another complicated issue is the distribution of the magnetizing current between primary and secondary. The amount of magnetizing current that flows in each winding depends in large part on the external circuit. For simplicity, this thesis assumes that the magnetizing current flows entirely in the primary. The intent of this chapter is to show

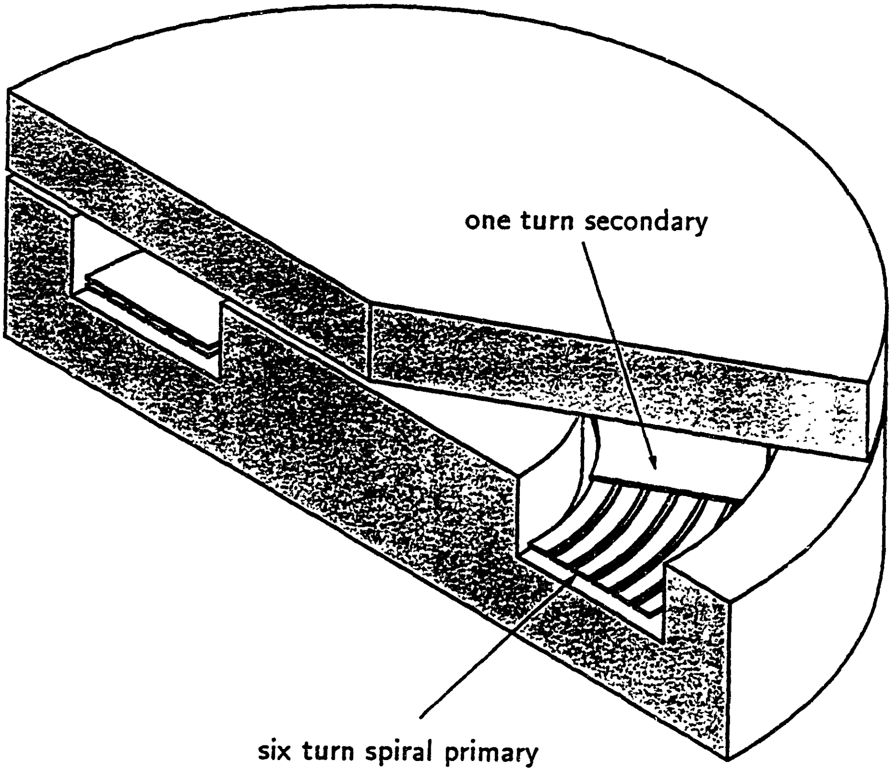

Fig. 4.4 Cutaway view of slotted gapped transformer with planar spiral winding.

what must be done to minimize the proximity effects, regardless of the detailed nature of the winding currents.

The work in this chapter shows that while in a simple sandwich transformer the ac resistance can be over eight times the dc resistance, by using such structures as the gapped slotted transformer, it is possible to reduce the ac resistance to the point where it is only 33% more than the dc resistance. This number, 33%, represents the smallest ac resistance that can be achieved with the structures discussed in this chapter, and is reached at the expense of a larger transformer. The nature of the tradeoff between size and loss is discussed later in this chapter.

4.1 Finite Element Analysis

The magnetic diffusion problems posed by the structures in this chapter were solved by means of finite element analyses. This section briefly describes the procedure used by

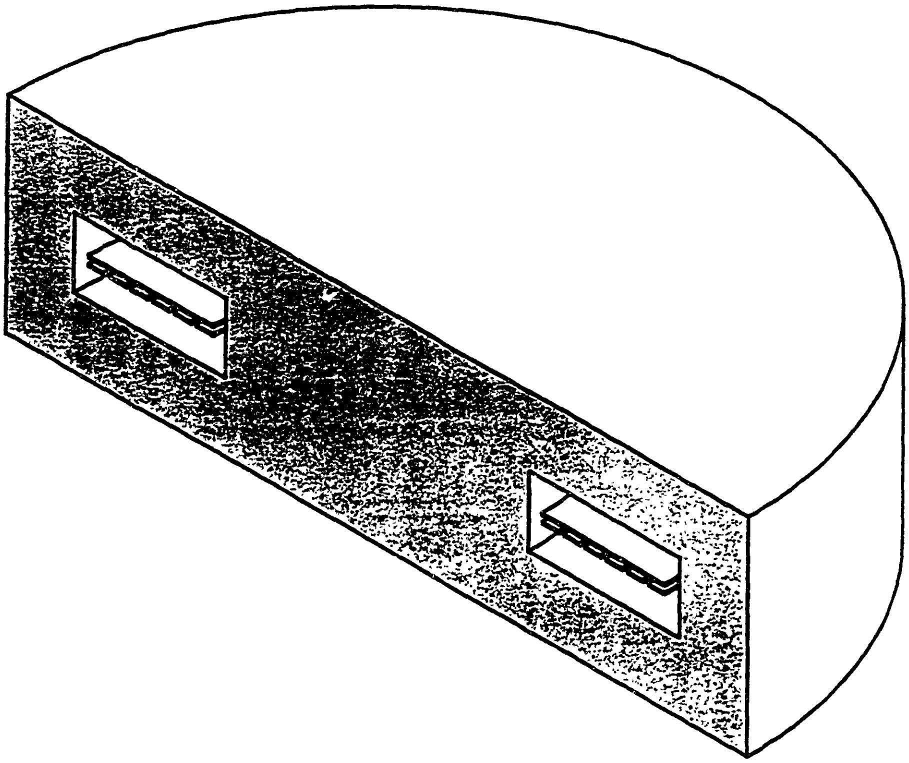

Fig. 4.5 Cutaway view of slotted ungapped transformer with planar spiral winding.

the finite element analysis computer program used in this thesis[1].

First, the program breaks up the geometry of the problem into a mesh of triangles. The program treats the transformers as being axisymmetric, so that the problem is reduced from three dimensions (r, θ, z) to two dimensions (r, θ). The length of each triangle side must be much shorter than the characteristic length of the solution in that region. For example, in the conductors the characteristic length is a skin depth, so that the sides of the triangles there must all be much shorter than a skin depth. The solution is computed at each vertex and midpoint; these positions are called nodes. Quadratic interpolation is used to determine the solution between nodes. Material properties are associated with triangles, sources are defined, and boundary conditions are imposed. It should be noted that this software models the permeability as a real constant, so that its solutions do not take into account either core loss or the variation of permeability with flux level.

---

[1] "Maxwell" finite element package, Ansoft Corporation, Pittsburgh, PA.

Second, the program computes the magnetic potential at each node. The structures studied in this chapter are all axisymmetric, so that the vector potential is given by $\tilde{A}_\phi(r,z)$. The computation is performed by means of an algorithm that employs variational techniques to transform the system of differential equations to a matrix of simultaneous equations[2]. This matrix is sparse, since nodes are coupled only to their neighbors. Preserving the sparseness of the matrix during the solution process is essential to minimizing the computer memory requirements. For this reason an iterative solution technique is preferred over such methods as Gaussian elimination.

The analysis software produced both numerical and graphical data from the magnetic potential distribution. The program was used to compute the energy storage and power dissipation in each material, and to graph the current distributions in the conductors.

Each analysis presented in this chapter contained 8000–10000 nodes and required about two hours to solve on a Digital Equipment Corp. Microvax II running the Ultrix operating system and the X10 window system. The solving program required about 8 MB of memory, not including the operating system requirements. The computer was configured with enough memory to run the solver in RAM, as the use of virtual (disk) memory incurs a substantial performance penalty.

4.2 Sandwich Transformer

Perhaps one of the simplest transformer designs to manufacture is the sandwich transformer of Fig. 4.1, in which the primary and secondary windings are patterned on each side of a substrate, such as a flexible printed circuit, that is sandwiched between two pieces of magnetic material. Note that the windings occupy the gap of the magnetic circuit. This is possible because the winding thickness in 1–10 MHz transformers is often less than that of the gap required.

In the sandwich transformer the load current, which is the component of the current that flows into the primary and out of the secondary, flows on the facing surfaces of the windings, as shown in Fig. 4.6. The separation between primary and secondary is very small compared to the width of the windings, so the field solution is similar to that of a long solenoid: the H field is uniform between the primary and secondary. Inside each conductor the H field, as well as the load current, decays exponentionally away from the facing surface. Under this solenoidal field approximation, the spatial decay constant is the

---

[2] J. Weiss and Z. Cendes, "Efficient Finite Element Solution of Multipath Eddy Current Problems," *IEEE Transactions on Magnetics*, **18**, 6 (1982).

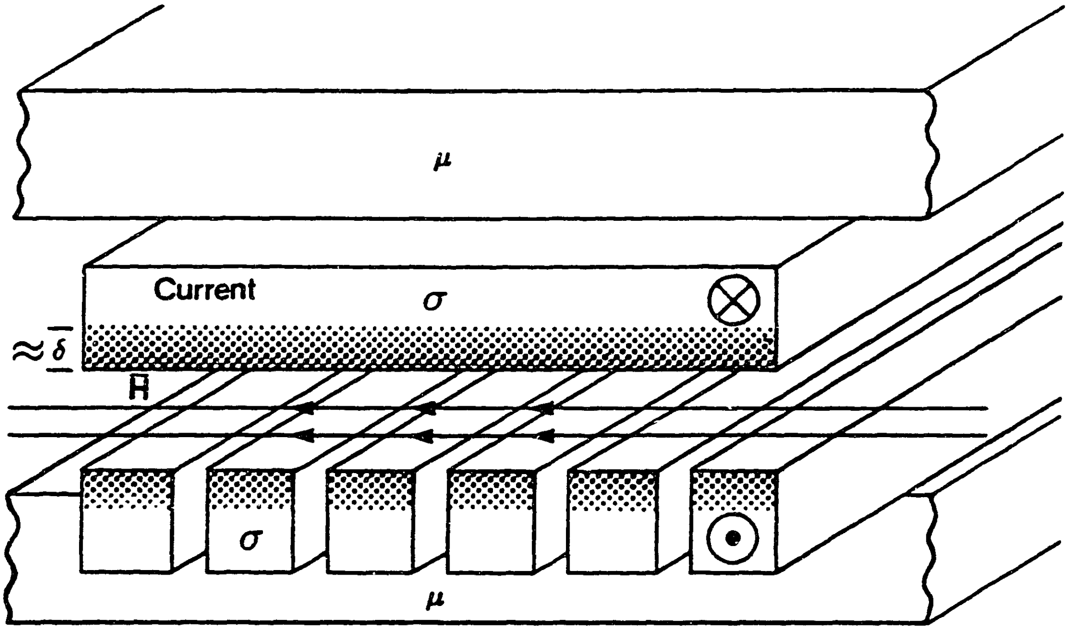

Fig. 4.6 Load current distribution in a sandwich transformer.

characteristic skin depth, δ.

Figure 4.6 shows windings that are much thicker than a skin depth. In this study however, the thickness of the windings will be assumed to be one skin depth. This limitation is imposed to avoid circulating currents induced by the magnetizing current that cause excessive loss, an effect that will be explained later in this chapter. It is shown in Appendix A that limiting the thickness of the windings to a skin depth increases the resistance to the load current by only 9% over the resistance of windings much thicker than a skin depth.

Although the useful copper thickness is limited to a skin depth, the useful copper width is not, so that the resistance to the load current can be reduced by increasing the width of the conductors. Therefore, windings are typically designed with widths that are much greater than their thicknesses. Increasing the conductor width, however, does not reduce the resistance to the magnetizing current. As this section will explain, the magnetizing current is not spread out over the horizontal surfaces, like the load current, but is instead concentrated on the conductors' vertical edges. While the load current decays exponentially in the $\hat{z}$ direction from the horizontal surfaces, the magnetizing current decays exponentially in the $\hat{r}$ direction from the vertical edges. Because the conductor thickness is assumed to be δ, the cross-sectional conductor area available to the magnetizing current is proportional to δ^2. Thus the effective resistance to the magnetizing current is much higher than it is for the load current.

In addition, due to the proximity effect, the magnetizing current induces large circulating currents in each turn that also crowd into these vertical edges and greatly increase dissipation. This section will show how these circulating currents arise. For simplicity, it will start by assuming that only the primary winding is present so that the magnetic fields and currents can be determined analytically. These results will be confirmed by a finite element analysis. The influence of the secondary winding will then be discussed qualitatively and verified by another finite element analysis.

4.2.1 Magnetizing Current Distribution in the Sandwich Inductor

Figure 4.7 shows a cross-sectional view of a six turn sandwich inductor whose dimensions are listed in Table 4.1. All the analyses presented in this chapter are for a core with the radial dimensions of a Ferroxcube 1107 pot core, because the experimental measurements reported in Chapter 9 used this core size. The windings in the sandwich inductor are positioned where the slot in the 1107 pot core would be. The analyses here use the 4 MHz operating frequency that was used in the measurements of Chapter 9, as well as in a prototype high density dc/dc converter.[3] The thickness of the windings was chosen to be 34 μm, which is both a standard thickness of the copper on commercially available flexible printed circuit board, and approximately equal to the skin depth in copper at 4 MHz (33 μm).

Table 4.1: Dimensions of Sandwich Inductor

Dimension	Symbol	Value
Core inner radius	r_i	955 μm
Core outer radius	r_o	5.55 mm
Winding inner radius	r_{wi}	2.47 mm
Winding outer radius	r_{wo}	4.32 mm
Conductor thickness	t	34 μm
Gap length	g	34 μm
Width of conductor		250 μm

To understand the source of the circulating currents, consider the field and current distributions in the gap of the sandwich inductor of Fig. 4.7. For simplicity, assume that the reluctance of the magnetic material is negligible, and that the winding carries a sinusoidal

---

[3] L. F. Casey and M. F. Schlecht, "A High Frequency, Low Volume Point-of-Load Power Supply for Distributed Power Systems," *IEEE Power Electronics Specialists Conference Record*, June 1987.

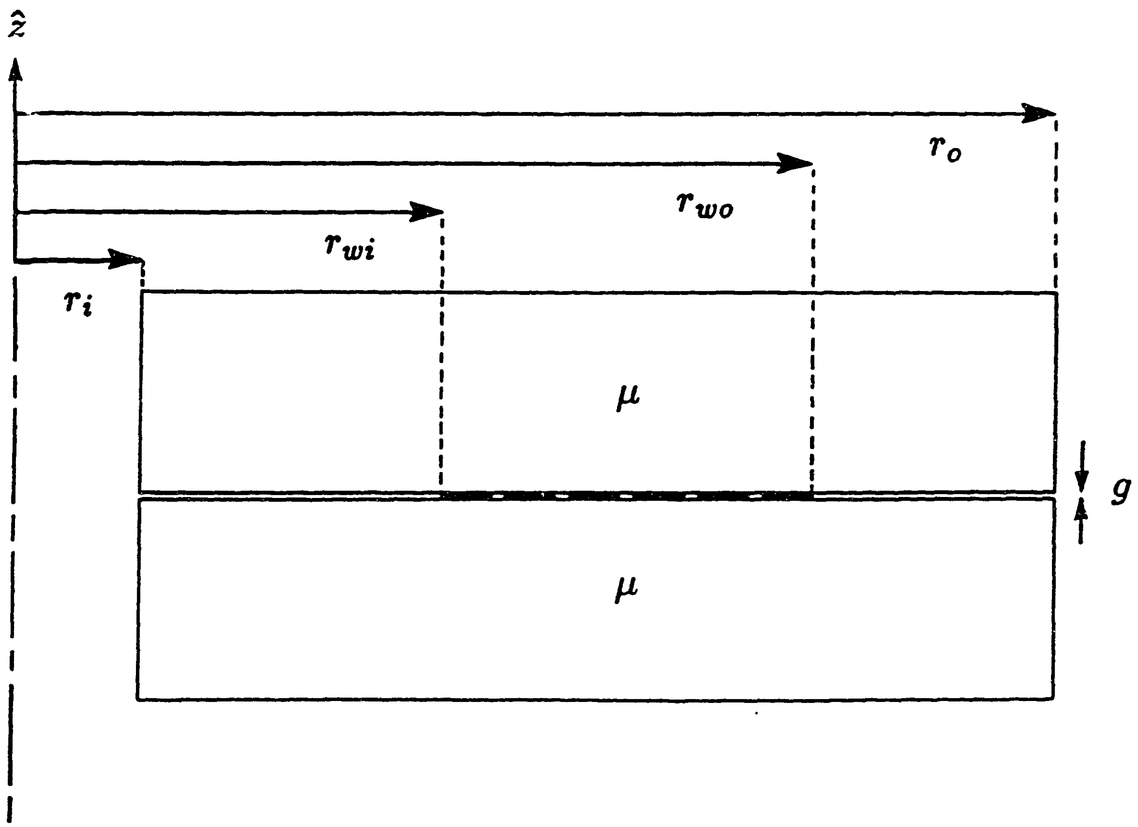

Fig. 4.7 Dimensioned view of a sandwich inductor. Note that in this and the following figures, the structures are shown with a hole along the $\hat{z}$ axis. This is because, as explained in the text, the radial dimensions of the cores studied in this chapter were set equal to those of the Ferroxcube 1107 pot core, which has such a hole.

magnetizing current, i_m, with a peak value of 1 A. Because the gap is small compared to the structure's horizontal dimensions and because $\mu \gg \mu_o$, it is reasonable to assume that the H field in the gap is purely $\hat{z}$ directed.

For a 4 MHz sinusoidal excitation each primary turn is more than seven skin depths wide, so that the $\hat{z}$ directed H field in the gap does not have enough time during its cycle to diffuse throughout the entire conductor. The field instead flows around the conductor and only penetrates to about a skin depth in the radial direction in each vertical edge. The magnetizing currents therefore only flow in the vertical edges of the conductors.

In order to obtain a simple expression for the H field in the gap, the total magnetic flux passing between the turns will be assumed to be negligible compared to the flux passing through the center of the winding and returning across the gap at the outer radius of the core. This is a good approximation because the total area of the spaces between the windings is small compared to the area of the center of the winding and the return area at the outer radius. The value of the magnetic field in the gap at the center of the winding can be found from Ampere's Law to be

$$H_z = \frac{6i_m}{g(1 + A_i/A_o)} \tag{4.1}$$

where g is the gap length and A_i/A_o is the ratio of the area of the center of the winding to the area outside the outer edge of the winding where the flux returns. In the 1107 pot core A_i is less than A_o. The area ratio can be expressed as

$$\frac{A_i}{A_o} = \frac{r_{wi}^2 - r_i^2}{r_o^2 - r_{wo}^2} \tag{4.2}$$

For the dimensions of Table 4.1, this gives a value for H_z of 120 kA/m.

The magnitude of the current flowing on the innermost edge of the innermost conductor can be calculated by multiplying the value of H_z (120 kA/m) by the winding thickness (34 μm), which gives 4.2 A. But since only a total of 1 A actually flows in the conductor, a return current of 3.2 A must be circulating in the opposite direction on the right edge of the innermost winding. This means that the H field tangential to the right edge of the innermost conductor has a magnitude of 3.2 A divided by 34 μm, which is 94 kA/m. This value is necessarily equivalent to the strength of the H field we would calculate between this and the next turn by using the integral form of Ampere's Law.

The circulating currents in the other turns can be estimated by extending the above calculation. The magnitude of the H field in the region between any two winding turns is given by

$$H_{n,n+1} = \left| \frac{ni_m}{g} - H_i \right| \tag{4.3}$$

where n is the number of turns between the center axis and the region being considered. The current that flows in any conductor edge can therefore be found by multiplying the appropriate field strength, $H_{n,n+1}$, by the winding thickness, t. The circulating currents that result for each turn of the sandwich inductor are listed in Table 4.2. Note that each conductor carries the the required 1 A net current.

Table 4.2: Circulating Currents in Each Conductor

Conductor	Left edge (A)	Right edge (A)
1 (innermost)	− 4.2	+ 3.2
2	− 3.2	+ 2.2
3	− 2.2	+ 1.2
4	− 1.2	+ 0.2
5	− 0.2	− 0.8
6 (outermost)	+ 0.8	− 1.8

The asymmetrical current distribution apparent in Table 4.2, in which only the outermost conductor carries a positive current in its left edge, arises because A_i is not equal to A_o. In order to understand the nature of this asymmetry, it is instructive to examine two limits: $A_i/A_o = 1$ and $A_i/A_o \ll 1$. Table 4.3 shows the current distribution that results for $A_i/A_o = 1$. In this limit the H field is of equal magnitude and opposite direction at the left edge of the innermost conductor and the right edge of the outrermost conductor, so that the current distribution is perfectly symmetrical. Table 4.4 shows the current distribution that results for $A_i/A_o \ll 1$. In this limit the magnitude of the H field at the left edge of the innermost conductor is $6i_m/g$, and the magnitude of the H field at the right edge of the outermost conductor is negligible, so that the current distribution is as asymmetrical as it can be. For the case described by Table 4.2, $A_i/A_o = 0.43$, so that the current distribution is between the two extremes of symmetry and asymmetry.

Table 4.3: Circulating Currents in Each Conductor for $A_i/A_o = 1$

Conductor	Left edge (A)	Right edge (A)
1 (innermost)	− 3.0	+ 2.0
2	− 2.0	+ 1.0
3	− 1.0	0.0
4	0.0	− 1.0
5	+ 1.0	− 2.0
6 (outermost)	+ 2.0	− 3.0

Table 4.4: Circulating Currents in Each Conductor for $A_i/A_o \ll 1$

Conductor	Left edge (A)	Right edge (A)
1 (innermost)	− 6.0	+ 5.0
2	− 5.0	+ 4.0
3	− 4.0	+ 3.0
4	− 3.0	+ 2.0
5	− 2.0	+ 1.0
6 (outermost)	− 1.0	0.0

The copper loss can be easily calculated once these currents are known. As mentioned previously, the current density decays exponentially away from each vertical edge with the characteristic skin depth, δ. For the purposes of computing copper loss, the current can be considered to flow uniformly to a depth of one skin depth.[4] Since the conductor thickness is also one skin depth, the effective cross-sectional area for the circulating current is δ^2. The

---

[4] S. Ramo, J. R. Whinnery, and T. Van Duzer, *Fields and Waves in Communication Electronics*, John Wiley and Sons, Inc., New York (1965), p. 288.

edge resistance is therefore

$$R = \frac{2\pi r}{\sigma \delta^2} \tag{4.4}$$

where r is the radius of the conductor's edge and σ is the conductivity of the copper. Returning to the case considered in Table 4.2, for the innermost conductor, the resistance of the left edge of the innermost conductor is 0.24 Ω, giving a power dissipation of 2.1 W, and the resistance of the right edge is 0.27 Ω, giving a power dissipation of 1.4 W. The total power dissipation in the innermost conductor is therefore 3.5 W, so that the effective resistance of the innermost turn to the net current of 1 A is 7.0 Ω.

Table 4.5 compares the power dissipation in each turn predicted by this simple estimate with a finite element solution of this problem. The agreement is good considering the simplifying assumptions that were made. The finite element analysis calculated a total power dissipation of 7.2 W, so that the effective resistance of the primary winding is 14.4 Ω. This resistance is more than 50 times larger than the dc resistance of the primary winding, 0.27 Ω.

Table 4.5: Power Dissipation in Each Conductor

Conductor	Estimate	Finite Element
1 (innermost)	3.5	3.2
2	2.1	1.9
3	1.0	0.83
4	0.25	0.19
5	0.13	0.16
6 (outermost)	0.82	0.92
Total	7.8	7.2

It is instructive to constrast the 15.6 Ω resistance calculated for this case with the resistances that would result for the symmetric $A_i/A_o = 1$ case and the asymmetric $A_i/A_o \ll 1$ case. The symmetric case would give a resistance of 12.8 Ω, while the asymmetric case would give a resistance of 42.2 Ω. The symmetric case, therefore, corresponds to the current distribution with the lowest copper loss, while the asymmetric case corresponds to the distribution with the highest copper loss. It is tempting to conclude that a criterion for minimum loss is that $A_i = A_o$, but it must remembered that the total loss also depends on the core loss, so that the total loss may be lower for $A_i \neq A_o$. This issue will be reexamined in Chapter 7.

Figure 4.8 shows the finite element computation of the current distribution along a horizontal line through the center of the primary windings. For clarity, the outline of the primary windings is superimposed on the horizontal axis. This figure assumes a sinusoidal current in the windings, $I_o \cos \omega t$ ($I_o = 1$ A, $\omega = 2\pi \times 4$ MHz), and shows a snapshot in time,

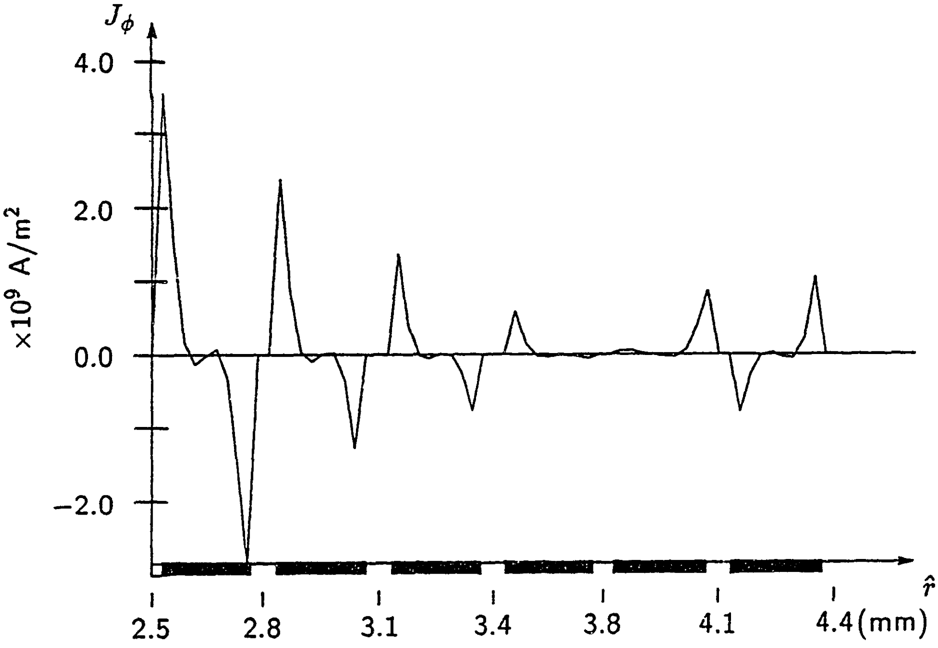

Fig. 4.8 Magnetizing current density in the primary winding. The windings are shown in outline in their position along the horizontal (radial) axis.

$\omega t = 0$, of the current distribution. The spikes of alternating polarity indicate the presence of circulating currents at the edges of the conductors.

4.2.2 Magnetizing Current Distribution in the Sandwich Transformer

Next, consider the effect on the copper loss of adding a one turn secondary to the structure, as shown in Fig. 4.1. As discussed in the introduction, the distribution of magnetizing current between the primary and secondary windings depends on the external circuit. However, the central problem of reducing the copper loss due to the proximity effect can be addressed without considering the details of this distribution. For simplicity, therefore, the secondary is open circuited so that all the magnetizing current flows in the primary. Although the net current in the secondary must be zero, the primary current induces eddy currents in the secondary that add to the copper loss. Despite the presence of these eddy currents, the total copper loss actually decreases, as this section will explain. The finite element program models the open circuited secondary by adding a distributed current source to the eddy currents induced in the secondary so that the net current in the secondary is

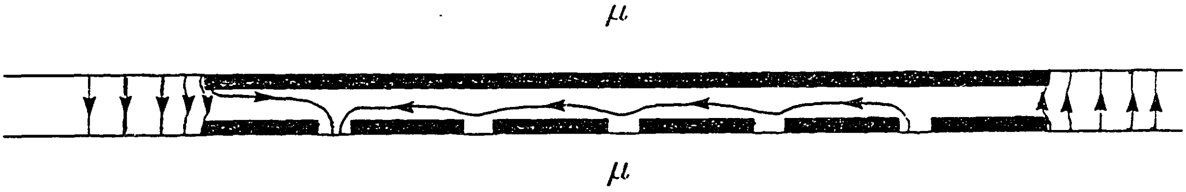

Fig. 4.9 *H* field distribution due to magnetizing current in a sandwich transformer.

zero, while ensuring that the total current distribution satisfies both the magnetic diffusion equation and the boundary conditions.

Figure 4.9 shows a sketch of the H field distribution in the gap. Although the secondary is only a skin depth thick, it is more than forty skin depths wide. As was the case with the primary, the excitation is too fast for the flux to diffuse fully into the secondary, and the flux must therefore flow around it. The H field is therefore forced to flow in the $\hat{r}$ direction, along the long dimension of the conductors, instead of vertically along only their thin edges. This field distribution serves to spread out the magnetizing current in the primary along the full width of each turn and to eliminate the circulating currents in all but the innermost conductor, where, since A_i is less than A_o, the field is most intense.

The new current density distribution in the primary is shown in Fig. 4.10a. With this spread out current distribution, the resistance of the primary itself is reduced from the 14.4 Ω of the sandwich inductor to 1.02 Ω. However, the primary current distribution is mirrored in the secondary, as shown in Fig. 4.10b, which gives rise to additional loss. And since the total current in the open circuited secondary must sum to zero, large positive currents must also flow in the edges of the secondary to oppose the negative mirrored currents. The resulting loss in the secondary is actually larger than the loss in the primary and adds 1.24 Ω to the effective primary resistance, for a total of 2.26 Ω. This resistance is less than 20% of the effective resistance of the sandwich inductor. Although the presence of the secondary greatly reduces the total copper loss, the effective resistance is still more than eight times larger than the primary winding's dc resistance of 0.27 Ω.

4.3 Cofired Transformer

One way to make the magnetizing current flow more uniformly in the primary is to embed the windings in a magnetic material. A material with a lower permeability is used so that the reluctance is the same as for the gapped transformer. This approach requires a different fabrication technique, e.g. the use of windings cofired with the magnetic material. In analyzing this structure the core permeability was chosen to be $21\mu_o$, so that

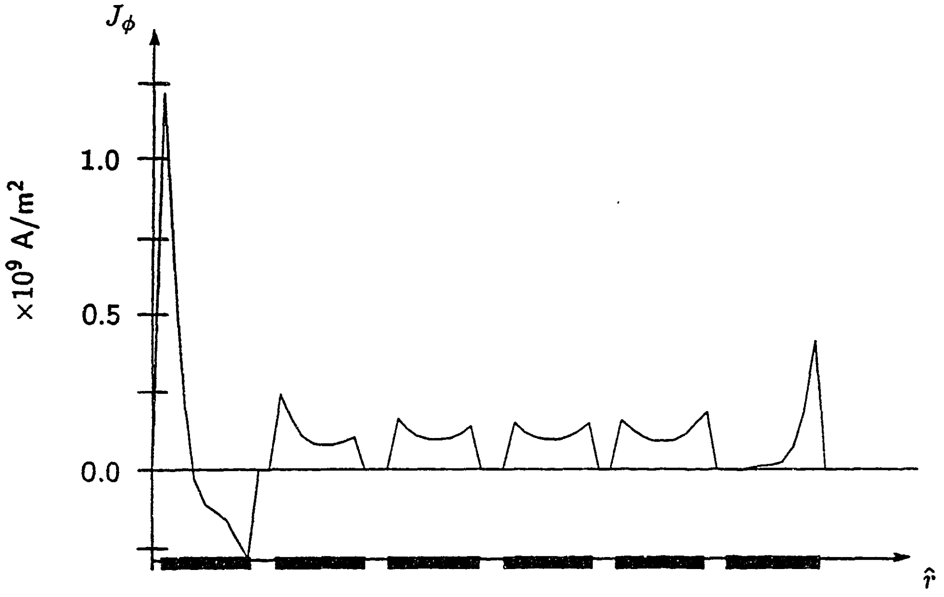

Fig. 4.10a Magnetizing current density in the primary winding of a sandwich transformer.

the inductance would be the same as the slotted structures discussed later in this chapter. The dimensions are the same as those of the sandwich transformer and are given in Table 4.1.

With the gap filled with permeable material, much of the flux created by the primary winding current flows horizontally between the windings, rather than enclosing the secondary. The magnetizing current is therefore spread out across the primary winding even more than before, and there is little current density in the secondary. A finite element analysis determined the effective resistance to the magnetizing current of this structure to be only 0.44 Ω, of which 0.35 Ω was due to loss in the primary, and 0.09 Ω was due to loss due to currents induced in the secondary. This effective resistance is only 60% higher than the dc resistance of the primary winding.

Unfortunately, since the flux generated by the primary tends not to enclose the secondary, the leakage inductance of this structure is 15 times higher than the 50 nH leakage inductance of the sandwich transformer of Fig. 4.1. Furthermore, its value is dependent on the exact value of the core permeability. In addition, if ferrites are used as the core material (as they are in this thesis), the interwinding capacitances is at least three times higher because magnetic material typically has a permittivity of at least $10\epsilon_o$, compared to

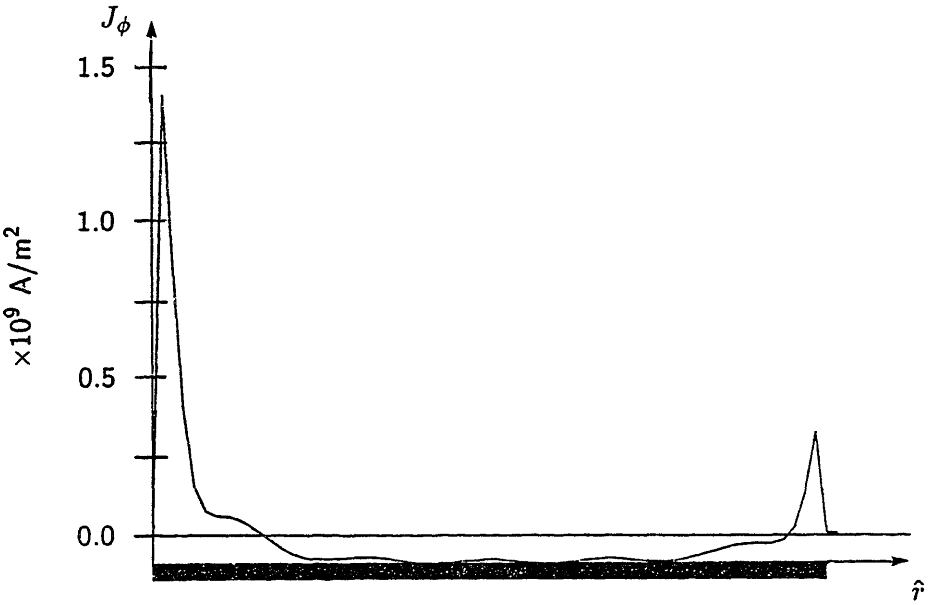

Fig. 4.10b Current density induced in the secondary winding of sandwich transformer by a magnetizing current in the primary. Since the secondary is open-circuited, the total area under the curve (the net current) sums to zero.

$3\epsilon_o$ for the polyimide insulator in a flexible printed circuit.[5] The high firing temperatures of ferrites precludes the use of copper, which would oxidize. A metal of lower conductivity, such as silver, must be used instead, increasing the ohmic loss. Although cofiring offers substantial reduction of ohmic loss due to the reduction of the proximity effects, such high leakage inductances and interwinding capacitances may rule out this approach for many applications.

4.4 Slotted Gapped Transformer

Another strategy for reducing the magnetizing loss is to recess the windings into a slot, as shown in Fig. 4.4. Although the load current distribution is not affected, the magnetizing current distribution is substantially altered and the circulating currents are greatly reduced. As before, this section will first develop a qualitative understanding of the influence of the slot on the magnetizing current's distribution and then present numerical results. The section begins by considering just the primary winding and then shows the

---

[5] Siemens AG, *Ferrites Data Book 1986/87*, Munich, Federal Republic of Germany (1986), p. 31.

effect of adding the secondary.

Figure 4.11 shows the primary winding recessed into a slot of width w to form a slotted inductor. The figure shows the H field lines associated with the magnetizing current. Since the gap presents a large reluctance to the flux in the upper half of the core, there is a substantial fringing field present in the slot between the windings and the gap. In comparison, the low reluctance of the magnetic path on the lower half of the core gives very little fringing field in the lower half of the slot.

If the slot is deep enough so that the winding is far away from the gap, the fringing field will be mostly tangential to the upper surface of the winding. The boundary condition imposed by this field results in a magnetizing current that is uniform across the winding surface and exponentially decaying with depth into the winding. Since the winding is only a skin depth thick, the effective resistance to the magnetizing current will be close to the winding's dc resistance. An analysis in Appendix A shows that the actual value will be about 9% higher. For the dimensions of Tables 4.1 and 4.6 this calculation gives an effective primary resistance of 0.29 Ω. A finite element analysis confirmed this number. In that analysis the slot depth (3.38 mm) was 1.5 times the slot width and the windings were placed 74 μm, the thickness of the flexible printed circuit, above the bottom of the slot.

Table 4.6: Dimensions of Slot

Dimension	Symbol	Value
Slot inner radius	r_{si}	2.29 mm
Slot outer radius	r_{so}	4.54 mm
Width of slot	w	2.25 mm

Figure 4.12 shows the deep slotted transformer formed when the secondary winding is added above the primary. Since the H field is already tangential to the surface of the conductors, the field distribution is relatively unchanged by the addition of the open circuited secondary. If the secondary is placed above the primary, in the fringing field generated by the magnetizing current, there will be induced eddy currents and copper loss in the secondary. If the secondary is placed below the primary, the induced current and loss will be smaller. But this low loss case only applies if the entire magnetizing current flows only in the primary winding. In reality, as mentioned in the introduction to this chapter, the amount of magnetizing current flowing in the secondary is determined in part by the external circuit. The external circuit must therefore be carefully analysed in order to determine whether placing the secondary above or below the primary gives a lower copper loss. Placing the secondary in the fringing field therefore gives a more realistic estimate of the induced losses, and is the case that will be considered here. This configuration is also the

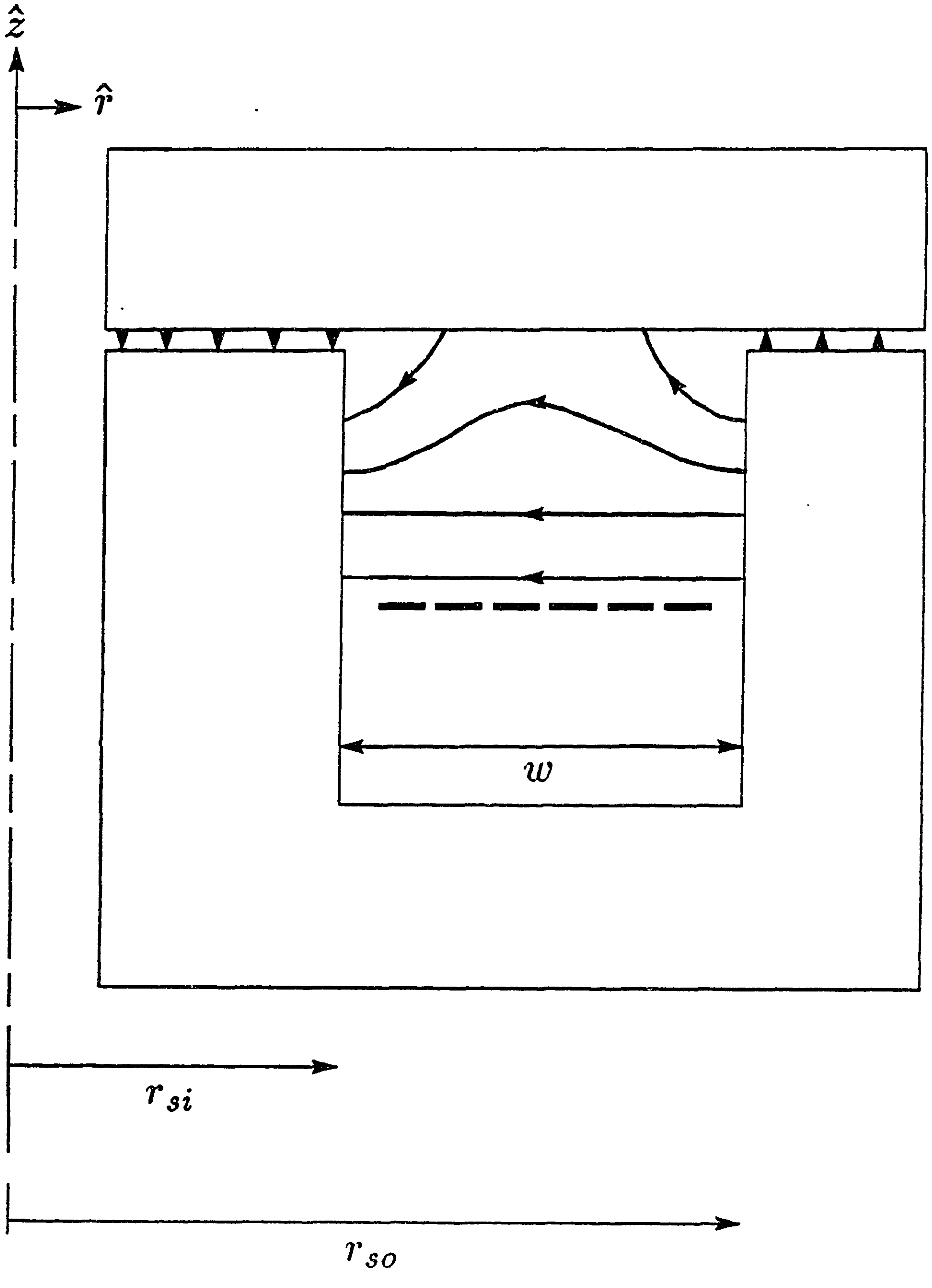

Fig. 4.11 Slotted inductor and its H field distribution.

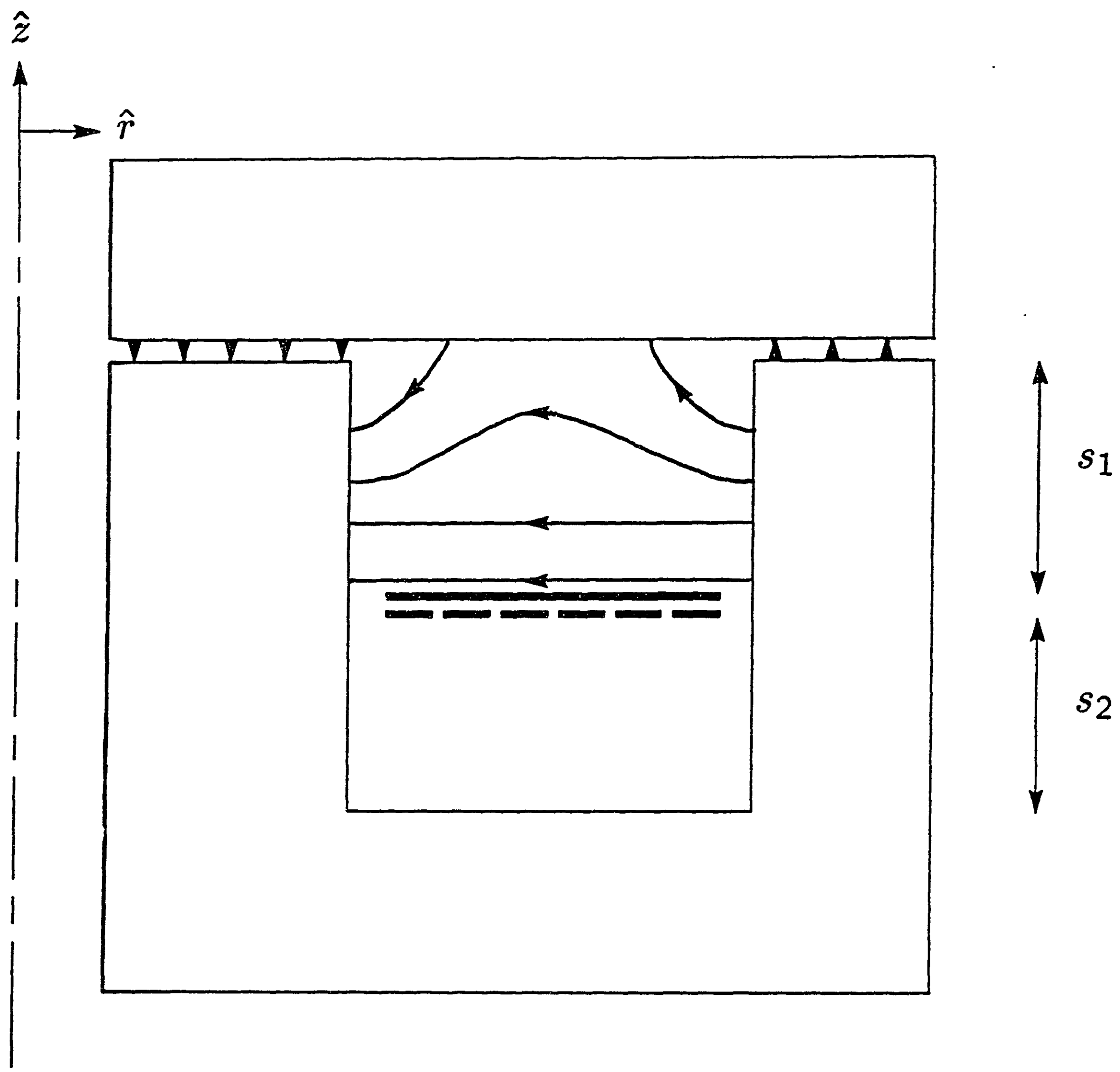

Fig. 4.12 Slotted gapped transformer and its H field distribution.

one that will be used for the design studies in Chapter 7.

If the secondary is much thicker than a skin depth, there will be currents induced on both the top and bottom surfaces of the secondary that decay exponentially with depth into the conductor. These circulating currents flow in opposite directions, which is consistent with the need to have a net induced current of zero in the secondary. If the secondary is this thick, the magnetizing current will cause about twice as much dissipation in the secondary as it will in the primary. Since the secondary's load current only flows on its lower surface, however, there is no need to make the winding thicker than a skin depth or two. A thinner secondary permits the induced circulating currents to overlap and cancel, which greatly reduces the dissipation. But if there is a dc component to the load current, the dissipation of that component is reduced by making the secondary thicker. A tradeoff between the dissipation due to the load current and the magnetizing current is therefore required to determine the thickness of the secondary that gives the lowest total loss. This tradeoff depends on the particular magnitudes of load and magnetizing currents that are considered. For the purposes of this general study, the thickness of the secondary will be taken to be one skin depth.

The dissipation caused by the currents induced in the secondary by the magnetizing current in the primary adds an additional resistance to the effective primary resistance. Appendix A shows that if the magnetic field were purely tangential to the secondary winding, this additional resistance is approximately

$$R_s = \frac{0.64\pi}{\sigma\delta}\left[\frac{N^2}{\ln\left(r_{wo}/r_{wi}\right)}\right] \tag{4.5}$$

In a transformer with the dimensions of Table 4.1, (4.5) predicts that the secondary adds 0.068 Ω to the effective primary resistance. A finite element analysis determined that the secondary adds 0.070 Ω to the effective primary resistance, showing excellent agreement with the prediction of (4.5).

The total effective primary resistance when the windings are recessed in a slot is therefore 0.36 Ω. This is only 33% more than the dc winding resistance, an improvement over the cofired transformer, whose effective resistance was 60% more than the dc resistance. In addition, the slotted transformer has the same leakage inductance as the sandwich transformer, while the cofired transformer had a much higher leakage inductance.

These improvements are achieved at the cost of a taller transformer. The question is, therefore, how deep does the slot need to be to gain most of the loss reduction? In order to gain most of the reduction, the fields must be essentially tangential to the windings. Clearly, the windings cannot be in the fringing field of the gap, so that the slot must be at least several gap lengths deep. Typical designs satisfy this constraint, because the windings must be far enough from the top plate of ferrite that the proximity of the top plate does not add a $\hat{z}$ directed component to the field near the windings. In order for this to be true, the reluctance from the top of the windings to the top plate must be substantially greater than the reluctance across the slot. The distance between the windings and the top plate required to avoid a substantial $\hat{z}$ component in the field near the windings is therefore dependent on the ratio of the slot depth to the slot width. Therefore, finite element analyses were performed in order to study the dependence of loss on the ratio of slot depth to slot width.

As indicated in Fig. 4.12, the two free parameters are s_1, the distance between the

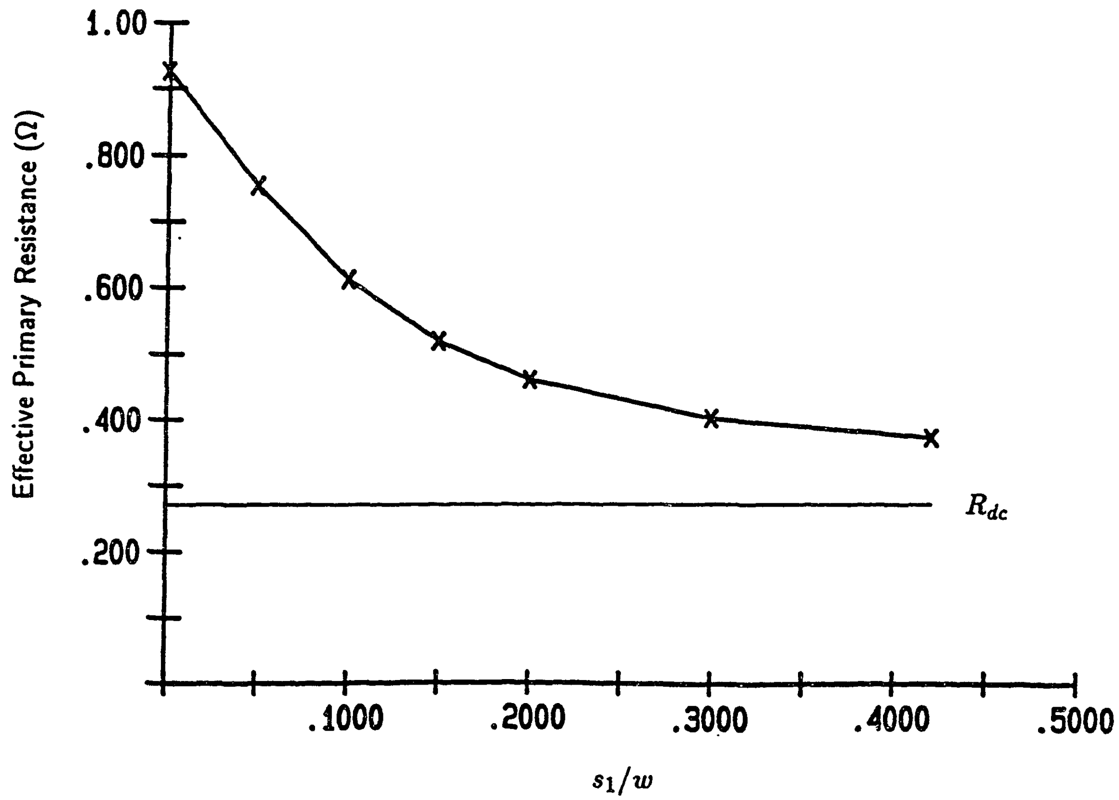

Fig. 4.13 Variation with s_1/w of the effective ac primary resistance to magnetizing current in a slotted gapped transformer. The horizontal line shows the dc resistance.

top of the winding and the bottom of the gap, and s_2, the distance between the bottom of the winding and the bottom of the slot. In these studies the permeability of the magnetic material was set at $150\mu_o$. This permeability is typical of the nickel-zinc ferrites used at these frequencies, as will be shown in Chapter 6. In addition, as the parameters s_1 and s_2 were varied, the gap thickness was varied slightly to hold the magnetizing inductance constant at 3.68 μH, as for the cofired transformer.

The results of the first parametric study are shown in Fig. 4.13, which shows the variation of effective primary resistance with s_1/w. In this study, s_2/w was fixed at 0.5, since increasing s_2/w above 0.5 did not appreciably alter the current distribution in the windings. Note that the ac resistance curve flattens out and approaches the 0.35 Ω calculated above when s_1/w is about 0.3.

A second study was then performed to study the variation of effective primary resistance with s_2/w, shown in Fig. 4.14. In this study, s_1/w was fixed at 0.3. The ac resistance curve flattens out and approaches 0.35 Ω when s_2/w is about 0.1.

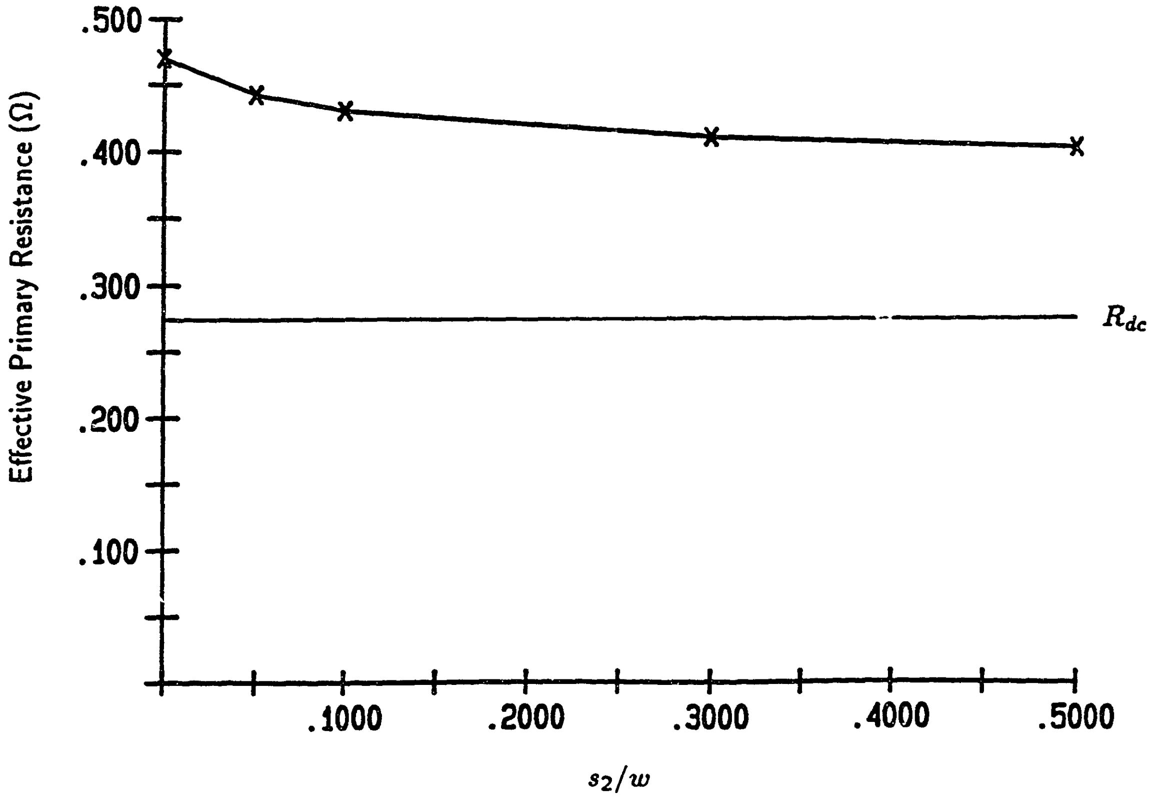

Fig. 4.14 Variation with s_2/w of the effective ac primary resistance to magnetizing current in a slotted gapped transformer. The horizontal line shows the dc resistance.

From these results it appears reasonable that an appropriate transformer design would have a slot whose depth is 40% of its width and that the winding would be placed one quarter of the way up from the bottom of the slot. A transformer reflecting this reasonable design would have an $s_1/w = 0.3$ and a $s_2/w = 0.1$. A finite element analysis determined that in this design, the primary would contribute an effective resistance of 0.30 Ω. This value is within 2% of the 0.29 Ω that was calculated above to be the lowest primary resistance that could be achieved with a slotted design. The loss induced in the secondary adds 0.13 Ω, which is twice the resistance that would be added if the windings were very far from the air gap. The additional loss that is added by having an s_1/w of only 0.3 appears almost entirely in the secondary. The total effective primary resistance to the magnetizing current, therefore, is 0.43 Ω, 60% higher than the dc resistance. This structure therefore achieves the same loss reduction as the cofired structure but without the added leakage inductance. This structure, however, is taller than the unslotted structures because of the slot height, which is 40% of the winding width.

It should be noted that with the addition of a slot there is an alternative to the planar windings of Fig. 4.4, which is essentially equivalent in terms of the magnetic circuit. Instead of planar windings, "barrel" windings can be formed by printing straight primary and secondary traces on either side of a flexible substrate. The substrate is then wrapped around the center post of the core, as shown in Fig. 4.15. The N turns of the primary must be connected in series with vias or tabs where the two ends of the substrate meet, complicating the fabrication. Planar spirals, on the other hand, do not have to be wrapped and joined. One via is required at the center of the planar spiral in order to connect to a trace that leads to the outer edge. This trace is not shown in Fig. 4.4. When layers of primary and secondary are interleaved, as discussed in the next section, barrel winding fabrication becomes even more difficult and consequently will not be considered.

4.5 Slotted Ungapped Transformer

Instead of cofiring the windings with the magnetic material, or keeping the windings far from an air gap, the windings could be put in a slotted structure without a gap. In such a structure, the permeability of the magnetic material is reduced in order to achieve the desired magnetizing inductance without an actual air gap. Figure 4.16 shows a cross-sectional view of this type of transformer, along with the H field lines created by the magnetizing current. The winding is centered in the window. As was the case for the gapped transformer, the deeper the slot, the more tangential the magnetic field is to the surface of the winding, and the lower the effective magnetizing resistance will be.

A parametric study was performed to determine the variation of the copper loss with s_3/w, the ratio of the slot height above and below the winding to the slot width. In this study the magnetizing inductance was again held constant at 3.68 μH, this time by varying the permeability of the core. The results, shown in Fig. 4.17, show that a reasonable compromise between transformer height and dissipation can be achieved with an s_3/w of 0.2. For that value of s_3, the core permeability that gave the required inductance was $34\mu_o$. The resistance and size for a given energy storage are very similar to the gapped transformer; the total effective resistance in this case is 0.42 Ω, and the slot again has a depth that is 40% of its width.

4.6 Selection of Transformer Geometry

The studies that have been presented in this chapter compared a slotted gapped transformer with a slotted ungapped transformer whose core permeability had been chosen

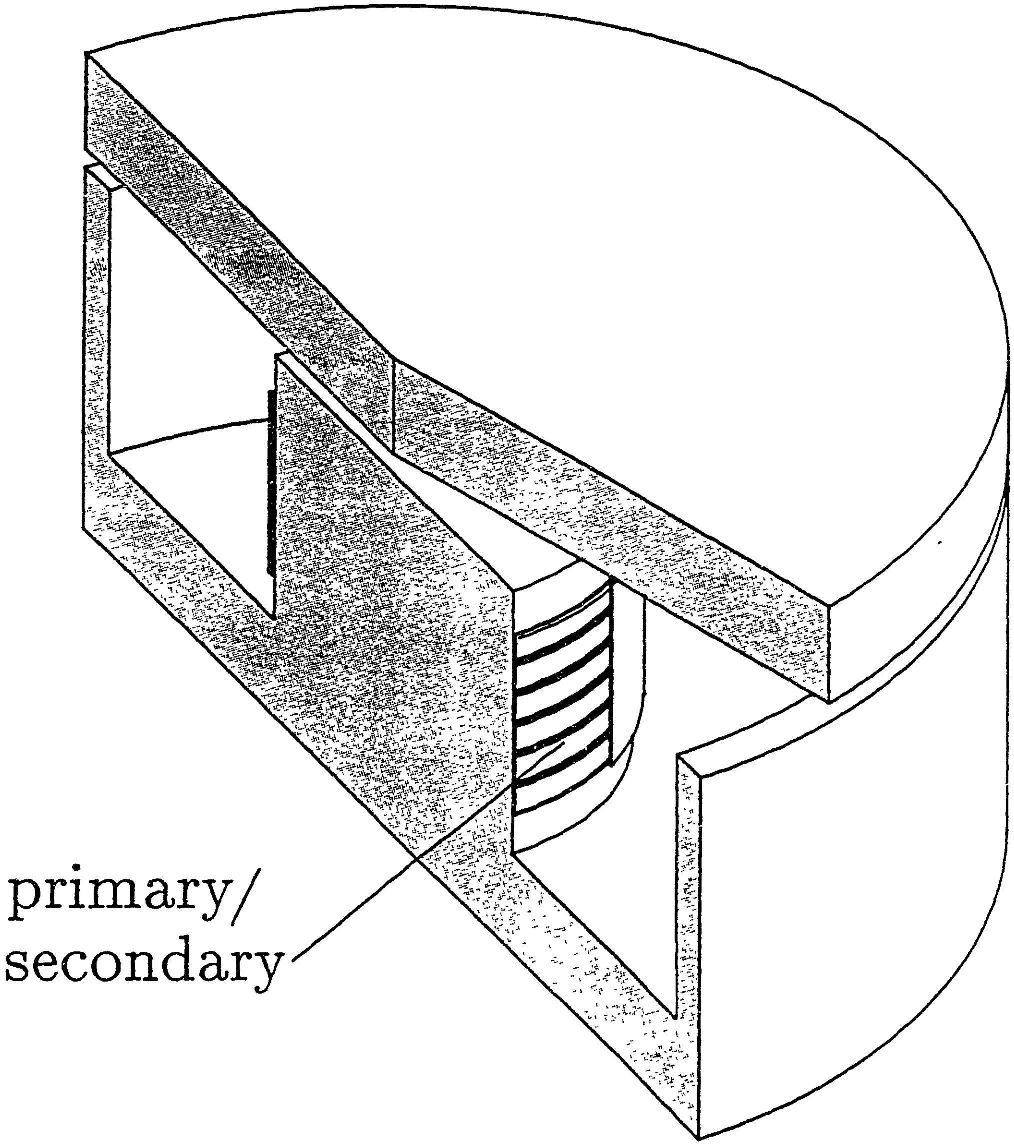

Fig. 4.15 Cutaway view of slotted gapped transformer with barrel winding.

to give the same reluctance as the gapped transformer. The transformers were found to occupy about the same total volume with about the same copper loss.

This section further shows that the core loss is about the same for the two transformers, and that for the dc/dc converter application, the typical process variation in magnetic material permeability does not affect the choice of geometry. The gapped transformer is chosen over the ungapped transformer for the dc/dc converter because its higher permeability core better contains the magnetic fields, and because the value of its magnetizing

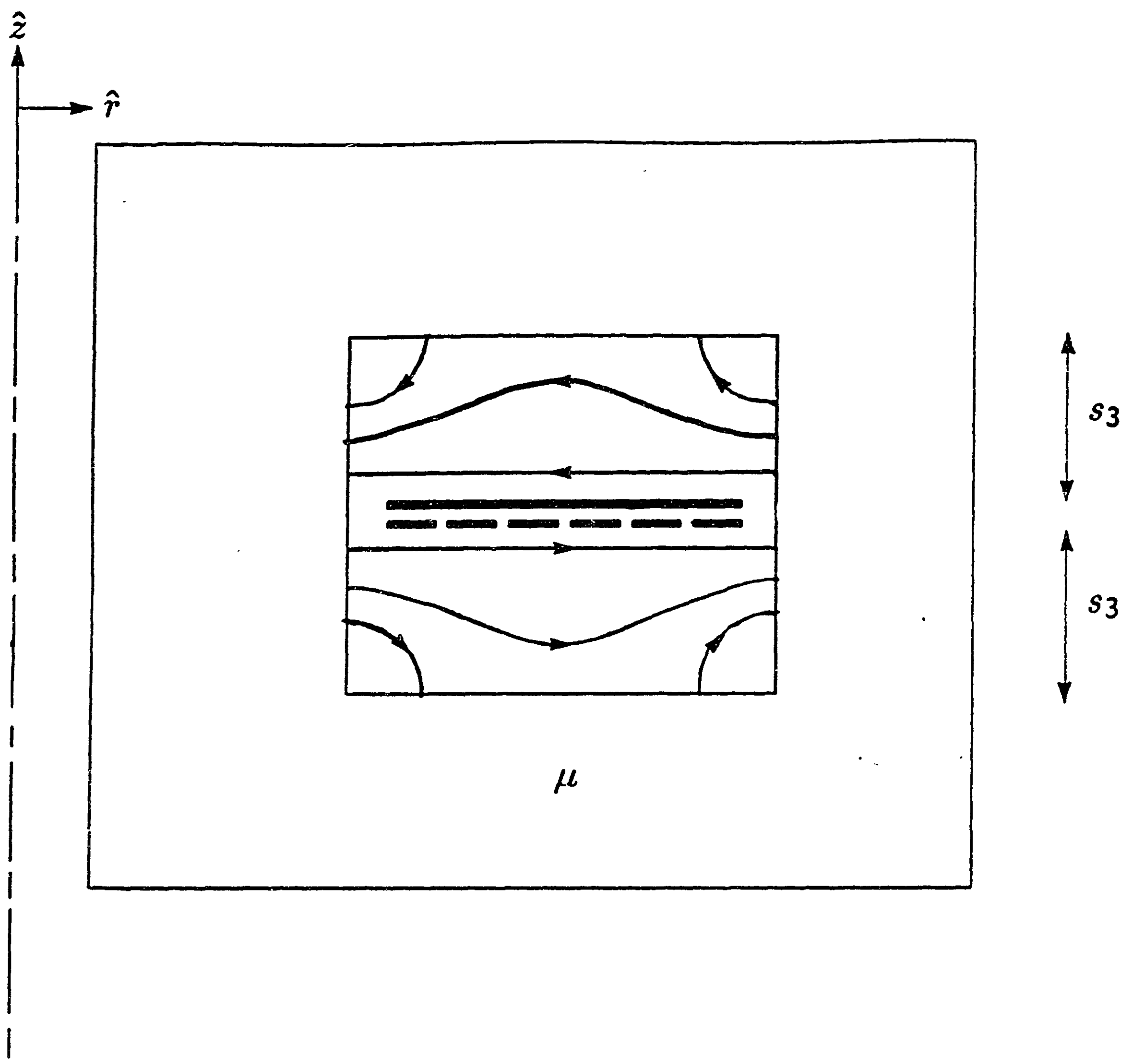

Fig. 4.16 Dimensioned cross-sectional view of a slotted ungapped transformer. The permeability has been reduced so that the reluctance is the same as the slotted gapped transformer discussed in the previous section.

inductance is more easily adjusted.

In the ungapped transformer all the magnetic energy is stored in the bulk of the magnetic material, so that in order for the two geometries to have the same core loss, the loss density of the ungapped core material must be less than that of the gapped transformer core material. Exactly how much less is estimated by the following analysis.

In order to compare the gapped and ungapped structures, the total energy stored should be the same. The total energy stored in a gapped transformer is approximately

$$W_{t,g} = \frac{1}{2}\,(Ni_m)^2 \left[1 + \frac{\Re_c}{\Re_g}\right] \frac{1}{\Re_g} \tag{4.6}$$

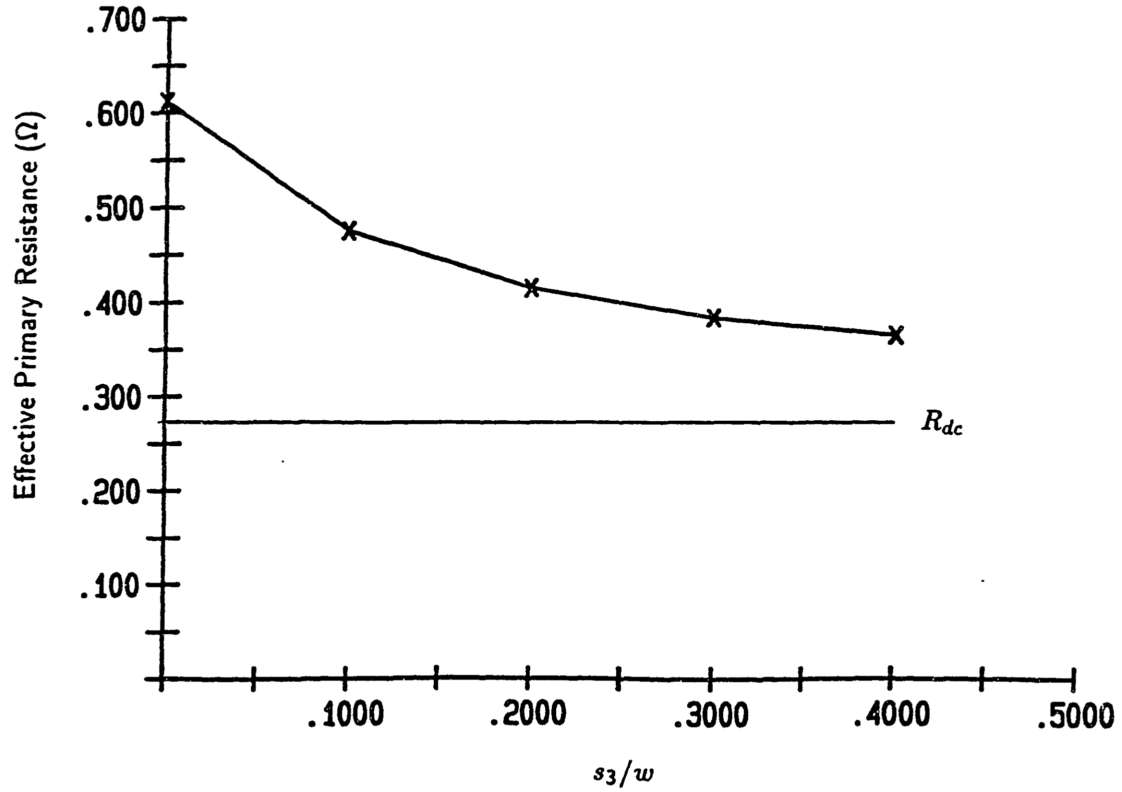

Fig. 4.17 Variation with s_3 of the effective ac primary resistance to the magnetizing current in a slotted ungapped transformer. The horizontal line shows the dc resistance.

where N is the number of turns, i_m is the magnetizing current, A is the cross sectional area of the core, and g is the length of the gap. $\Re_c$ and $\Re_g$ are the reluctances of the core and the gap, respectively, and are given by

$$\Re_c = \frac{l}{\mu_c A}, \quad \Re_g = \frac{g}{\mu_o A} \tag{4.7}$$

where μ_c is the permeability of the core and l is the magnetic path length around the core. The total energy stored in a ungapped transformer of the same dimensions is approximately

$$W_{t,d} = \frac{1}{2}\, \mu_d (N i_m)^2\, \frac{A}{l} \tag{4.8}$$

where μ_d is the permeability of the ungapped core material. As explained in Chapter 2, in a properly designed gapped transformer $\Re_c \gg \Re_g$, so that setting (4.7) equal to (4.8) gives the value for μ_d that is required in order for the gapped and the ungapped transformers to store the same energy,

$$\mu_d = \frac{\mu_o l}{g} \tag{4.9}$$

In this analysis it is assumed that the core loss in the gapped transformer is proportional to the portion of the total energy that is stored in the core. From (4.6), this core loss is given by

$$P_c \propto \frac{\alpha}{2}(Ni_m)^2 \frac{\Re_c}{\Re_g^2} \tag{4.10}$$

where α is a constant of proportionality whose value is dependent on the material. Similarly, the core loss in the ungapped transformer can be written, using (4.8) and (4.9), as

$$P_d \propto \frac{\beta}{2}(Ni_m)^2 \frac{1}{\Re_g} \tag{4.11}$$

where β is a material dependent constant. Since the permeability of the gapped core must be higher than the permeability of the ungapped core for a given inductance, α is presumably greater than β. Combining (4.10) and (4.11) gives the ratio of the core loss in the gapped transformer to the core loss in the ungapped transformer,

$$\frac{P_c}{P_d} = \frac{\alpha \Re_c}{\beta \Re_g} = \frac{\alpha}{\beta} \frac{l}{g} \frac{\mu_o}{\mu_c} \tag{4.12}$$

In a typical gapped transformer, $\Re_c/\Re_g \approx 0.1$, and the typical μ_c for a nickel-zinc ferrite would be about $150\mu_o$. From (4.7) it follows that $l/g \approx 15$, and, from (4.9), that $\mu_d \approx 15\mu_o$. With these numbers (4.12) says that in order for the core losses in the two transformers to be equal, $\alpha/\beta \approx 10$. In other words, the ungapped core material should have both an order of magnitude less permeability and an order of magnitude less core loss at a given B field.

The available data suggests that ferrite magnetic materials exist that can satisfy these requirements, so that each transformer geometry would give the same core loss. For example, Ferroxcube IV nickel-zinc ferrite was originally produced in five different grades, A–E, which represented different proportions of nickel and zinc. Grade A had the least nickel, the most zinc, the highest permeability, and the highest loss, while grade E had the most nickel, the least zinc, the lowest permeability, and the lowest loss. Table 4.7 compares the real and imaginary components of the relative permeability of grades C and E.[6,7] The imaginary component corresponds to core loss. While these numbers were measured at extremely low flux levels, they suggest that the order of magnitude differences in permeability and loss are possible to achieve.

---

[6] J. Smit and H. Wijn, "Physical Properties of Ferrites," in *Advances in Electronics and Electron Physics*, vol. vi, ed. L. Marton, Academic Press, Inc., New York (1954), p. 105.

[7] D. J. Craik, *Structure and Properties of Magnetic Materials*, Pion Limited, London (1971), p. 183.

Table 4.7: Ferroxcube 4C Ferrite

Grade	μ_r'	μ_r''
C	90	4
E	12	0.07

A usual concern with ungapped cores is the lack of precise control over the exact value of material permeability. Typical ferrite permeabilities are specified only to within ±20%, so that the magnetizing inductance would vary by the same amount. In this application, however, the importance of the value of the magnetizing inductance is that it sets the resonant frequency of a tank. Since the resonant frequency is inversely related to the square root of the inductance, the ±20% variation in inductance causes less than a ∓10% variation in resonant frequency, which would be acceptable.

One major drawback to the ungapped transformer is its poorly contained field. Since both structures must provide the same magnetizing inductance, the fringing field around a ungapped transformer is much larger than that of a gapped transformer, especially one in which the gap is confined to the center leg. This fringing field can induce eddy currents in surrounding conductors, causing additional loss, and can couple into other circuit elements, disrupting circuit operation.

4.7 Conclusions

In conclusion, this chapter has shown that a slotted gapped transformer should be used for this application. This structure has a reasonably low copper loss and is relatively easy to fabricate. In order to avoid magnetizing current proximity effects and the resulting high copper losses, the depth of the slot should be about 40% of its width, with the planar spiral windings placed about one quarter of the way up from the bottom of the slot.

Chapter 5

A LUMPED PARAMETER MODEL OF THE SLOTTED GAPPED TRANSFORMER

Basic magnetic circuit analysis can be used to find the lumped parameter model for the slotted gapped transformer of Fig. 4.4. This chapter presents the basic elements of the model, namely the magnetizing inductance, L_m, the leakage inductance, L_l, the magnetizing current resistance, R_m, and the load current resistance, R_l. Finite element analyses are used to validate the analytic model. In addition, capacitive effects are considered.

5.1 Magnetizing Inductance

The magnetizing inductance can be approximated in terms of the effective lumped reluctances of the air gap, $\Re_{gap}$, and the core, $\Re_{core}$, as

$$L_m = \frac{N^2}{\Re_{gap} + \Re_{core}} \tag{5.1}$$

In order to avoid storing energy in the lossy magnetic material and to reduce the dependence on the value of μ, the reluctances are chosen such that

$$\Re_{gap} \gg \Re_{core} \tag{5.2}$$

The magnetizing inductance is therefore approximately

$$L_m \approx \frac{\mu_o N^2 A_i}{g(1 + A_i/A_o)} \tag{5.3}$$

where g is the gap length and A_i/A_o is the ratio of the magnetic material's cross-sectional area at the center of the winding to its area outside the outer edge of the winding where the flux returns. The ratio A_i/A_o is given by (4.2). In order to improve the approximation, a correction term is added that reflects the energy stored in the fringing field above the windings and below the gap. The fringing field is shown in Fig. 4.12 and is given by (A14). The total magnetizing inductance is therefore approximately

$$L_m \approx \frac{\mu_o N^2 A_i}{g(1 + A_i/A_o)} + \frac{2\pi\mu_o N^2 s_1}{\ln(r_{so}/r_{si})} \tag{5.4}$$

where s_1 is the distance between the windings and the gap.

5.2 Leakage Inductance

The leakage inductance can also be estimated by a simple analysis. The leakage inductance is due to the flux that links one winding but not the other, as shown in Fig. 4.6.

Since the leakage field penetrates the conductors, the leakage inductance is due not only to the energy stored between the primary and secondary windings, but also to the energy stored within the conductors. For this reason, the effective cross sectional area A in the expression

$$L_l = \frac{\mu_o N^2 A}{w_e} \tag{5.5}$$

is not $2\pi r_{si} m$, where m is the distance separating the primary and secondary windings, but rather $2\pi r_{si}(m + \gamma\delta)$. For windings much thicker than a skin depth, $\gamma = 1$. In this transformer the windings are one skin depth thick, and it is shown in Appendix B that for these windings $\gamma = 0.65$. The total leakage referred to the primary is shown in Appendix B to be

$$L_l = \frac{2\mu_o \pi N^2}{\ln\left(r_{so}/r_{si}\right)}\left(m + 0.65\delta\right) \tag{5.6}$$

It is important to note that there is a minimum leakage inductance, no matter how closely the primary and secondary are spaced ($m \rightarrow 0$), due to the energy stored in the conductors. Reducing the conductor separation increases the interwinding capacitance, however, since the primary and secondary form a parallel plate capacitor. This tradeoff will be explored in Chapter 7.

5.3 Computing Copper Loss

Finding simple expressions for the copper loss in a transformer is in general extremely complicated, since the copper loss must be computed from the the sum of the load and magnetizing currents, and magnetic diffusion adds a different spatially varying phase shift to each of these two currents. In the gapped slotted transformer, however, the loss computation is greatly simplified, as explained by the following discussion.

Note that the currents in the bottom winding have approximately the same spatial distribution. The load current distribution, shown in Fig. 4.6, flows on the upper surface of the bottom winding and decays exponentially away from the surface. As for the magnetizing current distribution, it was explained in Section 4.4 that since the windings are far from the gap, the fringing field generated by the magnetizing current flowing in the primary is mostly tangential to the upper surface of the bottom winding, giving the magnetizing current approximately the same spatial distribution as the load current. If the currents associated with interwinding capacitances and the phase shifts introduced by core loss are both negligible, then the phase difference between the load current and the magnetizing current in any incremental volume of the bottom winding is the same as the phase difference at the terminals. It is shown at the end of this chapter that interwinding capacitances are typically negligible. The core loss is shown in Chapter 7 to be typically small compared to the copper loss.

If both the load and magnetizing currents are approximated to have the same spatial distribution in the bottom winding, then a single expression can be derived for the effective resistance of the bottom winding. If there are no harmonics present in the current waveforms, then the copper loss in the bottom winding can be computed directly from this effective resistance and the rms value of the current at the bottom winding's terminals. If there are harmonics present in the current, then the effective resistance can be computed at each harmonic frequency and, since in this approximation the load and magnetizing current have the same spatial distribution, the average power in each harmonic can be computed separately. An example of this procedure is given in the design studies of Chapter 7.

Unfortunately, in the top winding the distributions of the load and magnetizing currents differ. While the load current distribution in the top winding decays away from the bottom surface, as in Fig. 4.6, the magnetizing current distribution depends on the amount of magnetizing current in the bottom winding. This chapter will therefore follow the approach of the previous chapter, and the effective resistances associated with the load and magnetizing currents will be computed separately. The design studies in Chapter 7 present an example of extending the analysis to correctly compute the copper loss for a particular distribution of magnetizing current.

5.4 Magnetizing Current Resistance

The effective resistance of the primary winding to the magnetizing current is computed here for the case where the primary is the bottom winding. It was shown in Appendix A that since the primary is one skin depth thick, the ac resistance it presents to the magnetizing current is 9% higher than its dc resistance. In order to compute the dc resistance of the primary winding, the flat N turn spiral can be approximated as N concentric annuli. The windings that were actually fabricated were in fact concentric annuli connected by radial segments, and they will be described in detail in Chapter 8. The dc resistance of a flat annulus is

$$R_{a,dc} = \frac{2\pi}{\sigma t} \frac{1}{\ln(r_o/r_i)} \tag{5.7}$$

where t is the thickness of the winding, and r_i and r_o are the inner and outer radii of the annulus. The dc resistance for the planar spiral primary can therefore be approximated as

$$R_{p,dc} = \frac{2\pi}{\sigma t} \sum_{n=1}^{N} \frac{1}{\ln(r_{on}/r_{in})} \tag{5.8}$$

where r_{in} and r_{on} are the inner and outer radii of the n^{th} annulus.

The ac resistance of the primary is therefore given by multiplying (5.8) by 1.09, and adding the resistance associated with the eddy currents induced in the secondary. This secondary resistance was shown in Appendix A to be 32% of the dc secondary resistance, given by (4.5). Combining (5.8) and (4.5) gives the total ac resistance to the magnetizing current,

$$R_m = 1.09\ R_{p,dc} + 0.32\ N^2 R_{s,dc} = \frac{2\pi}{\sigma\delta}\left[\frac{0.32N^2}{\ln(r_{wo}/r_{wi})} + \sum_{n=1}^{N} \frac{1.09}{\ln(r_{on}/r_{in})}\right] \tag{5.9}$$

where the winding thickness, t, is assumed to be the skin depth, δ.

In order to evaluate (5.9), the radii r_n must be specified. This problem is equivalent to specifying the widths of each primary turn. For simplicity, the studies of this and the last chapter assume that each concentric ring had the same width. The value of the resulting $R_{p,dc}$ is evaluated in Appendix B. But because of the cylindrical geometry, this assumption does not give the minimum copper loss. The minimum copper loss is achieved by choosing the width of each ring so that each ring has the same resistance. If the spacing between primary turns is negligible, the minimum primary resistance is equal to the reflected resistance of a one turn secondary with the same total width. These assertions are also proved in Appendix B and result in the criterion for minimum copper loss,

$$r_{n+1} = r_n \left(\frac{r_{wo}}{r_{wi}}\right) \tag{5.10}$$

Using (5.10) to determine the width of each primary turn, instead of simply making all the primary turns of equal width, typically reduces the copper loss by over 20%. Equation (5.10) is therefore used to choose the winding widths in the design studies of Chapter 7.

At this point it should be reiterated that (5.9) approximates the N turn planar spiral primary winding as N concentric rings. For the windings that were actually fabricated for the experimental work described in Chapter 9, this approximation is a very good one, since the fabricated primary approximated the spiral with concentric rings connected in series. These fabricated windings will be discussed in more detail in Chapter 8.

5.5 Load Current Resistance

As with the magnetizing current resistance, the load current ac resistance can be easily computed using the results of Appendix A. As shown in Fig. 4.6, the field due to the load current is uniform between the skin depth thick conductors and zero outside them, so that the load current resistance is simply the dc resistance of the windings times 1.09, giving

$$R_l = 1.09\left(R_{p,dc} + N^2 R_{s,dc}\right) = \frac{2.18\pi}{\sigma\delta}\left[\frac{N^2}{\ln(r_{wo}/r_{wi})} + \sum_{n=1}^{N}\frac{1}{\ln(r_{on}/r_{in})}\right] \qquad (5.11)$$

5.6 Comparison of Analytic Model with Finite Element Analysis

The section compares the values of the inductances and resistances that are predicted by the analytic models presented above with the values that were generated by finite element analyses. In this study, as well as in the experimental transformer described in Chapter 8, the primary turns were assumed to be all the same width. The resulting primary resistance is derived in Appendix B. Table 5.2 summarizes the results of the comparison and show very good agreement between the model and the numerical solutions. These calculations were made for a gapped slotted transformer with the parameters of Table 5.1 and a lossless material with a permeability of $10^4\mu_o$.

5.7 Capacitive Effects

While the 1–10 MHz transformer is a magnetoquasistatic (MQS) system, it still possesses parasitic capacitances that can significantly affect circuit operation. This section models this capacitance as common and differential mode capacitances, and computes these capacitances from the electric fields that follow from the MQS magnetic field distribution.[1]

5.7.1 Voltage Distribution

The voltage distribution in the windings will be assumed to be that of an ideal transformer, so that the voltage per turn is equal for all turns, and the build up of this voltage is uniform around every turn. The effects of the winding resistance and leakage inductance can be neglected not only because their impedances are small, but also because their distributed nature does not disturb the uniformity of the voltage distribution. Each turn has approximately the same resistance and links approximately the same leakage flux as the other turns. The effect of the capacitance on the voltage distribution is neglected since the amount of electric energy storage is very small compared to magnetic energy storage. This can be demonstrated by computing, for example, the resonant frequency of the leakage

---

[1] L. F. Casey, A. F. Goldberg, M. F. Schlecht, "Issues Regarding the Capacitance of 1–10 MHz Transformers," *IEEE Applied Power Electronics Conference*,

Table 5.1: Test Transformer Parameters

Dimension	Symbol	Value
Frequency	f	4 MHz
Core inner radius	r_i	955 μm
Core outer radius	r_o	5.55 mm
Gap length	g	128 μm
Core permeability	μ	$10^4\mu_o$
Slot inner radius	r_{si}	2.29 mm
Slot outer radius	r_{so}	4.54 mm
Width of slot	w	2.25 mm
Distance between windings and gap	s_1	3.38 mm
Distance between windings and bottom of slot	s_2	74 μm
Winding inner radius	r_{wi}	2.47 mm
Winding outer radius	r_{wo}	4.32 mm
Conductor thickness	t	33 μm
Width of conductor	w_t	250 μm
Distance between primary and secondary	m	74 μm
Permittivity of winding substrate	ϵ	$3.2\epsilon_o$
Number of turns	N	6
Turn spacing	ς	0.28

Table 5.2: Comparison of Calculated Parameters with Finite Element Results

Parameter	Symbol	Equation	Calculation	Finite Element
Magnetizing inductance	L_m	(5.4)	5.4 μH	5.6 μH
Leakage inductance	L_l	(5.6)	48.5 nH	48.2 nH
Dc primary resistance	$R_{p,dc}$	(5.7)	0.27 Ω	0.27 Ω
Dc secondary resistance	$R_{s,dc}$	(5.5)	0.21 Ω	0.22 Ω
Ac resistance to magnetizing current from primary alone	R_{mp}	(5.9)	0.29 Ω	0.29 Ω
Ac resistance to magnetizing current from secondary alone	R_{ms}	(4.5)	0.068 Ω	0.070 Ω
Total ac resistance to magnetizing current	R_m	(5.9)	0.36 Ω	0.36 Ω
Ac resistance to load current from primary alone	R_{lp}	(5.11)	0.29 Ω	0.29 Ω
Ac resistance to load current from secondary alone	R_{ls}	(5.11)	0.23 Ω	0.24 Ω
Total ac resistance to load current	R_l	(5.11)	0.52 Ω	0.53 Ω

inductance and the capacitance. A typical leakage inductance of 15 nH and capacitance of 20 pF (these values calculated in the design studies of Chapter 7) gives rise to a resonant frequency of about 300 MHz, much higher than the 1–10 MHz region of operation.

5.7.2 Stored Electric Energy

In order to determine the capacitance of the transformer, the stored electric energy must be computed. Consider the transformer connection of Fig. 5.1, in which the primary is excited by a sinusoidal voltage, the secondary is open circuited, and the primary and secondary share a common ground. Figure 5.2 shows the voltage at the high side of each turn. For clarity, in Fig. 5.2 the circular windings have been straightened. A voltage of V_t/N is induced around each turn, so that the voltage between primary and secondary builds up from zero around the first primary turn, to $(N-1)V_t/N$ around the N^{th} primary turn.

In computing the stored energy, the windings can be considered as a parallel plate capacitor. The capacitance is therefore of the form $C = \epsilon A/m$, where ϵ is the dielectric constant of the winding substrate, A is the effective winding area, and m is the separation between windings. Since each turn is much wider than the separation between windings, the effect of the fringing field can be ignored. The stored electric energy in the structure of

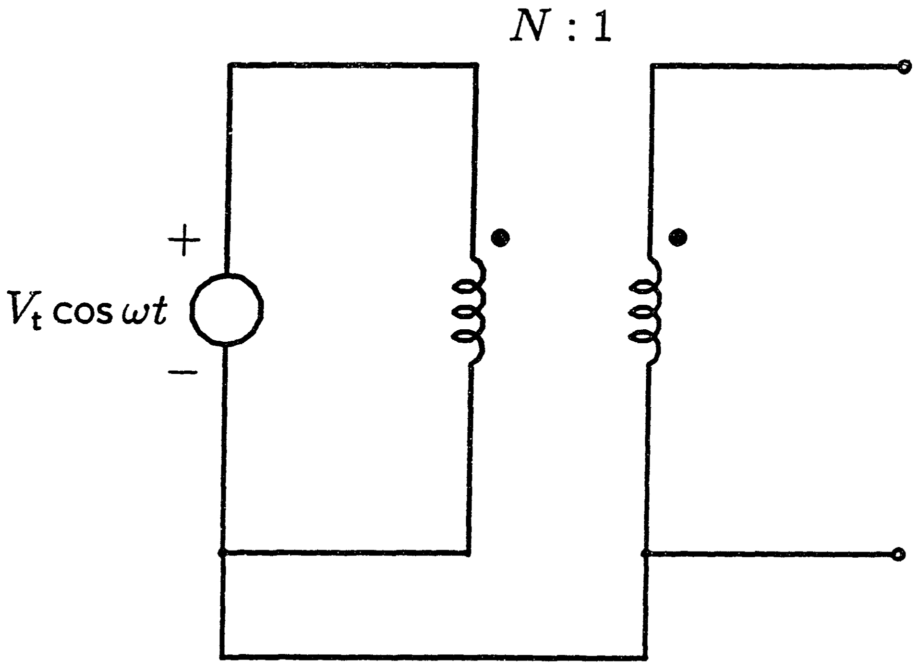

Fig. 5.1 Electrical connection of transformer for computation of stored electric energy.

Fig. 5.2 is of the form $W_{et} = \frac{1}{2} C_t V_t^2$ and is given by

$$W_{et} = \frac{1}{2}\left(\frac{\epsilon w_t}{m}\right) \sum_{n=1}^{N} 2\pi r_n \left(\frac{nV_t}{N} - \frac{V_t}{N}\right)^2 \tag{5.12}$$

where w_t is the width of each turn, derived in Appendix B as (B6); and r_n is the effective radius of the n^{th} turn, derived in Appendix B as (B21). The capacitance, C_t is consequently

$$C_t = \frac{2\pi \epsilon w_t}{N^2 m} \sum_{n=1}^{N} r_n (n-1)^2 \tag{5.13}$$

5.7.3 Differential and Common Mode Capacitance

Although the analysis of the last section derived an expression for the transformer capacitance, the exact placement of the capacitance in the lumped parameter model depends on where the capacitive charging current actually flows. Some of the charging current, known as the differential mode current, returns to the source from the primary winding, while the rest of the current, the common mode current, crosses to the secondary winding

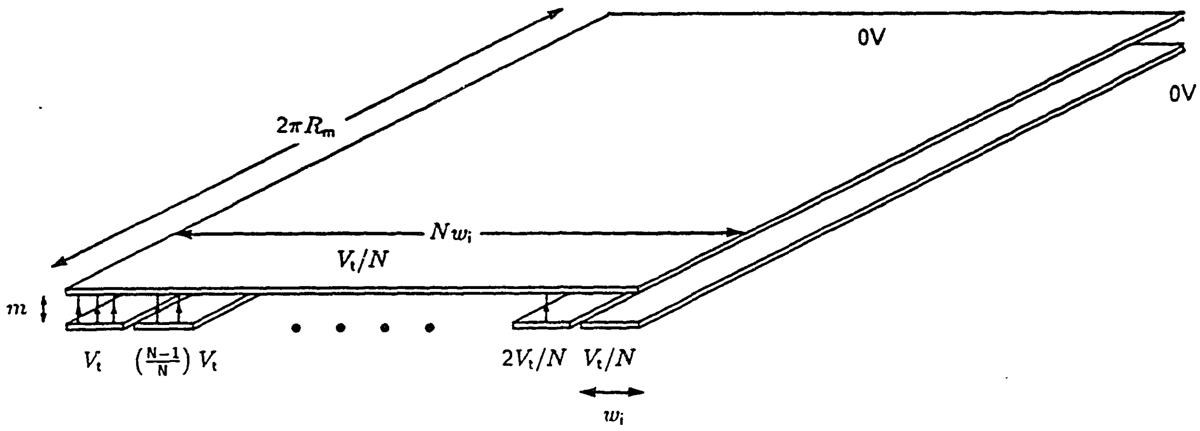

Fig. 5.2 Voltage and field distribution in transformer for computation of stored electric energy. For clarity, the circular windings have been straightened.

and returns through the ground connection. Since there are two distinct capacitive current paths, the capacitance must be modelled by two distinct capacitors, the differential mode and the common mode capacitors, as shown in Fig. 5.3. The differential mode capacitance appears in parallel with the magnetizing inductance, while the common mode capacitance is connected between the high side of the primary and the low side of the secondary.

The differential mode capacitance can be calculated by breaking the ground connection between primary and secondary, which prevents common mode current from flowing. Without a connection by which current can return from the secondary winding to the voltage source, the total net charge induced on the secondary must be zero. The charge Q_n induced on the secondary by the n^{th} primary turn is

$$Q_n = \frac{1}{2}(2\pi w_t r_n)\left(V_s - \frac{nV_t}{N}\right) \tag{5.14}$$

where V_s is the voltage that the high side of the secondary has floated to. The value of V_s can be calculated by using the fact that the sum of the Q_n must be zero,

$$\sum_{n=1}^{N} r_n \left(V_s - \frac{nV_t}{N}\right) = 0 \tag{5.15}$$

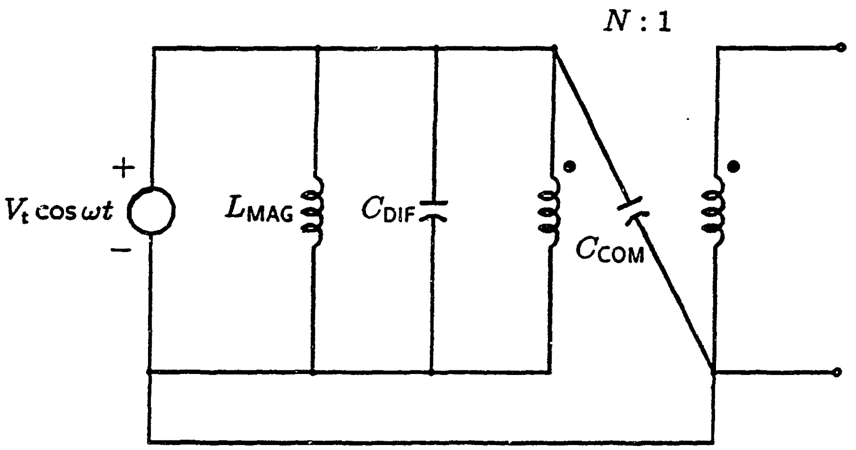

Fig. 5.3 Lumped element capacitor placement in transformer model.

Equation (5.15) can be solved to yield

$$V_s = \gamma \frac{V_t}{N} \tag{5.16}$$

where γ is derived in Appendix B as (B25). The low side of the secondary is therefore at a potential of $(\gamma - 1)V_t/N$.

Figure 5.4 shows the resulting differential mode voltage distribution. The stored differential mode energy, W_{ed}, can be computed in a similar fashion to (5.12), giving

$$W_{ed} = \frac{1}{2}\left(\frac{\epsilon w_t}{m}\right) \sum_{n=1}^{N} 2\pi r_n \left(\frac{\gamma V_t}{N} - \frac{nV_t}{N}\right)^2 \tag{5.17}$$

The differential mode capacitance, C_d, is therefore given by

$$C_d = \frac{2\pi\epsilon w_t}{N^2 m} \sum_{n=1}^{N} r_n(\gamma - n)^2 \tag{5.18}$$

If the ground is reconnected to the low side of the secondary, the potential on the secondary is reduced by $(\gamma-1)V_t/N$, causing an additional charge to appear on the windings. The resulting common mode voltage distribution is shown in Fig. 5.5. As before, the stored common mode energy, W_{ec}, is given by

$$W_{ec} = \frac{1}{2}\left(\frac{\epsilon w_t}{m}\right) \sum_{n=1}^{N} 2\pi r_n \left(\frac{\gamma V_t}{N} - \frac{V_t}{N}\right)^2 \tag{5.19}$$

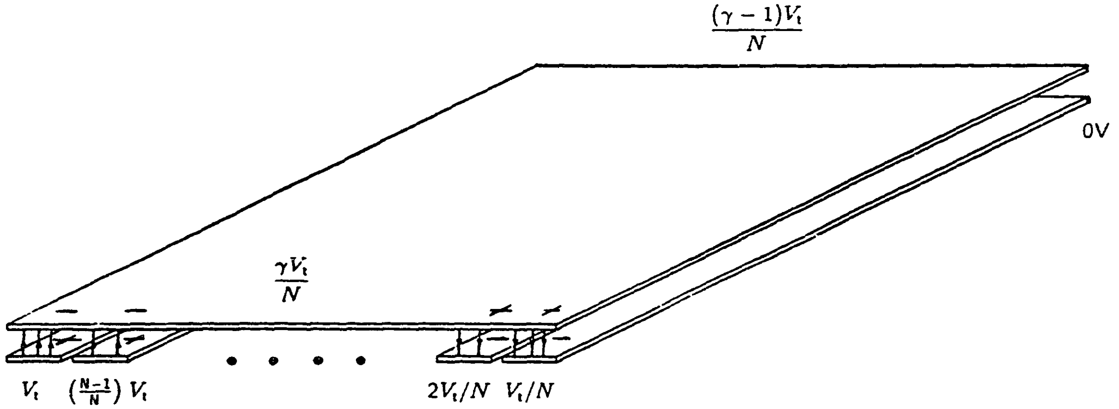

Fig. 5.4 Voltage and field distribution in transformer for computation of stored differential mode electric energy.

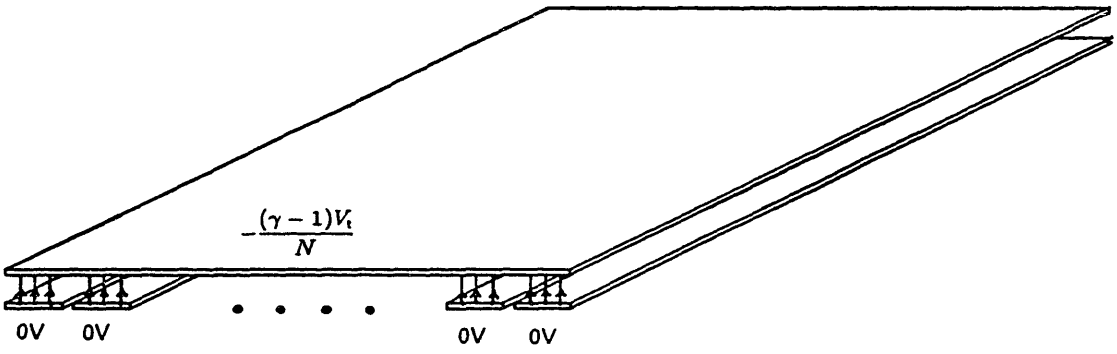

Fig. 5.5 Voltage and field distribution in transformer for computation of stored common mode electric energy.

The common mode capacitance, C_c, is given by

$$C_c = \frac{2\pi\epsilon w_t}{N^2 m} \sum_{n=1}^{N} r_n(\gamma-1)^2 \tag{5.20}$$

Table 5.4 shows the values for these capacitances that were predicted for the gapped slotted transformer with the parameters of Table 5.1. Note that since the two capacitances represent the two modes of electric energy storage, the differential mode capacitance, computed from (5.18), and the common mode capacitance, computed from (5.20), sum to the total capacitance, computed from (5.13). Unfortunately, the finite element program could not calculate values for these capacitances. However, the capacitance measurements of the experimental windings described in Chapter 8 are shown there to be close to the values predicted for the winding used in that chapter.

Table 5.4: Test Transformer Capacitance

Parameter	Symbol	Equation	Value
Differential mode capacitance	C_d	(5.18)	0.95 pF
Common mode capacitance	C_c	(5.20)	2.6 pF
Total capacitance	C_t	(5.13)	3.5 pF

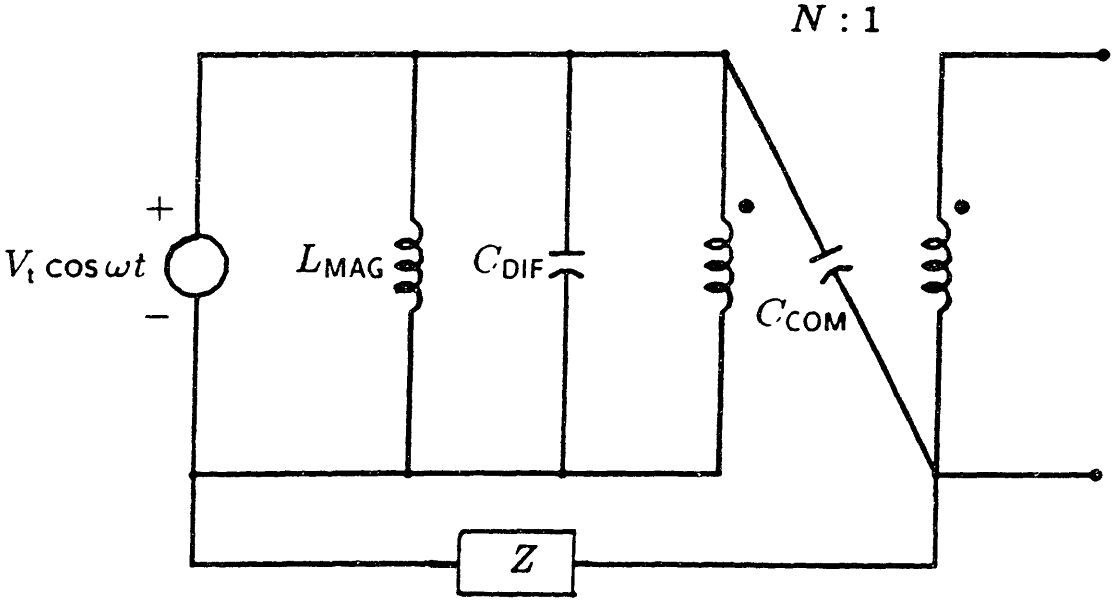

Fig. 5.6 Transformer model showing common mode capacitance and scaled ground impedance.

5.7.4 Effect of Ground Impedance

The model for the common mode capacitance, shown in Fig. 5.6, implicitly assumed that the impedance of the ground connection between the low sides of the primary and secondary was zero. If this impedance is non-zero, indicated in Fig. 5.6 by Z', the model must be adjusted in order to preserve the model's assumption that the capacitive currents are not a source of net ampere-turns for the transformer. The following analysis determines the voltages and currents present in the ground impedance and indicates the modifications that must consequently be made to the model.

Figure 5.7 shows the common mode capacitor repositioned so that it is connected between the center taps of the primary and secondary. This connection emphasizes that for a spiral winding the actual winding-to-winding capacitance, C_{w-w}, is subjected to a voltage equal to the difference between the two midpoint voltages. In this approximate

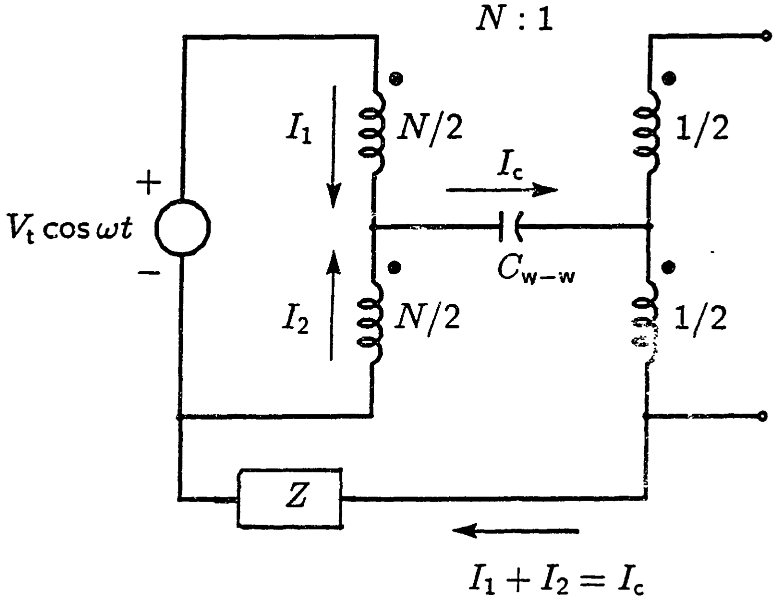

Fig. 5.7 Transformer model showing winding-to-winding capacitance and actual ground impedance.

analysis, C_{w-w} will be considered to be a parallel plate capacitor, and each turn will be assumed to have the same area, $2\pi w_t\ r_{av}$, where r_{av} is the average radius of the turns. The winding-to-winding capacitance can therefore be written as

$$C_{w-w} = \frac{2\pi\epsilon N w_t\ r_{av}}{m} \tag{5.21}$$

Since the net ampere-turns in the transformer must be zero, the following equation can be written for the circuit of Fig. 5.7,

$$I_1\frac{N}{2} + (I_1 + I_2)\frac{1}{2} = I_2\frac{N}{2} \tag{5.22}$$

Solving for I_c, the current through C_{w-w}, gives

$$I_c = I_1 + I_2 = \left(\frac{2N}{N-1}\right) I_1 \tag{5.23}$$

Kirchoff's voltage law gives another equation,

$$V_c = \frac{V_t}{2} - I_c Z - \frac{V_t}{2N} \tag{5.24}$$

where V_c is the voltage across C_{w-w}. Dividing (5.24) by X_c, the impedance of C_{w-w}, gives

$$I_c = \frac{V_c}{X_c} = \frac{V_t}{X_c}\left[\frac{N-1}{2N}\right] - \frac{I_c Z}{X_c} \tag{5.25}$$

Solving for V_t/I_c gives

$$\frac{V_t}{I_c} = (X_c + Z)\left[\frac{2N}{N-1}\right] \tag{5.26}$$

Finally, substituting (5.23) into (5.26) gives

$$\frac{V_t}{I_1} = (X_c + Z)\left[\frac{2N}{N-1}\right]^2 \tag{5.27}$$

Equation (5.27) states that the capacitance and ground impedance of Fig. 5.7 must be scaled by $(2N/N-1)^2$ in order to fit the model of Fig. 5.6. For the common mode capacitance, C_c, this means that

$$C_c = \left[\frac{2N}{N-1}\right]^2 C_{w-w} = \frac{2\pi\epsilon N w_t\ r_{av}}{m}\left[\frac{2N}{N-1}\right]^2 \tag{5.28}$$

This is consistent with our earlier calculation of C_c, since in the approximation where the area of each turn is equal,

$$\gamma = \frac{N+1}{2} \tag{5.29}$$

Substituting (5.29) into the original expression for C_c, (5.20), gives (5.28), as required.

Similarly, for the ground impedance, Z, the above analysis states that

$$Z' = \left[\frac{2N}{N-1}\right]^2 Z \tag{5.30}$$

The actual ground impedance must be scaled in order to be used in the model of Fig. 5.6. This scaling yields a more accurate model of the ground impedance for such applications as designing filters to prevent common-mode signals in the system ground. However, this model fails to preserve the voltage across the ground impedance. In Fig. 5.7 $V_z = I_1 Z(2N/N-1)$, while in Fig. 5.6 $V_z = I_1 Z(2N/N-1)^2$.

Chapter 6

SELECTION AND CHARACTERIZATION OF THE MAGNETIC MATERIAL

The 1–10 MHz magnetic materials that are commercially available were developed for telecommunications applications, not for power circuits. For this reason the permeability and loss data available from the manufacturers and the technical literature is for very low flux levels, less than ten Gauss, rather than the flux levels of several hundred Gauss that will be called for by the designs of Chapter 7. This chapter surveys the magnetic materials available, explains the choice of nickel-zinc ferrite, describes a measurement technique for experimentally determining permeability and loss at power flux levels, and presents data for six commercially available nickel-zinc ferrites from eight different manufacturers.

6.1 Survey of Magnetic Materials

The four magnetic materials generally available for use in high frequency transformers are powdered iron, powdered amorphous metal (for example $Fe_{81}B_{13.5}Si_{3.5}C_2$), manganese-zinc ferrite, and nickel-zinc ferrite. This section presents a brief review of material properties that shows that, of the currently available materials, nickel-zinc ferrite is the best choice for this application.

6.1.1 Powdered Iron and Amorphous Metal

Ferromagnetic materials like iron generally have high electrical conductivity and must be laminated even at 60 Hz to prevent excessive eddy current loss. At 10 MHz the skin depth in 4% silicon-iron, which has a permeability of about $5000\mu_o$ and a conductivity of $2\times10^6\,(\Omega\text{m})^{-1}$, is about 2 μm. In order to avoid high losses due to eddy currents, the iron would have to be laminated thinner than the skin depth. Laminations of much less than 2 μm are impractical.[1]

Amorphous metals are metals that have been prepared in the glassy state in order to lower their conductivity. Unfortunately, this process typically lowers the conductivity of a particular material by a factor of three at best.[2] Since the skin depth is inversely

---

[1] C. Heck, *Magnetic Materials and Their Applications*, Butterworth and Co., Ltd., London (1974), p. 437.

[2] D. Nathasingh and C. H. Smith, "A New High-Flux, Low-Loss Magnetic Material

proportional to the square root of the conductivity, the potential increase in skin depth is limited to a factor of 1.7. Typical amorphous metals have skin depths, as silicon-iron does, on the order of 2 μm at 10 MHz.[3]

One approach to lowering the conductivity of either iron or amorphous metal is to prepare it in a powdered form in which individual particles are insulated from each other by an insulating coating. Cores formed of powdered metal therefore possess a "distributed gap" represented by the spacing between particles. In order to reduce eddy current loss, the metal particles must have radii that are substantially less than the 2 μm skin depth.

Table 6.1 compares the permeability and loss of two representative powdered iron materials, GQ–4 and GS–6, with those of two nickel-zinc ferrites, 4C4 and Q1, for a 2.5 MHz, 200 G sinusoidal excitation.[4,5,6] The loss of the powdered iron materials is substantially higher than that of the nickel-zinc ferrites. Note that the particle radii of the powdered iron materials are not substantially smaller than a skin depth, and that for these particular materials, a small decrease in particle size does not appear to affect the loss. The discussion of Section 4.6 explained that in order for an ungapped transformer composed of powdered iron to be superior to a discrete gap transformer composed of ferrite, the loss per unit volume in the powdered iron would have to be an order of magnitude lower than that of the ferrite. Therefore, for this application, ferrites would appear to be preferable to powdered iron.

It should be noted, however, that powdered iron materials have substantially higher saturation flux densities than ferrites; Carbonyl GQ–4 has a saturation flux density of 12 kG, while Ferroxcube 4C4, a typical nickel-zinc ferrite, has a saturation flux density of only 3 kG. While high saturation flux density is not a advantage that the transformer in the

---

for High Frequency Applications," *Proceedings of Powercon 7*, Power Concepts, Inc., San Diego, California (1980).

[3] A. Tago, C. Nishimura, and K. Yanagisawa, "Magnetic Properties of Ion-Beam Sputtered Co-Zr and Co-Zr-Re Amorphous Films," *IEEE Transactions on Magnetics*, **21**, 5 (1985).

[4] "Carbonyl Iron Powders," Pub. no. 2303–73, GAF Corporation, Wayne, N.J. (1986), pp. 3 and 8.

[5] "High Frequency Core Loss Graphs," Micrometals, Inc., Anaheim, California (1986).

[6] Philips Electronic Components and Materials Division, *Components and Materials Book C4: Ferroxcube Potcores, Square Cores, and Cross Cores*, Eindhoven, the Netherlands (1984), p. 40.

Table 6.1: Material Properties at 2.5 MHz and 200 G				
Manufacturer	Material	Particle Radius	Permeability	Loss
GAF	GQ–4	2–4 μm	$35\mu_o$	2.5 W/cc
GAF	GS–6	1.5–2.5 μm	$25\mu_o$	2.5 W/cc
Ferroxcube	4C4	—	$125\mu_o$	1.0 W/cc
Indiana General	Q1	—	$125\mu_o$	0.5 W/cc

MIT converter can utilize, since excessive core loss will limit the purely ac flux excitation to a value far below saturation, powdered iron might be the appropriate choice in those high frequency converter topologies in which a magnetic component carries a current with a large dc offset.[7]

6.1.2 Ferrites

Ferrites are ferrimagnetic iron oxides, prepared commercially as ceramics, and distinguished by their high electrical resistivity compared to metals. The two commonly manufactured ferrite compounds are manganese-zinc (Mn-Zn) ferrite and nickel-zinc (Ni-Zn) ferrite. Mn-Zn ferrite typically displays a permeability on the order of 2000 μ_o and a conductivity of about $1\,(\Omega m)^{-1}$. Ni-Zn ferrite has a lower permeability, on the order of $200\mu_o$, but a much lower conductivity, 10^{-5} $(\Omega m)^{-1}$.

Mn-Zn ferrite is not appropriate for application above approximately 2 MHz because of its high core loss, due to both eddy current loss and loss due to irreversible magnetic processes. The eddy current loss can be exacerbated by dimensional resonances in the material, since the dielectric constant at 1 MHz is greater than $10^4\epsilon_o$.[8] This extremely high dielectric constant is due to grain boundary effects which cause the material to look like a very lossy dielectric.[9] The very high ϵ, together with the relatively high permeability, reduces the wavelength in the material to about 2 cm at 2 MHz.[10] Since 1–10 MHz magnetic

---

[7] "A New Family of Resonant Rectifier Circuits for High Frequency Dc-Dc Converter Applications," W. A. Nitz, W. C. Bowman, F. T. Dickens, F. M. Magalhaes, W. Strauss, W. B. Suiter, and N. G. Ziesse, *IEEE Applied Power Electronics Conference Record*, February 1988, pp. 12–22.

[8] Siemens AG, *Ferrites Data Book 1986/87*, Munich, Federal Republic of Germany (1986), p. 31.

[9] P. A. Miles, W. B. Westphal, and A. von Hippel, "Dielectric Spectroscopy of Ferromagnetic Semiconductors," *Reviews of Modern Physics*, **29**, 3 (1957), pp. 279–307.

[10] F. G. Brockman, P. H. Dowling, and W. G. Steneck, "Dimensional Effects Resulting from a High Dielectric Constant Found in a Ferromagnetic Ferrite," *Physical Review*, **77**,

components have typical diameters on the order of 1 cm, lossy dimensional resonances will occur. Furthermore, at 1 MHz the domain wall movement in Mn-Zn ferrite is close to its resonant frequency. As the material is driven closer to its resonance, the permeability increases slightly, but the magnetic loss becomes very large.[11].

Ni-Zn ferrite is an appropriate choice for circuits operating at 2–10 MHz. Because of Ni-Zn ferrite's extremely low conductivity, eddy current loss can be ignored, and the dielectric constant is only about $10\epsilon_o$. Core loss in Ni-Zn ferrite is primarily associated with domain wall movement. Although the domain wall resonant frequency in these ferrites is higher than in the Mn-Zn ferrites, and the loss correspondingly lower, the resonant frequency is still low enough so that in the 1–10 MHz range, small increases in operating frequency cause large increases in core loss.

6.2 Characterization of Permeability and Loss

The permeability and loss of magnetic materials can not be predicted theoretically and instead require the development of empirical models based on measured data. Development of these models requires more data about the nickel-zinc ferrites used in these components than is currently available from the manufacturers or the literature. Manufacturers usually specify only the initial permeability and the small signal loss. These parameters are measured at the extremely low flux densities (below 3 G) characteristic of commercial impedance analyzers and are poor indicators of the actual permeability and loss at power flux levels (above 50 G). Permeability and loss are also dependent on frequency, temperature, and dc bias.

This lack of permeability and loss data is due, at least in part, to the difficulty of making and interpreting measurements in the 1–10 MHz range. Parasitic elements can cause large errors in the measurements. The nonuniform flux densities in the core, together with the field-dependent permeability, complicate the interpretation of the measured data.

This section describes an experimental procedure and mathematical analysis designed to determine the dependence of permeability and power loss density on the applied B field at frequencies between 1 and 10 MHz. This section also presents experimentally determined characteristics of eight different commercially available nickel-zinc ferrites from

---

1 (1950), pp. 85–93.

[11] J. Smit and H. Wijn, "Physical Properties of Ferrites," in *Advances in Electronics and Electron Physics*, vol. vi, ed. L. Marton, Academic Press, Inc., New York (1954), pp. 105–110.

six manufacturers.

6.2.1 Experimental Procedure

Experimental procedures for measuring permeability and loss may be classified as either direct or indirect. This section will discuss these two approaches and describe the measurement procedure used in this work.

Direct measurements of sinusoidal voltage and current are typically made with the circuit of Fig. 6.1.[12] In this scheme a toroid of the material under test is wound with both an excitation and a sense winding. The flux in the toroid is inferred from a voltage measurement made at the open circuited sense winding, so that the effect of leakage inductance and winding resistance is avoided. The current is measured with a sense resistor in the excitation winding. The voltage and current signals, proportional to the B and H fields, respectively, are plotted against each other on an oscilloscope, and the area of the resulting hysteresis loop is calculated to find the energy lost each cycle. In the 1–10 MHz range, significant phase errors can be introduced by parasitic inductances and capacitances in the circuit and by time delays in the oscilloscope. These phase errors make accurate loss measurement difficult.[13,14].

Above 1 MHz indirect methods are often employed in order to avoid these phase errors. Typical high frequency core loss measurement techniques include balanced bridges[15],

---

[12] H. P. J. Wijn and J. J. Went, "The Magnetization Process in Ferrites," *Physica,* **17** 11–12 (1951), pp. 976–992.

[13] V. J. Thottuvelil, "High-Frequency Magnetic-Core Measurements for Power Conditioning Systems with Emphasis on Amorphous Metallic-Alloy Tape-Wound Cores," Ph. D. Dissertation, School of Engineering, Duke University, Durham, North Carolina (1984), p. 94.

[14] T. Sato and Y. Sakaki, "100 kHz–10 MHz Iron Loss Measuring System," *IEEE Transactions on Magnetics,* **23** 5 (1987), pp. 2593–2595.

[15] Miles, Westphal, von Hippel.

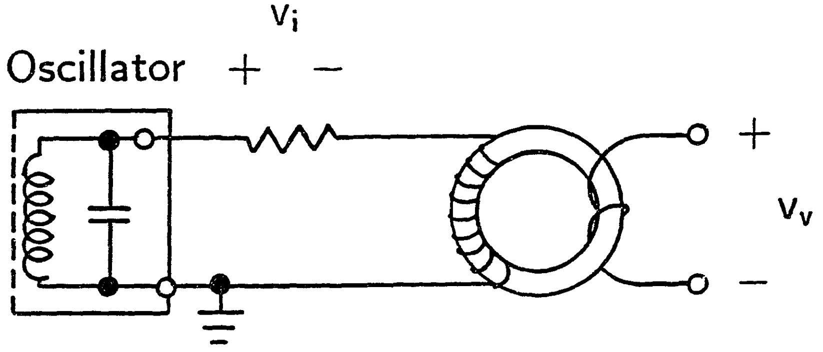

Fig. 6.1 Circuit for determining hysteresis loss in a toroidal sample by measuring excitation voltage and current.

wattmeters[16], H-bridges[17], resonant tanks[18], and calorimetry[19]. Indirect measurements necessarily include the losses of the rest of the measurement circuit, such as the dissipation in the copper windings. Proximity effects in the conductors, which are affected by the permeability of the neighboring material, complicate efforts to segregate the copper loss by measuring the dissipation using a nonmagnetic core. Losses in resonating capacitor leads and electrodes can also be significant.

Because of the fundamental limitations of indirect measurements, the results presented in this paper are based on the direct measurement approach. Considerable care was taken to reduce parasitic inductances and capacitances, and the voltage and current waveforms were digitized with a high bandwidth digital oscilloscope to permit a mathematical correction for the remaining parasitics. A block diagram of the measurement circuit is shown in Fig. 6.2, and the equipment listed in Table 6.2. A toroidal core of each material

---

[16] G. E. Schaller, "Power Ferrites for 1 Megahertz (and up) Switchers," *Technical Papers of the Second International High Frequency Power Conversion Conference,* April 1987, pp. 205–210.

[17] B. Carsten, "Fast, Accurate Measurement of Core Loss at High Frequencies," *Power Conversion and Intelligent Motion,* March 1986, pp. 29–33.

[18] J. G. De Lau, "Influence of Chemical Composition and Microstructure on High-Frequency Properties of Ni-Zn-Co Ferrites," *Philips Research Reports Supplements,* 6 (1975), p. 39.

[19] A. Estrov, "1-MHz Resonant Converter Power Transformer is Small, Efficient, Economical," *Power Conversion and Intelligent Motion,* August 1986, pp. 14–24.

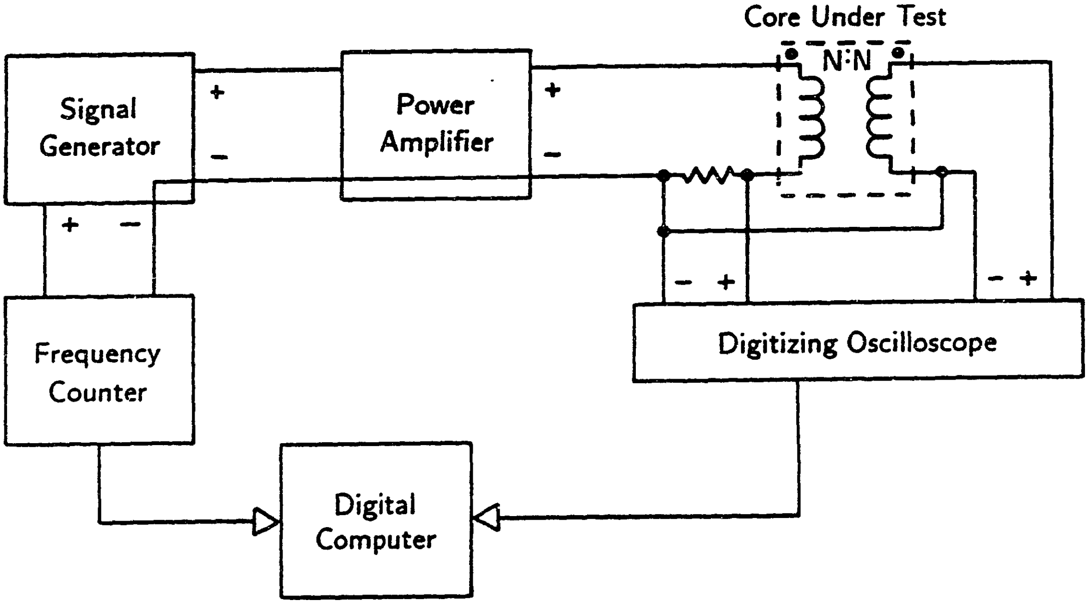

Fig. 6.2 Block diagram of the circuit used to measure the excitation voltage and current in a toroidal sample of the ferrite under test.

under test was wound as an $N{:}N$ transformer with a bifilar winding pair in order to avoid inducing a differential mode voltage across the interwinding capacitance. As mentioned earlier, in the direct method the voltage is measured from the open-circuited secondary to avoid the effects of leakage inductance and winding resistance. The current was measured with a coaxial sense resistor in the primary. This resistor, developed for RF applications, is composed of constantan foil and has a value of 0.5 Ω. The voltage and current waveforms were digitized by the oscilloscope and transferred to a digital computer for analysis. The programs that performed the analyses are described in Appendix D.

Note that the oscilloscope and the voltage source share the same ground. If they did not, there would be another current path in parallel with the current sense resistor, through the interwinding capacitance in the isolation transformers of the equipment power supplies and the inductance of the ground loop. The parasitic impedance of this alternate path can be low enough to introduce significant error in the measurement of the current. It was therefore avoided by connecting the oscilloscope and the voltage source to a common ground.

Two parasitic circuit elements that significantly affect the measurement and could

Table 6.2: Measurement Equipment

Item	Manufacturer	Model
Signal Generator	Hewlett-Packard	8116A
RF Power Amplifier	Electronic Navigation Industries	3100LA
RF Sense Resistor	T&M Instruments	VLBNC–PT5–5
Digitizing Oscilloscope	Tektronix	2430
Frequency Counter	Hewlett-Packard	5834A
Personal Computer	IBM	PC/XT
GPIB Bus Controller	National Instruments	GPIB–PC
Analysis Software	Asyst Software Technologies	ASYST V. 5.3

not be totally eliminated are the series inductance inside the RF sense resistor ($\sim$ 0.1 nH) and the parasitic capacitance across the core ($\sim$ 30 pF). The latter element is composed of both the capacitance of the coaxial cable connecting the secondary to the oscilloscope and the input capacitance of the oscilloscope. These parasitics were measured and their effects were compensated for by the software. In addition, the effect of the time delay between oscilloscope channels ($\sim$ 70 psec) was removed analytically during data analysis.

Each of the eight ferrite samples was tested at three frequencies: 2.5 MHz, 5 MHz, and 10 MHz. At each frequency the magnitude of the sinusoidal voltage source was varied in order to give a range of peak flux levels that would represent the practical domain of interest. The lowest voltage was chosen so that the peak flux in the core would be approximately 70 Gauss, while the highest voltage was chosen so that the power loss density would be about 5 W/cc. Before each measurement was performed, the core was demagnetized with the circuit of Fig. 6.3.[20]

6.2.2 Mathematical Analysis

The goal of the mathematical analysis is to relate the digitized voltage and current waveforms to the B and H fields in the core, and to determine the dependence of the permeability and loss on the flux level for a particular frequency of excitation. This section describes the harmonic analysis of the voltage and current waveforms, the expressions used to model the material permeability and loss density, and the approach used to fit the data to the analytical models.

---

[20] "Apparatus for Magnetic Conditioning with Capacitor Discharge," in *Cores for Inductors and Transformers for Telecommunications: Part 1, Measuring Methods,* International Electrotechnical Commission Publication 367–1 Geneva (1982), pp. 89–91.

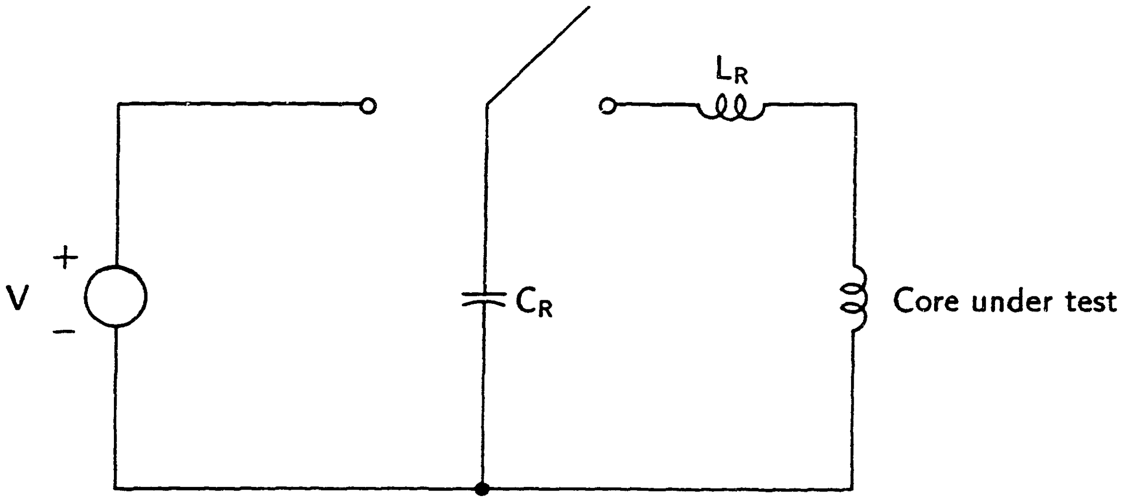

Fig. 6.3 IEC standard circuit for demagnetizing cores.

6.2.2.1 Harmonic Analysis of Voltage and Current Waveforms

The first step in the procedure is a discrete Fourier analysis of the digitized voltage and current waveforms to find the magnitudes and the relative phase of their fundamental components. The excitation frequency is measured independently by a frequency counter, as shown in Fig. 6.2, in order to avoid the error introduced by deriving the frequency from the data.

Below about 8 MHz, the harmonics in the voltage and current waveforms were found to be negligible, so that the hysteresis loops were nearly perfect ellipses. These ellipses are characteristic of ferrites at small magnetizations[21] Note that the largest flux density applied to the cores, about 300 G, is only 10% of the saturation flux density of about 3000 G. As will be shown later, the maximum flux density applied to the ferrites is limited by the core loss. Above about 8 MHz, second and third harmonics were present, each less than 3% of the fundamental, due primarily to distortion in the signal generator. However, the power dissipated in these modes was computed by a discrete Fourier analysis and found to be negligible. The harmonics were therefore not included in the analysis.

6.2.2.2 Determination of Material Permeability

Next, the material permeability is determined from the experimental voltage and current measurements. This section first presents equations relating the permeability to

---

[21] C. Chen, *Magnetism and Metallurgy of Soft Magnetic Materials*, North-Holland Publishing Company, Amsterdam (1977), p. 116.

the measured voltage and current for materials whose permeability and loss do not depend on flux level. The analysis is then extended for the ferrites, whose properties were observed to depend on flux level. The expression proposed for the permeability contains constants that are determined by fitting the voltage and current data to an equation derived in this section. The permeability model does not include frequency, so a separate fit must be made at each frequency.

The permeability, μ, which relates the B and H fields inside the magnetic material, is defined by the constitutive relation

$$B = \mu H \tag{6.1}$$

Ampere's and Faraday's Laws are used to relate the current and voltage of the magnetizing inductance to the internal H and B fields in the toroid. The core is modelled as a non-dissipative magnetizing inductance in parallel with a dissipative element that represents the core loss. Ampere's Law relates the current in the magnetizing inductance, i_m, to the H field inside the core, giving

$$H(r) = \frac{N}{2\pi r} i_m \tag{6.2}$$

where N is the number of turns and r is the radius. Similarly, Faraday's Law relates the voltage, v, to the B field, giving

$$v = Nh \frac{d}{dt} \int_a^b B(r)\, dr \tag{6.3}$$

where a is the inner radius of the core, b the outer radius, and h the height of the rectangular cross-section, as illustrated in Fig. 6.4. Given v and i_m, (6.1), (6.2), and (6.3) can be solved for the permeability.

Permeability and loss analyses typically neglect the radial dependence of (6.2) and (6.3) by replacing r with the average radius, $(a+b)/2$.[22] This approximation is not appropriate for the commercially available toroids available for these tests, however, since in these toroids a and b are substantially different from the average radius. Therefore, the radial dependence is retained in the work presented here.

For a material in which μ is independent of flux level, (6.1), (6.2), and (6.3) yield

$$\mu = \frac{1}{f N^2 h \ln(b/a)} \left(\frac{v}{i_m} \right) \tag{6.4}$$

where f is the excitation frequency. If μ were indeed independent of flux level, only one measurement of voltage and current would be necessary to determine its value. However,

---

[22] Schlicke, p. 9.

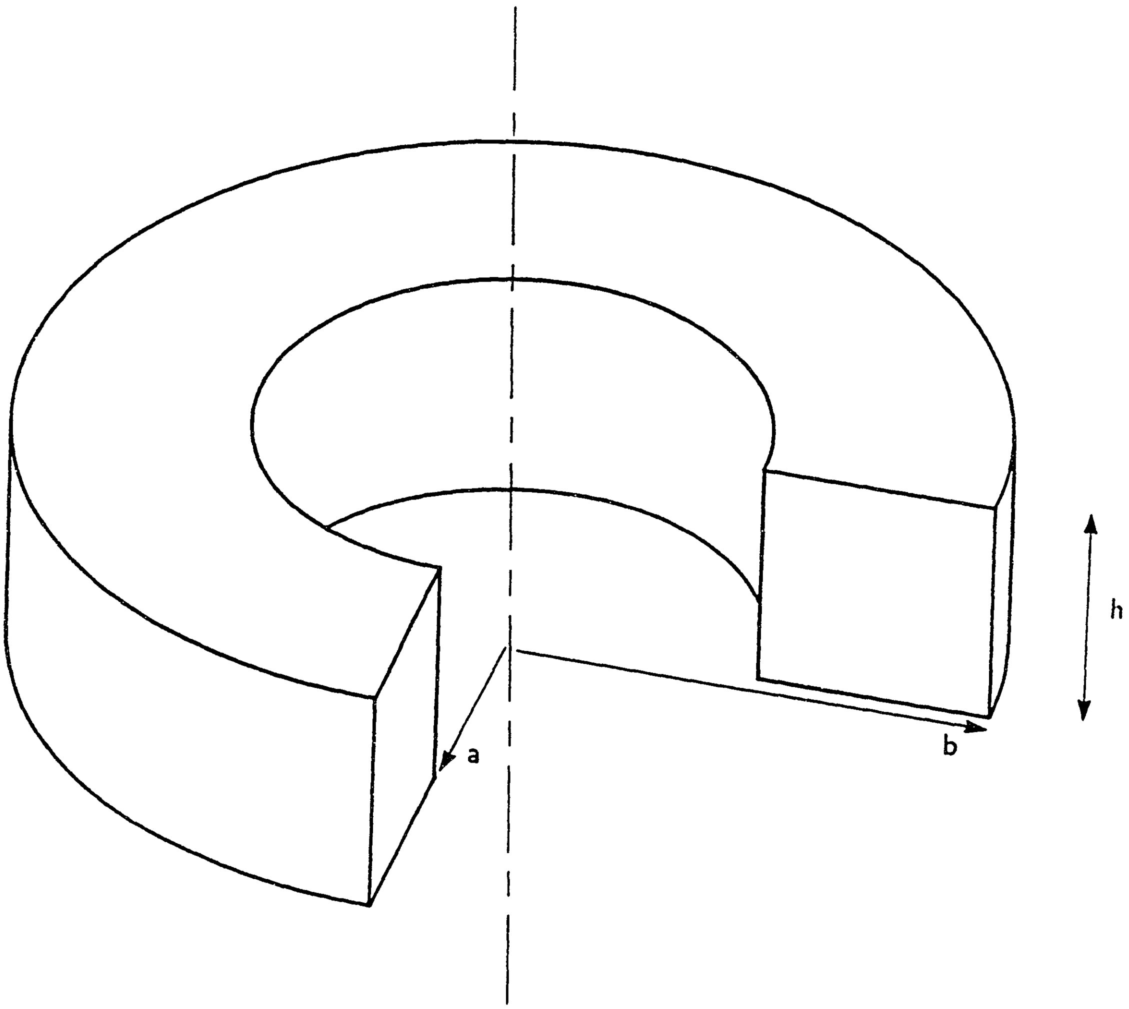

Fig. 6.4 Dimensioned diagram of toroid.

in the ferrite samples measured, μ was found to increase with increasing flux level, which is typical of magnetic materials.

The dependence of permeability on excitation was empirically modelled by

$$\mu(H) = \mu_i \sqrt{1 + \alpha^2 \left|H\right|^2} \tag{6.5}$$

a function that was chosen because it fit the data very well. In this equation, μ_i is the initial permeability, similar to the initial permeability specified by manufacturers, and α gives the dependence of μ on the H field. The constitutive relation, (6.1), then becomes the nonlinear expression

$$B = \mu(H)\, H = \mu_i H \sqrt{1 + \alpha^2 \left|H\right|^2} \tag{6.6}$$

and (6.4) becomes a transcendental equation in μ_i and α,

$$\mu_i = \frac{1}{f N^2 h\, \xi(a, b, \mu_i, \alpha, i_m)} \left(\frac{v}{i_m}\right) \tag{6.7}$$

In this equation, which is derived in Appendix A, ξ is a function of a, b, μ_i, α, and i_m.

Ideally, measurements at two different levels of voltage and current would be sufficient to determine μ_i and α. In practice, voltage and current measurements over the range of the excitation must be examined in order to find the best (i.e., least square error) values for these parameters.

6.2.2.3 Determination of Loss Density

The next step of the analysis is the determination of the power loss density as a function of flux level. This section first presents equations describing core loss in materials whose permeabilities do not depend on flux level. The analysis is then extended to the ferrite materials, whose permeabilities do depend on flux level. As in the last section, the expression for core loss contains constants that are determined by fitting the voltage and current data to an equation derived in this section. The model for core loss, like the model for permeability, does not include frequency, so a separate fit must be made at each frequency.

For a material with a permeability, μ, that does not depend on the applied field, the energy stored each cycle is

$$W_m = \frac{1}{2}\mu H^2 \tag{6.8}$$

The core loss, P_h, can be expressed as a fraction, γ, of the total energy stored in the volume of the material, times the frequency f of the excitation, giving

$$P_h = \gamma f \int W_m \, dV \tag{6.9}$$

The hysteresis loss is found by substituting (6.2) and (6.8) into (6.9), giving

$$P_h = \frac{\gamma f}{2} \int \mu H^2 \, dV = \gamma \left(\frac{\mu f h N^2}{4\pi} \ln \frac{b}{a} \right) |i_m|^2 \tag{6.10}$$

This equation shows that the hysteresis loss is a function of the current, i_m. Ideally, only one measurement of current and power dissipation would be necessary to determine the value of γ.

However, as was found with the permeability, γ is not a constant, but rather increases with flux level. This dependence was modelled by adding higher order correction terms to (6.10), with a different γ_n associated with each term, as shown in (6.11).

$$P_h = \frac{f}{2} \int \left[\gamma_1 \left[\mu(H) H^2\right] + \gamma_2 \left[\mu(H) H^2\right]^2 + \gamma_3 \left[\mu(H) H^2\right]^3 \right] dV \tag{6.11}$$

In this expression $\mu(H)$ is given by (6.5), H is given by (6.2), and γ_1, γ_2, and γ_3 are constants whose values were determined by fitting (6.11) to the experimental data. This expression can be rewritten as

$$P_h = \pi f h \mu_i \left(\frac{N}{2\pi}\right)^2 |i_m|^2 \sum_{n=1}^{3} \gamma_n K_n(i_m, \mu_i, \alpha, a, b) \tag{6.12}$$

where the K_n, which depend on the current, the permeability, and the core geometry, are evaluated in the Appendix. The resulting expression, (C6), which relates the core loss to the magnetizing current and the permeability model, was found to fit the experimental data very well.

6.2.2.4 Fitting Data to Models

The previous sections presented analytical models that relate permeability and loss to the measured voltage and current. These models contain constants — μ_i, α, γ_1, γ_2, and γ_3 — whose values can be determined at each frequency by fitting the expression to the measured voltage and current data. This section describes the procedure by which this fit was performed.

For experiments that have normal error distributions, a well established procedure for fitting a curve to the data is the least square error fit.[23] In this procedure, a function, $f(x)$, is chosen to relate N measurements of a dependent variable, y, to the associated independent variable, x. The free parameters of the function are chosen to minimize the error χ^2, given by

$$\chi^2 = \sum_{n=1}^{N} [f(x_n) - y_n]^2 \tag{6.13}$$

The least square error criterion was used to determine the permeability. The current was considered the independent variable, the voltage the dependent variable, and the function that relates them is given by (C2). The curve fitting routine determined the free parameters, μ_i and α. The model fit the data very well. Although the test voltage ranged between 3 V and 25 V, the standard deviation of the fit was typically less than 0.03 V.

To determine the loss density, the current was considered the independent variable and the power dissipation the dependent variable. The function that relates them is given by (C6). Here, the fit determines the parameters γ_1, γ_2, and γ_3. However, unlike the

---

[23] P. R. Bevington, *Data Reduction and Error Analysis for the Physical Sciences*, McGraw Hill Book Company, Inc., New York (1969), pp. 66–91.

permeability, whose value typically varies by 20% over the range of excitation, the loss density can vary by a factor of 50. If the error function given by (6.13) were used for this study, an error of 0.5 mW out of 1 mW would have the same weight as an error of 0.5 mW out of 350 mW. In order to correct this imbalance, the error at low power was weighted more heavily than the error at high power.

The weighting represents a tradeoff; with no weighting, the error at low power is much worse than the error at high power, while with heavy weighting, the fit as a whole was found to degrade. The following weighting was felt to represent a good compromise and was used in the fit:

$$\chi^2 = \sum_{n=1}^{N} \sqrt{\frac{|y_{max}|}{|y_n|}} \left[f(x_n) - y_n\right]^2 \tag{6.14}$$

The resulting fit error was examined on a point-by-point basis in order to assure a satisfactory fit. The error typically rolled off quickly from ±10% at the lowest power levels to less than ±3% at moderate and high power levels. The computer programs that performed these curve fits are described in Appendix D.

6.2.3 Experimental Measurements

The experimental procedure and mathematical analysis described above were used to determine the permeability and loss of samples of eight commercially available ferrites in response to a purely ac field. The properties of three representative materials were then measured in response to an ac field with a dc offset.

In every case the measurements were performed at three frequencies: 2.5, 5.0, and 10 MHz. As mentioned previously, each sample was demagnetized before each measurement. The ferrite temperature was kept at the ambient temperature, 25°C, by the use of forced air cooling and brief excitations. The surface temperature of the ferrite was monitored by means of a thermistor probe.

6.2.3.1 AC Excitation

Eight ferrites, listed in Table 6.3, were measured in response to a purely ac excitation. A dc blocking capacitor was added to the output of the RF power amplifier in order to remove a small offset introduced by the amplifier. The corresponding permeability and loss curves are shown in Figs. 6.5(a)–(f).

The following conclusions can be drawn from these data:

1. Core loss increases faster than frequency. This effect is further illustrated by Fig. 6.6,

Table 6.3: Nickel-Zinc Ferrites		
Sample	Ferrite	Manufacturer
1	Q1	Indiana General
2	4C4	Ferroxcube
3	C2025	Ceramic Magnetics
4	C2050	Ceramic Magnetics
5	K1	Siemens
6	K5	TDK
7	K6a	TDK
8	K01	Krystinel

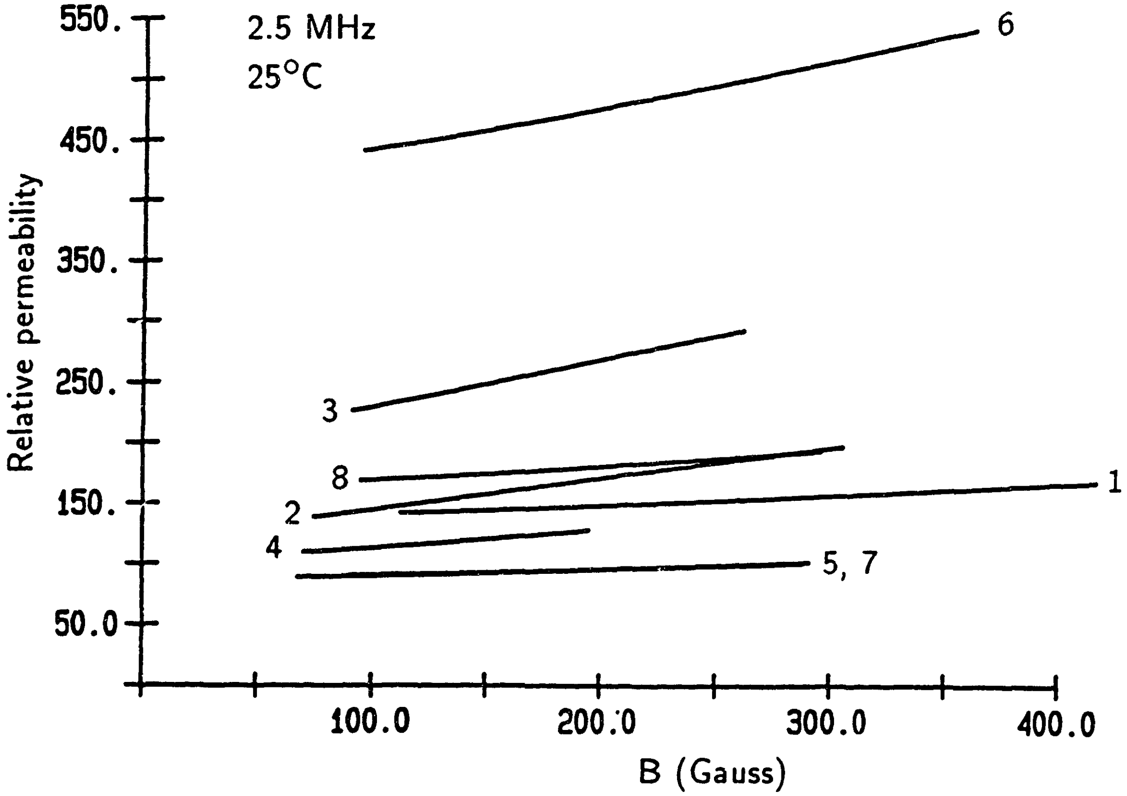

Fig. 6.5a Relative permeability versus peak B field (Gauss) for ac excitation at 2.5 MHz and 25°C.

which shows the energy density lost per cycle as a function of excitation frequency for Q1, 4C4, and C2025 materials. These curves are drawn for an ac excitation of 125 G (peak).

2. Increased permeability is generally associated with increased loss.
3. The loss density increases rapidly with flux level, limiting practical flux levels to less

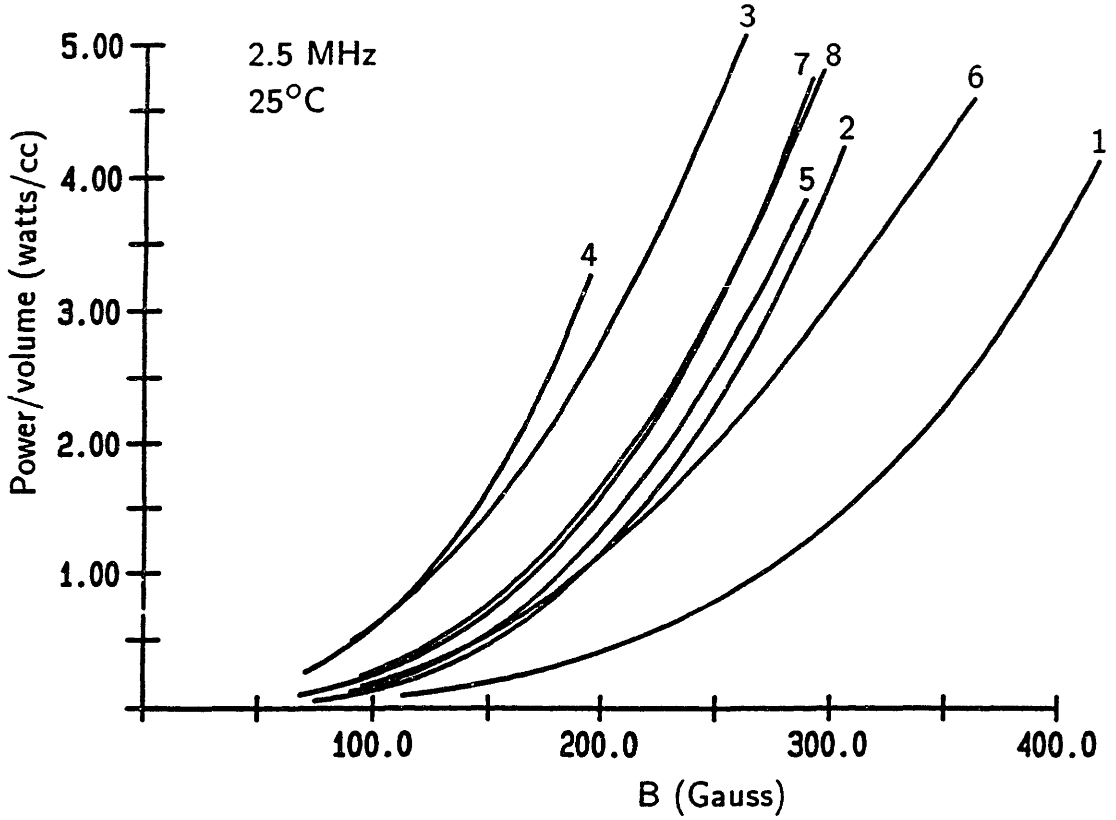

Fig. 6.5b Power loss density (watts/cm^3) versus peak B field (Gauss) for ac excitation at 2.5 MHz and 25°C.

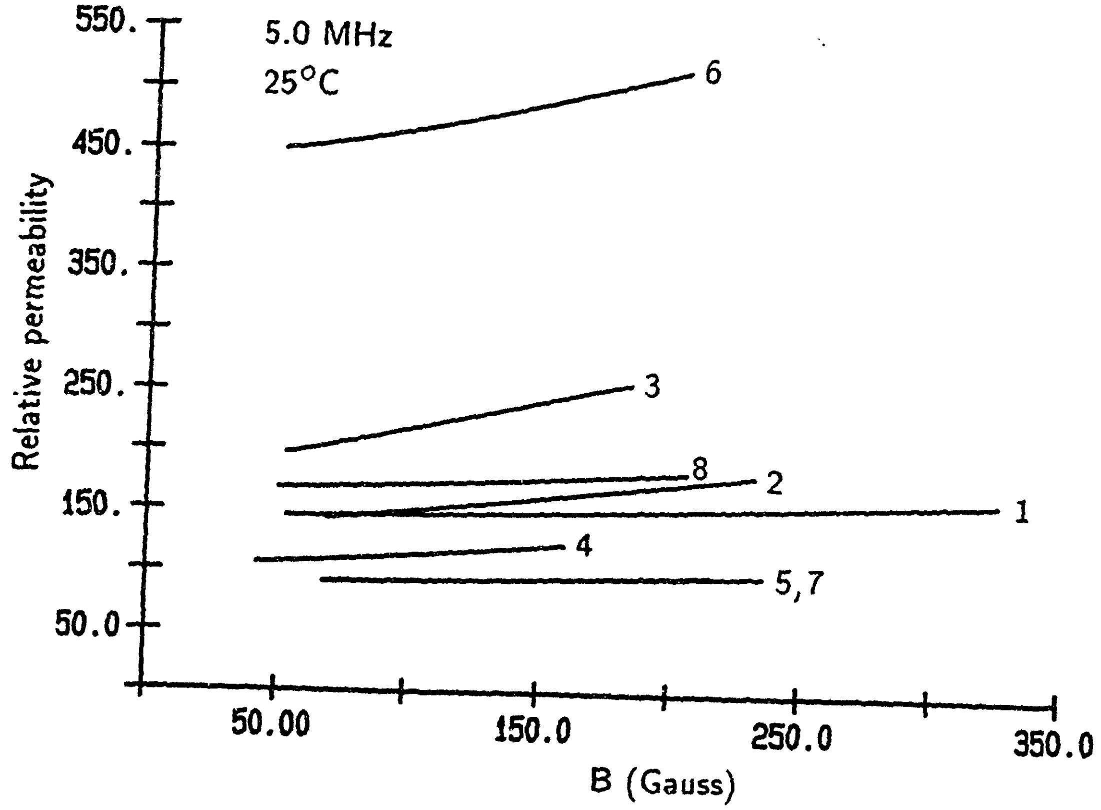

Fig. 6.5c Relative permeability versus peak B field (Gauss) for ac excitation at 5.0 MHz and 25°C.

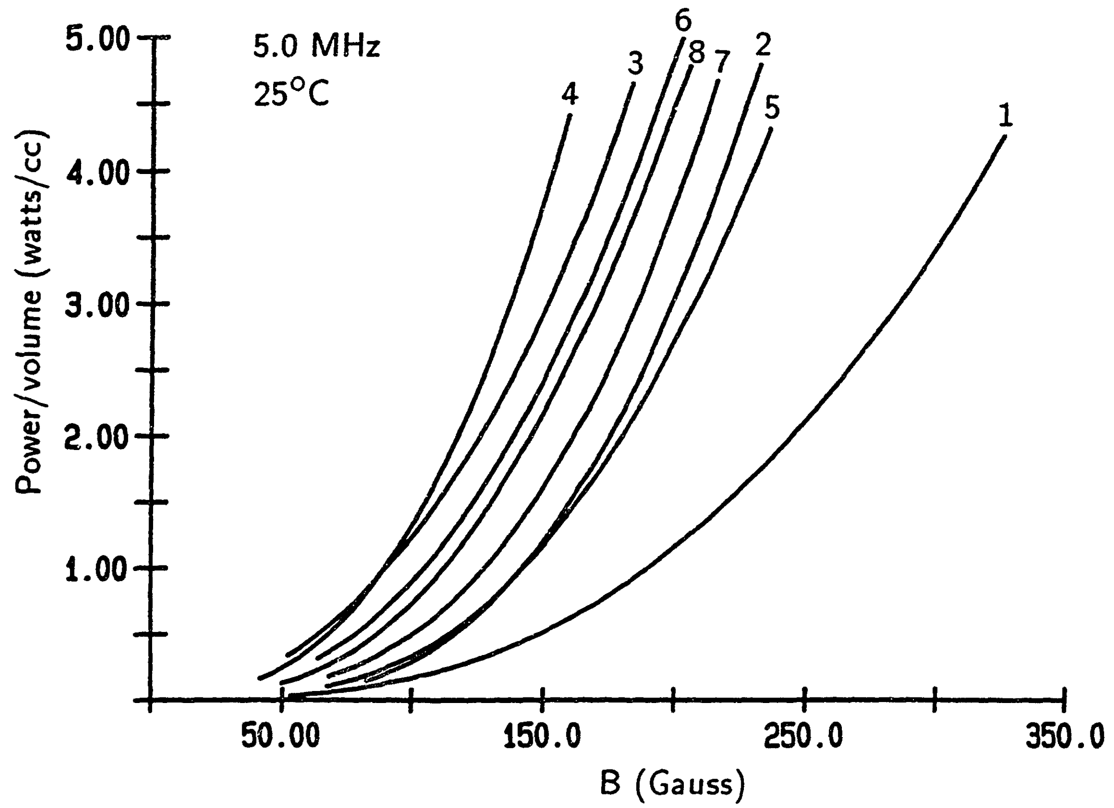

Fig. 6.5d Power loss density (watts/cm^3) versus peak B field (Gauss) for ac excitation at 5.0 MHz and 25°C.

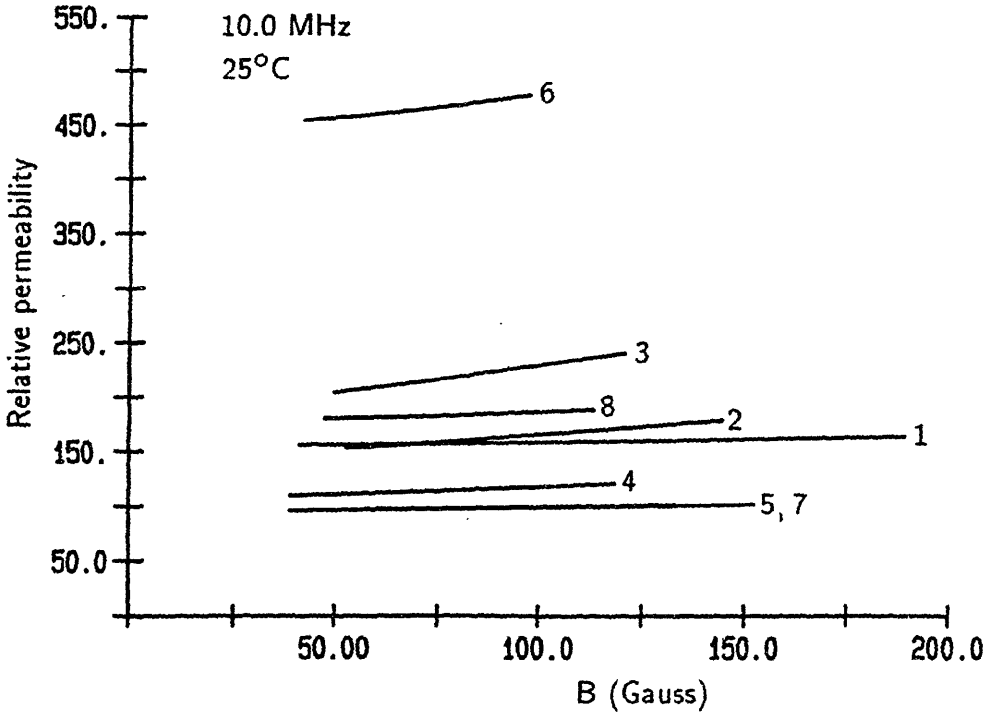

Fig. 6.5e Relative permeability versus peak B field (Gauss) for ac excitation at 10.0 MHz and 25°C.

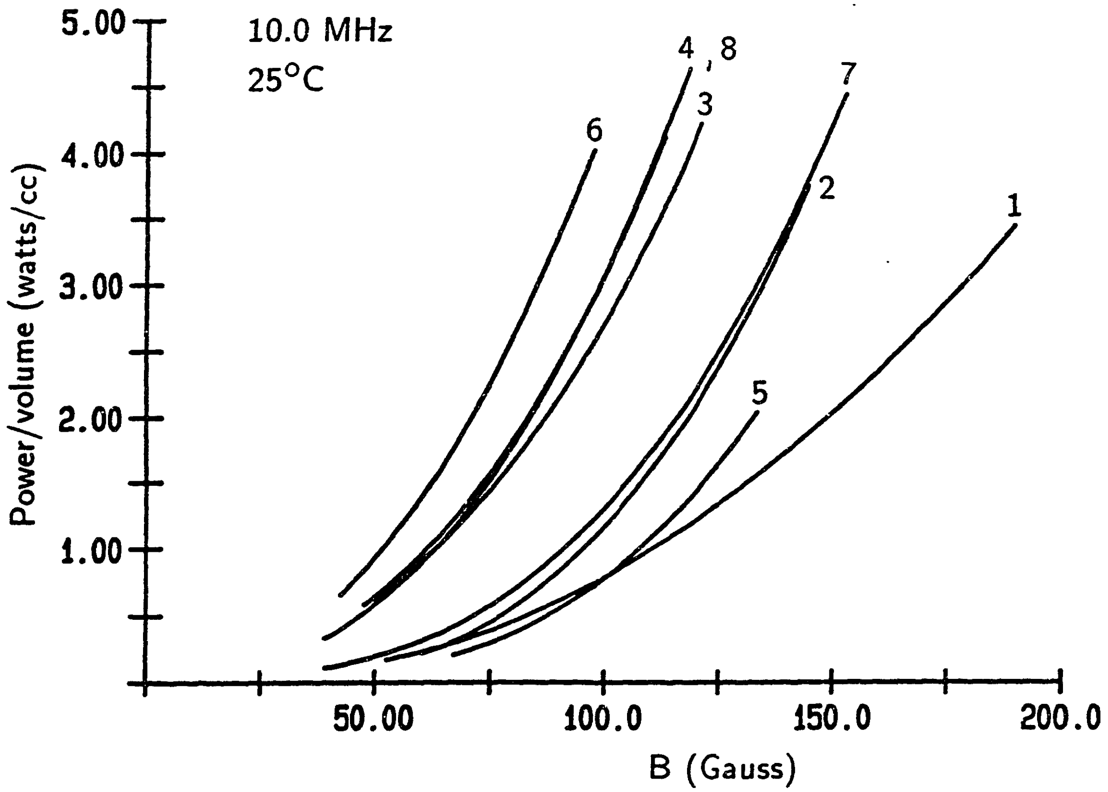

Fig. 6.5f Power loss density (watts/cm^3) versus peak B field (Gauss) for ac excitation at 10.0 MHz and 25°C.

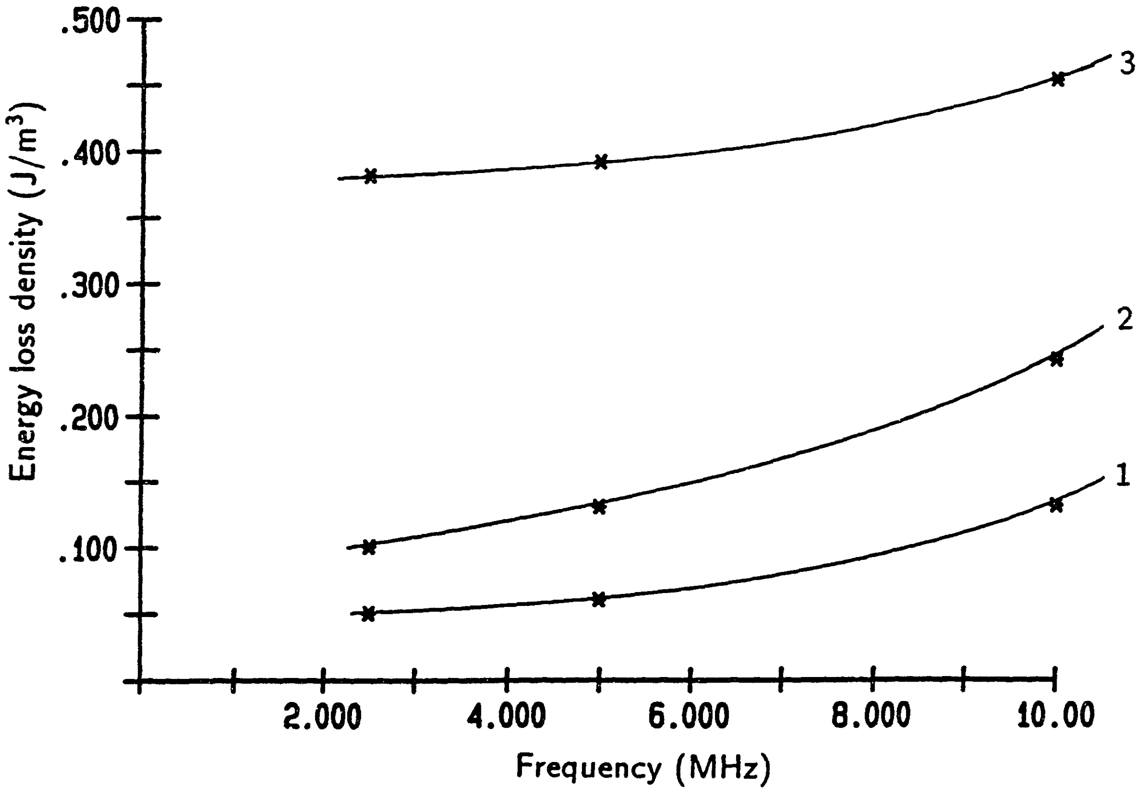

Fig. 6.6 Energy loss density per cycle (J/m^3) versus frequency (MHz) for Q1, 4C4, and C2025 materials, for an ac excitation of 125 G (peak).

than 10% of the saturation flux density of about 3000 G.

4. For applications with purely ac excitations, the Q1 material appears to offer the lowest loss.

An issue requiring further investigation is the sample-to-sample variation of properties for a particular ferrite. For each ferrite in this study, a small number of samples was acquired from manufacturers or distributors. The results presented here are based on measurements of a representative sample from each small group. For a particular ferrite recipe, the permeability and loss were found to vary from sample to sample by up to ±20%. An increased permeability was associated with increased loss, which is consistent with conclusion (2) above.

The observed variation is consistent with the ±20% tolerance specified by the manufacturers for the initial permeability. In order to investigate properly the sample-to-sample variation of permeability and loss for a particular ferrite, samples must be acquired from different processing lots. Unlike semiconductor devices, ferrites do not bear any lot information, so this investigation would require the cooperation of the ferrite manufacturers.

6.2.3.2 Excitation with DC Offset

The measurements were repeated for the first three samples listed in Table 6.3, with a dc offset added to the flux that was equal to the peak ac flux excitation. In other words, for each measurement the flux offset was chosen so that the minimum flux was zero and the maximum was the peak-to-peak amplitude of the ac excitation. This type of offset is present in some single-ended dc/dc converter topologies. The results are shown in Figs. 6.7(a)–(f).

The following conclusions can be made:

1. The dc offset generally increases the loss, most significantly for the Q1 material that performed best in the purely ac tests.
2. No irreversible changes were made to the ferrites by the dc offset.
3. At 10 MHz the 4C4 material has a lower loss density than the Q1 material, demonstrating that the material must be carefully matched to the application.

6.2.4 Error Analysis

The errors in the models of permeability and loss result from both the measurement error and the curve fit error. This section considers these error mechanisms.

The efforts to minimize measurement error by compensating for measured parasitics in software have already been described. One remaining source of error is the measurement of the core dimensions. The error in the micrometer used to measure the core dimensions is ±1 mil, which corresponds to an error of less than ±2% in each measurement. The relations for μ and P_h depend linearly on one dimension, h, but less strongly on the radii. A reasonable estimate for the error in μ and P_h introduced by the micrometer error is ±5%.

The error in the permeability curve fit is less than ±1% at each point for the purely ac excitations, and less than ±2% at each point for the excitations with a dc offset. The scatter in this fit is therefore very small. The error in the core loss curve fits, as discussed previously, rolled off from ±10% at the lowest power levels to less than ±3% at moderate and high power levels.

The overall error in the permeability curves, therefore, is less than ±7%. The error in the power loss curves is less than ±15% at the lowest power levels, rolling off to less than ±8% at moderate and high power levels.

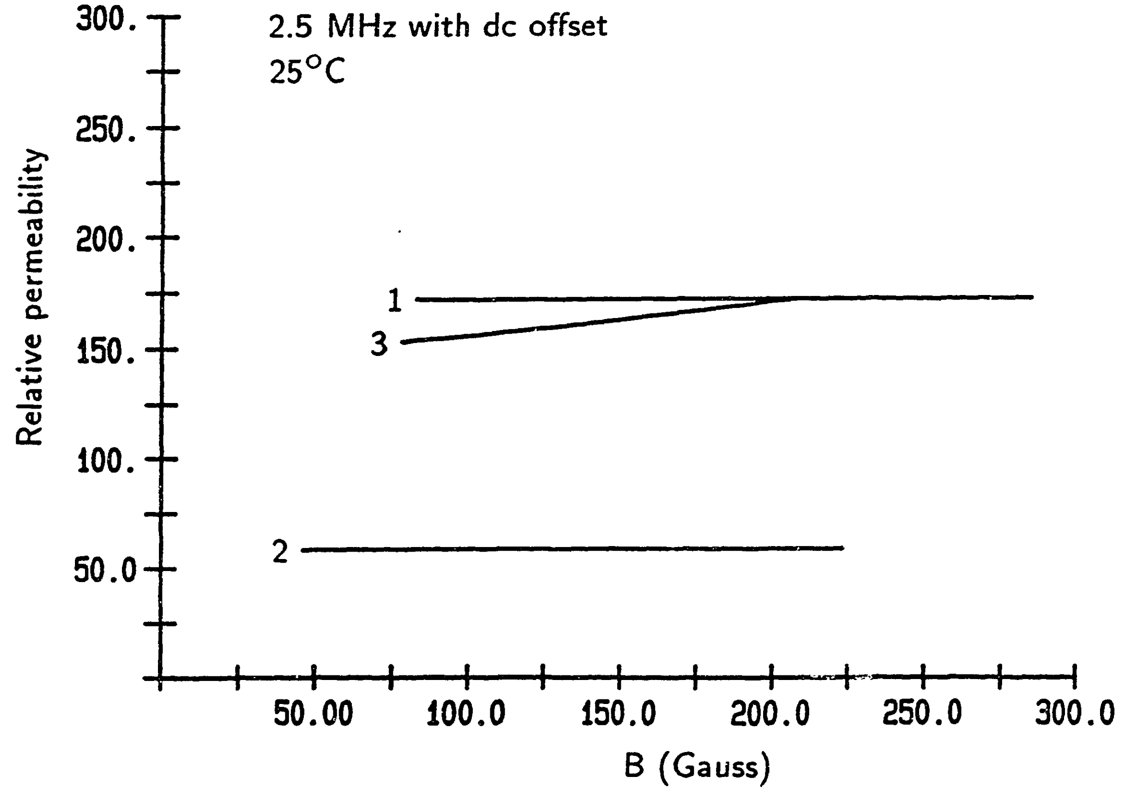

Fig. 6.7a Relative permeability versus peak B field (Gauss) for ac excitation with dc offset at 2.5 MHz and 25°C.

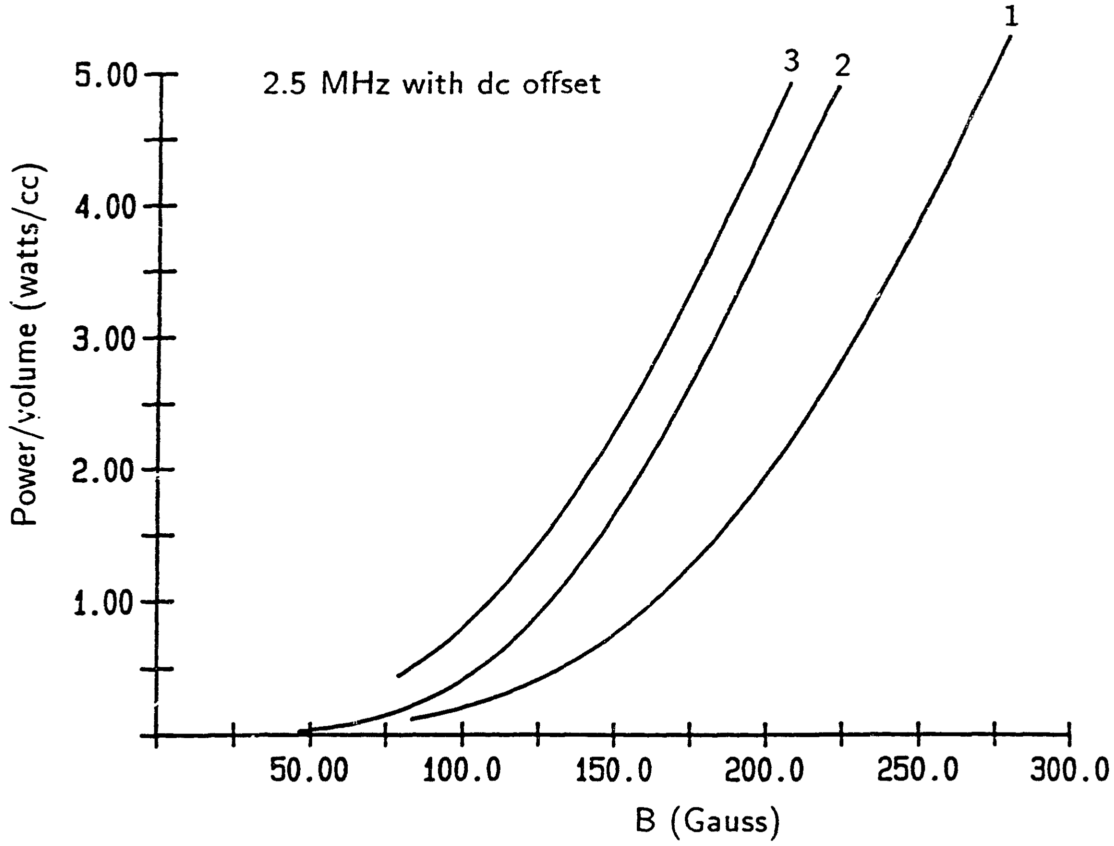

Fig. 6.7b Power loss density (watts/cm^3) versus peak B field (Gauss) for ac excitation with dc offset at 2.5 MHz and 25°C.

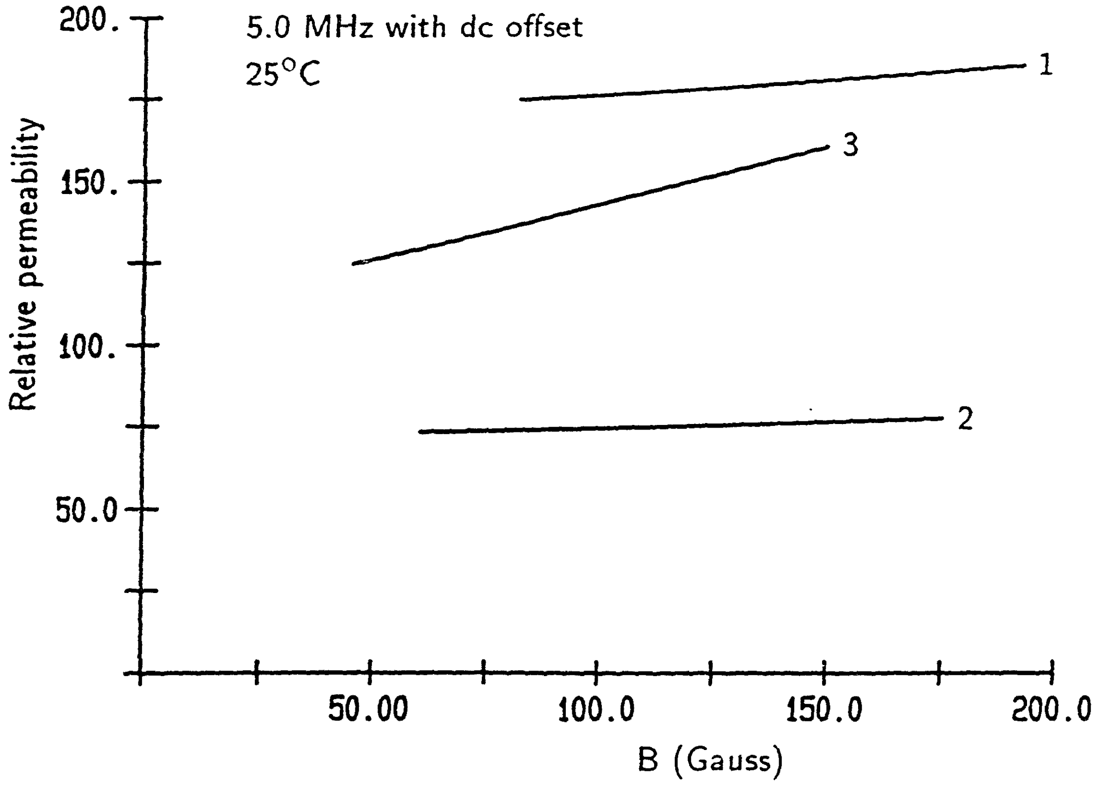

Fig. 6.7c Relative permeability versus peak B field (Gauss) for ac excitation with dc offset at 5.0 MHz and 25°C.

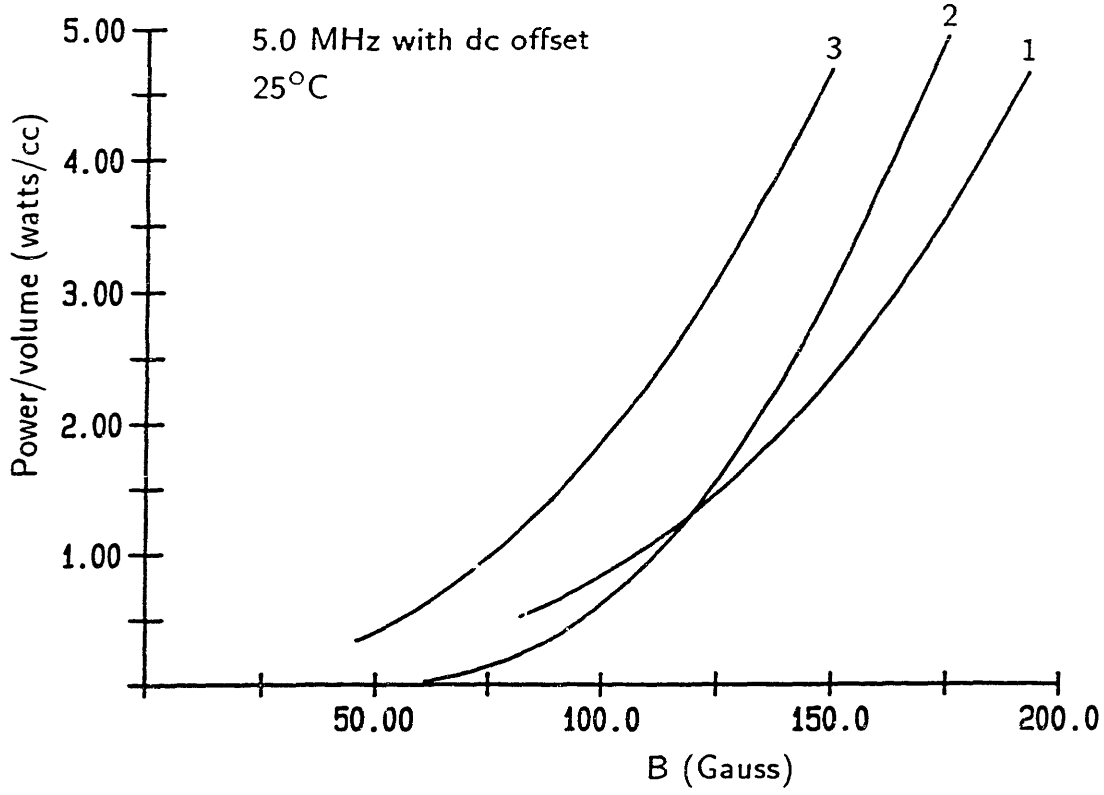

Fig. 6.7d Power loss density (watts/cm^3) versus peak B field (Gauss) for ac excitation with dc offset at 5.0 MHz and 25°C.

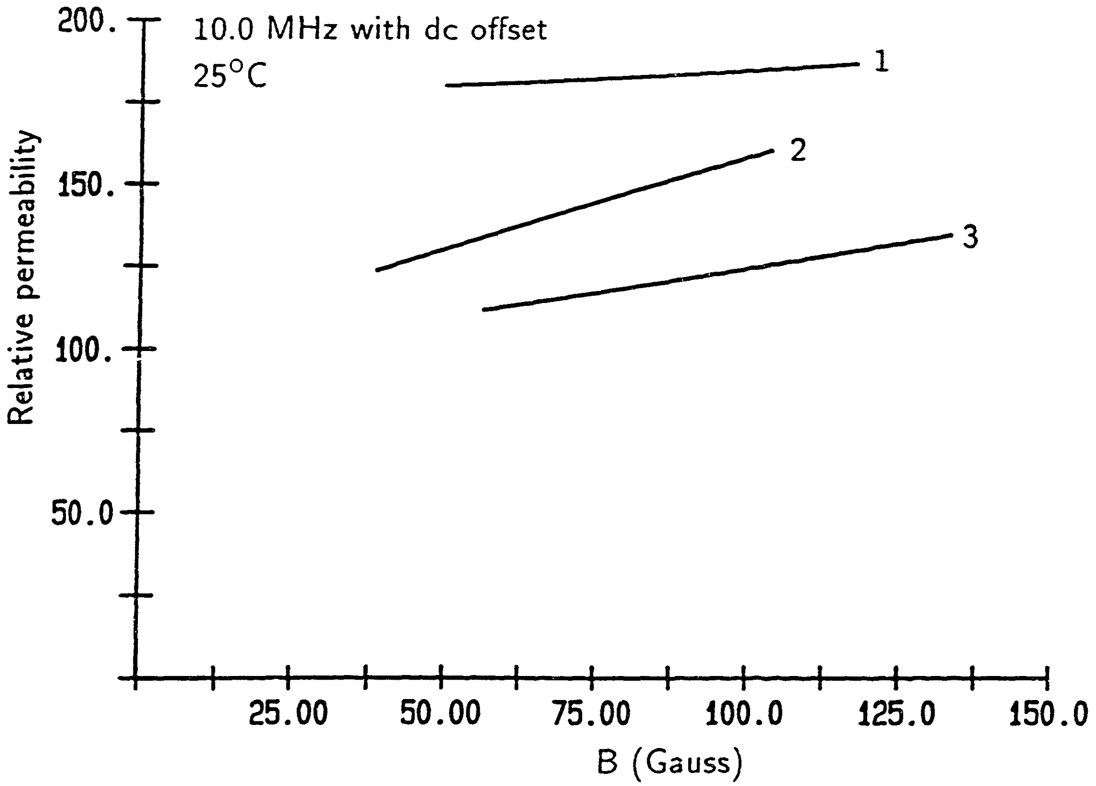

Fig. 6.7e Relative permeability versus peak B field (Gauss) for ac excitation with dc offset at 10.0 MHz and 25°C.

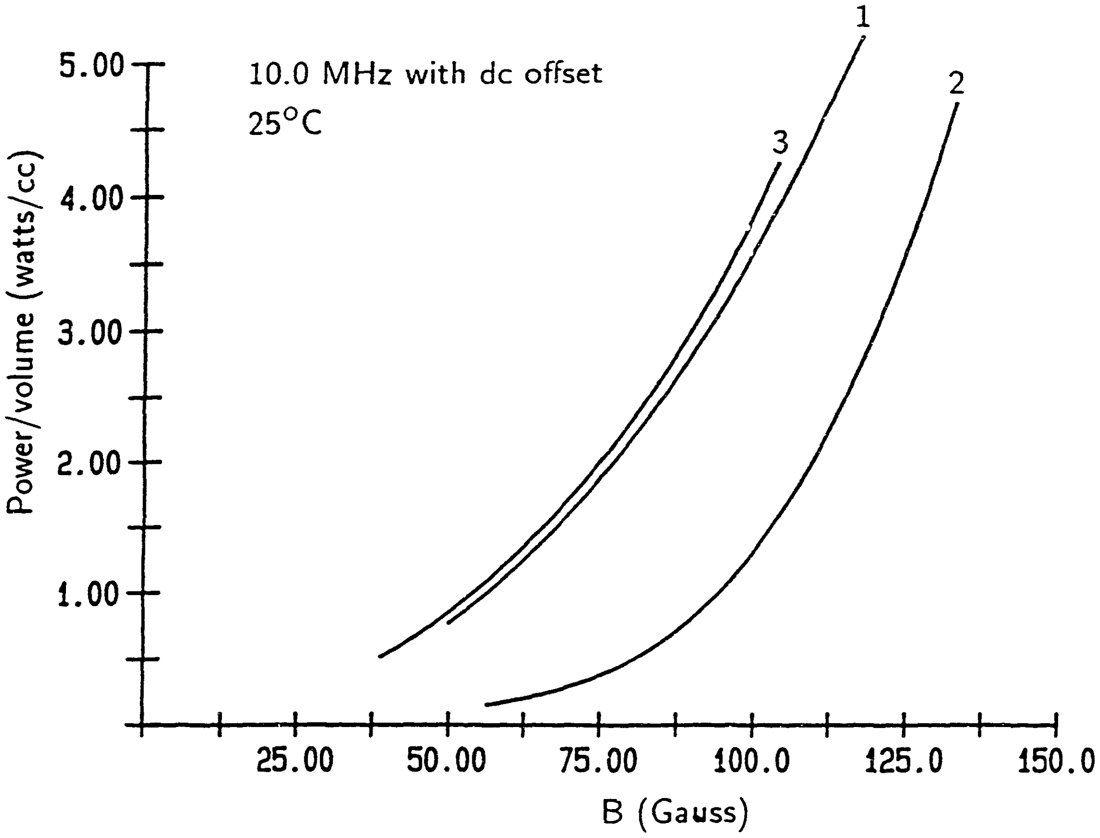

Fig. 6.7f Power loss density (watts/cm^3) versus peak B field (Gauss) for ac excitation with dc offset at 10.0 MHz and 25°C.

Chapter 7

DESIGN ANALYSIS

As a vehicle for examining some typical design tradeoffs in 1–10 MHz transformers, this chapter considers the design of a 7:1 gapped slotted transformer for the MIT high density power supply project's hybrid prototype 50 W, 42/5 V, 10 MHz dc/dc converter. This converter uses the dual resonant forward topology shown in Fig. 7.1.[1,2] First, the transformer requirements of the power circuit are discussed. Next, various design studies are presented that illustrate the relationships between frequency, volume, efficiency, and other fundamental transformer parameters. These studies first consider the designs that can be achieved with the planar windings described in Chapter 4, in which the primary and secondary were each a single layer. It should be reiterated that the copper fills only a small proportion of the available core window area, since it was found in Chapter 4 that the copper loss is greatly decreased by positioning the windings far from the slot. After the single layer windings are discussed, studies are presented that consider multilayer windings, in which multiple layers of primary and secondary are interleaved in order to reduce the copper loss. A transformer design for the MIT prototype converter is then presented.

These studies were performed by means of a computer program that incorporated both the analyses of Chapters 4 and 5 and the core loss measurements that were presented in Chapter 6. The program employs sophisticated optimization algorithms to produce a design that minimizes the transformer footprint area for a specified energy storage and total power dissipation.

It should be stressed that while the actual numbers presented in this chapter are important in that they are indicative of the performance that can be achieved with these components, the real significance of the analyses presented here is the underlying tradeoffs between the design parameters, or in other words, how the individual results found in previous chapters interact in the design of the transformer. For each issue discussed in this chapter, the numerical results produced by the program will be used as a starting point for discussion, while the analytical results of previous chapters will be used to explain *why* the numerical results turned out as they did. If the inductance or power dissipation were

---

[1] L. F. Casey and M. F. Schlecht, "A High Frequency, Low Volume Point-of-Load Power Supply for Distributed Power Systems," *IEEE Power Electronics Specialists Conference Record,* June 1987, pp. 439–450.

[2] B. Miwa, "Hybrid Construction of a 10 MHz Dc-Dc Converter for Distributed Power Systems," MIT SM Master's Thesis, September 1988.

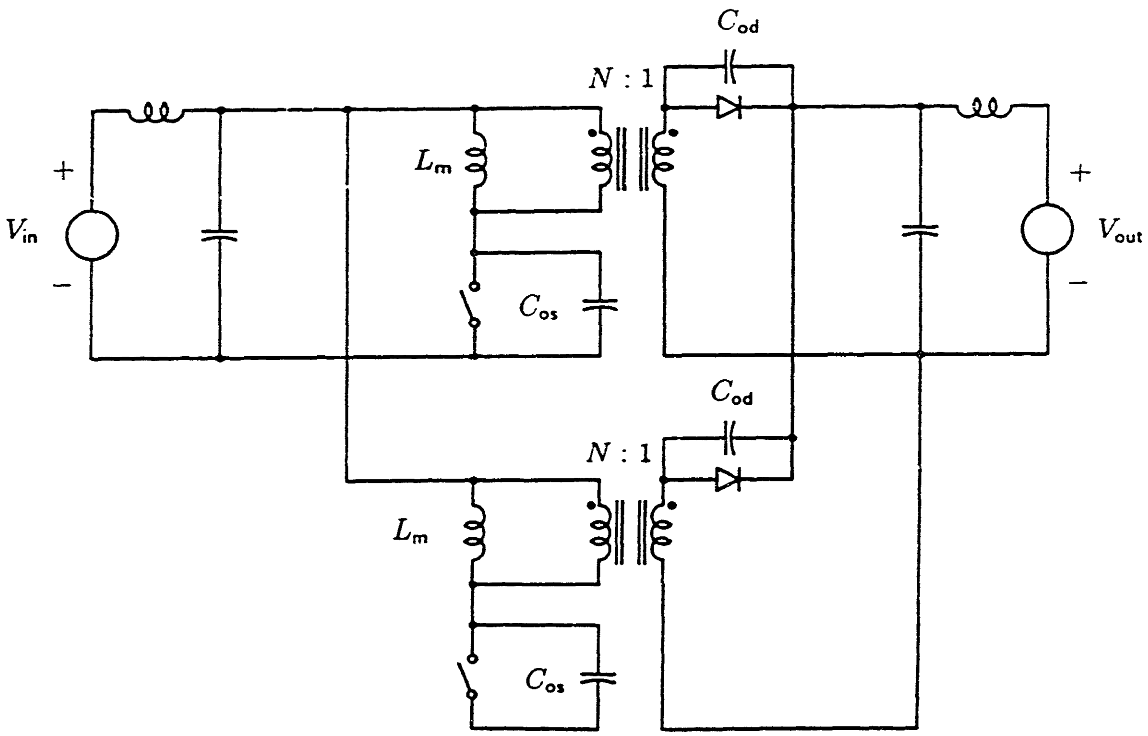

Fig. 7.1 Dual resonant forward converter.

different from those assumed here, or different core materials or conductors were used, the dimensions of the resulting transformer would be different. But the underlying tradeoffs should remain the same.

7.1 The Dual Resonant Forward Converter

The dual resonant forward converter used in the MIT prototype converter is composed of two of the resonant forward converters discussed in Chapter 1. The resonant forward converter delivers power to its load during half of its cycle. In the dual configuration two converters are operated 180° out of phase in order to deliver power to the load continuously. Since the prototype converter transfers 50 W, each of the two transformers must transfer 25 W. As described in Section 1.3, each side of the converter contains a resonant tank composed of the parasitic output capacitances of the MOSFET and the output rectifier, and the magnetizing inductance of the transformer. Since this transformer must store energy in its magnetizing inductance, the design of this component involves issues of both inductor and transformer design. Ideally, the two resonant tanks in the dual converter do not have to be matched to each other, since the harmonics in the output are ideally determined by the frequency, duty cycle, and phasing of the switches.

Table 7.1: Prototype Transformer Requirements

Parameter	Symbol	Value
Turns ratio	$N:1$	7:1
Frequency	f_o	10 MHz
Magnetizing inductance	L_m	1.3 μH
Leakage inductance	L_l	0.03 L_m
Common mode capacitance	C_c	20 pF
Differential mode capacitance	C_d	5.0 pF
Total Capacitance	$C_t = C_c + C_d$	25 pF
Total power dissipation	P_t	0.75 W

The design parameters for each of the two transformers in the dual converter are listed in Table 7.1. The value of magnetizing inductance should be achieved within about ±10%, since it determines the resonant frequency of the power circuit tank, while the values of the other energy storage elements simply represent maximum values above which they will disrupt the circuit operation. The maximum allowable leakage inductance is expressed as a fraction, approximately 3%, of the magnetizing inductance. At 10 MHz the maximum allowable leakage inductance is therefore 39 nH. The maximum values of the parasitics are determined by the requirements of the power circuit and the rationale for their choice is not considered here.[3] The switching frequency, 10 MHz, is at the top of the range considered in this thesis. Although this frequency may not necessarily result in the "best" design for the transformer, it has been chosen for the prototype converter in order to minimize the size of the entire hybrid converter. Operation at frequencies between 1–10 MHz will also be considered in this chapter and the required value of the magnetizing inductance will be assumed to be inversely proportional to the frequency, as explained in Chapter 1.

The allowable power dissipation in the transformer, given here as 0.75 W, must be determined by an analysis of the converter system as a whole. Although such a global analysis is beyond the bounds of this thesis, the general approach it would take can be outlined. First, a system analysis would determine the total converter power dissipation. One way to do this is simply to satisfy an arbitrary efficiency specification. Another way is to recognize that the converter itself will function properly only as long as its most delicate component does not exceed its operating temperature. The total allowable power loss can then be determined from a thermal analysis that considers the maximum converter operating temperature, the ambient temperature, and the thermal resistance of the converter substrate

---

[3] L. F. Casey, "Point of Load Conversion for Distributed Power Systems," MIT PhD Thesis (in progress).

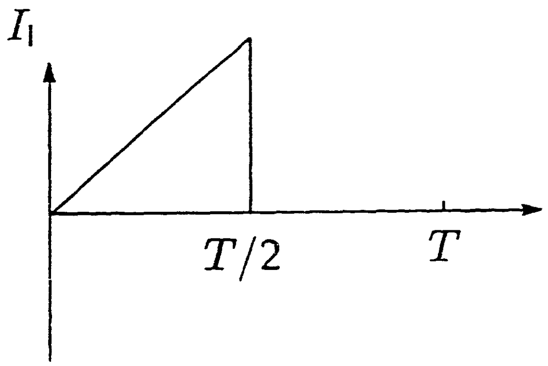

Fig. 7.2 Primary load current.

and its heat sink. Once the total converter power dissipation has been determined, a power loss budget can be allocated to each component of the transformer. For the purposes of this design, each of the two transformers has been allocated a loss budget of 0.75 W. The effect of varying the loss budget will be presented later in this chapter.

The impact of the loss budget on the transformer design depends on the nature of the magnetizing and load currents. The currents present in the prototype converter are graphed in Figs. 7.2 and 7.3, and their amplitudes given in Table 7.2. Note that the magnetizing current has essentially no harmonics. This fact will greatly simplify the calculation of the copper loss given in the next section. The triangular load current, on the other hand, has harmonics, some of which are in phase with the magnetizing current. The amplitude of the load current is given in terms of the turns ratio, since the constraint that determines the load current is that the converter deliver 50 W at 5 V. This mandates an average load current of 10 A, so that each of the two transformers must deliver an average load current at the secondary of 5 A. The average value of the triangular load current is 25% of its peak. The peak load current at the secondary of each transformer is therefore 20 A, and the peak load current reflected to the primary is ($20/N$ A).

7.2 Copper Loss

This section derives expressions for the copper loss in the gapped slotted transformer, based on the lumped parameter model that was derived in Chapter 5 and the magnetizing and load currents of Figs. 7.2 and 7.3. These expressions were used in the computer program that generated the design studies. These studies will assume that the widths of the primary turns are chosen in order to minimize the copper loss, as discussed in Chapter 5. The

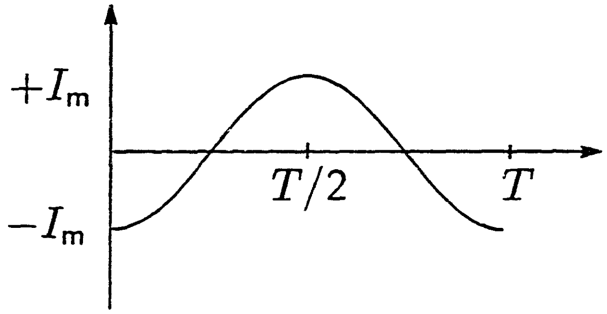

Fig. 7.3 Primary magnetizing current.

Table 7.2: Current Amplitudes		
Parameter	Symbol	Value
Magnetizing Current	I_m	0.75 A
Load Current	I_l	$20/N$ A

transformer that was actually built and measured and is discussed in the next chapter had, for simplicity of fabrication, primary turns of equal width.

Before the copper loss can be computed, the distribution of the magnetizing current between primary and secondary must be considered. Determining the distribution of magnetizing current between primary and secondary in the resonant forward converter is a complicated task, especially since this circuit has a time varying circuit topology. Therefore, this analysis will use the approximation described in Section 4.4, in which the primary is below the secondary and is assumed to carry all of the magnetizing current. This approximation is justified by the following argument, which attempts to show that for the values of current in this study there is a negligible difference between assuming that all the magnetizing current flows in one winding and assuming that the magnetizing current splits evenly between primary and secondary.

First, neglect the spacing between the primary turns, so that the primary resistance is equal to the reflected secondary resistance. Since the spacing is small compared to the width of each turn, this is a reasonable approximation. Second, assume that the load and magnetizing currents have the same distribution in both windings. It was shown in Section 5.4 that in this transformer the load and magnetizing currents have the same distribution in the bottom winding, but not the top winding. If all the magnetizing current flows in the primary, then the total copper loss, using the current waveforms of Figs. 7.2 and 7.3, is equal to

$$P_c = R_p\left[\frac{1}{2}I_m^2 + \frac{1}{3}I_l^2 + \frac{I_m I_l}{\pi^2}\right] \tag{7.1}$$

If, on the other hand, half of the magnetizing current flows in the primary and half flows in the secondary, then the total copper loss is given by

$$P_c = R_p\left[\frac{1}{4}I_m^2 + \frac{1}{3}I_l^2 + \frac{I_m I_l}{\pi^2}\right] \tag{7.2}$$

For the currents given by Table 7.2 for the 7:1 transformer considered in this chapter, (7.1) is only about 4% larger than (7.2). This would suggest that only a small error is added by assuming all the magnetizing current is in the primary winding. Since in this study the load current is much larger than the magnetizing current, it is asserted that the error introduced by assuming that the magnetizing current flows entirely in the primary is small. Therefore, the expression for the copper loss derived below is similar to (7.1) and has been adjusted for the difference in resistance between the primary and secondary.

In order to facilitate the computation of the copper loss, the magnetizing and load currents are expressed below as Fourier series. The magnetizing current shown in Fig. 7.2 is essentially sinusoidal and can be expressed as

$$i_m(t) = -I_m\cos(2\pi f_o t) \tag{7.3}$$

where I_m is the amplitude of the magnetizing current and f_o is its switching frequency of the converter. The triangular load current can be expressed by the Fourier series,

$$i_l(t) = I_l\left[\frac{1}{4} + \sum_{m=1}^{\infty}\frac{(-1)^{m+1}}{\pi m}\sin(2\pi f_o mt) - \sum_{n=0}^{\infty}\frac{2}{\pi^2(2n+1)^2}\cos(2\pi f_o nt)\right] \tag{7.4}$$

Equation (7.4) shows that the load current is composed of a dc component, a square wave (represented by the second term, whose harmonics fall off as $1/m$), and a triangle wave (represented by the third term, whose harmonics fall off as $1/n^2$).

7.2.1 Copper Loss in the Primary Winding

First, consider the copper loss in the primary winding. There is a dc term due to the dc component of the load current that can clearly be computed separately from the ac components. On the other hand, the power loss associated with the ac terms must be computed from the sum of the magnetizing current's cosine term and the load current's sines and cosines. However, as discussed in Section 5.4, this computation can be greatly simplified in the case of the gapped slotted transformer. In the primary the field distribution associated with the load and magnetizing currents are both essentially the same. The field is maximum at the top surface of the primary, and negligible below the primary, so that in any incremental volume of the primary, the load and magnetizing currents maintain the same relative phase difference present at the transformer terminals and are subject to the same effective resistance. For a skin depth thick winding, this effective resistance was shown in Appendix A to be 1.09 times the primary's dc resistance. As explained in Chapter 4, the windings are assumed to be a skin depth thick at the fundamental frequency. Since the skin depth is inversely proportional to the square root of the frequency, the effective resistance presented to the harmonics also increases with frequency. But at higher harmonics, the physical thickness of the winding is larger than a skin depth and the 1.09 correction factor is dropped. Therefore, in this analysis the approximation is made that the resistance presented to the n^{th} harmonic is

$$R_n = R_{dc}\sqrt{f_n/f_o} = \sqrt{n}R_{dc}, \qquad n > 1 \tag{7.5}$$

where f_o is the fundamental frequency and f_n is the n^{th} harmonic.

In the primary winding, therefore, the copper loss can be computed from (7.3), (7.4), and (7.5) as

$$\begin{aligned} P_{c,p} = \left(\frac{I_l}{4}\right)^2 R_{p,dc} + \frac{I_l^2}{2\pi^2}\left[1.09 + \sum_{m=2}^{\infty}\left(\frac{(-1)^{m+1}}{m}\right)^2\right](\sqrt{m}R_{p,dc}) \\ + \frac{1}{2}\sum_{n=0}^{\infty}\left(I_m\delta_{0n} + \frac{2I_l}{\pi^2(2n+1)^2}\right)^2 (1+0.9\delta_{0n})\sqrt{2n+1}\; R_{p,dc} \end{aligned} \tag{7.6}$$

where δ_{0n} is the Kronecker delta function[4] and $R_{p,dc}$ is given by (5.6), repeated here as (7.7),

$$R_{p,dc} = \frac{2\pi}{\sigma t}\sum_{n=1}^{N}\frac{1}{\ln(r_{n+1}/r_n)} \tag{7.7}$$

In the studies of this chapter, the r_n are chosen according to (5.10), the condition for minimum copper loss, repeated here as (7.8),

$$r_{n+1} = r_n\left(\frac{r_{wo}}{r_{wi}}\right) \tag{7.8}$$

The harmonics of the square wave component of the load current will add substantial power loss. Although the harmonics of the square wave component of i_l^2 are falling off as $1/m^2$, the decrease in the skin depth causes the power dissipation of the harmonics to roll

---

[4] $\delta_{mn} = 1$ for $m = n$, else $\delta_{mn} = 0$.

off slower, as $1/m^{3/2}$. The harmonics of the triangle wave component of the load current, on the other hand, do not add significantly to the power loss. The power dissipation of the harmonics of the triangle wave component of i_l rolls off as $1/n^{7/2}$, and the first nonzero harmonic is $n = 3$. This only adds about 2% to the power dissipation, so that only the fundamental of the triangle wave component will be included in the power dissipation analysis. In order to evaluate the summation associated with the square wave component of the load current, the conservative approximation was made that the current waveforms in the power circuit are limited to below 150 MHz, which at 10 MHz would correspond to the first 15 harmonics. The summations in (7.6) were consequently evaluated, replacing the upper limit of ∞ with 15, giving

$$P_{c,p} = R_{p,dc}\left[I_l^2\left[\frac{1}{16}+\frac{2.19}{\pi^2}\right]+\frac{1.09}{2}(I_m+0.20I_l)^2\right] \tag{7.9}$$

7.2.3 Copper Loss in the Secondary Winding

Since this analysis assumes that all the magnetizing current flows in the primary, the copper loss in the secondary will be due to the load current and to the eddy current induced by the magnetizing current in the primary. Appendix E shows that the copper loss in the secondary is, under this approximation, given by

$$\begin{aligned} P_{c,s} = {} & \left(\frac{I_l}{4}\right)^2 N^2 R_{s,dc} + \frac{I_l^2}{2\pi^2}\left[1.09 + \sum_{m=2}^{\infty}\left(\frac{(-1)^{m+1}}{m}\right)^2\right]\left(\sqrt{m}N^2 R_{s,dc}\right) \\ & + \frac{1}{2}\sum_{n=0}^{\infty}\left(\frac{2I_l}{\pi^2(2n+1)^2}\right)^2(1+0.9\delta_{0n})\sqrt{2n+1}\;N^2 R_{s,dc} \\ & + \frac{0.32N^2 R_{s,dc}}{2}\left(I_m^2+\frac{2I_l I_m}{\pi^2}\right) \end{aligned} \tag{7.10}$$

Equation (7.10), when evaluated for the first 15 harmonics, becomes

$$\begin{aligned} P_{c,s} &= N^2 R_{s,dc} I_l^2\left[\frac{1}{16}+\frac{2.19}{2\pi^2}+\frac{1.09(0.20)^2}{2}\right] \\ &\quad + \frac{0.32N^2 R_{s,dc}}{2}(I_m^2+0.20I_l I_m) \\ &= N^2 R_{s,dc}(0.20I_l^2+0.16I_m^2+0.032I_m I_l) \end{aligned} \tag{7.11}$$

where $R_{s,dc}$ is given by

$$R_{s,dc} = \frac{2\pi}{\sigma\delta\ln(r_{wo}/r_{wi})} \tag{7.12}$$

It should be reiterated here that although limiting the secondary thickness to a skin depth minimizes the eddy currents induced by the magnetizing current in the primary, the loss associated with the dc component of the load current would be decreased by increasing the thickness. This issue of trading off circulating current loss with dc current loss by varying the secondary thickness was first raised in Section 4.4. Although this tradeoff is not addressed in this work, which assumes that the windings are all one skin depth thick, it is an important issue for future investigation.

7.3 Description of Design Study Computer Program

This section describes the computer program that was used to study the design tradeoffs. The source code for the program, ZZCHAP7.C, is given in Appendix G. The program contained a list of independent variables, given in Table 7.3, and a list of dependent variables, given in Table 7.4. These independent and dependent variables were related by formulas based on those developed in Chapter 5, and the material properties were based on measurements of the Indiana General $Q1$ material described in Chapter 6. The value of the magnetizing inductance, given in Table 7.1 as 1.3 μH at 10 MHz, is assumed here to vary inversely with frequency, as explained in Section 1.3. The specific procedures used by the program are outlined below.

The program iterates to find the inner slot radius, r_{wi}, outer slot radius, r_{wo}, and outer radius, r_o, that result in a transformer that occupies the minimum total area while providing both the required magnetizing inductance and the required total power dissipation. At every step in the iteration to minimize the total transformer area, the program guesses values for r_{wi} and r_o and then performs a secondary iteration to find the value of r_{wo} that would give the required total power loss. The program uses the Powell multidimensional optimization algorithm to determine r_{wi} and r_o, and the Brent root finding algorithm to determine r_{wo} at each iteration of the Powell algorithm.[5] The last parameter computed is the gap length. The program neglects the reluctance of the magnetic material, so the gap may in reality need to be somewhat smaller than the computed value.

The rest of this section discusses the relationships between the core dimensions, power dissipation, and size at a fixed frequency. For simplicity, in this discussion r_o is constrained to be equal to the value that would make the area of the center post equal to that of the flux return area at the edge of the core. Although the computer program did not operate under this constraint, the assumption simplifies the discussion without significantly changing the underlying behavior.

---

[5] W. H. Press et al., *Numerical Recipes in C: The Art of Scientific Computing*, Cambridge University Press, New York (1988), pp. 255–352.

Table 7.3: Independent Variables of Design Study

Variable	Symbol	Value(s)
Total Power Loss	P_t	0.75–1.5 W
Frequency	f	1–10 MHz
Turns Ratio	N_r	7
Turns on Secondary	N_s	1,2
Peak Magnetizing Current	I_m	0.75 A
Peak Load Current	I_l	$(20/N)$ A
Magnetizing Inductance	L_m	$13.3/f$ H
Primary Turn Spacing	Δ	70 μm
Primary / Secondary Separation	m	25 μm
Winding Thickness	t	δ
Dielectric Constant of Winding Substrate	ϵ	$3.2\epsilon_o$
Conductivity of Copper (25°C)	σ	$5.8\times10^7\ (\Omega\text{m})^{-1}$

Table 7.4: Dependent Variables of Design Study

Variable	Symbol
Inside Slot Radius	r_{wi}
Outer Slot Radius	r_{wo}
Outer Core Radius	r_o
Gap Length	g
Total Transformer Height	
Total Transformer Area	
Dc Primary Resistance	$R_{p,dc}$
Dc Secondary Resistance	$R_{s,dc}$
Maximum B field	B_{max}
Copper Loss	P_c
Core Loss	P_h
Leakage Inductance	L_l
Differential Mode Capacitance	C_d
Common Mode Capacitance	C_c

It should also be noted that the core loss, P_h, occurs almost entirely in the center post and in the core's outer edge, and not in the top and bottom plates. Although the core plates increase in area as r_{wo} is increased, they do not contribute appreciably to the total core loss. Their core loss is nevertheless calculated by the program and included in the design procedure. Due to the cylindrical geometry, the flux density in the top and bottom plates falls off as $1/r$. The thickness of the top and bottom plates was chosen to be $r_{wi}/2$, so that the flux density at the center of the plate is equal to the flux density in the center post. Consequently, at large r the flux density and core loss in the top and bottom plates is negligible.

Since the core loss is small in the top and bottom plates, one might conclude that their thickness should be reduced. While this can be done, it should be remembered that on a printed circuit board, the primary requirement is that each component have a small area footprint. And while achieving a low profile is an important, but secondary objective, it should be pointed out that even with the thick top and bottom plates, the transformers are typically less than 10 mm high. The much easier fabrication possible with thicker ferrite plates will probably greatly outweigh the advantage of reducing the transformer height by 1–2 mm.

A typical curve relating the total core area with r_{wi} is shown in Fig. 7.4. Note first that the total area increases rapidly when r_{wi} approaches small values. In order to give the required magnetizing inductance, the flux density varies inversely with the area of the center post, given by $A_i = \pi r_{wi}^2$. Since only the center post and the outer edge contribute significantly to the core loss,

$$P_h \propto (B^2 + k_1 B^4)A_i \propto \left(\frac{1}{A_i} + \frac{k_2}{A_i^3}\right) \tag{7.13}$$

where the dependence of P_h on B comes from the core loss model developed in Chapter 6, and k_1 and k_2 are constants. Equation (7.13) shows that the core loss increases as A_i decreases. To maintain the constant total power dissipation, the copper loss must decrease, so that r_{wo} must increase in order to accommodate more copper. Hence the total transformer area increases.

The increase in area for large r_{wi} occurs because as r_{wi} is increased, the length of the winding turns increases, so that r_{wo} must increase in order to limit the increase in copper loss. Although the core loss decreases with increasing r_{wi}, it is only a small percentage of the total; typically, even for the minimum area design the core loss is only 20% of the total loss.

The secondary iteration that determines r_{wo} for each guess of r_{wi} and r_o finds the

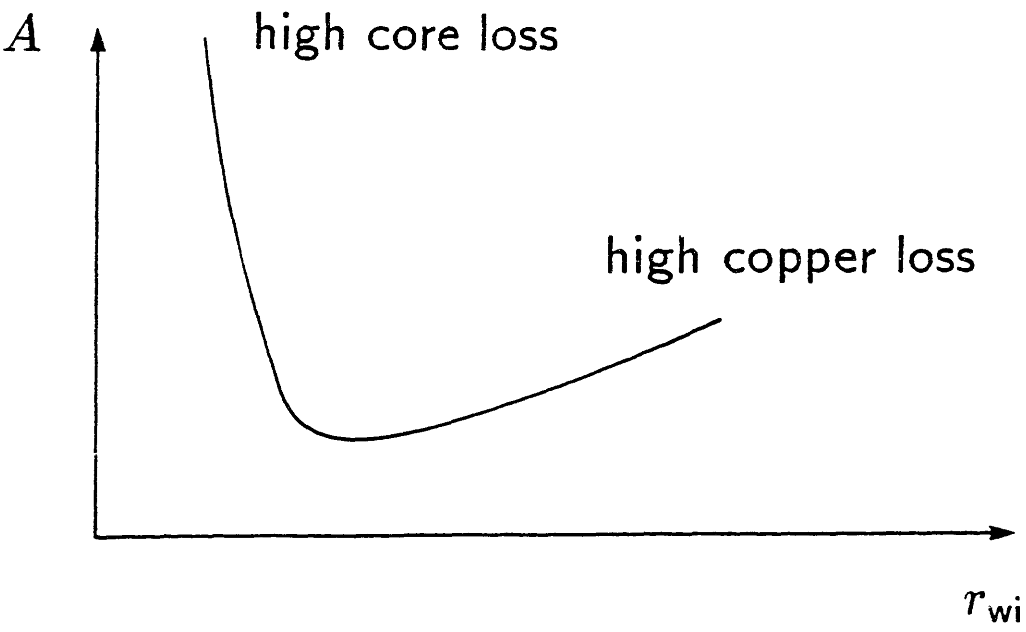

Fig. 7.4 Variation of transformer footprint area with r_{wi}.

value of r_{wo} that makes the computed total power dissipation, P_t', equal to the required total power dissipation, P_t. Figure 7.5 shows a typical curve relating $P_t - P_t'$ to r_{wo}. Note that there are two roots. The smaller one corresponds to a transformer with a smaller area, and is therefore the required root in this application. The shape of the curve is explained by the following discussion.

For small r_{wo} near r_{wi}, the small slot width causes the copper loss to be very high, so that $P_t' > P_t$. As r_{wo} is increased, it reaches the value where the sum of the copper and core loss equals the required total dissipation. This value of r_{wo} is the required root in this application. As r_{wo} is increased beyond this point, the total power dissipation falls increasingly below the value that the design will tolerate, so that the transformer is unnecessarily large. However, as r_{wo} is further increased, the core loss increases as the copper loss decreases, for a reason explained in the next paragraph. The computed total loss, P_t', eventually reaches a minimum, corresponding to the maximum in Fig. 7.5. As r_{wo} is raised above this point P_t' increases, until r_{wo} reaches a value where P_t' again is equal to P_t, corresponding to the second root in Fig. 7.5. But this second root yields a much larger transformer than the first root, so that the first root is used for the design.

The reason that the core loss increases with increasing r_{wo} is that the height of the transformer, and therefore the core volume, is increasing. While the area of the top

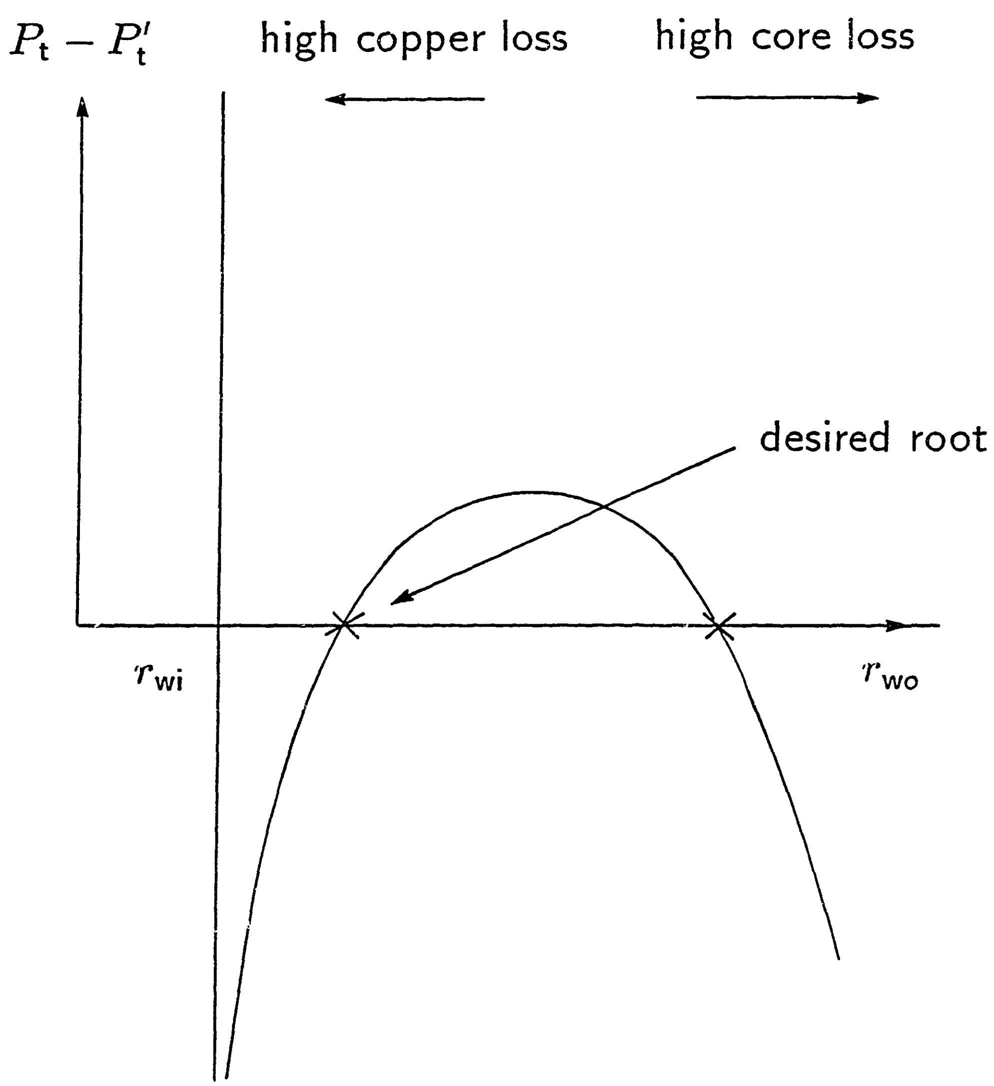

Fig. 7.5 Variation of $P_t - P_t'$ with r_{wo}.

and bottom core plates is also increasing, it was explained above that these plates do not contribute significantly to the core loss. As explained in Chapter 4, in order to minimize proximity effects and copper loss, the slot depth should be at least 40% of the slot width. This is the constraint used by the program. As r_{wo} increases and r_{wi} is held fixed, the slot width increases. The height of the transformer consequently increases, increasing the core volume and the core loss. Of course, although making the slot depth 40% of its height may minimize the copper loss, it may not minimize the total loss. This tradeoff is not considered here, but since reasonable designs will be shown to be typically dominated by copper loss, including the tradeoff should not alter the results significantly.

For the particular values of conductivity and core loss that were used in this study, the first root corresponds to a high copper loss, low core loss, minimum area design, while the second root corresponds to a low copper loss, high core loss, larger area design. This result is typical for the conductors and magnetic materials used at these frequencies. It should be pointed out, however, that the fact that the minimum area solutions are dominated by copper loss depends on the actual numbers that are used for conductivity and core loss. If the conductivity were raised and the other parameters held constant, eventually both roots would be high core loss solutions, while if the conductivity were lowered and the other parameters held constant, eventually both roots would be high copper loss solutions.

Figure 7.6 shows a representative curve relating the transformer footprint area to P_t. This particular curve is for a 5 MHz design, but the general shape of the curve is the same at other frequencies. This curve has a pronounced knee. To the left of the knee, a small reduction in the allowable power dissipation has a large cost in increased transformer area. To the right of the knee, allowing a large increase in power dissipation buys only a small decrease in transformer area. The transformer design corresponding to the knee of the curve therefore represents a reasonable balance between transformer area and power dissipation. The knee can be moved to the left by incorporating more copper into the structure through interleaving layers of primary and secondary, a strategy that is discussed later in this chapter.

The shape of the curve in Fig. 7.6 is explained by the following discussion. First, consider the region to the left of the knee. Decreasing the allowable power dissipation corresponds to raising the axes in Fig. 7.5 relative to the curve. The value of r_{wo} that corresponds to the minimum area root steadily increases as the axes are raised, and if the axes of Fig. 7.5 are raised high enough, then it would appear that there would be no root. In order for there to be a root, the core loss must be decreased so that the curve is moved up, relative to the axes, and in order to reduce the core loss, as explained above, r_{wi} has to be increased. Since the copper loss is proportional to $1/\ln(r_{wo}/r_{wi})$, as was shown in Appendix B, the dependence of r_{wo} on r_{wi} and the copper loss, P_c, is given by

$$r_{wo} = r_{wi} e^{k/P_c} \tag{7.14}$$

where k is a constant. While (7.14) obviously shows that the increase in r_{wi} increases r_{wo}, it more importantly shows that as P_c is forced to decrease by the fall in allowable total dissipation, r_{wo} increases *exponentially* as e^{k/P_c}. This relationship gives rise to the steep

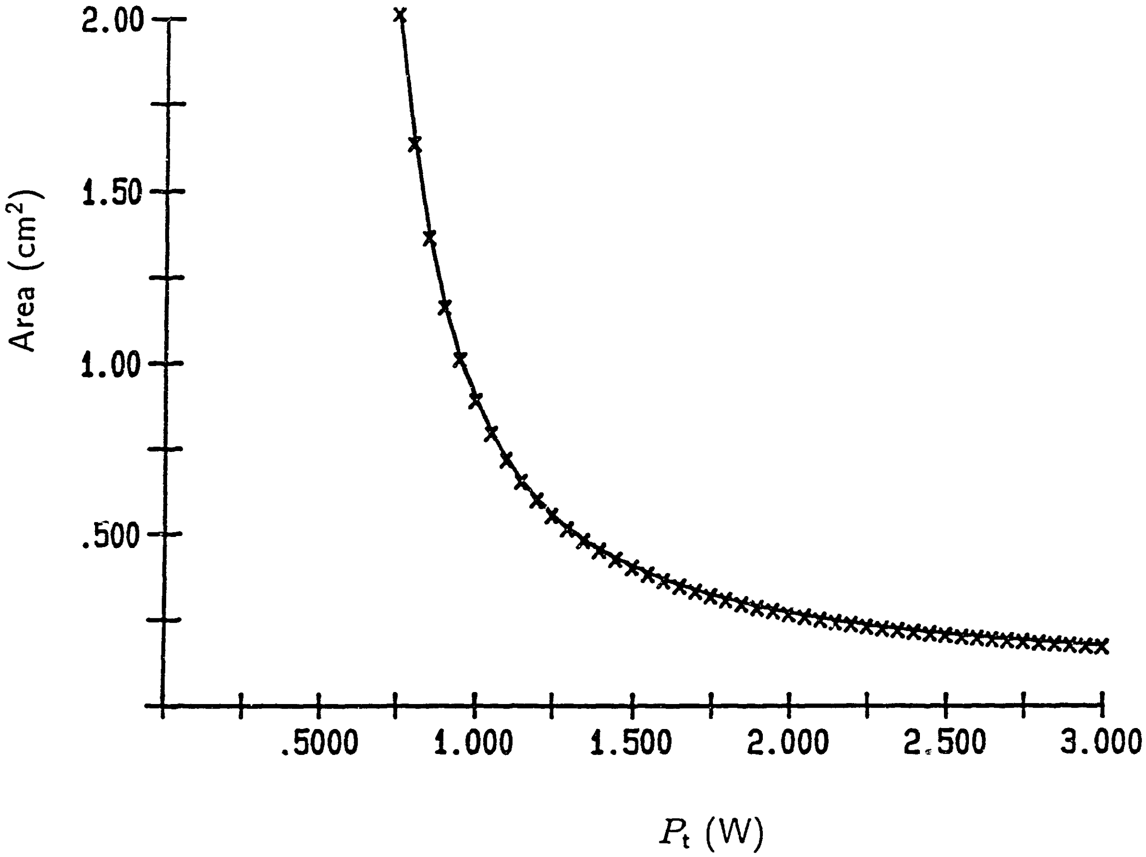

Fig. 7.6 Variation of transformer footprint area with P_t.

increase in transformer area to the left of the knee in Fig. 7.6.

Second, consider the region to the right of the knee in Fig. 7.6, where a large increase in allowable power dissipation buys only a small decrease in transformer footprint. Increasing the allowable power dissipation corresponds to lowering the axes in Fig. 7.5 relative to the curve. Since the part of the curve in Fig. 7.5 to the left of the required root is almost vertical, lowering the axes will not change the position on the root on the r_{wo} axis by very much, so that the transformer footprint does not change very much. Equivalently, the e^{k/P_c} factor in (7.14) is very close to unity and changes its value very little with increasing P_c for $k/P_c \ll 1$.

The existence of the knee in the footprint vs. power loss curve is of great importance to the transformer designer. In designing 1–10 MHz transformers, one should generate such a curve in order to avoid producing a design that dissipates an unnecessarily large amount of power or occupies an unnecessarily large area.

Table 7.5: Comparison of 7:1 and 14:2 Designs
A_i/A_o Constrained

Parameter	Symbol	7:1 Design	14:2 Design
Maximum B field	B_{max}	290 G	71 G
Ratio of Center Post Area to Outer Edge Area (Constrained)	A_i/A_o	1.0	1.0
Inside Slot Radius	r_{wi}	1.8 mm	2.5 mm
Outer Slot Radius	r_{wo}	5.2 mm	81.1 mm
Transformer Outer Radius	r_o	5.4 mm	81.2 mm
Transformer Height	h	3.3 mm	34 mm
Core Loss	P_h	0.20 W	0.11 W
Copper Loss	P_c	0.80 W	0.89 W

7.4 The Importance of A Single Turn Secondary

The analyses of Chapters 4 and 5 all assume that the required turns ratio is realized with a one turn secondary. But it has not yet been shown that a one turn secondary necessarily yields the smallest transformer. If the area of the center post were held constant, then more turns would provide the same inductance with a lower B field in the core. The lower core loss might outweigh the increase in copper loss from the additional turns and might permit a smaller transformer with the same loss as one with a single turn secondary.

This is not the case, as one might expect from the statement in the previous section that core loss is typically only 20% of the total dissipation. Table 7.5 gives a comparison between two 5 MHz transformer designs. Each provides the same magnetizing inductance (2.8 μH), but one uses a 7:1 planar spiral winding and the other uses a 14:2 planar spiral winding. In order to simplify the understanding of the underlying relationships, in the designs of Table 7.5, the outer radius was constrained to be equal to the value that would make the area of the center post equal to that of the flux return area at the edge of the core. After the relationships have been explained, a pair of designs for which the full optimization has been performed will be presented.

The inductance is essentially proportional to $N^2 r_{wi}^2/g$, so that doubling N means that r_{wi}^2/g must fall by a factor of 4. Inspection of Table 7.5 shows that this occurs by r_{wi} increasing as $\sqrt{2}$, so that the gap length must have increased by a factor of 8. Therefore, the B field, which is proportional to N/g, falls by a factor of 4. The small increase in r_{wi} combined with the large decrease in B_{max} permits the core loss to fall. The winding resistance, however, was shown in Appendix B to be proportional to $N^2/\ln(r_{wo}/r_{wi})$, so

Table 7.6: Comparison of 7:1 and 14:2 Designs

Parameter	Symbol	7:1 Design	14:2 Design
Maximum B field	B_{max}	320 G	120 G
Ratio of Center Post Area to Outer Edge Area	A_i/A_o	0.73	0.10
Inside Slot Radius	r_{wi}	1.7 mm	2.0 mm
Outer Slot Radius	r_{wo}	5.0 mm	61.0 mm
Transformer Outer Radius	r_o	5.3 mm	62.0 mm
Transformer Height	h	3.2 mm	25.3 mm
Core Loss	P_h	0.21 W	0.10 W
Copper Loss	P_c	0.79 W	0.90 W

that

$$r_{wo} = r_{wi} e^{kN^2} \tag{7.15}$$

where k is a constant. Since r_{wi} is not decreasing, r_{wo} must grow exponentially with N^2 in order to accommodate enough copper to maintain the required power dissipation. This large increase in r_{wo} is present in Table 7.5.

Table 7.6 repeats the comparison of Table 7.5 without the previously mentioned constraint on r_o. Although the 14:2 design is now somewhat smaller, since changing A_i/A_o permitted some optimization of the core loss, the 14:2 design is still much larger than the 7:1 design.

Since the power dissipation of minimum transformer area designs is typically dominated by copper loss, any strategy that further increases copper loss will not enable further size reduction. It is therefore necessary to implement designs with one turn secondaries. This result is not altered by the use of multilayer windings; multiple layers of secondary should be placed in parallel, not series, as is discussed later in this chapter.

7.5 Dependence of Transformer Size on Frequency

At this point one of the central questions of this thesis can be addressed: how does the transformer size scale with frequency? It was established in Section 2.3 by means of a general analysis that there would be some frequency at which the transformer size would begin to increase. This section presents studies for a single layer winding that show that this limiting frequency can indeed occur in the 1–10 MHz range. The next section will consider the effect of multilayer windings.

The computer program described above was used to generate the curves of Fig. 7.7,

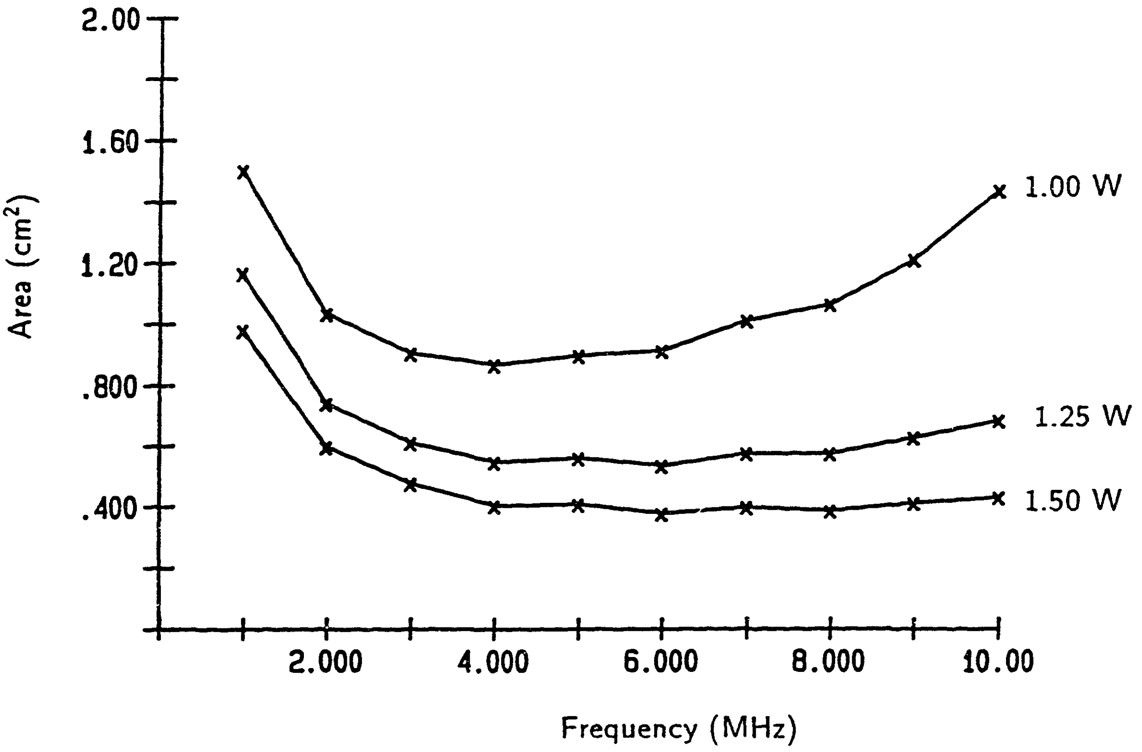

Fig. 7.7 Variation of transformer footprint area with frequency for various fixed total power dissipations.

which show the variation of minimum transformer area with frequency. Each curve corresponds to a different level of total power dissipation. Each curve was dominated by copper loss. The curve for 1.0 W, for example, varied from about 70% copper loss at 1 MHz to about 79% copper loss at 10 MHz. One immediately notices that the area curve for the smallest value of power dissipation, 1.0 W, has a distinct minimum at 4 MHz, indicating that 4 MHz is the limiting frequency for that set of design constraints. The shape of these curves is explained by the following discussion.

Consider first the region in Fig. 7.6 between 1–4 MHz. Increasing the frequency reduces the value of inductance required, enabling the inner radius to decrease while maintaining the same core loss. In order to maintain the same copper loss, the slot width must be made larger to compensate for the smaller skin depth. If r_{wi} decreases faster than the slot width increases, then higher frequency yields a smaller transformer. This is the case for all the curves in Fig. 7.7 from 1 MHz to about 4 MHz. However, as was shown in Fig. 6.6, above 4 MHz the core loss in the Q1 material grows with a greater than linear dependence on the frequency, limiting the amount that r_{wi} can be reduced.

Figure 7.8 shows the variation of r_{wi} with frequency for the 1.0 W design. The 1.0 W total power dissipation level is sufficiently low that above 4 MHz the core loss will not permit significant reduction of r_{wi}. In order to limit the copper loss, r_{wo} must instead be increased. The dependence of r_{wo} on frequency can be found from the expression for the winding resistance. Neglecting the spacing between turns, Appendix B showed that the total (primary plus secondary) resistance is

$$R_t = \frac{4\pi N^2}{\sigma\delta \ln(r_{wo}/r_{wi})} \tag{7.16}$$

The frequency dependence in this expression is in the skin depth, which increases as $f^{1/2}$. Equation (7.16) can therefore be rewritten as

$$R_t = \frac{kf^{1/2}}{\ln(r_{wo}/r_{wi})} \tag{7.17}$$

where k is a constant. Figure 7.9 shows the variation of P_h/P_c with frequency for the 1 W design. The ratio stays approximately constant above 4 MHz, so that R_t, representing the copper loss, is approximately constant. Equation (7.17) can be solved for r_{wo}, giving

$$r_{wo} = r_{wi}e^{kf^{1/2}/R_t} \tag{7.18}$$

This result shows that if r_{wi} or R_t do not decrease with increasing frequency, then r_{wo}, and therefore the total transformer area, must increase exponentially with $f^{1/2}$. Table 7.7 shows the design that corresponds to the minimum point of the 1.0 W curve of Fig. 7.7.

The P_h/P_c curve of Fig. 7.9, in which P_h/P_c rolls off from 0.45 to 0.3, appears to contradict the generally accepted design rule that P_h/P_c should be equal to unity. A derivation of that rule is given in Appendix F. An examination of the derivation shows that it is not applicable here. The derivation considers an N:1 transformer of a given size and determines the N that gives the lowest loss. If N is larger than its optimal value then the copper loss causes the total to increase; if N is smaller than its optimal value then the core loss causes the total to increase. This application, on the other hand, considers transformers of given N and loss and determines the design with the smallest area. The problems are not equivalent.

It is difficult to draw general conclusions from Fig. 7.9. If a simple formula for P_h/P_c could be shown, then there would be no need for the optimization algorithms of the computer program. The value of P_h/P_c that corresponds to the minimum area design depends on the relative size of the core loss density and the copper conductivity. If the conductivity is increased by a factor of 10, for example, the value of P_h/P_c at 5 MHz increases from 0.28 to 0.63, reflecting the decreased importance of the copper loss.

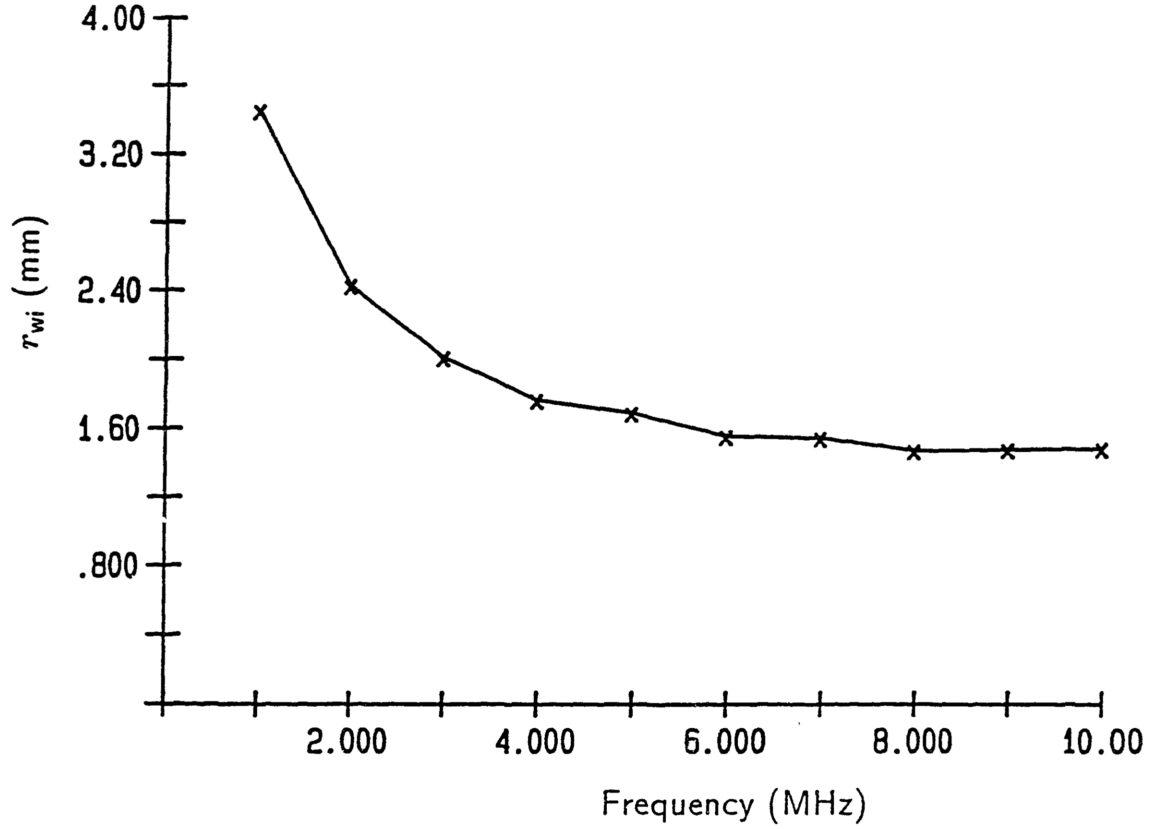

Fig. 7.8 Variation of r_{wi} with frequency for 1 W total power dissipation.

7.6 Multiple Winding Layers

The results of the previous section make it clear that for a single layer of primary and secondary, the only way to reduce the copper loss is to make the windings wider. If reducing the copper loss to an acceptable level requires that the conductors, and therefore the transformer, be made unacceptably wide, then the effective copper thickness can be increased by interleaving layers of primary and secondary.

This strategy is illustrated in Fig. 7.10, which shows two three-turn primary windings connected in series and two one-turn secondary windings connected in parallel to achieve a 6:1 transformer. In order for the load current to share between the two paralleled layers of secondary, each secondary winding must be adjacent to a primary winding, forming two pairs of the primary-secondary double layer shown in Fig. 4.6. Incorporating two double layers halves the resistance and the leakage inductance. The capacitance, however, increases. If the spacing between the two double layers were very large, the capacitance would be twice that of the noninterleaved winding. But because of the coupling between the lower primary

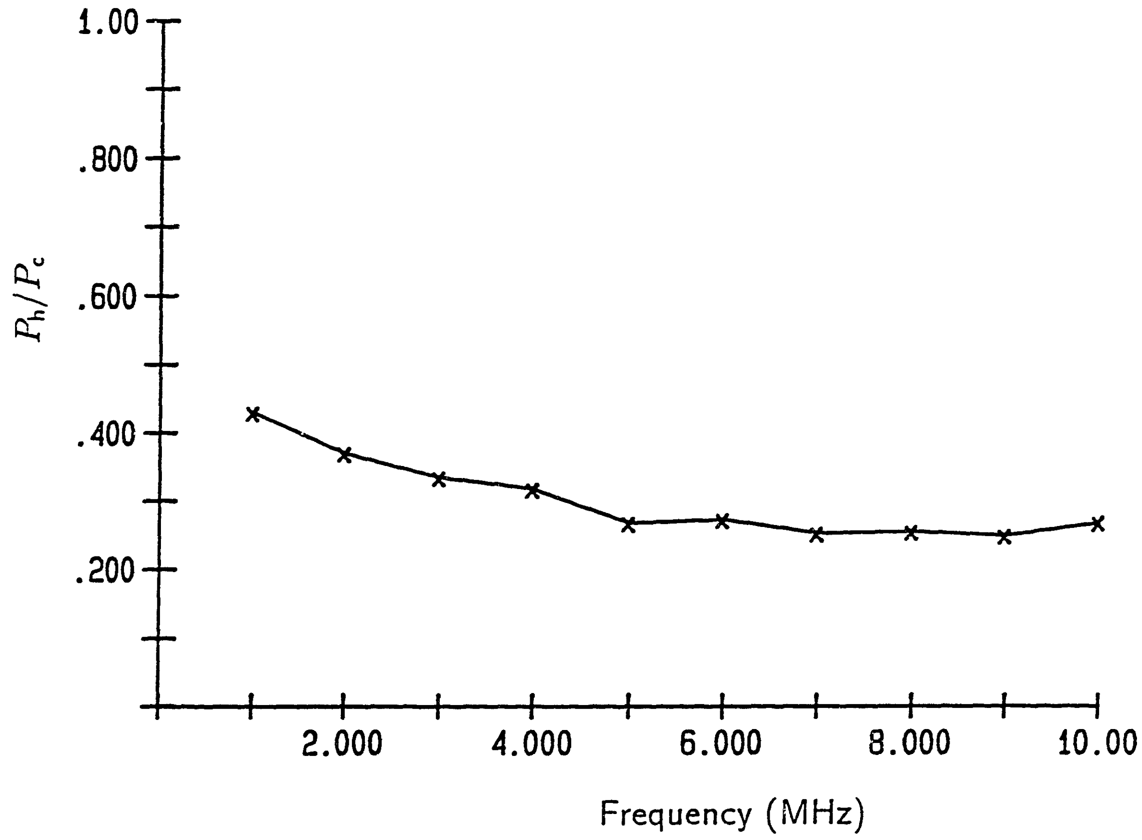

Fig. 7.9 Variation of P_h/P_c with frequency for 1 W total power dissipation.

winding and the upper secondary winding, the capacitance more than doubles. In order to reduce the energy stored in this coupling, the primary turns that are sandwiched between the secondary layers should be those that have voltages closest to the secondary voltage. For the flexible printed circuit process described in the next chapter, the insulating layers all have the same thickness. The capacitance would therefore treble. Table 7.8 summarizes the effect of interleaving two layers of primary and secondary. While this chapter only considers two double layers of windings, this strategy could be extended to several double layers of windings, with the number limited by the fabrication complexity and the difficulty of getting the heat out of the middle of the windings.

Figure 7.11 repeats the study of Fig. 7.7 for a transformer with the simple interleaving of Fig. 7.10. The axes of Figs. 7.7 and 7.11 are the same. Note that there is no longer a minimum in the 1.0 W curve; now the total power dissipation can be reduced to 0.75 W before the area curve shows a distinct minimum. Table 7.9 shows the design that corresponds to a 10 MHz transformer dissipating 0.75 W. This design satisfies the requirements of Table 7.1. Figure 7.12 shows that this 10 MHz, 0.75 W interleaved design is right on

Table 7.7: Sample Design of 4 MHz Transformer

Variable	Symbol	Value(s)
Magnetizing Inductance	L_m	3.3 μH
Leakage Inductance	L_l	18 nH
Dc Primary Resistance	$R_{p,dc}$	0.193 Ω
Dc Secondary Resistance	$R_{s,dc}$	3.35 mΩ
Common Mode Capacitance	C_c	16 pF
Differential Mode Capacitance	C_d	4.7 pF
Inner Slot Radius	r_{wi}	1.8 mm
Outer Slot Radius	r_{wo}	4.8 mm
Transformer Outer Radius	r_o	5.2 mm
Transformer Height	h	3.2 mm
Skin Depth	δ	33 μm
Gap Length	g	120 μm
Maximum B-field	B_{max}	360 G
Ratio of Center Post Area to Outer Edge Area	A_i/A_o	0.75
Copper Loss	P_c	0.76 W
Core Loss	P_h	0.24 W

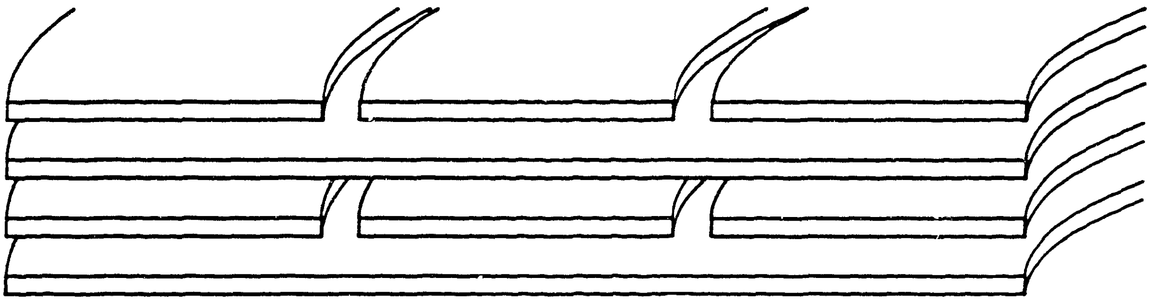

Fig. 7.10 Interleaved windings for a 6:1 transformer. The two one-turn secondaries are connected in parallel, and the two three-turn primaries are connected in series.

the knee of the footprint area vs. P_t curve. It was argued in Section 7.3 that a reasonable design would indeed be on the knee of this curve. Figure 7.12 also shows that interleaving moves the curve to the left, as explained in Section 7.3.

However, the outer edge of this core would be very thin (0.3 mm), and consequently difficult to fabricate. In practice, the outer edge would need to be at least about 1.6 mm thick. Part of this increased edge thickness is achieved because an actual core, like a pot

Parameter	Symbol	Multiplier
Magnetizing inductance	L_m	×1
Leakage inductance	L_l	$\times\frac{1}{2}$
Resistance to magnetizing current	R_m	$\times\frac{1}{2}$
Resistance to load current	R_l	$\times\frac{1}{2}$
Differential mode capacitance	C_d	×3
Common mode capacitance	C_c	×3

Table 7.8: Effect of Interleaving

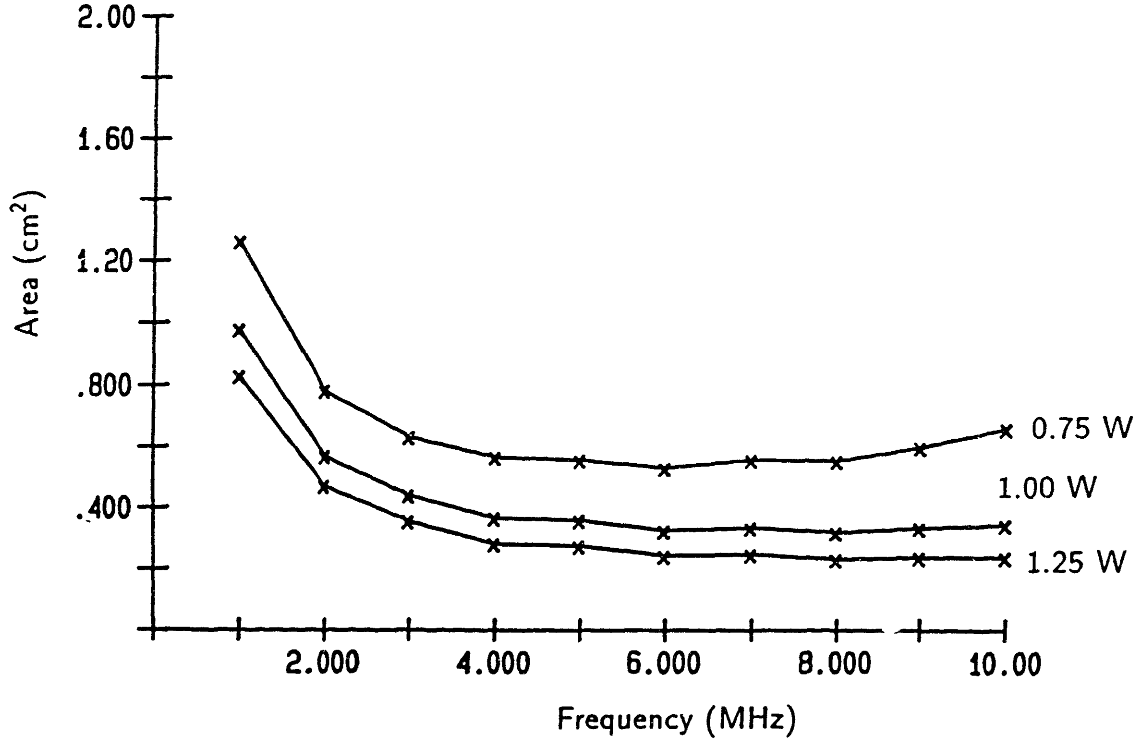

Fig. 7.11 Variation of transformer footprint area with frequency for various fixed total power dissipations and simple interleaving of conductors.

core, would need an opening in the outer edge so that the windings can be connected to the external circuit. In order to maintain the total edge area required by the design, the edge would have to be made slightly thicker. Further adjustment could be made by making the gap smaller.

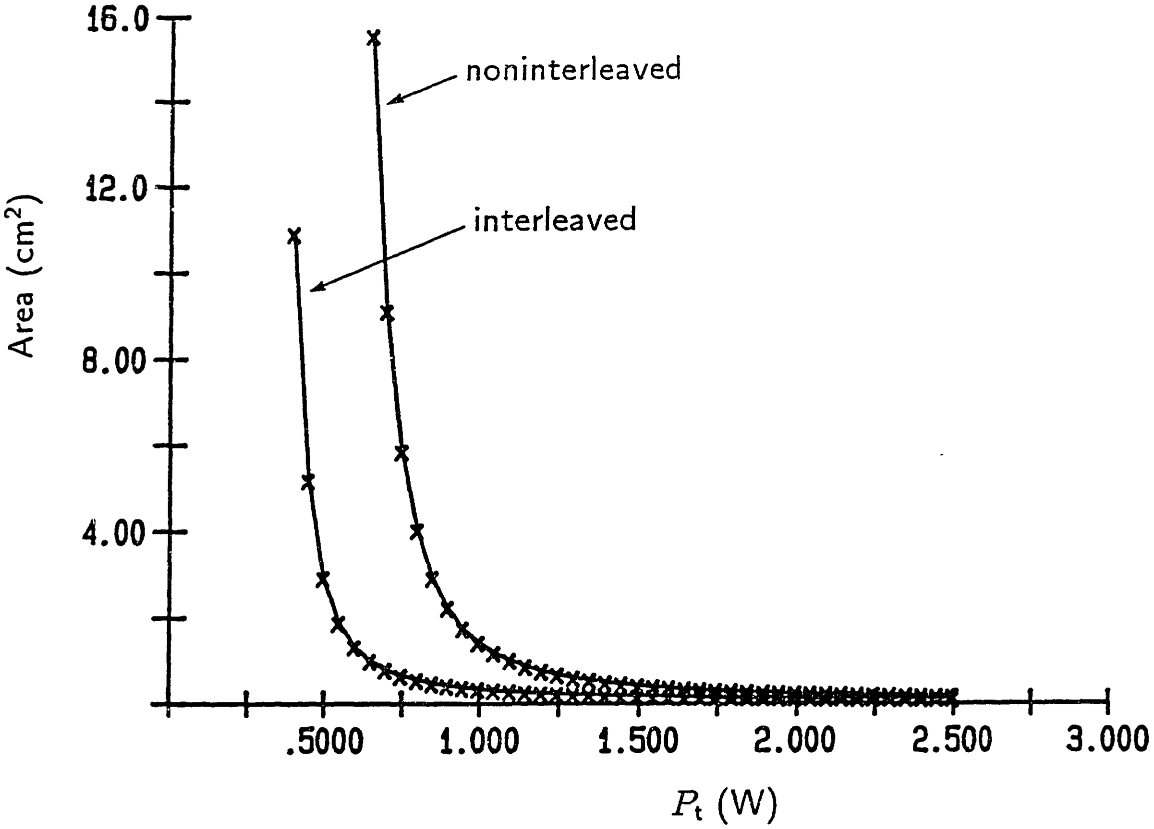

Fig. 7.12 Variation of transformer footprint area with allowable power dissipation at 10 MHz for noninterleaved and interleaved structures.

7.7 Leakage Inductance and Interwinding Capacitance

The total leakage inductance, L_l, and the interwinding capacitance, C_t, were shown in Chapter 5 to be determined by the width of the slot, w, and the separation between the traces, m. The product of L_l and C_t is essentially fixed by the width of the slot, which is determined by the loss and minimum area requirements described above. Their relative magnitudes, however, can be traded off against each other by varying m.

Figures 7.13 and 7.14 show the dependence of L_l and C_t on m for the design of Table 7.9. The capacitance calculations used $\epsilon = 3.2\epsilon_o$, which is valid for the kapton winding substrates used in the fabricated windings described in Chapters 8 and 9. As indicated by (5.9), L_l varies linearly with m, and as indicated by (5.12), C_t is inversely proportional to m.

The design of Table 7.9 lists L_l, C_d, and C_c for $m = 75\mu m$ (3 mil). The value of L_l, 15 nH, is far below the required value of 39 nH shown in Table 7.1. This allows ample margin for the additional 2 nH that will be contributed by the connection to the external

Table 7.9: Sample Design of 0.75 W, 10 MHz Transformer With Interleaved Winding

Variable	Symbol	Value(s)
Magnetizing Inductance	L_m	1.3 μH
Leakage Inductance	L_l	15 nH
Dc Primary Resistance	$R_{p,dc}$	0.14 Ω
Dc Secondary Resistance	$R_{s,dc}$	2.4 mΩ
Common Mode Capacitance	C_c	13 pF
Differential Mode Capacitance	C_d	3.7 pF
Total Capacitance	$C_t = C_c + C_d$	17 pF
Inner Slot Radius	r_{wi}	1.4 mm
Outer Slot Radius	r_{wo}	4.3 mm
Transformer Outer Radius	r_o	4.6 mm
Transformer Height	h	3.0 mm
Skin Depth	δ	21 μm
Gap Length	g	225 μm
Winding Substrate Thickness	m	75 μm
Maximum B-field	B_{max}	230 G
Ratio of Center Post Area to Outer Edge Area	A_i/A_o	0.67
Footprint		0.66 cm^2
Copper Loss	P_c	0.55 W
Core Loss	P_h	0.20 W

circuit.[6] The value of C_d, 3.7 pF, is below its maximum value of 5.0 pF, and the value C_c, 17 pF, is below its maximum value of 20 pF. Figs. 7.13 and 7.14 show that a slight increase in m will bring a reduction in C_t, and therefore C_d and C_c, without bringing L_l near its limit.

7.8 Thermal Dependence

The thermal requirement imposed on the transformer by the converter is that the performance of the transformer not significantly change either under the temperature rise resulting from steady state operation or from a rise in the temperature of the hybrid substrate. The conservative approximations in this section show that this requirement is satisfied.

A very simple thermal model is shown in Fig. 7.15. In this conservative model all the

---

[6] B. Miwa, private communication.

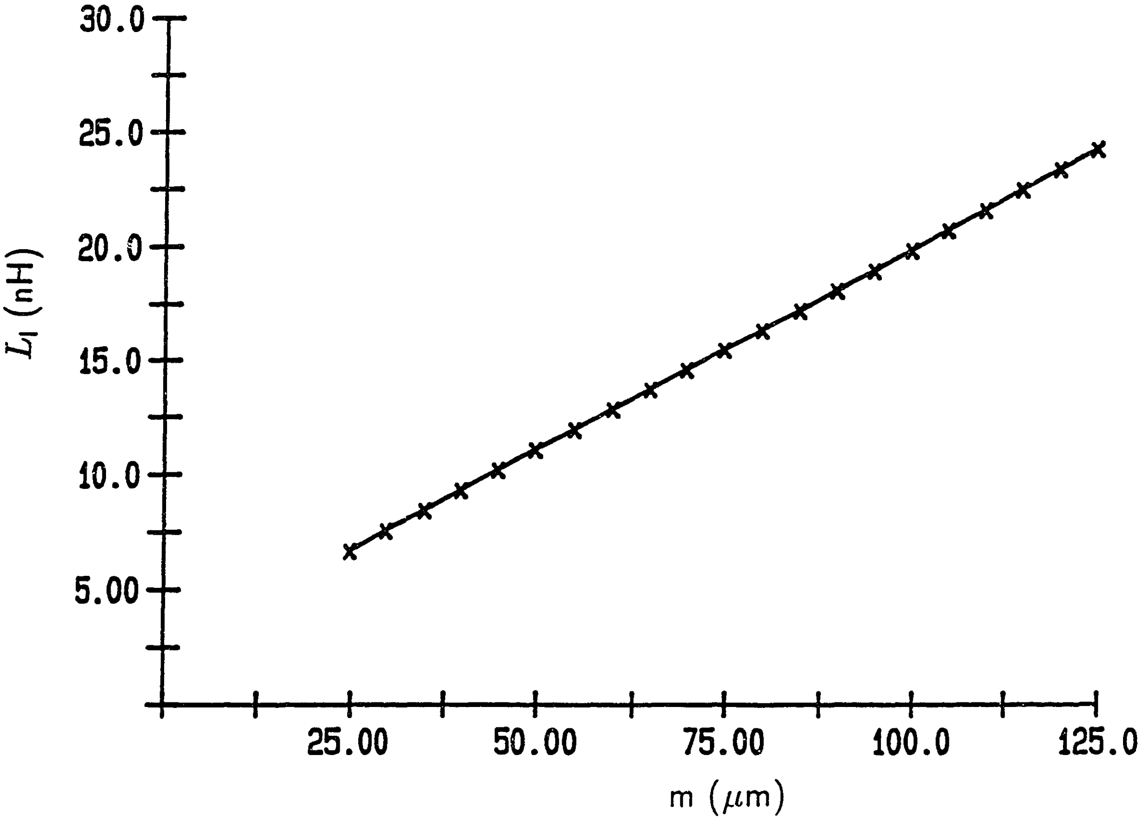

Fig. 7.13 Variation of leakage inductance with trace separation.

power dissipation of 0.75 W, both core and copper loss, is assumed to be injected at the winding. Half of the power is assumed to be dissipated at the top surface of the winding and half at the bottom surface. The winding is fixed at the bottom of the slot with a 0.2 mm layer of thermal epoxy. The heat is assumed to diffuse from the winding through the epoxy and the bottom of the ferrite core to the heat sink and the surrounding air without spreading laterally, which would reduce the thermal resistance.

The thermal resistance for each material layer is given by

$$\Theta_t = \frac{\rho_t t}{A} \tag{7.19}$$

where ρ_t is the thermal resistivity, t is the material thickness, and A the area through which the heat must diffuse. Table 7.10 gives the thermal resistivity of the materials used.[7] In

---

[7] L. D. Pitzele, "The System Fabrication of a 10 MHz, Dc/Dc Switching Power Supply," MIT Master's Thesis, September 1986, p. 164.

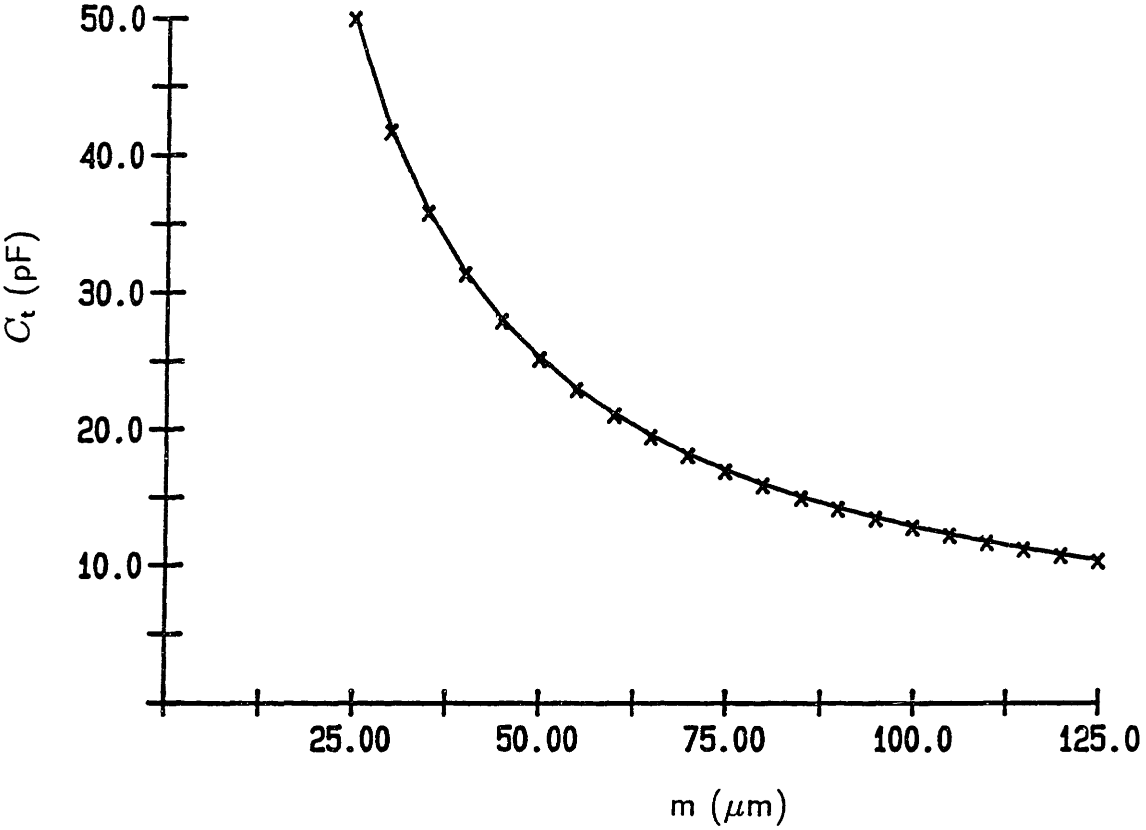

Fig. 7.14 Variation of total interwinding capacitance with trace separation.

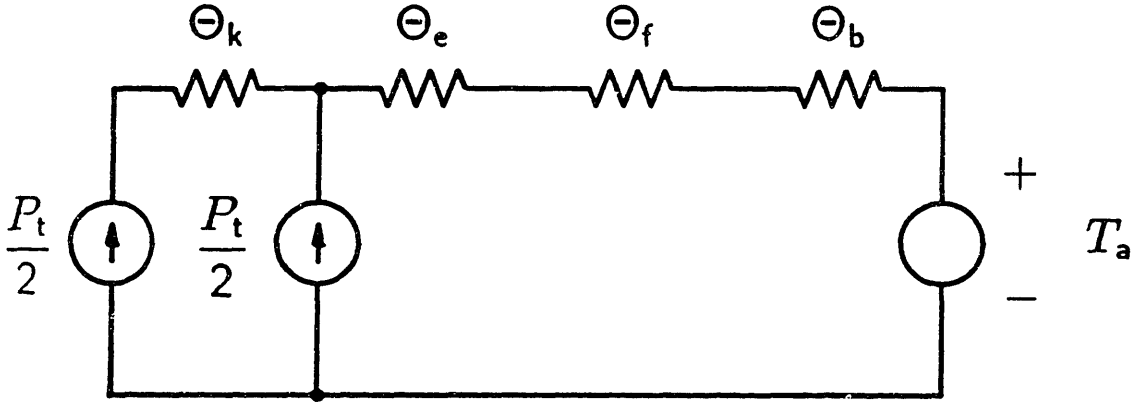

Fig. 7.15 Thermal resistance model.

these calculations A will be taken to be the winding area, $A = \pi(r_{wo}^2 - r_{wi}^2)$. For the design of Table 7.9, $A = 0.52\ \text{cm}^2$.

Table 7.11 gives the values of the thermal resistances for the model of Fig. 7.15. The value for Θ_b, the thermal resistance from the alumina substrate through the heat sink to

Table 7.10: Thermal Resistivities

Material	ρ_t (°C-cm/W)
Ferrite	23.3
Kapton	500
Thermal Epoxy	125

Table 7.11: Thermal Resistances of 10 MHz, 0.75 W Design

Resistance	Symbol	Thickness	Value
Kapton	Θ_k	75 μm	7.2 °C/W
Thermal Epoxy	Θ_e	0.2 mm	4.8 °C/W
Ferrite	Θ_f	1.0 mm	7.0 °C/W
Substrate	Θ_b	—	0.84 °C/W

the air, is determined from hybrid system design and is outside the scope of this thesis.[8] For a total dissipation of 0.75 W, this model states that the temperature rise at the substrate is about 11°C over ambient, a very modest increase. The available data suggest that for nickel zinc ferrites, the core loss will decrease with increasing temperature, so that the data used in the design at 25°C gives a conservative approximation.[9] Of course, the core temperature must stay below the Curie temperature of about 300°C. The dependence of the electrical conductivity of the copper, σ_{Cu}, is given by the well-known formula[10]

$$\sigma_{Cu} = \sigma_o \frac{T_o + 234.5°C}{T + 234.5°C} \tag{7.20}$$

where σ_o is the conductivity at T_o (°C) and T is the new temperature (°C). This formula gives about a 4% decrease in conductivity for a 10°C rise in temperature around 25°C.

Fig. 7.16 shows the dependence of transformer area on winding temperature for a 10 MHz, 0.75 W design. This study includes the dependence of copper conductivity on temperature and assumes that the core loss, which is in any case less than 30% of the total, remains constant. The dependence of the copper loss on conductivity is found from (7.7) as

$$P_c \propto \frac{1}{\sigma\delta} \propto \sigma^{-1/2} \tag{7.21}$$

---

[8] Pitzele, p. 207.

[9] Philips Electronic Components and Materials Division, *Components and Materials Book C4: Ferroxcube Potcores, Square Cores, and Cross Cores*, Eindhoven, the Netherlands (1984), pp. 33 and 40.

[10] Prof. J. H. Lang, private communication.

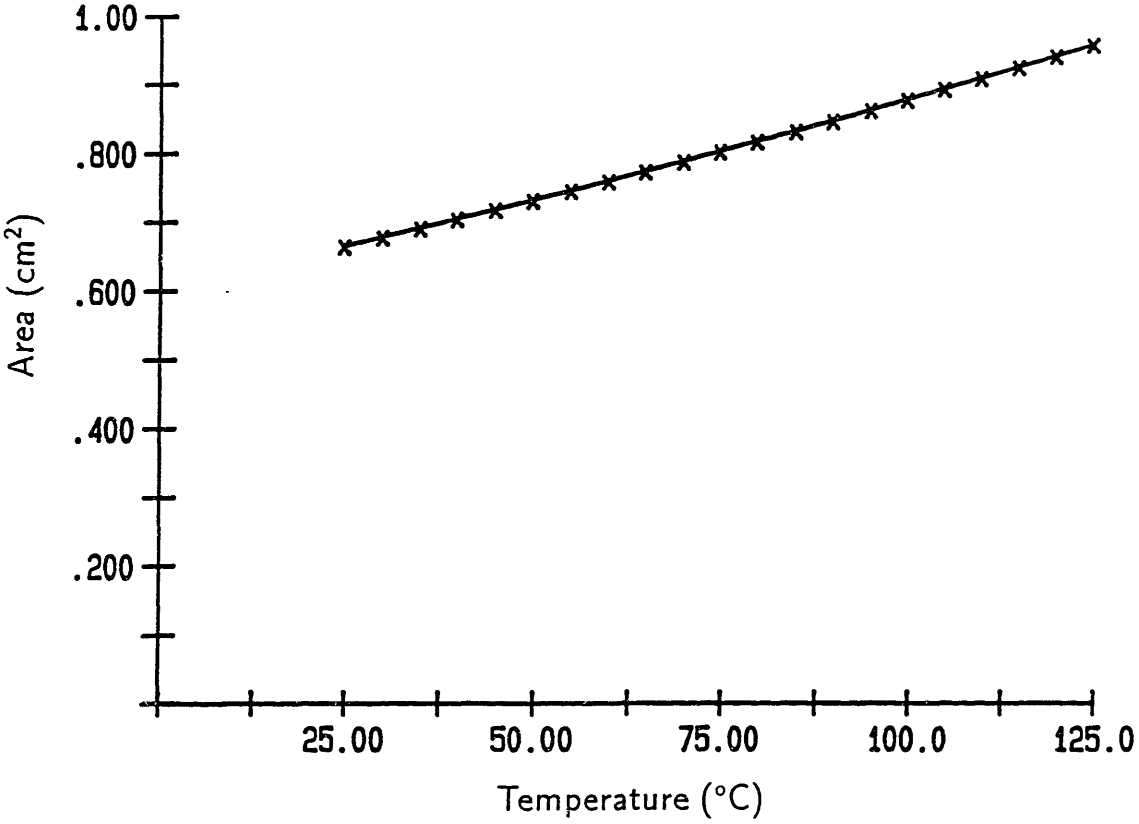

Fig. 7.16 Variation of transformer area with winding temperature for 10 MHz, 0.75 W design.

The weak dependence of P_c on σ given by (7.21), together with the weak dependence of σ on T given by (7.20), yields the small increase of transformer area with temperature shown by Fig. 7.16. For a five fold increase in winding temperature, the area of the transformer increased only by a factor of 1.4.

7.9 Scaling Issues

This section discusses how the transformer design changes with different levels of transferred power and bus voltage. While this chapter considers the design of a transformer to transfer 25 W, larger or smaller amounts of power may need to be transferred for different applications. The MIT prototype converter is designed for a bus voltage of about 40 V, but different equipment and safety standards may require the use of higher or lower bus voltages. The figure of merit that is used to characterize the transformer design over the range of transferred power and bus voltage is A/P, the ratio of the transformer footprint area to the transferred power.

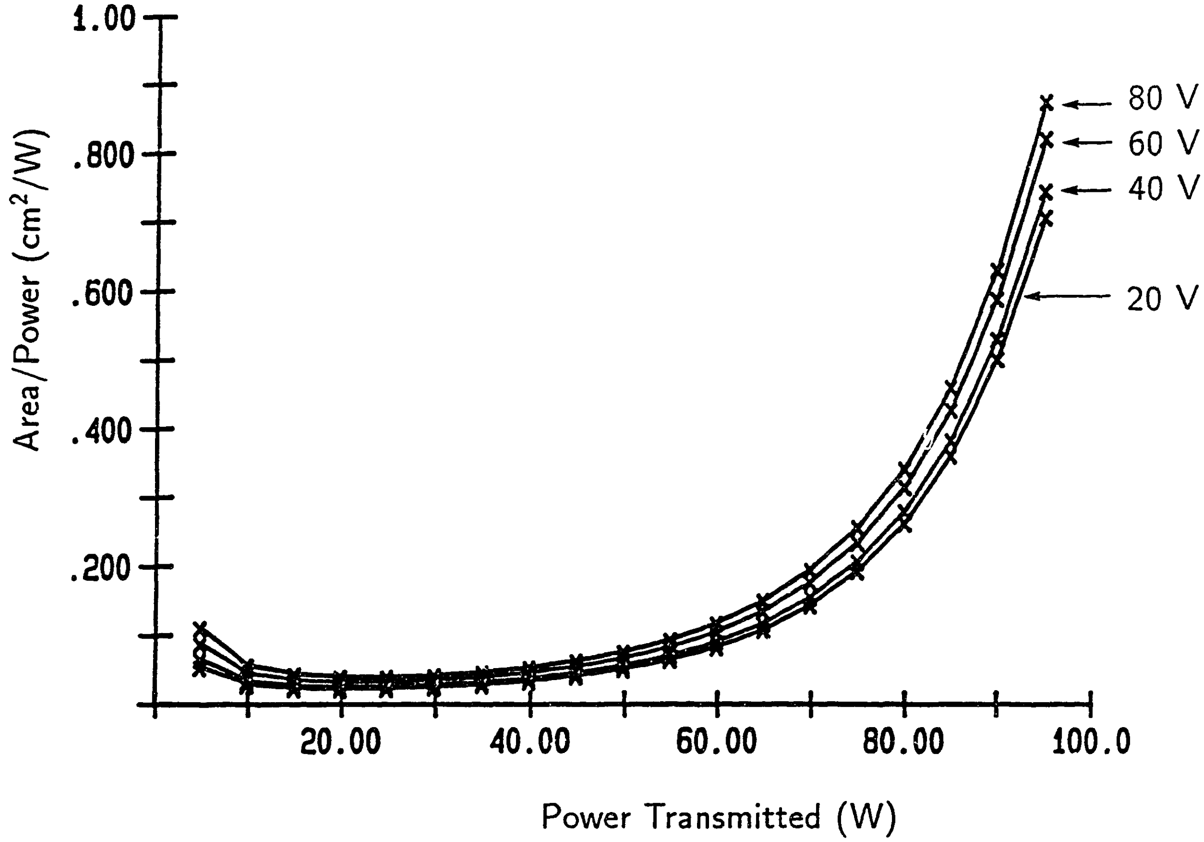

Fig. 7.17 Variation of transformer area with transferred power for different values of bus voltage. The designs are for a 10 MHz, interleaved, 97% efficient transformer.

Figure 7.17 shows the variation of A/P with transferred power for four different values of bus voltage. The transferred power was varied from 10 W to 100 W, and a curve relating A/P to the transferred power was generated for each of the following bus voltages: 20 V, 40 V, 60 V, and 80 V. This study was carried out by scaling the design of Table 7.9, so that the designs represented by the points on the curves are for 10 MHz, interleaved, 97% efficient transformers. The point on the 40 V curve corresponding to a transferred power of 25 W therefore represents the design of Table 7.9.

Before interpreting these curves, it is necessary to explain exactly how they were generated. For a given bus voltage, changing the transferred power by a factor of ψ means changing the load current by a factor of ψ. In order to accommodate the increased current, the die area of the semiconductor switch in the converter circuit is assumed to be changed also by a factor of ψ, so that its on-state resistance is changed by a factor of ψ. But this increase in die area changes the switch's output capacitance by a factor of ψ, so that in order to keep the resonant frequency of the power circuit tank constant, the magnetizing inductance of the transformer must be changed by a factor of $1/\psi$. Since the bus voltage is held constant, the magnetizing current must also be changed by a factor of ψ. In order to maintain a constant efficiency, the allowable total power dissipation in the transformer is also changed by a factor of ψ.

The difference in bus voltage was handled by changing the number of turns of the primary to maintain 5 V at the secondary (it was shown in Section 7.4 that the secondary should only have one turn). If the turns ratio was changed by a factor of γ, then in order to keep the power transferred constant, the input currents were scaled by a factor of $1/\gamma$. Changing the turns ratio by a factor of γ increased the magnetizing inductance by a factor of γ^2.

The curves show that for a given bus voltage, above a certain power level the size of the transformer per power transferred increases quickly with power transferred. These results suggest that rather than design one transformer to transfer 100 W, the total footprint would be much smaller if two 50 W transformers were used. This rapid increase in A/P with power transferred occurs because these designs occur increasingly to the left of the knee in the footprint area vs. power dissipation curve discussed in Section 7.3. This effect again highlights the importance of investigating the position of any design on the footprint area vs. power dissipation curve. For small values of power transferred, A/P again increases. This effect occurs because the finite spacing between primary turns mandates a minimum slot width, which in turn means a minimum slot height (due to the 40% rule discussed in Section 7.3), and a minimum core loss. As the transferred power is decreased, the allowable power dissipation is also decreased, so that in order to reduce either the core loss or the copper loss, the footprint area must increase. The finite spacing between turns also accounts for the small increase in A/P with bus voltage. As the bus voltage is increased, the number of primary turns is increased, and because of the fixed spacing between turns, the proportion of slot width occupied by primary copper decreases. Hence the footprint must increase in order to meet the required power dissipation.

7.10 Comparison Between Minimum Area Design and Existing Component

This section presents a comparison between a transformer design using a conventional pot core and a design produced by the computer program described in this chapter for a customized core and planar windings. Table 7.13 compares a 1.2 W design by Miwa using a standard Ferroxcube 1107 pot core for a 5 MHz hybrid prototype converter with a design using a single layer planar spiral winding and with a design using a two layer interleaved

Table 7.13: Design Comparison for 5 MHz, 1.2 W Transformer

Parameter	Miwa	Single Layer	Interleaved
L_m	2.5 μH	2.5 μH	2.5 μH
L_l	39 nH	17 nH	13 nH
r_o	5.5 mm	5.1 mm	3.4 mm
footprint	0.95 cm^2	0.82 cm^2	0.36 cm^2
h	4.3 mm	3.2 mm	2.4 mm

winding. The windings used by Miwa were of the barrel type described in Chapter 4 and were painstakingly fabricated by hand in order to minimize the leakage inductance.[11]

The design using a single layer planar spiral matches the size of the conventional pot core but has less than half of the leakage inductance. With a double interleaved layer of primary and secondary, as described in Section 7.6, the transformer takes up less than 40% of the area of the conventional design, while further decreasing the leakage inductance. For high volume manufacture the easily manufactured single layer spiral winding offers slightly better performance for a fraction of the fabrication cost of a hand wound barrel winding. For hybrid converters where physical size must be minimized, the interleaved winding offers a substantially smaller transformer.

7.11 Conclusion

The studies of this chapter have shown that there is a limit to the transformer volume reduction that can be achieved with higher frequency operation. Moreover, these studies have shown that for the components and converter application considered, this limiting frequency occurs around 5 MHz, although other system design issues besides transformer size, such as capacitor size, may justify a converter frequency above 5 MHz.

---

[11] B. Miwa, private communication.

Chapter 8

EXPERIMENTAL MEASUREMENTS ON A SLOTTED GAPPED TRANSFORMER

This chapter describes measurements performed on a prototype 6:1 transformer with planar spiral windings. This transformer was not intended to represent a best design, but rather was intended to demonstrate the feasibility of fabricating planar spirals with thin line widths and close spacing, to provide a check on the design analysis, and to validate the measurement procedure.

The primary and secondary winding patterns were photolithographed and etched on each side of a polyimide-copper laminate flexible printed circuit. The exposed polyimide was cut away and the windings slid over the center post of one half of a Ferroxcube 1107PL00 pot core composed of 4C4 nickel-zinc ferrite. The top of the core was then covered with a 4C4 ferrite plate separated by a gap of 120 μm. The dimensions and parameters of the transformer and windings conformed to those of Table 5.1, except for the depth of the slot, which in the 1107 core is equal to the slot width (2.25 mm). Also, the permeability of the 4C4 ferrite is about $150\mu_o$, not the $10^4\mu_o$ of Table 5.1. The polyimide-copper laminate and the ferrite core are discussed in more detail in Appendix H.

The winding resistance and leakage inductance were determined by measuring the transformer impedance at the primary with the secondary short-circuited. The primary winding was connected to the measurement apparatus of Fig. 7.2 and driven with a sinusoidal current with a frequency of 4 MHz and a peak amplitude of 0.8 A. The impedance was calculated from measurements of the magnitude and phase of the primary voltage and current. The lead impedance was also measured and subtracted from the previous measurement, and the result was separated into the winding resistance, R_w, and the leakage inductance, L_l. The contribution of the magnetizing inductance was neglected, since the L_m/L_l ratio was greater than 75. Since the secondary was short-circuited in this measurement, the flux level in the core was extremely low, so that core loss was negligible. The finite element analysis predicted that even near the windings, the flux level in the ferrite was less than 4 G. Table 8.1 shows the calculated and measured values of R_w and L_l. They show good agreement.

The magnetizing inductance, and the hysteresis and copper loss associated with the magnetizing current, were determined by measuring the transformer impedance at the primary with the secondary open-circuited. The primary winding was driven with a sinusoidal voltage with a frequency of 4 MHz and a peak amplitude of 40.8 V. The results are shown

Table 8.1: Short Circuit Test

Parameter	Estimated	Finite El.	Measured
L_l	49 nH	48 nH	44 nH
R_w	0.52 Ω	0.53 Ω	0.52 Ω

Table 8.2: Open Circuit Test

Parameter	Estimated	Finite El.	Measured
L_m	3 μH	3.6 μH	3.4 μH
P_c	64 mW	64 mW	—
P_h	0.19 W	—	—
P_t	0.25 W	—	0.25 W

in Table 8.2. The estimated value for L_m was 12% lower than the measured value of 3.4 μH, primarily because the estimate did not take into account the energy stored in the fringing field. The estimate for L_m, however, did take into account the reluctance of the magnetic material, as well as the fact that the area enclosed by the windings was not equal to the area at the periphery of the core, through which the flux returns. The finite element program predicted a value for L_m that was 6% larger than the measured value, primarily because the axisymmetric solver of the finite element program could not model the notches in the side of the Ferroxcube pot core. These notches reduce the return area for the flux, thereby reducing the magnetizing inductance.

The total power dissipation in this open-circuit test was measured as 0.25 W. This is accounted for as follows. The lead resistance was measured and found to account for 22 mW, and the finite element program predicted a copper loss in the windings of 42 mW. Since the secondary was open-circuited in this measurement, the B-field was substantial, and its magnitude was calculated to be 20 mT in the inner leg of the core and 0.8 mT in the outer leg. Loss measurements on 4C4 toroids found that these flux densities correspond at 4 MHz to loss densities of 1.9 W/cc and 0.12 W/cc, respectively. These loss densities correspond to a total core loss of 0.19 W, so that the total loss is 0.25 W, as required.

Table 5.3 lists the capacitances predicted in Chapter 5 and the values that were actually measured. The winding-to-winding capacitance (C_{w-w}) was measured at low frequency with an impedance analyser (HP4192A) and found to agree closely with the predicted capacitance. The total capacitance (C_t) was measured by connecting the transformer as in Fig. 5.1, and measuring the admittance with a network analyser (HP3577A). The resulting admittance curve is shown in Fig. 8.1. This frequency at which this admittance approaches

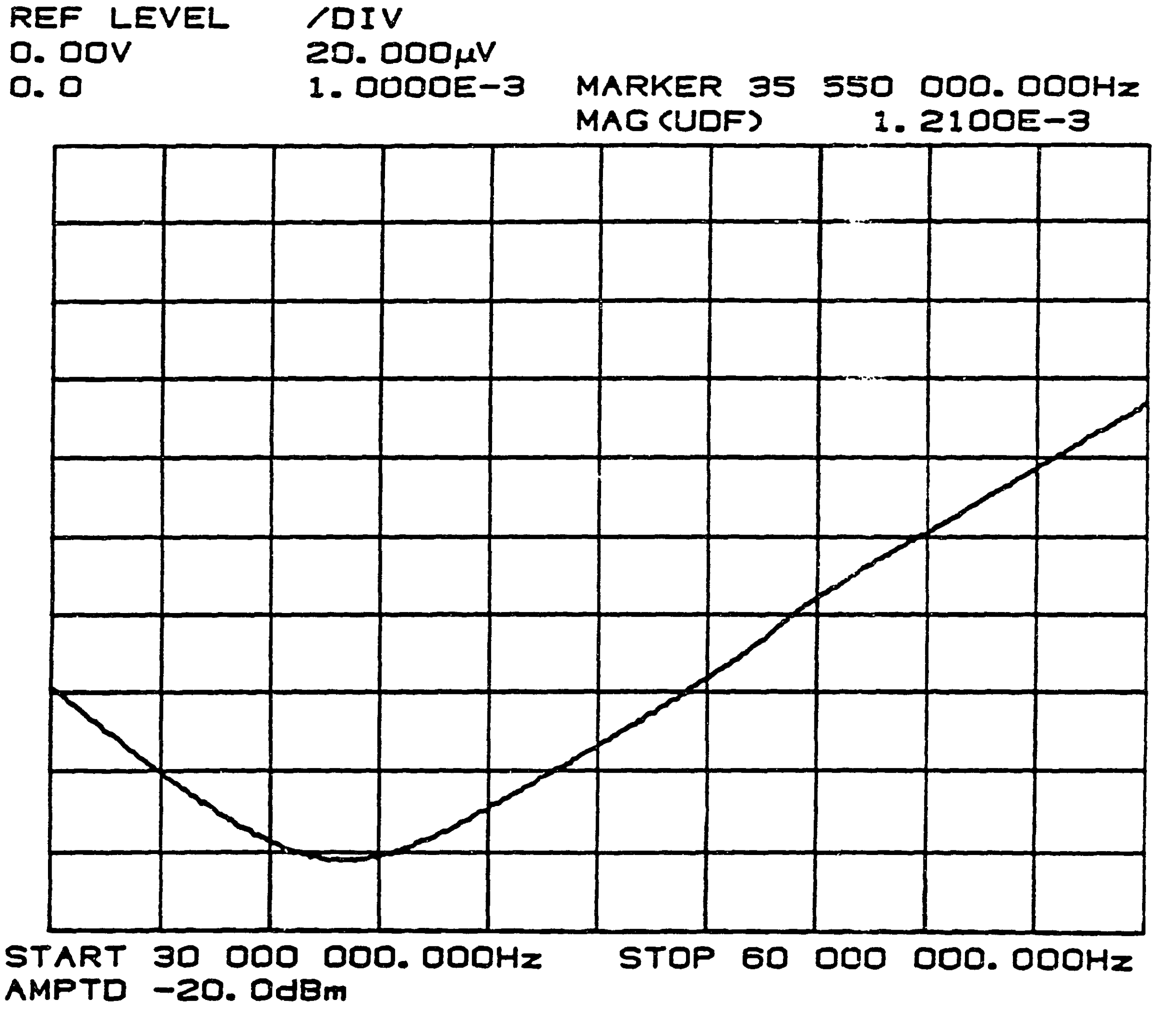

Fig. 8.1 Admittance curve for transformer showing resonance of L_m with C_t.

zero is determined by the product of C_t and L_m. Figure 8.1 shows this resonant frequency to be about 38 MHz, which for an L_m of 3.4 μH corresponds to a C_t of 5.1 pF. Approximately 1 pF of this capacitance is due to the current probe (Tektronix CT–1/P6040), so that the actual C_t was about 4.1 pF, close to the predicted quantity. The measurement was repeated with the ground connection removed in order to find C_d. The admittance curve is shown in Fig. 8.2. The resonant frequency of 53 MHz corresponds to a capacitance of 2.6 pF. Subtracting the probe capacitance from this gives a value for C_d of 1.6 pF, reasonably close to the predicted value of 0.95 pF, given the difficulty of measuring such small capacitances.

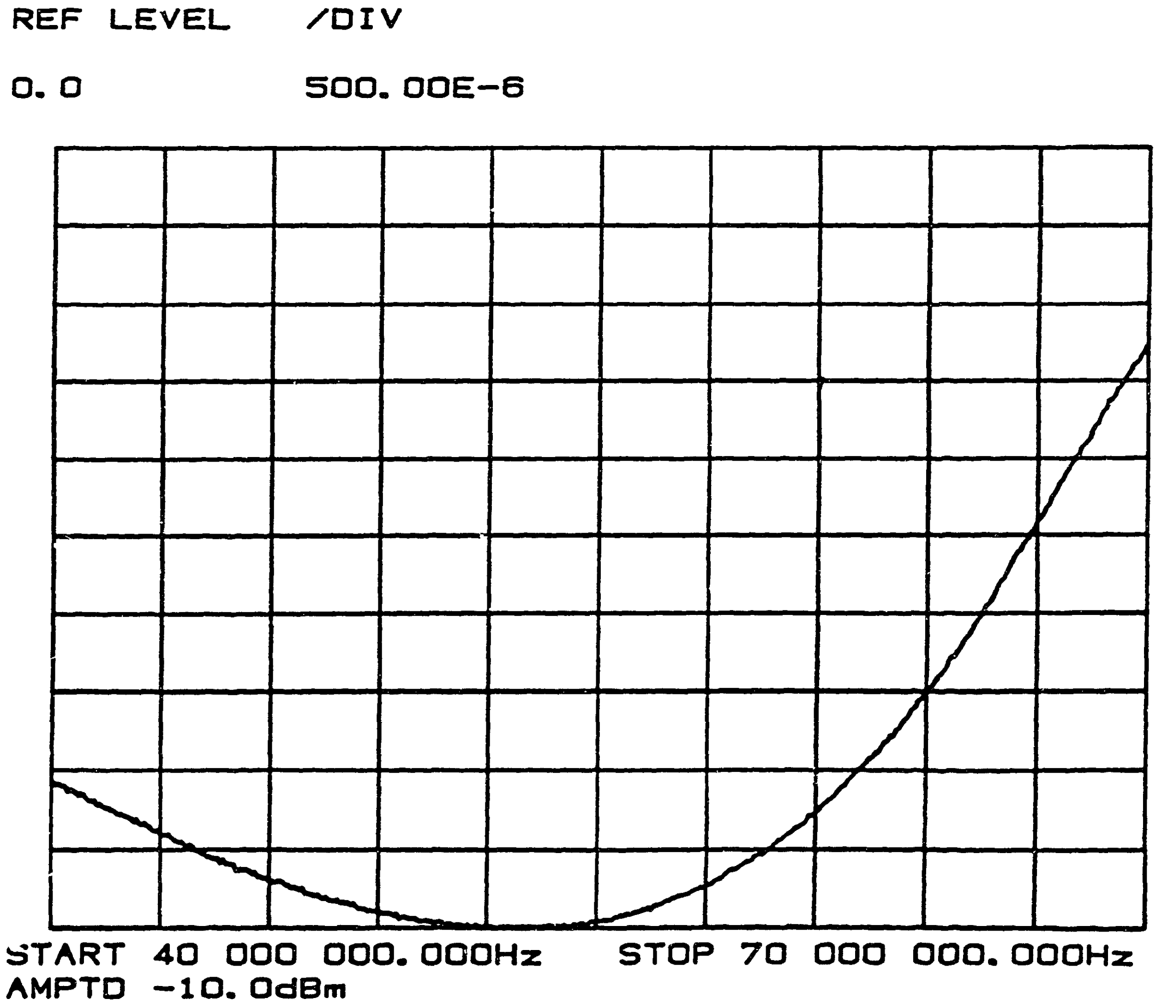

Fig. 8.2 Admittance curve for transformer showing resonance of L_m with C_d.

Table 8.3: Capacitance Measurement

Parameter	Estimated	Measured
C_{w-w}	15 pF	15 pF
C_t	3.5 pF	4.1 pF
C_d	0.95 pF	1.6 pF

Chapter 9

CONCLUSIONS AND DIRECTIONS FOR FUTURE WORK

This thesis has shown that by carefully analyzing copper and core loss, the physical size of the magnetic components required by the emerging generation of high power density 1–10 MHz dc/dc converters can be reduced significantly over present designs. The design presented in Chapter 7 for the transformer of the MIT prototype converter was shown to occupy less than 40% of the footprint area of the component presently used, for the same energy storage and total power dissipation. In addition, the new design, with its planar copper/kapton windings, is much more amenable to economical mass production than the conventional technology of magnet wire and bobbins.

In order to make quantitative predictions of the copper loss in windings whose current distributions were greatly complicated by skin and proximity effects, finite element programs were used that have themselves only become recently available. And in order to make quantitative predictions of the core loss in the ferrite magnetic materials, whose permeability and loss vary greatly with flux density and frequency, a detailed measurement and analysis procedure was developed and used to measure the properties of eight commercially available nickel-zinc ferrites. These analyses were used to choose a core and winding geometry for the transformer of the prototype 10 MHz, 50 W dc/dc converter under development at MIT. The analyses were also used to derive a lumped parameter model of the transformer, and the model was verified by experimental measurements using a 6:1 transformer that was fabricated with planar spiral windings.

The analytic models of copper and core loss were combined in a computer program that designed the transformer with the smallest footprint for a given energy storage, power dissipation, and frequency. This program was used not only to produce designs at particular operating points and to develop a design for the transformer of the MIT prototype converter, but also to investigate the design tradeoffs. It was found, for example, that if the copper loss is not reduced by a strategy such as interleaving layers of primary and secondary, then the footprint area of the transformer can increase with increasing frequency, thereby negating one of the motivations for operating at high frequency. It was also found that the curve relating footprint area with the allowable power dissipation has a pronounced knee, so that constraining the power dissipation to be too low results in an unreasonably large transformer, while allowing the power dissipation to be unnecessarily large hardly buys any reduction in the transformer footprint.

Although the previous work described in Chapter 3 represents important initial research, it does not constitute an organized effort to identify the limits of magnetic component miniaturization. This thesis is intended not just to determine how small the transformer for the MIT converter can be made, but rather to develop a methodology that can be used to reduce the size of energy storage components for other applications as well. The remainder of this chapter considers some important avenues for further research.

There are several important issues of copper loss that deserve further attention. The studies of Chapter 4 focus on reducing the loss due to ac currents, and conclude that the windings should be made only a skin depth thick. As is discussed in the chapter, however, the loss associated with a dc component in the load current is reduced by making the windings thicker. This tradeoff between the copper loss due to ac and dc currents was not addressed in this thesis, but is nevertheless important. Another issue related to copper loss that should be further explored is that of interleaved windings. Finite element analyses of interleaved windings were not performed, due to limitations of both hardware and software. The hardware did not possess the memory or the speed required to process the large amount of nodes in an interleaved structure, and the software was limited in its ability to model the inherently three dimensional nature of the interleaved windings. The finite element software could also be extended to use the analytic models for the dependence of the core permeability and loss on flux density that were developed in Chapter 6.

Since there are so many different types of magnetic materials and since their properties depend strongly on so many parameters, the challenge in indicating directions for further research in core loss is to choose only the most important. One important task is to analyse the properties of the manganese-zinc ferrites, which are appropriate for use below about 2 MHz. Not only is there still great interest in the development of 1 MHz converters, but manufacturers are introducing new, low loss MnZn ferrites intended specifically for power use at 1 MHz. The next most important direction might be to broaden the understanding of both NiZn and MnZn ferrites by studying the variation of their properties with temperature, sample, and different types of dc bias than that discussed in Chapter 6.

Chapter 7 describes a transformer design program that essentially acts as a one-port: given a set of requirements, it designs the optimal transformer, where optimal here is defined to mean smallest footprint area. This approach could be extended to the other components in the hybrid converter, so that the design of each component would be performed by a one-port program, which would accept a set of requirements and then design the component which was considered to be optimal. These programs, each of which would be responsible for the optimization of an individual components, could be used by a higher level, or meta-program which performed a system optimization. In this way, for example, the smallest hybrid converter for a given power dissipation could be designed. This kind of optimization, which in previous years required expensive computer resources, can be easily done on the personal computers that are available today. The designs presented in Chapter 7, for example, typically required less than 3 seconds each to compute on a desktop computer (based on the Intel 80386/80387) worth, in 1988, only about $4,000.

Finally, the experimental work described in this thesis only used single layers of primary and secondary, rather than the interleaved layers recommended in Chapter 7 for the prototype transformer. This was due to the present unavailability at MIT of a multilayer process. Multilayer copper/kapton processes are under development at MIT, as elsewhere, and it is hoped that multilayer copper/kapton windings will soon be fabricated for the transformer of the MIT prototype converter.

APPENDICES

Appendix A: Calculations of Winding Loss

Resistance to Load Current of a One Skin Depth Thick Winding

This section shows that the resistance to the load current of a winding whose thickness is one skin depth is only 9% higher than the resistance that would result if the winding were many skin depths thick.

As illustrated in Fig. A1 for both the primary and secondary windings, at one surface of each winding the H field is $H_o(r)$, and at one surface of each winding the field is close to zero. Therefore, this section considers a winding for which the field at $z = 0$ is $H_o(r)$, and the field at $z = -\delta$ is close to zero. The complex H field distribution inside the winding is given by

$$\tilde{H}_r = \tilde{A}(r)e^{z(1+j)/\delta} + \tilde{B}(r)e^{-z(1+j)/\delta} \tag{A1}$$

where $A(r)$ and $B(r)$ are determined from the boundary conditions

$$\tilde{A}(r) + \tilde{B}(r) = \tilde{H}_o(r), \qquad z = 0 \tag{A2}$$

and

$$\tilde{A}(r)e^{-(1+j)} + \tilde{B}(r)e^{(1+j)} = 0, \qquad z = -\delta \tag{A3}$$

These three equations can be evaluated tc yield

$$\tilde{H}_r = \left[\frac{e^{z(1+j)/\delta}}{1 - e^{-2(1+j)}} + \frac{e^{-z(1+j)/\delta}}{1 - e^{2(1+j)}}\right]\tilde{H}_o(r) \tag{A4}$$

The current, $\tilde{J}_\phi$, is given by

$$\tilde{J}_\phi = \frac{\partial}{\partial z}\tilde{H}_r = \frac{(1+j)}{\delta}\left[\frac{e^{z(1+j)/\delta}}{1 - e^{-2(1+j)}} - \frac{e^{-z(1+j)/\delta}}{1 - e^{2(1+j)}}\right]\tilde{H}_o(r) \tag{A5}$$

and the power dissipation density is given by

$$P_d = \frac{1}{2\sigma}\int_{-\delta}^{0} \tilde{J}_\phi \cdot \tilde{J}_\phi^* \, dz \tag{A6}$$

Substituting (A5) into (A6) gives[1]

$$P_d = \frac{1}{2\sigma\delta}|\tilde{H}_o(r)|^2 \cdot 1.09 \tag{A7}$$

---

[1] Equation (A6) was evaluated by MACSYMA, an expert system for performing both numerical and symbolic mathematical manipulations. MACSYMA was developed by the Mathlab Group of the MIT Laboratory for Computer Science and is available from Symbolics, Inc. of Cambridge, Massachusetts.

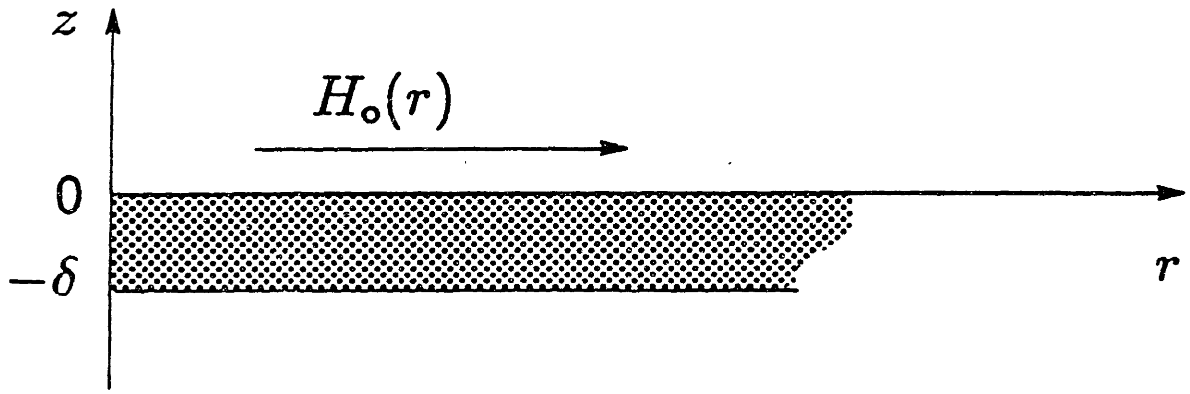

Fig. A1 Illustration of windings for loss calculations.

If the winding were much thicker than a skin depth, then the power dissipation density would be given by

$$P_d = \frac{1}{2\sigma\delta}|\tilde{H}_o(r)|^2 \tag{A8}$$

Equation (A8) states that the loss can be computed as if the current were uniformly distributed in z to a thickness of one skin depth, δ. The fact that the winding is only a skin depth thick increases the loss by the factor of 1.09 over the loss that would occur in a winding much thicker than a skin depth. Since the winding is one skin depth thick, (A8) also states that the effective resistance is 9% higher than the winding's dc resistance.

Resistance to Magnetizing Current of a Winding Far From the Gap

If the primary winding is a skin depth thick and is recessed in a slot so that it is far from the gap, then the field at the top of the primary is $H_o(r)$, and the field at the bottom of the primary is close to zero. This case is identical to the case considered above. The resistance of the primary is therefore 9% higher than its dc resistance.

If the secondary winding is a skin depth thick and placed above the primary, the field at the top surface of the winding at $z = 0$ and the field at the bottom surface of the winding at $z = -\delta$ are both equal to $\tilde{H}_o(r)$. The complex H field distribution inside the secondary is again given by (A1), but in this case the boundary conditions are

$$\tilde{A}(r) + \tilde{B}(r) = \tilde{H}_o(r), \qquad z = 0 \tag{A9}$$

and

$$\tilde{A}(r)e^{-(1+j)} + \tilde{B}(r)e^{(1+j)} = \tilde{H}_o(r), \qquad z = -\delta \tag{A10}$$

These three equations can be evaluated to yield

$$\tilde{H}_r = \left[\frac{1-e^{-(1+j)}}{1-e^{-2(1+j)}}e^{z(1+j)/\delta} + \frac{1-e^{(1+j)}}{1-e^{2(1+j)}}e^{-z(1+j)/\delta}\right]\tilde{H}_o(r) \tag{A11}$$

The current, $\tilde{J}_\phi$, is given by

$$\tilde{J}_\phi = \frac{\partial}{\partial z}\tilde{H}_r = \frac{(1+j)}{\delta}\left[\frac{1-e^{-(1+j)}}{1-e^{-2(1+j)}}e^{z(1+j)/\delta} - \frac{1-e^{(1+j)}}{1-e^{2(1+j)}}e^{-z(1+j)/\delta}\right]\tilde{H}_o(r) \tag{A12}$$

and the power dissipation density is again given by (A6). Substituting (A12) into (A6) yields

$$P_d = \frac{1}{2\sigma\delta}|\tilde{H}_o(r)|^2 \cdot 0.32 \tag{A13}$$

If the reluctance of the magnetic material is negligible, Ampere's Law can be used to find $\tilde{H}_o(r)$,

$$\tilde{H}_o(r) = \frac{Ni_m}{\ln\left(r_{wo}/r_{wi}\right)}\frac{1}{r} \tag{A14}$$

where i_m is the magnetizing current in the primary, N is the number of turns in the primary, and the spacing between the winding and the edges of the slot is assumed to be small.

The total power dissipation can be found by substituting (A14) into (A13), and integrating over r and ϕ,

$$P_c = \frac{0.16}{\sigma\delta}\int_0^{2\pi} d\phi \int_{r_{wi}}^{r_{wo}} r\, dr\, |\tilde{H}_o(r)|^2 \tag{A15}$$

The integration is performed to yield

$$P_c = \frac{0.32\pi}{\sigma\delta}\left[\frac{N^2 i_m^2}{\ln\left(r_{wo}/r_{wi}\right)}\right] \tag{A16}$$

The resistance that the secondary adds to the effective primary resistance, follows from substituting (A16) into

$$R_s = \frac{2P_c}{i_m^2} \tag{A17}$$

giving

$$R_s = \frac{0.64\pi}{\sigma\delta}\left[\frac{N^2}{\ln\left(r_{wo}/r_{wi}\right)}\right] \tag{A18}$$

which is the same expression as (4.5). Note also that the additional resistance the secondary adds is equal to 32% of its dc value, referred to the primary.

Appendix B: Calculations of Lumped Parameter Model

Computation of L_l

The first major component of the leakage inductance is due to the leakage field between the traces, given by (A14). Each turn links the same leakage flux, so (A14) can be evaluated at $r = r_{si}$, multiplied by $\mu_o N$ and the cross sectional area, $2\pi r_{si} m$, and divided by i_m to yield

$$L_{l,air} = \frac{2\mu_o N^2 \pi m}{\ln\left(r_{so}/r_{si}\right)} \qquad (B1)$$

The second component of leakage inductance is due to the energy stored in the skin depth thick windings. The inductance added by each of the two windings is equal to

$$L_{l,cu} = \frac{\mu_o}{i^2}\int_{-\delta}^{0} dz \int_{0}^{2\pi} d\phi \int_{r_{si}}^{r_{so}} \tilde{H}_r \cdot \tilde{H}_r^* \; r \, dr \qquad (B2)$$

where $\tilde{H}_r$ is given by (A4). This expression can be evaluated[2] to yield

$$L_{l,cu} = 0.325\delta \left[\frac{2\mu_o N^2 \pi}{\ln\left(r_{so}/r_{si}\right)}\right] \qquad (B3)$$

The total leakage inductance is therefore equal to (B1) plus twice (B3), giving (5.6).

Computation of $R_{p,dc}$ for Primary Turns of Equal Width

If each primary turn is assumed to be of equal width, then (5.8) can be rewritten in terms of r_{wi} and r_{wo}, the innermost and outermost radii of the winding, using the relations

$$r_{in} = r_{wi} + (n-1)(1+\varsigma)w_t \qquad (B4)$$

and

$$r_{on} = r_{wi} + w_t + (n-1)(1+\varsigma)w_t \qquad (B5)$$

where w_t is the width of each turn, given by

$$w_t = \frac{r_{wo} - r_{wi}}{N + (N-1)\varsigma} \qquad (B6)$$

and ςw_t is the spacing between turns.

Equation (5.8) can then be rewritten as

$$R_{p,dc} = \frac{2\pi}{\sigma t}\sum_{n=1}^{N} \frac{1}{\ln\left(1 + \frac{1}{(n-1)(\varsigma+1) + r_{wi}/w_t}\right)} \qquad (B7)$$

---

[2] Equation (B2) was evaluated by MACSYMA.

Derivation of Primary Annulus Width for Minimum Copper Loss

In this analysis, the N turn spiral primary is modelled as N concentric rings connected in series. For simplicity, previous chapters have assumed that each of these rings had the same width. This assumption, however, did not result in a primary with the lowest possible resistance for the total width available. This appendix determines the distribution of ring widths that gives the lowest total resistance.

First, it was found by numerical analysis that the minimum copper loss is achieved by choosing the width of each ring so that each ring has the same resistance. A necessary condition for this can be shown analytically by means of the following simple analysis. Equation (5.9) can be rewritten as

$$\begin{aligned} R = \frac{2\pi}{\sigma\delta}\sum_{n=1}^{N}\frac{1}{\ln(r_{n+1}/r_n)} = \frac{2\pi}{\sigma\delta}\Bigg[&\frac{1}{\ln(r_2/r_1)} + \dots + \frac{1}{\ln(r_n/r_{n-1})} \\ &+ \frac{1}{\ln(r_{n+1}/r_n)} + \dots + \frac{1}{\ln(r_N/r_{N-1})}\Bigg] \end{aligned} \tag{B8}$$

Since the r_n are all independent variables, the minimum resistance occurs when $\partial R/\partial r_n = 0$.[3] Taking the derivative of (B8) gives

$$\frac{\partial R}{\partial r_n} = \frac{\partial}{\partial r_n}\left[\frac{1}{\ln(r_n/r_{n-1})} + \frac{1}{\ln(r_{n+1}/r_n)}\right] = 0 \tag{B9}$$

Evaluating (B9) gives a necessary criterion for minimum copper loss,

$$\frac{r_n}{r_{n-1}} = \frac{r_{n+1}}{r_n} \tag{B10}$$

In other words, the ratio of the ring's outer radius to its inner radius should be equal for each ring. Inspection of (5.9) shows that this is equivalent to choosing the width that gives each concentric ring the same resistance.

The resistance of a primary winding that satisfies (B10) is given by

$$R_{p,dc} = N\,\frac{2\pi}{\sigma\delta\ln(r_{n+1}/r_n)} = \frac{2\pi}{\sigma\delta\ln(r_{n+1}/r_n)^{1/N}} \tag{B11}$$

It was found by numerical analysis that if the spacing between primary turns is neglected, then the minimum primary resistance given by (B11) is equal to the reflected resistance of a one turn secondary winding with the same total width, given by

$$R_{p,dc} = \frac{2\pi N^2}{\sigma\delta\ln(r_{wo}/r_{wi})} = \frac{2\pi N^2}{\sigma\delta\ln(r_{N+1}/r_1)} \tag{B12}$$

---

[3] F. B. Hildebrand, *Methods of Applied Mathematics*, 2nd ed., Prentice-Hall, Inc., Englewood Cliffs, New Jersey (1965), p. 120.

Comparison of (B11) and (B12) shows that

$$\frac{r_{N+1}}{r_1} = \left(\frac{r_{n+1}}{r_n}\right)^N \qquad (B13)$$

which can be recast to yield the recurrence relation, (5.10).

An analytic proof of (B13) follows.[4] First, note that

$$\frac{r_{n+1}}{r_n} = \frac{r_{N+1}}{r_N} \qquad (B14)$$

This expression can be recast as

$$\frac{r_{n+1}}{r_n}\frac{r_N}{r_n} = \frac{r_{N+1}}{r_n} \qquad (B15)$$

But r_N/r_n can be rewritten, using (B10), as

$$\frac{r_N}{r_n} = \frac{r_{n+1}}{r_n}\frac{r_{n+2}}{r_{n+1}} \dots \frac{r_{n+(N-n)}}{r_{n+(N-n-1)}} = \left(\frac{r_{n+1}}{r_n}\right)^{N-n} \qquad (B16)$$

Substituting (B16) into (B15) gives the general relation

$$\left(\frac{r_{n+1}}{r_n}\right)^{N-n+1} = \frac{r_{N+1}}{r_n} \qquad (B17)$$

Equation (B13) follows from taking (B17) with $n = 1$.

Computation of r_n for Primary Turns of Equal Width

The primary and secondary windings can be considered as a parallel plate capacitor. The area of each primary turn, A_n, can be computed as

$$A_n = \pi(r_{on}^2 - r_{in}^2) \qquad (B18)$$

Using (B18) with (B4) and (B5), A_n can be rewritten as

$$A_n = 2\pi w_t \left[r_{wi} + w_t \left[(n-1)(1+\varsigma) + \frac{1}{2}\right]\right] \qquad (B19)$$

Equation (B19) can be rewritten as

$$A_n = 2\pi w_t r_n \qquad (B20)$$

where r_n is identified as the effective radius of the n^{th} turn, and is given by

$$r_n = r_{wi} + w_t \left[(n-1)(1+\varsigma) + \frac{1}{2}\right] \qquad (B21)$$

---

[4] Proof by Jay Damask.

Computation of γ for Primary Turns of Equal Width

The differential mode secondary voltage can be computed from (5.15), which expresses the constraint that the net charge on the secondary must be zero. Equation (5.15) can be expanded to give

$$\sum_{n=1}^{N}\left[V_s-\frac{nV_t}{N}\right]\left[r_{wi}-w_t\left(\frac{1}{2}+\varsigma\right)\right]+\left[V_s-\frac{nV_t}{N}\right]\left[w_t n(1+\varsigma)\right]=0 \tag{B22}$$

The summations can be eliminated by use of the relations

$$\sum_{i=1}^{j} i=\frac{j(j+1)}{2} \tag{B23}$$

and

$$\sum_{i=1}^{j} i^2=\frac{j(j+1)(2j+1)}{6} \tag{B24}$$

to yield (5.16), where

$$\gamma=\frac{r_{wi}-w_t\left(\frac{1}{2}+\varsigma\right)+\frac{w_t(1+\varsigma)(2N+1)}{3}}{\frac{2}{N+1}\left[r_{wi}-w_t\left(\frac{1}{2}+\varsigma\right)\right]+w_t(1+\varsigma)} \tag{B25}$$

Appendix C: Derivation of Chapter 6 Results

1) ξ (Eq. 6.7)

Eqs. (6.2) and (6.6) are substituted into (6.3) to yield

$$v = \mu_i N^2 h f i_m \int_a^b \sqrt{1+\left(\frac{\alpha N}{2\pi r}\right)^2 |i_m|^2}\,\frac{1}{r}\,dr \tag{$C1$}$$

This integral is evaluated to yield

$$v = \mu_i N^2 h f i_m \left[\varphi(a) - \varphi(b) + \frac{1}{2}\ln\left[\frac{(\varphi(b)+1)(\varphi(a)-1)}{(\varphi(b)-1)(\varphi(a)+1)}\right]\right] \tag{$C2$}$$

where

$$\varphi(r) = \sqrt{\left(\frac{\alpha N}{2\pi r}\right)^2 |i_m|^2 + 1} \tag{$C3$}$$

Comparing (C2) with (6.7) gives

$$\xi(a, b, \mu_i, \alpha, i_m) = \varphi(a) - \varphi(b) + \frac{1}{2}\ln\left[\frac{(\varphi(b)+1)(\varphi(a)-1)}{(\varphi(b)-1)(\varphi(a)+1)}\right] \tag{$C4$}$$

2) P_h (Eq. 6.11)

The integral in (6.10) is evaluated as follows.

$$P_h = \pi f h \sum_{n=1}^{3} \int_a^b \gamma_n \left[\mu_i \varphi(r) \left(\frac{\alpha N}{2\pi}\right)^2 \frac{|i_m|^2}{r^2}\right]^n r\,dr \tag{$C5$}$$

The result can be expressed as

$$P_h = \pi f h \mu_i \left(\frac{N}{2\pi}\right)^2 |i_m|^2 \left[\gamma_1 I_1 + \gamma_2 I_2 + \gamma_3 I_3\right] \tag{$C6$}$$

where

$$\gamma_1 = \varphi(a) - \varphi(b) + \frac{1}{2}\ln\left[\frac{(\varphi(b)+1)(\varphi(a)-1)}{(\varphi(b)-1)(\varphi(a)+1)}\right] \tag{$C7$}$$

$$\gamma_2 = \frac{\mu_i}{4\alpha^2}\left(\varphi(a)^4 - \varphi(b)^4\right) \tag{$C8$}$$

$$\gamma_3 = \frac{\mu_i^2}{\alpha^4}\left[\frac{1}{5}\left(\varphi(b)^5 - \varphi(a)^5\right) + \frac{1}{7}\left(\varphi(a)^7 - \varphi(b)^7\right)\right] \tag{$C9$}$$

Appendix D: Material Measurement Software

D.1 ASYST programs

ASYST is an interpretive high level language whose primitive operations provide for data acquisition, statistical analysis, and graphical display.[5]

This section describes the routines that were written in the ASYST language to control the measurement apparatus, acquire voltage and current data, correct for parasitics, and determine the amplitude and phase of the waveforms. The source code for these programs has been published separately.[6]

The software is menu driven and self explanatory. The programs are well documented and the new user should read ANL.A before using the rig, in order to understand exactly what the analysis routines do.

PLOT.BAT	This is a batch procedure that starts the program. The package is invoked by typing "PLOT" from the DOS command prompt.
INIT.A	This is an ASCII file that contains site-dependent parameters that can be changed at run time. Examples include the value of the current sense resistor, values of the parasitics, and the type of oscilloscope.
LDPLT.A	This module contains the instructions that read in the modules and save an image, PLOT, of the interpreted code. Since ASYST is a one-pass interpreter, GLB.A must appear first in this file, and DRV.A must appear last. The saved image is constructed by typing "ASYST LOAD LDPLT.A" at the DOS command prompt.
GLB.A	This module contains definitions and routines used by the other modules.
DRV.A	This module contains the driving loop. It presents the top level menu of commands to the user. The modules listed below (ACQ, ANL, PLT, DSK) are accessed from this menu.
ACQ.A	This module controls the GPIB bus to which the instruments and the computer are connected. The instruments should be set to the bus addresses listed in

---

[5] Asyst Software Technologies, Inc., Rochester, New York.

[6] A. F. Goldberg, "Software for Magnetic Material Analysis," Laboratory for Electromagnetic and Electronics Systems Technical Report, Massachusetts Institute of Technology, Cambridge, Mass. (1988).

Table B.1. Two oscilloscopes are currently supported, the Tektronix 2430 and the Tektronix 11401. The choice of oscilloscope must be noted in INIT.A. The 2430, which gives 8 bits of vertical resolution, should be set to collect 1024 samples, and the 11401, which gives 10 bits of vertical resolution, should be set to collect 2048 samples.

When the module is invoked, it initializes the bus and presents the menu of commands. The commands allow the user to set approximately the frequency and voltage of the excitation. These parameters are set open loop, so that if particular values are required, the user may need to manually adjust the equipment controls. The "Get Data" command assumes that the voltage signal is on channel 2 of the oscilloscope and that the current signal is on channel 1.

Table B.1: GPIB Bus Addresses

Device	Bus Address
Computer	0
Oscilloscope	1
Signal Generator	2
Frequency Counter	3

PLT.A This module displays the voltage and current waveforms on the screen and on any plotter, attached to the COM1 serial port, that understands the Hewlett-Packard graphics language (HPGL).

DSK.A This module stores and reads data from the disk, and its commands are part of the main menu. Data that is stored and read is ordinarily in the internal ASYST format. There is a command to read ASCII files containing x,y pairs, but the command to store data as ASCII x,y pairs has not be written. The ASCII file must contain one pair per line in scientific notation. If the exponentiation character 'E' is present it must be capitalized. The x and the y numbers must be separated by a space, a comma, and a space. The file must be terminated by a control-Z (1A Hex) followed by a null (00 Hex). Note that this termination is not the default produced by either Lattice-C V. 3 or Microsoft C V. 4.0. For this reason the routine good_fclose() is provided in AIO.C, listed below.

ANL.A This module analyses the data acquired from the measurement rig. The program determines the magnitude and phase of the Fourier components of the digitized data by means of a discrete Fourier analysis.[7] When invoked, the program prompts for the frequency that the measurement was made at. The program is commented and should be read by the new user. There are two commands for scaling the acquired data. "Impedance scale" is used for measurements of one-ports (voltage and current measured from the same terminal pair). "Hysteresis scale" is used for two-port measurements of hysteresis loss in toroids, where the current is measured on the primary side and the voltage is measured on the secondary side. Parasitic compensation is automatically performed for two-port measurements, but must be explicitly requested for one-port measurements by invoking the "parasitic compensation" command after the "impedance scale" command.

There are three commands for recalibration. These commands are independent of the calibration routines built into the digitizing oscilloscope. These commands also do not determine the scope input capacitance, the inductance of the current sense resistor, and the capacitance of the cable that connects the toroidal transformer secondary to the oscilloscope. These three parameters must be determined independently and adjusted in INIT.A. Note that the oscilloscope, signal generator, and frequency counter should be left on for several days prior to the measurement in order for their components to reach a thermal steady state. The recalibration routines must be performed in order. If their results are to affect future sessions, the values displayed must be entered in the INIT.A file next to the appropriate parameter. The first calibration routine, "delay calibration", determines the time delay between channels and assumes that none of the other ANL.A commands have been executed yet. For the "delay calibration" measurement, the same signal must have been applied to both channels, and the same cable lengths must be the same. Next the "open circuit calibration" can be performed. This assumes that the measurement rig is set up for one-port measurements, and that a measurement has been made with the measurement port open-circuited. Before the "open circuit calibration" command can be executed, the "impedance scale" command must be given. Finally, the "short circuit calibration" can be performed. The procedure is identical to that of the "open circuit calibration", except that the

---

[7] F. B. Hildebrand, *Introduction to Numerical Analysis*, McGraw-Hill Book Company, Inc., New York (1956), pp. 373–378.

measurement port is short circuited.

D.2 C programs

These programs convert voltage and current data generated by the ASYST package to permeability and loss data. They compile under the Microsoft C compiler, version 4.0. The source code for these programs has been published separately.[8]

Each data file contains the voltage, current, phase shift, and power dissipation data generated by the ASYST package at different voltages at a particular frequency. Each line of the data file corresponds to one measurement and has the format: voltage, current, power dissipation, phase shift. Each item is in scientific notation, and the units are MKS and degrees. If the optional exponentiation character, 'E', is used, it must be capitalized. The items must be separated by a space, a comma, and a space. The lines must be arranged in order of ascending voltage.

The programs all assume MKS units unless otherwise specified. The routines generally read data files, process them, and write the output files. These files can be specified from the DOS command line. If omitted, the program will ask for them. Input files must be specified. If no output files are specified (by hitting a carriage return only when asked for the output file name), the program will continue without saving its data on disk. The output files that are created are all readable with the ASYST package above in order to be plotted on the screen or the hard copy device.

CHECK.C	This program checks a data file for internal consistency, since any entry in a line can be derived from the other three. It is invoked by typing "CHECK datafilename" at the DOS command prompt.
MUFIT3.C	This program determines the parameters μ_i and α associated with the material permeability in (6.5). It prompts the user for the toroid dimensions and other relevant information, and asks for an initial guess for μ_i and α. This routine uses the Powell conjugate directions minimization alogorithm to find the values for μ_i and α that give the least square error.[9] The program produces three output files. The first is the current-voltage curve fit, described in Sec. 6.2.2.2,

---

[8] A. F. Goldberg, "Software for Magnetic Material Analysis," Laboratory for Electromagnetic and Electronics Systems Technical Report, Massachusetts Institute of Technology, Cambridge, Mass. (1988).

[9] W. H. Press et al., *Numerical Recipes in C: The Art of Scientific Computing*, Cambridge University Press, New York (1988), pp. 290–317.

	and the second is the B-μ curve that corresponds to the input data. The third file contains the fit error at each point. The program also displays the standard deviation.
NLHYST2.C	This program determines the values for the γ_n associated with the power loss density in Sec. 6.2.2.3. The program prompts for the geometry of the toroid and other experimental parameters. It also asks for the values of μ_i and α determined by FMUFIT3 and for the number of γ_n to use in the model. The program performs a nonlinear least squares curve fit using the Marquardt gradient expansion algorithm to determine the γ_n.[10] The program will also asks if the user want to introduce weighting, discussed in Sec. 6.2.2.4, into the fit. Three output files are produced: the current-power curve fit, the B-power density curve that corresponds to the input data, and the fit error at each point. The program displays the standard deviation, the average per-cent error, and the minimum and maximum values of power dissipation.
GRAFNL2.C	The B-power density curve produced by NLHYST2 has points only at flux levels where the input data file had measurements. GRAFNL2 is a version of NLHYST2 that produces many points along the curve fit. This program is useful for generating plots for documents.
AIO.C	This is a collection of i/o routines common to all the C programs. It is compiled as a library and linked with each object file.

---

[10] Bevington, pp. 204–246.

Appendix E: Loss in Secondary Winding

This section derives (7.10), the loss in the secondary winding when all the magnetizing current flows in the primary. An inspection of (7.3) and (7.4) shows that the current in the secondary, I_s, can be expressed as

$$I_s = I_{l,dc} + \sum_{n=1}^{\infty} I_{l,sn}\sin(2\pi f_o nt) - \sum_{n=1}^{\infty} I_{l,cn}\cos(2\pi f_o nt) - I_m\cos(2\pi f_o t) \qquad (E1)$$

where the terms are defined in Table E1.

Table E1: Definition of Terms in (E1)

Symbol	Definition
$I_{l,dc}$	dc component of load current
$I_{l,sn}$	sine coefficient of n^{th} harmonic of load current
$I_{l,cn}$	cosine coefficient of n^{th} harmonic of load current
I_m	cosine coefficient of magnetizing current

The dc power can be computed separately and is dropped from the following analysis. The field due to the load current is maximum below the secondary, and negligible above the secondary, so that the load current density associated with each harmonic is given by adjusting (A5),

$$\tilde{J}_{l,\phi n} = -(I_{l,cn} + jI_{l,sn})\frac{(1+j)}{\delta}\left[\frac{e^{z(1+j)/\delta}}{1-e^{-2(1+j)}} - \frac{e^{-z(1+j)/\delta}}{1-e^{2(1+j)}}\right]\frac{N}{\ln\left(r_{wo}/r_{wi}\right)}\frac{1}{r} \qquad (E2)$$

The field generated by the magnetizing current in the primary, which only has a fundamental mode, is the same above and below the secondary and is given by adjusting (A12),

$$\tilde{J}_{m,\phi} = -I_m\frac{(1+j)}{\delta}\left[\frac{1-e^{-(1+j)}}{1-e^{-2(1+j)}}e^{z(1+j)/\delta} - \frac{1-e^{(1+j)}}{1-e^{2(1+j)}}e^{-z(1+j)/\delta}\right]\frac{N}{\ln\left(r_{wo}/r_{wi}\right)}\frac{1}{r} \qquad (E3)$$

The power dissipated by each mode can be computed separately, since they are orthogonal. The power in the n^{th} is computed by evaluating (A6) with[11]

$$\tilde{J}_{\phi} = \tilde{J}_{l,\phi n} + \delta_{0n}\tilde{J}_{m,\phi} \qquad (E4)$$

giving a power loss density of

$$P_d = \frac{1}{2\sigma\delta}\left(\frac{N}{r\ln\left(r_{wo}/r_{wi}\right)}\right)^2\left(1.09I_{l,sn}^2 + 1.09I_{l,cn}^2 + 0.32\delta_{0n}I_m^2 + 0.32\delta_{0n}I_{l,cn}I_m\right) \qquad (E5)$$

---

[11] Equation (A6) was evaluated by MACSYMA.

Equation (7.10) follows from integrating (E5) over the volume of the secondary and adding the dc power.

Appendix F: Derivation of P_h/P_c Constraint

This appendix gives the derivation of a constraint on P_h/P_c for an N:1 transformer.[12,13] The derivation considers an N:1 transformer of a given size and determines the N that gives the lowest loss. The approach is to express P_t in terms of N, then treat N as an independent variable and derive a minimum power constraint from $\partial P_t/\partial N = 0$.

If R_l is the load impedance referred to the primary and V the voltage applied to the primary, then the dependence of P_c on N is given by

$$P_c \propto \left(\frac{V}{R_l}\right)^2 R_t \propto V^2 N^2 \tag{F1}$$

where R_t is given by (7.13). The core loss is assumed to be proportional to B^n, where n is an empirically determined material constant. The dependence of P_h on N is given by

$$P_h \propto B^n \propto \left(\frac{V}{N}\right)^n \tag{F2}$$

The minimum power loss constraint follows from

$$\frac{\partial P_t}{\partial N} = \frac{\partial}{\partial N}\left(k_1 V^2 N^2 + k_2 \frac{V^2}{N^2}\right) = 0 \tag{F3}$$

where k_1 and k_2 do not depend on N. Equation (F3) can be evaluated and combined with (F1) and (F2) to yield

$$\frac{P_h}{P_c} = \frac{2}{n} \tag{F4}$$

For a material whose core loss is proportional to B^2, (F4) states that $P_c = P_h$.

---

[12] E. C. Snelling and A. D. Giles, *Ferrites for Inductors and Transformers*, Research Studies Press, Ltd., Letchworth, Hertfordshire, England (1983), p. 128

[13] S. Smith, *Magnetic Components: Design and Applications*, Van Nostrand Reinhold Company, New York (1985), p. 43.

Appendix G: ZZCHAP7.C

```
/*
        zzchap7.c
        design studies for thesis
        A. F. Goldberg,  May/June 1988
        Copyright Massachusetts Institute of Technology, 1988,
        except as indicated
*/


#include <stdio.h>
#include <math.h>
#include <string.h>
#include <malloc.h>

#define TRUE 1
#define FALSE -1
#define VARS_PER_LINE 3
#define MAX_VAR_LEN 10
#define PI 3.141592654
#define MUO 1.256637062E-6
#define EPO 8.8541853e-12

char token[80];
char fname[80];
int command;

struct var_list
        {
        char *var_name;
        double var_val;
        char *var_desc;
        };

struct var_list ind_var[] =
                {
                "temp",25.0,"temperature",
                "epr",3.2,"dielectric constant of winding substrate",
                "rtol",0.5e-6,"tolerance for root solver",
                "freq",5.0e6,"frequency",
                "Pt",1.0,"total power dissipated",
                "Lo",13.3,"magnetizing inductance is Lo / freq",
                "Nrat",7.0,"turns ratio",
                "Nmul",1.0,"turns on secondary",
                "Im",0.75,"amplitude of magnetizing current",
                "Ils",20.0,"peak of secondary sawtooth load current",
                "sigma",5.8e7,"conductivity of copper",
                "spacing",70.0e-6,"primary turn spacing",
                "leaf",1.0,"number of interleaving",
                "m",25.4e-6,"distance between primary and secondary",
                "tr_wi",2.0e-3,"initial guess for r_wi",
                "t_delta",2.0e-3,"initial guess for delta",
                "core",1.0,"if zero then neglect core loss",
                "stats",0.0,"if nonzero then print root solver statistics"
                 };
#define NUM_IND (sizeof(ind_var) / sizeof(struct var_list))

struct var_list dep_var[] =
```

```
                        {
                        "Arat",0.0,"ratio of Ai to Ao",
                        "sigma",0.0,"conductivity of copper at temp",
                        "delta",0.0,"thickness of outer ferrite wall",
                        "Il",0.0,"load current in primary",
                        "Prat",0.0,"ratio of hysteresis loss to copper loss",
                        "fres",0.0,"leakage-capacitance self resonant frequency",
                        "diam",0.0,"diameter of core",
                        "CapC",0.0,"common mode capacitance",
                        "CapD",0.0,"differential mode capacitance",
                        "CapT",0.0,"total capacitance",
                        "B2",0.0,"coefficient of B**2 term",
                        "B4",0.0,"coefficient of B**4 term",
                        "B6",0.0,"coefficient of B**6 term",
                        "skdep",0.0,"skin depth",
                        "Lm",0.0,"magnetizing inductance",
                        "Pc",0.0,"copper loss",
                        "r_wi",0.0,"inside radius of slot",
                        "r_wo",0.0,"outside radius of slot",
                        "R_p_dc",0.0,"dc resistance of primary",
                        "R_s_dc",0.0,"dc resistance of secondary",
                        "height",0.0,"total height of structure",
                        "Ll",0.0,"leakage inductance",
                        "Lrat",0.0,"ratio of magnetizing to leakage inductance",
                        "w",0.0,"width of groove",
                        "Bmax",0.0,"maximum B-field in Gauss",
                        "Ph",0.0,"core loss",
                        "gap",0.0,"length of gap",
                        "area",0.0,"footprint",
                        "volume",0.0,"volume",
                        "Ro",0.0,"outer radius"
                        };
#define NUM_DEP (sizeof(dep_var) / sizeof(struct var_list))

/*************************************************************************/
/*********** Driving Loop ************************************************/
/*************************************************************************/

void main(argc, argv)
int argc;
char *argv[];
{
void sort(), signon(), print_all(), vary_ind(), parametrize();
void describe(), vary_ind_find_min();
int savedata(), getdata(), ask_ind(), find_var();

signon();
sort(ind_var,NUM_IND);
sort(dep_var,NUM_DEP);

if (argc > 1)
        {
        command = TRUE;
        sscanf(argv[1], "%s", fname);
        getdata();
        }
else
        {
        command = FALSE;
/*      print_all(); */
```

```
        }

do {
        printf("\nMUNG> ");
        scanf("%s",token);
        if(ask_ind(find_var(token, ind_var, NUM_IND)) == FALSE)
                switch(*token)
                        {
                        case 'C':
                        case 'c':
                                print_all();
                                break;
                        case 'V':
                        case 'v':
                                vary_ind();
                                break;
                        case 'P':
                        case 'p':
                                parametrize();
                                break;
                        case 'W':
                        case 'w':
                                savedata();
                                break;
                        case 'D':
                        case 'd':
                                describe();
                                break;
                        case 'R':
                        case 'r':
                                getdata();
                                break;
                        case 'S':
                        case 's':
                                vary_ind_find_min();
                                break;
                        case 'Q':
                        case 'q':
                                return;
                                break;
                        case '?':
                        case 'H':
                        case 'h':
printf("\nC: Compute, V: Vary, W: Write, R: Read, P: Parametrize\nD: Describe, Q
: Quit, ? or H: Help");
printf("\nS: Minimize -- For more help consult MUNG reference guide.\n");
                                break;
                        default:
                                printf("\n?Eh? What is %s?",token);
                                break;
                        }
   }
while (TRUE);

}

/********************************************************************/
/*********** Subroutines ********************************************/
/********************************************************************/

void signon()
```

```
{
printf("\nThis is MUNG 6.0\nPrototype Transformer Analysis for Thesis\n\n");
}

int ndepen, nindep, nsweep;
void vary_ind_find_min()
/*
        vary one indep. variable and at each point find minimum of one
        dependent variable with respect to another indep. var
        can be expanded to handle more than one indep var.
*/
{
double start_ind,end_ind,incr,answer;
double get_ind(),get_dep();
double vifm1();
char depen[80],indep[80],sweep[80];
FILE *fp,*fopen();
double indlist[1];
void powell(), compute_dep();
int max_iter,iter;

printf("\nThis will sweep over a range of independent variable (a)");
printf("\nand at each point adjust independent variable (b) so as to");
printf("\nminimize dependent variable (c).  The algorithm uses the");
printf("\nPowell conjugate directions algorithm. The output");
printf("\nfile contains (a,c) pairs.");

printf("\n\nFile for ASYST output: ");
scanf("%s",fname);
if ( (fp = fopen(fname,"w")) == NULL)
        {
        printf("Error opening file %s for writing.\n",fname);
        return;
        }

printf("\nSweep independent variable: ");
scanf("%s",sweep);
if ((nsweep = find_var(sweep, ind_var, NUM_IND)) == FALSE)
        {
        printf("%s is not an independent variable.\n",sweep);
        return;
        }

printf("Vary independent variable: ");
scanf("%s",indep);
if ((nindep = find_var(indep, ind_var, NUM_IND)) == FALSE)
        {
        printf("%s is not an independent variable.\n",indep);
        return;
        }

printf("Minimize dependent variable: ");
scanf("%s",depen);
if ((ndepen = find_var(depen, dep_var, NUM_DEP)) == FALSE)
        {
        printf("%s is not a dependent variable.\n",depen);
        return;
        }

printf("Starting value of %s: ",sweep);
```

```
scanf("%lf",&start_ind);
printf("Final value of %s: ",sweep);
scanf("%lf",&end_ind);
printf("Increment: ");
scanf("%lf",&incr);

indlist[0] = ind_var[nindep].var_val;
max_iter = ((int) (1.5 + (end_ind - start_ind) / incr));
for (iter = 0; iter < max_iter; iter++)
        {
        ind_var[nsweep].var_val = start_ind;
        powell(vifml,indlist,1);
        ind_var[nindep].var_val = indlist[0];
        compute_dep();
        fprintf(fp,"%1.6lE , %1.6lE\n", ind_var[nsweep].var_val,
                dep_var[ndepen].var_val);
        if ( ((int) (get_ind("stats") + 0.5)) != 0) printf("\n");
        printf("%s is %1.6lE, %s is  %1.6lE, at %s = %1.6lE\n",
                sweep, ind_var[nsweep].var_val,
                depen, dep_var[ndepen].var_val,
                indep, ind_var[nindep].var_val);
        start_ind += incr;
        }

fputc(0x1a,fp);                                 /* cntrl-Z */
fputc(0x00,fp);                                 /* null */
fclose(fp);
}

double vifml(p)
double p[];
{
void compute_dep();

ind_var[nindep].var_val = p[0];
compute_dep();
return(dep_var[ndepen].var_val);
}

#define pITLIM 200
#define FTOL 1.0e-6

void powell(f,p,n)
double (*f)(), p[];
int n;
/*
        minimize function using Powell conjugate directions algorithm
        code adapted from "Numerical Recipes in C" by Press et al.
        f:  function
        p:  vector of independent variables initialized to starting guess
        n:  number of independent variables
*/
{
double *pt, *ptt, **xi, *xit, *mkvec(), **mkmat();
double y,t,fptt,fp,del;
double linmin(), fabs(), sqr();
void rmvec(), rmmat();
int iter, jter, count, ibig;
double get_ind();
```

```
/* initialize starting guess of direction to unit vectors */
xi = mkmat(n,n);
for (iter = 0; iter < n; iter++)
        for (jter = 0; jter < n; jter++)
                if (iter == jter)
                        xi[iter] [jter] = p[iter];
                else
                        xi[iter] [jter] = 0.0;

pt = mkvec(n);
ptt = mkvec(n);
xit = mkvec(n);

y = (*f)(p);
for (iter = 0; iter < n; iter++)
        pt[iter] = p[iter];

count = 1;
do
        {
        fp = y;
        ibig = 0;
        del = 0.0;
        for (iter = 0; iter < n; iter++)
                {
                for (jter = 0; jter < n; jter++)
                        xit[jter] = xi[jter] [iter];
                fptt = y;
                y = linmin(f,p,n,xit);
                if (fabs(fptt - y) > del)
                        {
                        del = fabs(fptt - y);
                        ibig = iter;
                        }
                }
        if (2.0 * fabs(fp - y) <= FTOL * (fabs(fp) + fabs(y)))
                {
                rmvec(xit,n);
                rmvec(ptt,n);
                rmvec(pt,n);
                rmmat(xi,n,n);
                return;
                }
        for (jter = 0; jter < n; jter++)
                {
                ptt[jter] = 2.0 * p[jter] - pt[jter];
                xit[jter] = p[jter] - pt[jter];
                pt[jter] = p[jter];
                }
        fptt = (*f)(ptt);
        if (fptt < fp)
                {
                t = 2.0 * (fp - 2.0 * y + fptt) * sqr(fp - y - del) -
                    del * sqr(fp - fptt);
                if (t < 0.0)
                        {
                        y = linmin(f,p,n,xit);
                        for (jter = 0; jter < n; jter++)
                                xi[jter] [ibig] = xit[jter];
                        }
```

```
                }
        }
while (count++ < pITLIM);
printf("\n from powell: Too many iterations (%d)", pITLIM);
}

#define TOL 2.0e-4
int ncom=0;
double *pcom=0, *xicom=0, (*nrfunc)();

double linmin(f,p,n,xi)
double (*f)(), p[], xi[];
int n;
/*
        Given function, point, and direction vector, finds
        minimum along line in direction given from point given.
        Resets direction vector to displacement of point, resets
        point, and returns value of function at point
        code adapted from "Numerical Recipes in C" by Press et al.

        f       function
        p       point
        n       number of independent variables
        xi      direction vector
*/
{
int iter;
double xx,xmin,fx,fb,fa,bx,ax;
double fp,brent(),f1dim(),*mkvec();
void mnbrak(),rmvec();

ncom = n;
pcom = mkvec(n);
xicom = mkvec(n);
nrfunc = f;
for (iter = 0; iter < n; iter++)
        {
        pcom[iter] = p[iter];
        xicom[iter] = xi[iter];
        }
ax = 0.0;
xx = 1.0;
bx = 2.0;
mnbrak(&ax,&xx,&bx,&fa,&fx,&fb,f1dim);
fp = brent(ax,xx,bx,f1dim,TOL,&xmin);
for (iter = 0; iter < n; iter++)
        {
        xi[iter] *= xmin;
        p[iter] += xi[iter];
        }
rmvec(xicom,n);
rmvec(pcom,n);
return(fp);
}

double f1dim(x)
double x;
{
int iter;
double answer,*xt,*mkvec();
```

```
void rmvec();

xt = mkvec(ncom);
for (iter = 0; iter < ncom; iter++)
        xt[iter] = pcom[iter] + x * xicom[iter];
answer = (*nrfunc)(xt);
rmvec(xt,ncom);
return(answer);
}

#define GOLD 1.618034
#define GLIMIT 100.0
#define TINY 1.0e-20
#define MAX(a,b) ((a) > (b) ? (a) : (b))
#define SIGN(a,b) ((b) > 0.0 ? fabs(a) : -fabs(a))
#define SHFT(a,b,c,d) (a)=(b);(b)=(c);(c)=(d)

void mnbrak(ax,bx,cx,fa,fb,fc,f)
double *ax,*bx,*cx,*fa,*fb,*fc;
double (*f)();
/*
        bracket minimum. Given function f and initial points (ax, bx),
        search downhill and return bracket (ax,bx,cx) and values of f
        at bracket points (fa, fb, fc)
        code adapted from "Numerical Recipes in C" by Press et al.
*/
{
double ulim,u,r,q,fu,dum;
*fa = (*f)(*ax);
*fb = (*f)(*bx);
if (*fb > *fa)
        {
        SHFT(dum,*ax,*bx,dum);
        SHFT(dum,*fb,*fa,dum);
        }
*cx = (*bx) + GOLD * (*bx - *ax);
*fc = (*f)(*cx);

while (*fb > *fc)
        {
        r = (*bx - *ax) * (*fb - *fc);
        q = (*bx - *cx) * (*fb - *fa);
        u = (*bx) - ((*bx - *cx) * q - (*bx - *ax) * r) /
                (2.0 * SIGN(MAX(fabs(q - r),TINY), q - r));
        ulim = (*bx) + GLIMIT * (*cx - *bx);

        if ((*bx - u) * (u - *cx) > 0.0)
                {
                fu = (*f)(u);
                if (fu < *fc)
                        {
                        *ax = (*bx);
                        *bx = u;
                        *fa = (*fb);
                        *fb = fu;
                        return;
                        }
                else
                        if (fu > (*fb))
                                {
```

```
                                *cx = u;
                                *fc = fu;
                                return;
                                }
                        u = (*cx) + GOLD * (*cx - *bx);
                        fu = (*f)(u);
                        }
                else
                        if ((*cx - u) * (u - ulim) > 0.0)
                                {
                                fu = (*f)(u);
                                if (fu < (*fc))
                                        {
                                        SHFT(*bx, *cx, u, *cx + GOLD * (*cx - *bx));
                                        SHFT(*fb, *fc, fu, (*f)(u));
                                        }
                                }
                        else
                                if ((u - ulim) * (ulim - *cx) >= 0.0)
                                        {
                                        u = ulim;
                                        fu = (*f)(u);
                                        }
                                else
                                        {
                                        u = (*cx) + GOLD * (*cx - *bx);
                                        fu = (*f)(u);
                                        }
                SHFT(*ax,*bx,*cx,u);
                SHFT(*fa,*fb,*fc,fu);
                }
}

#define bITLIM 100
#define CGOLD 0.3819660
#define ZEPS 1.0e-10

double brent(ax,bx,cx,f,tol,xmin)
double ax,bx,cx,tol,*xmin;
double (*f)();
/*
        given function f and bracket for minimum (ax,bx,cx),
        isolate minimum to fractional precision tol using Brent's
        method. Return minimum (xmin) and brent returns f(xmin).
        code adapted from "Numerical Recipes in C" by Press et al.
*/
{
int iter;
double a,b,d,etemp,fu,fv,fw,fx,p,q,r,tol1,tol2,u,v,w,x,xm;
double e=0.0;

a = ((ax < cx) ? ax : cx);
b = ((ax > cx) ? ax : cx);
x = w = v = bx;
fw = fv = fx = (*f)(x);

for (iter = 0; iter < bITLIM; iter++)
        {
        xm = 0.5 * (a + b);
        tol2 = 2.0 * (tol1 = tol * fabs(x) + ZEPS);
```

```
if (fabs(x - xm) <= (tol2 - 0.5 * (b - a)))
        {
        *xmin = x;
        return(fx);
        }
if (fabs(e) > tol1)
        {
        r = (x - w) * (fx - fv);
        q = (x - v) * (fx - fw);
        p = (x - v) * q - (x - w) * r;
        q = 2.0 * (q - r);
        if (q > 0.0)
                p = -p;
        q = fabs(q);
        etemp = e;
        e = d;
        if (fabs(p) >= fabs(0.5 * q * etemp) ||
            p <= q * (a - x) || p >= q * (b - x))
                d = CGOLD * (e = (x >= xm ? a - x : b - x));
        else
                {
                d = p / q;
                u = x + d;
                if ((u - a) < tol2 || (b - u) < tol2)
                        d = SIGN(tol1, xm - x);
                }
        }
else
        d = CGOLD * ( e = (x >= xm ? a - x : b - x));
u = (fabs(d) >= tol1 ? x + d : x + SIGN(tol1,d));
fu = (*f)(u);
if (fu <= fx)
        {
        if (u >= x)
                a = x;
        else
                b = x;
        SHFT(v,w,x,u);
        SHFT(fv,fw,fx,fu);
        }
else
        {
        if (u < x)
                a = u;
        else
                b = u;
        if (fu <= fw || w == x)
                {
                v = w;
                w = u;
                fv = fw;
                fw = fu;
                }
        else
                if (fu <= fv || v == x || v == w)
                        {
                        v = u;
                        fv = fu;
                        }
        }
```

```
        }
printf("\n from brent: Too many iterations (%d)", bITLIM);
*xmin = x;
return(fx);
}

double *mkvec(length)
int length;
{
double *vec;
char *err;

vec = (double *) (err = malloc((unsigned) (length * sizeof(double))));
if (err == NULL)
        printf("\n from mkvec: Insufficient space for %d byte vector",
                length * sizeof(double));
return(vec);
}

void rmvec(vec, length)
double *vec;
int length;
{
free((char *) vec);
}

double **mkmat(maxrow,maxcol)
int maxrow, maxcol;
{
double **mat, *mkvec();
char *err;
int iter;

mat = (double **) (err = malloc((unsigned) (maxrow * sizeof(double *))));
if (err == NULL)
        printf("\n from mkmat: Insufficient space for %d byte vector",
                maxrow * sizeof(double *));
for (iter = 0; iter < maxrow; iter++)
        mat[iter] = mkvec(maxcol);
return(mat);
}

void rmmat(mat,maxrow,maxcol)
double **mat;
int maxrow, maxcol;
{
int iter;
void rmvec();

for (iter = maxrow-1; iter >= 0; iter--)
        rmvec(mat[iter],maxcol);
rmvec(mat);
}

void describe()
/* print descriptive info about variable */
{
char var[80];
int pos, find_var();
```

```
printf("\nDescribe: ");
scanf("%s",var);

if ((pos = find_var(var,ind_var,NUM_IND)) != FALSE)
        printf("\nIndep. var. %s is the %s.",var,ind_var[pos].var_desc);
else
if ((pos = find_var(var,dep_var,NUM_DEP)) != FALSE)
        printf("\nDep. Var. %s is the %s.",var,dep_var[pos].var_desc);
else
        printf("\nCan't find variable %s.",var);
}

void parametrize()
{
char name1[80],name2[80];
double target,start_ind,end_ind,incr,big_dep,this_dep,big_ind;
double get_ind(),get_dep(),fabs();
int find_var(), put_ind();
void compute_dep(), print_all();

printf("\nVary independent variable: ");
scanf("%s",name1);
if (find_var(name1, ind_var, NUM_IND) == FALSE)
        {
        printf("%s is not an independent variable.\n",name1);
        return;
        }

printf("Observe dependent variable: ");
scanf("%s",name2);
if (find_var(name2, dep_var, NUM_DEP) == FALSE)
        {
        printf("%s is not a dependent variable.\n",name2);
        return;
        }

printf("Starting value of %s: ",name1);
scanf("%lf",&start_ind);
printf("Final value of %s: ",name1);
scanf("%lf",&end_ind);
printf("Increment: ");
scanf("%lf",&incr);
printf("Desired value of %s: ",name2);
scanf("%lf",&target);

big_ind = start_ind;
put_ind(name1,start_ind);
compute_dep();
big_dep = get_dep(name2);

start_ind += incr;
while (start_ind <= end_ind)
        {
        put_ind(name1,start_ind);
        compute_dep();
        this_dep = get_dep(name2);
        if (fabs(this_dep - target) < fabs(big_dep - target))
                {
                big_ind = start_ind;
                big_dep = this_dep;
```

```
                }
        start_ind += incr;
        }
put_ind(name1,big_ind);
print_all();
}

void vary_ind()
{
char name1[80],name2[80];
double start_ind,end_ind,incr,scale1,scale2;
double get_ind(),get_dep();
FILE *fp,*fopen();
int max_iter, iter, find_var();
void compute_dep();

printf("\nFile for ASYST output: ");
scanf("%s",fname);
if ( (fp = fopen(fname,"w")) == NULL)
        {
        printf("Error opening file %s for writing.\n",fname);
        return;
        }

printf("\nVary variable: ");
scanf("%s",name1);
if (find_var(name1, ind_var, NUM_IND) == FALSE)
        {
        printf("%s is not an independent variable.\n",name1);
        return;
        }
printf("Scale factor for %s: ", name1);
scanf("%lf", &scale1);

printf("Observe variable: ");
scanf("%s",name2);
if (find_var(name2, dep_var, NUM_DEP) == FALSE)
        {
        printf("%s is not a dependent variable.\n",name2);
        return;
        }
printf("Scale factor for %s: ", name2);
scanf("%lf", &scale2);

printf("Starting value of %s: ",name1);
scanf("%lf",&start_ind);
printf("Final value of %s: ",name1);
scanf("%lf",&end_ind);
printf("Increment: ");
scanf("%lf",&incr);

max_iter = ((int) (1.5 + (end_ind - start_ind) / incr));
for (iter = 0; iter < max_iter; iter++)
        {
        put_ind(name1,start_ind);
        compute_dep();
        fprintf(fp,"%1.6lE , %1.6lE\n", scale1 * start_ind,
                scale2 * get_dep(name2));
        printf("%s is %1.6lE, %s is  %1.6lE\n",
                name1, start_ind, name2, get_dep(name2));
```

```
        start_ind += incr;
        }

fputc(0x1a,fp);                                 /* cntrl-Z */
fputc(0x00,fp);                                 /* null */
fclose(fp);
}

int savedata()
{
FILE *fp,*fopen();
int iter;

printf("\nFilename: ");
scanf("%s",fname);
if ( (fp = fopen(fname,"w")) != NULL)
        {
        for (iter=0; iter < NUM_IND; iter++)
                fprintf(fp,"%s %1.6le\n", ind_var[iter].var_name,
                                          ind_var[iter].var_val);
        fputc(0x1a,fp);                                /* cntrl-Z */
        fputc(0x00,fp);                                /* null */
        fclose(fp);
        return(TRUE);
        }
else
        {
        printf("Error opening file %s for writing.\n", fname);
        return(FALSE);
        }
}

int getdata()
{
FILE *fp,*fopen();
int iter;

if (command == FALSE)
        {
        printf("\nFilename: ");
        scanf("%s",fname);
        }
else
        command = FALSE;

if ( (fp = fopen(fname,"r")) != NULL)
        {
        for (iter=0; iter < NUM_IND; iter++)
                fscanf(fp,"%*s %lf", &ind_var[iter].var_val);
        fclose(fp);
        print_all();
        return(TRUE);
        }
else
        {
        printf("Error opening file %s for reading.\n", fname);
        return(FALSE);
        }
}
```

```
void sort(array, max_array)
/* sort tables */
struct var_list array[];
int max_array;
{
int gap, i, j;
double ftemp;
char *stemp,*dtemp;

for (gap = max_array/2; gap > 0; gap /= 2)
        for (i = gap; i < max_array; i++)
                for (j = i - gap; j >= 0; j-= gap)
                        {
                if (strcmp(array[j].var_name, array[j+gap].var_name) <= 0)
                                break;

                        stemp = array[j].var_name;
                        ftemp = array[j].var_val;
                        dtemp = array[j].var_desc;

                        array[j].var_name = array[j+gap].var_name;
                        array[j].var_val = array[j+gap].var_val;
                        array[j].var_desc = array[j+gap].var_desc;

                        array[j+gap].var_name = stemp;
                        array[j+gap].var_val = ftemp;
                        array[j+gap].var_desc = dtemp;
                        }
}

int ask_ind(num)
/* change independent variable value in table */
int num;
{
if (num != FALSE)
        {
        printf("Enter value of variable %s (currently %1.6lE): ",
                ind_var[num].var_name,ind_var[num].var_val);
        scanf("%lf",&ind_var[num].var_val);
        }
return(num);
}

int put_ind(var,val)
char *var;
double val;
{
int put_var();

return(put_var(var,val,ind_var,NUM_IND));
}

int put_dep(var,val)
char *var;
double val;
{
int put_var();

return(put_var(var,val,dep_var,NUM_DEP));
}
```

```
int put_var(var, val, array, max_array)
char *var;
double val;
struct var_list array[];
int max_array;
{
int num, find_var();

if ((num = find_var(var, array, max_array)) != FALSE)
        array[num].var_val=val;
return(num);
}

double get_ind(var)
char *var;
{
double get_var();

return(get_var(var,ind_var,NUM_IND));
}

double get_dep(var)
char *var;
{
double get_var();

return(get_var(var,dep_var,NUM_DEP));
}

double get_var(var, array, max_array)
char *var;
struct var_list array[];
int max_array;
{
int find_var(),num;

return(((num = find_var(var, array, max_array)) == FALSE) ? 0.0 : array[num].var
_val);
}

int find_var(var, array, max_array)
/* binary search to find variable in value table */
char *var;
struct var_list array[];
int max_array;
{
int low, high, mid, cond;

low = 0;
high = max_array - 1;
while (low <= high)
        {
        mid = (low + high)/2;
        if ((cond = strcmp(var,array[mid].var_name)) < 0)
                high = mid - 1;
        else if (cond > 0)
                low = mid + 1;
        else
                return(mid);
        }
```

```
return(FALSE);
}

void print_all()
/* print contents of both tables */
{
void compute_dep(), print_var();

compute_dep();
printf("\nIndependent Variables:\n\n");
print_var(ind_var, NUM_IND);
printf("\nDependent Variables:\n\n");
print_var(dep_var, NUM_DEP);
putchar('\n');
}

void print_var(array, max_array)
/* Print contents of variable value table */
struct var_list array[];
int max_array;
{
int iter;

for (iter = 0; iter < max_array; iter++)
        {
        printf("%s = %1.6lE", array[iter].var_name, array[iter].var_val);
        printf("%c",((iter + 1) % VARS_PER_LINE == 0) ? '\n' : '\t');
        }
if ((max_array % VARS_PER_LINE) != 0) printf("\n");
}

double sqr(x)
double x;
{
return(x*x);
}

double power(x,y)
double x;
int y;
{
double answer;
int i,j,abs();

answer = 1.0;
for (i = 1, j = abs(y); i <= j; ++i)
        answer *= x;
return(y > 0? answer : 1.0 / answer);
}

#define ITMAX 100
#define EPS 3.0e-8
double zbrent(func,x1,x2,tol)
double x1,x2,tol;
double (*func)();
{
int iter;
double a=x1, b=x2, c, d, e, min1, min2, fabs();
double fa = (*func)(a), fb = (*func)(b), fc, p, q, r, s, tol1, xm;
```

```
if ((fb * fa) > 0.0)
        {
        printf("\nfrom zbrent: Root must be bracketed.");
        return(0.0);
        }
fc=fb;
for (iter = 1; iter <= ITMAX; iter++)
        {
        if ((fb*fc) > 0.0)
                {
                c = a;
                fc = fa;
                e = d = b - a;
                }
        if (fabs(fc) < fabs(fb))
                {
                a = b;
                b = c;
                c = a;
                fa = fb;
                fb = fc;
                fc = fa;
                }
        tol1 = 2.0 * EPS * fabs(b) + 0.5 * tol;
        xm = 0.5 * (c-b);
        if ((fabs(xm) <= tol1) || (fb == 0.0))
                return(b);
        if ((fabs(e) >= tol1) && (fabs(fa) > fabs(fb)))
                {
                s = fb / fa;
                if (a == c)
                        {
                        p = 2.0 * xm * s;
                        q = 1.0 - s;
                        }
                else
                        {
                        q = fa / fc;
                        r = fb / fc;
                        p = s * (2.0 * xm * q * (q - r) - (b - a) * (r - 1.0));
                        q = (q - 1.0) * (r - 1.0) * (s - 1.0);
                        }
                if (p > 0.0)
                        q = -q;
                p = fabs(p);
                min1 = 3.0 * xm * q - fabs(tol1 * q);
                min2 = fabs(e * q);
                if ((2.0 * p) < (min1 < min2 ? min1 : min2))
                        {
                        e = d;
                        d = p / q;
                        }
                else
                        {
                        d = xm;
                        e = d;
                        }
                }
        else
                {
```

```
                d = xm;
                e = d;
                }
        a = b;
        fa = fb;
        if (fabs(d) > toll)
                b += d;
        else
                b += (xm > 0.0 ? fabs(toll) : - fabs(toll));
        fb = (*func)(b);
        }
printf("\nfrom zbrent: Failed to converge after %d iterations.",ITMAX);
return(0.0);
}

/**********************************************************************/
/****** user supplied routines ****************************************/
/**********************************************************************/
double Nrat, Nmul, Np, Ns, spacing, Pt, Pc, Ph, sigma;
double freq, Lo, Im, Il, Prat, skdep, Lm;
double gap, Ro, area, height, Rcoef, Pcp, Pcs, BA;
double leaf, w, r_wi, r_wo, rtol, lr_wo, hr_wo, delta, m, Arat;
int core, stats, MHz;

/* the following table is the coefficients for igql material for 1--10MHz */
/* in the following formula for loss per unit volume */
/* Ph/v = alpha b**2 + beta b**4 + gamma b**6 */

static double btable[3] [10] = {
{9.3871e7, 6.0085e8, 1.1217e9, 1.2152e9, 1.2083e9, 2.0540e9, 2.4359e9,
3.3357e9,4.1962e9,6.1880e9},
{3.1292e11, 2.8393e11, 3.0825e11, 1.4335e12, 2.8268e12, 2.9044e12, 4.9115e12,
5.3128e12,7.7859e12,8.8010e12},
{5.5036e13, 1.8254e14, 3.3144e14, 0.0, 0.0, 2.3848e13, 0.0,
0.0,0.0,0.0}
};

double copper_loss(r_wi,r_wo)
double r_wi, r_wo;
{
double answer, R_p_dc(), R_s_dc();

answer =  Pcp * R_p_dc(r_wi,r_wo) + Pcs * R_s_dc(r_wi,r_wo);
return(answer);
}

double R_s_dc(r_wi,r_wo)
double r_wi,r_wo;
/*
        computes Rs,dc given r_wi and r_wo
        assumes spacing at sides and between turns
*/
{
double answer, wrat, r_in, r_on, log(), pow();
int iter, max_iter;

wrat = pow(r_wo/r_wi,1.0/Ns);
max_iter = (int) (Ns + 0.5);
for (r_in = r_wi, answer = 0.0, iter = 0; iter < max_iter; iter++)
        {
```

```
        r_on = r_in * wrat;
        answer += 1.0 / log((r_on - spacing) / (r_in + spacing));
        r_in = r_on;
        }
return(Rcoef * Nrat * Nrat * answer);
}


double R_p_dc(r_wi,r_wo)
double r_wi,r_wo;
/*
        computes Rp,dc given r_wi and r_wo
        assumes spacing at sides and between turns
*/
{
double answer, wrat, r_in, r_on, log(), pow();
int iter, max_iter;

wrat = pow(r_wo/r_wi,1.0/Np);
max_iter = (int) (Np + 0.5);
for (r_in = r_wi, answer = 0.0, iter = 0; iter < max_iter; iter++)
        {
        r_on = r_in * wrat;
        answer += 1.0 / log((r_on - spacing) / (r_in + spacing));
        r_in = r_on;
        }
return(Rcoef * answer);
}

double vol_eff(r_wi,r_wo,delta,nB)
double r_wi, r_wo, delta;
int nB;
{
double power(),sqr(),log(),temp,answer;

if (nB == 2)
        answer = log(r_wo/r_wi);
else
        answer = ( (1.0 / power(r_wi,nB-2)) -
                   (1.0 / power(r_wo,nB-2)) ) / (((double) nB) - 2.0);

answer *= power(r_wi,nB-1);
answer += 0.5 * r_wi;
answer *= 2.0 * PI * sqr(r_wi);
/* allow for unequal area at outer edge */
Arat = r_wi * r_wi /(delta * (2.0 * r_wo + delta));
temp = 0.4 * (r_wo - r_wi) + leaf * (2.0 * skdep + m);
temp *= PI * sqr(r_wi) * (1.0 + power(Arat, nB));
return(answer + temp);
}

double core_loss(r_wi, r_wo, delta)
double r_wi, r_wo, delta;
{
double answer, Bmax, vol_eff();
int iter;

/* compute Bmax */
Bmax = BA / sqr(r_wi);
```

```
for (answer = 0.0, iter = 1; iter <= 3; iter++)
        answer += vol_eff(r_wi,r_wo,delta,iter*2) *
                  btable[iter-1][MHz-1] * power(Bmax, iter*2);
return(answer);
}

#define VBIG 1.0e10

double find_r2(r_wo)
double r_wo;
{
double loss, copper_loss(), core_loss(), fabs(), power();

r_wo = fabs(r_wo);
loss = copper_loss(r_wi.r_wo) + (core ? core_loss(r_wi,r_wo,delta) : 0.0);
return(Pt - loss);
}

double find_lr_wo(r_wi, spacing, N)
double r_wi, spacing, N;
{
double answer;

answer = r_wi * power((1.001 + spacing * 2.001 / r_wi) , ((int) N));
return(answer);
}

double find_r1(r)
double r[];
{
double core_loss(), find_r2(), zbrent(), find_lr_wo();

/* powell may ask for negative radius */
r_wi = r[0] = fabs(r[0]);
delta = r[1] = fabs(r[1]);

/* get bracket for zbrent */
lr_wo = find_lr_wo(r_wi, spacing, Np);

/* make sure that solution is possible */
if (core && (core_loss(r_wi,lr_wo,delta) >= Pt))
        {
        if (stats != 0)
                printf("\nfrom find_r1: Core loss exceeds total allowable.");
        return(VBIG * (core_loss(r_wi,lr_wo,delta) - Pt));
        }
/* find upper bracket */
hr_wo = 2.0 * lr_wo;
while(find_r2(hr_wo) < 0.0)
        if (hr_wo/r_wi > 500.0)
                {
                /* r_wi too small, forcing B field and loss too high */
                if (stats != 0)
                        printf("\nfrom find_r1: Core loss too high: Bmax = %1.6l
e",
                                1.0e4 * BA / (r_wi * r_wi));
                return(VBIG / r_wi);
                }
        else
                hr_wo *= 2.0;
```

```
r_wo = zbrent(find_r2, lr_wo, hr_wo, rtol);
if (stats != 0)
printf("\nfind_r1: after zbrent: r_wi = %1.6le, r_wo = %1.6le\ndelta = %1.6le",
                r_wi, r_wo, delta);

return(r_wo + delta);
}

double get_sigma(sigma_o,temp)
double sigma_o, temp;
{
double answer;

answer = 259.5 * sigma_o / (temp + 234.5);
return(answer);
}

void compute_dep()
/* Evaluate dependent variable */
{
double get_ind(), get_dep(), sqr(), sqrt(), log(), fabs();
double r[2], R_p_dc(), R_s_dc();
double find_lr_wo(), find_r1(), find_r2(), zbrent(), copper_loss(), core_loss();
double L1;
double capt, capc, capd, temp, gamma, epr, n;
int iter;
void powell();
double zeta,w_t,get_sigma();

Pt = get_ind("Pt");
sigma = get_sigma(get_ind("sigma"),get_ind("temp"));
put_dep("sigma",sigma);
freq = get_ind("freq");
Nrat = get_ind("Nrat");
Nmul = get_ind("Nmul");
Np = Nrat * Nmul;
Ns = Nmul;
Lo = get_ind("Lo");
Im = get_ind("Im");
Il = get_ind("Ils") / Nrat;
put_dep("Il",Il);
spacing = 0.5 * get_ind("spacing");
m = get_ind("m");

/* compute magnetizing inductance */
Lm = Lo / freq;
put_dep("Lm",Lm);

/* compute skin depth */
skdep = 1.0 / sqrt(PI * freq * MUO * sigma);
put_dep("skdep",skdep);

/* Bmax = BA / sqr(ri) */
BA = Lm * Im / (PI * Np);

/* compute frequency in MHz */
MHz = (int) (freq * 1.0e-6 + 0.5);

/* get loss coefficients */
leaf = get_ind("leaf");
```

```
Rcoef = 2.0 * PI / (leaf * skdep * sigma);
Pcp = 0.5 * (0.357 * sqr(Il) + 1.09 * sqr(Im + 0.2 * Il));
Pcs = 0.2 * sqr(Il) + 0.16 * sqr(Im) + 0.032 * Im * Il;
put_dep("B2", btable[0] [MHz-1]);
put_dep("B4", btable[1] [MHz-1]);
put_dep("B6", btable[2] [MHz-1]);

/* compute r_wi, r_wo */
r[0] = get_ind("tr_wi");
r[1] = get_ind("t_delta");
rtol = get_ind("rtol");
stats = ((int) (get_ind("stats") + 0.5));
core = ((int) (get_ind("core") + 0.5));
powell(find_r1, r, 2);
put_dep("r_wi",r_wi = fabs(r[0]));
put_dep("delta",delta = fabs(r[1]));

/* get bracket for zbrent */
lr_wo = find_lr_wo(r_wi, spacing, Np);
hr_wo = 2.0 * lr_wo;
while(find_r2(hr_wo) < 0.0)
        hr_wo *= 2.0;

r_wo = zbrent(find_r2, lr_wo, hr_wo, rtol);
put_dep("r_wo", r_wo);

put_dep("w", (w = r_wo - r_wi));

/* compute resistances */
put_dep("R_p_dc",R_p_dc(r_wi, r_wo));
put_dep("R_s_dc",R_s_dc(r_wi, r_wo));

/* compute loss */
put_dep("Pc",Pc = copper_loss(r_wi,r_wo));
put_dep("Ph",Ph = (core ? core_loss(r_wi,r_wo,delta) : 0.0));
put_dep("Prat", Ph/Pc);
put_dep("Arat",Arat);

Ro = r_wo + delta;
put_dep("Ro",Ro);
put_dep("diam", Ro * 2.0);
area = PI * sqr(Ro);
put_dep("area",area);

put_dep("Bmax",1.0e4 * BA / sqr(r_wi));

/* compute the gap length */
gap = (Lm / (MUO * sqr(Np) * PI)) - (0.6 * w / log(r_wo/r_wi));
gap = sqr(r_wi) / (gap * (1.0 + Arat));
put_dep("gap",gap);

/* compute the height */
height = leaf * (2.0 * skdep + m) + gap + 0.4 * w + r_wi;
put_dep("height",height);

/* compute the volume */
put_dep("volume",area * height);

/* compute leakage inductance */
Ll = 2.0 * MUO * PI * sqr(Np) * (m + 0.65 * skdep) / (leaf * log(r_wo/r_wi));
```

```
put_dep("Ll",Ll);
put_dep("Lrat",Lm/Ll);

/* compute capacitances */
zeta = 2.0 * spacing * Np / w;
w_t = w / (Np + (Np - 1.0) * zeta);
put_dep("w_t",w_t);
epr = get_ind("epr");
temp = r_wi - w_t * (0.5 + zeta);
gamma = temp + w_t * (1.0 + zeta) * (2.0 * Np + 1.0) / 3.0;
gamma /= (w_t * (1.0 + zeta) + 2.0 * temp / (Np + 1.0));

capt = capd = capc = 0.0;
for (iter = 1; iter <= ((int) (Np + 0.5)); iter++)
        {
        n = ((double) iter);
        capt += sqr(n - 1.0) *
               (r_wi + w_t * ((n - 1.0) * (1.0 + zeta) + 0.5));
        capd += sqr(n - gamma) *
               (r_wi + w_t * ((n - 1.0) * (1.0 + zeta) + 0.5));
        capc += sqr(1.0 - gamma) *
               (r_wi + w_t * ((n - 1.0) * (1.0 + zeta) + 0.5));
        }
temp = 2.0 * PI * epr * EPO * w_t * (2.0 * leaf - 1.0) / (sqr(Np) * m);
capt *= temp;
capd *= temp;
capc *= temp;
put_dep("CapT",capt);
put_dep("CapD",capd);
put_dep("CapC",capc);
put_dep("fres", 0.5 / (PI * sqrt(capt*Ll)));
}
```

Appendix H: Fabrication Techniques

H.1 Polyimide

Polyimide[14] is an insulating organic compound developed for use as a dielectric layer between metallization layers in integrated circuits.[15] Polyimide is attractive as a winding substrate for the transformers described in this thesis because copper/polyimide windings are flexible and can be bent to connect the transformer with the hybrid substrate or with other components (in the case of the MIT prototype converter, the output diodes[16]). In addition, polyimide has a high dielectric breakdown strength ($\sim 10^8$ V/m) and relatively low dielectric constant ($\sim 3.5\epsilon_o$).[17]

There are two ways of preparing copper/polyimide windings. The first method is to start with sheets of polyimide which have been laminated on one or both sides with copper. These sheets may be photolithographically patterned with windings using the same processes used for conventional printed circuit boards. While this method is inexpensive, multiple winding layers, such as the interleaved windings discussed in Chapter 7, are very difficult to connect and align. In addition, commercially available copper/polyimide is relatively thick; the polyimide layer is typically 25 μm thick, with a 25 μm thick layer of adhesive between it and the copper. This 50 μm spacing between primary and secondary may give too high a leakage inductance.

The second method, especially appropriate for multiple winding layers, is to purchase the polyamic acid from which polyimide is formed and build up alternating layers of polyimide and conductors.[18] Polyamic acid is either spun or sprayed to form a layer between 1.5–25μm thick. The polyamic acid is converted to polyimide by heating it above 200°C, a process called *curing*. Layers thicker than 25 μm can be built up by incompletely curing

---

[14] Also known as Kapton, a registered mark of E. I. DuPont.

[15] A. C. Adams, "Dielectric and Polysilicon Film Deposition," in *VLSI Technology*, S. M. Sze, ed., Mc-Graw Hill Book Company, New York (1983), p. 125.

[16] L. D. Pitzele, "The System Fabrication of a 10 MHz, Dc/Dc Switching Power Supply," MIT Master's Thesis, September 1986, p. 134.

[17] A. M. Wilson, "Polyimide Insulators for Multilevel Interconnections," *Thin Solid Films*, **83** (1981), pp.145–163.

[18] R. J. Jensen, J. P. Cummings, and H. Vora, "Copper Polyimide Materials System for High Performance Packaging," *IEEE Electronic Components Conference Record*, (1984), pp. 73–81.

one layer and applying another directly on top. Once the polyimide is cured, it can be subjected to temperatures up to its melting point of 450°C without affecting its properties. Conductors can be patterned on top of the polyimide. However, in building up multilayer structures it is usually necessary to keep each layer flat, so that grooves are etched into the polyimide and conductors are evaporated, sputterred, and/or plated into the grooves.[19]

H.2 Test Transformer

The goal of fabricating the 6:1 slotted gapped transformer whose electrical properties are presented in Chapter 8 was to verify the analyses of the previous chapters. The core could be purchased commercially; one half of a Ferroxcube 1107 pot core made from 4C4 ferrite was used for the bottom half of the transformer, and the top plate of the core was formed by a independent company which sliced off and polished part of a 4C4 I-bar from a standard E-I core to form a rectangular plate.[20] A 120 μm gap was formed between the pot core half and the top plate by the insertion of mylar spacers, and the assembly was clamped together.

The planar spiral windings, on the other hand, had to be fabricated especially for this experiment.[21] The windings were patterned using a computerized layout and mask fabrication process available in the MIT Microsystems Technology Laboratories. The mask layout for the six turn primary is shown in Fig. E.1. Note that the six concentric turns are laid out as six concentric rings connected in series with short radial lengths. In this experiment each primary turn was of equal width. Another layout was produced for the one turn secondary. The winding dimensions of both primary and secondary correspond to those in Table 5.1. Chrome masks were produced and used to make contact prints on each side of a sheet of photoresist-covered copper clad kapton.[22] The prints were developed and etched with a conventional printed circuit board process. The center hole of the windings was cut out and the windings were slid over the center post of the pot core.

---

[19] J. L. Vossen and W. Kern, eds., *Thin Film Processes*, Academic Press, Inc., New York (1978).

[20] Accumet, Inc., Hudson, Massachusetts.

[21] The windings were fabricated by Mr. D. Richards.

[22] Fortin Flex Epoxy Poly-Core EP, Fortin Industries, Inc., Sylmar, California.

Fig. H.1 Close up of section of mask layout for six turn planar primary winding.

H.3 Ferrites

The preparation of ferrites from their raw materials is a complicated process characterized by proprietary techniques and additives. Yet a basic understanding of the general methods of preparation is necessary to determine appropriate core shapes and manufacturing methods.

The nickel-zinc ferrite cores considered in this thesis are typically prepared by a four step process. First, the raw materials containing nickel, zinc, iron, and oxygen are mixed together. Second, the materials are fired together to make the ferrite. Third, the ferrite is powdered and formed into the required shape. Fourth, the shaped ferrite is refired at high temperature and sometimes under pressure in order to merge the finely powdered particles together.[23]

There are several methods of mixing the raw materials together. Oxides of nickel, zinc, and iron can be milled together. Alternatively, these metals can be precipitated or dried from solutions of carbonates, nitrates, sulfates, or oxalates.[24,25,26] During this step special ingredients, such as cobalt oxide and manganese oxide, are also added to raise the permeability or to lower core loss.[27]

Once the raw materials are mixed together, they are fired at temperatures between 900–1200°C. This step is known as *prefiring* or *calcining*. The high heat enables the metal cations to diffuse and undergo a solid state reaction, forming particles of polycrystalline ferrite. The details of the firing cycle, such as the exact kiln temperatures, firing times, and kiln atmospheres, are typically trade secrets.

The ferrite particles are then ground into powder and formed into the required core shapes. The ferrite material is at this point referred to as *green*, or *unfired* ferrite, as it has not yet been through the final firing step. There are several different forming processes. One of the least expensive is to pour the dry powder into a die and then compress it.[28] Often the powder is mixed with a liquid binder in order to form a viscous fluid, known as *slip*. Thick films of slip are prepared by wiping a blade, known as a *doctor blade*, over a pool of slip. The film of slip then dries to form a rubbery mat. If the slip contained a photosensitive agent, the mat can be photolithographically patterned.[29] Alternately, conductive windings

---

[23] C. Chen, *Magnetism and Metallurgy of Soft Magnetic Materials*, North-Holland Publishing Company, Amsterdam (1977), pp. 221–222.

[24] Chen, p. 223.

[25] J. G. M. De Lau, Composition and Microstructure on High-Frequency Properties of Ni-Zn-Co Ferrites," *Philips Research Reports Supplements*, 6 (1975), p. 32.

[26] E. B. Rigby, W. D. Kehr, and C. B. Meldrum, "Preparation of Coprecipitated NiZn Ferrite," *IEEE Transactions on Magnetics*, 20, 5 (1984), pp. 1506–1508.

[27] G. Zerbes (Indiana General Corp.), "Ferromagnetic, Ceramic Body With High Quality at High Frequency," U. S. Patent 3,036,009, 22 May 1962.

[28] H. M. Schlicke, *Essentials of Dielectromagnetic Engineering*, John Wiley and Sons, Inc., New York (1961), p. 71.

[29] B. Schwartz (IBM), "Process of Making Patterned Unitary Solid Bodies From Finely

can be patterned on the slip with thick film pastes. Another film of slip can be laminated on top of the conductors and the entire assembly refired together.[30] This process, for example, might be used to produce the sandwich structures discussed in Chapter 4. Another option is to prepare a block of ferrite that will be machined into its final state after refiring.[31]

The final step is to refire the core at temperatures between 1000–1400°C. During this firing, known as *sintering*, the individual powder particles merge together. By increasing the density of the material, this process raises the permeability. The resulting volume shrinkage can be up to 20%.[32] The final two steps of forming and sintering are often combined in order to streamline the production process and raise the ferrite density. This procedure is known as *isostatic hot pressing*.[33]

As mentioned above, sintered ferrite can be machined, although since it is a brittle material the minimum feature thickness is on the order of 1.5 mm. Finer features can be formed through ion etching, although the etch rate is only about 2 μm/hour, and the procedure may be too expensive for volume production.[34] The surfaces of a sintered core or machined piece can be mechanically lapped to a smoothness limited by the grain size of the sintered ferrite, typically between 0.2–35 μm.[35,36] Laser beams may also be used for etching ceramics such as ferrite; a typical CO_2 laser can etch a 0.5 mm diameter hole in 2.5 mm thick alumina in 0.25 sec.[37]

Divided Discrete Particles," U. S. Patent 3,502,520, 24 March 1970.

[30] C. Wentworth (RCA), "Method of Making a Laminated Ferrite Memory," U. S. Patent 3,505,139, 7 April 1970.

[31] A. B. van Groenou and J. D. B. Veldkamp, "Grinding Brittle Materials," *Philips Technical Review*, **38**, 4/5 (1978), pp. 105–118.

[32] Schlicke, p. 72.

[33] K. H. Härtdl, "A Simplified Method for the Isostatic Hot Pressing of Ceramics," *Philips Technical Review*, **35**, 2/3 (1975), pp. 65–72.

[34] T. Nakanishi, T. Toshima, K. Yanagisawa, and N. Tsuzuki, "Narrow Track Magnetic Head Fabricated by Ion-Etching Method," *IEEE Transactions on Magnetics*, **15**, 3 (1979), pp. 1060–1064.

[35] De Lau, p. 91.

[36] J. K. Emery, "Surface Characteristics of Ceramic Substrates for Hybrid and Microwave Electronic Circuits," in *The Science of Ceramic Machining and Surface Finishing*, S. J. Schneider, R. W. Rice, eds., U. S. National Bureau of Standards Special Publication no. 348 (May 1972), pp. 293–300.

[37] S. A. Llewellyn, "Laser Cutting - State of the Art," *Proceedings of the Conference*

A serious drawback to the use of the Mn-Zn ferrites appropriate below about 2 MHz is the presence of a surface layer of lower permeability and higher loss. This surface layer forms during the fabrication process in ferrites containing manganese when the constituent chemicals are fired together to form the ceramic.[38,39] The surface layer can be removed through polishing from large blocks of ferrite, but when small pieces like the cores described in this thesis are mass produced, they are typically pressed and fired in the final shape, rather than milled from large blocks.[40] The mechanical polishing itself introduces surface stresses that can reduce permeability and increase loss. The thickness of this layer has been variously reported as being as large as 5 μm or as thin as tens of nanometers.[41,42] Acid etching has been explored as a method for removing the surface layer in small Mn-Zn ferrite cores, but this process adds to the difficulty of assuring precise dimensions.[43] Unlike Mn-Zn ferrites, Ni-Zn ferrites do not develop lossy surface layers during firing, although Ni-Zn ferrites develop a thicker dead layer than Mn-Zn ferrites in response to mechanical polishing.[44]

---

on the the Laser vs the Electron Beam in Welding, Cutting, and Surface Treatment, Bakish Materials Corporation, Englewood, New Jersey (1985), pp. 175-176.

[38] Heck, pp.175–181.

[39] G. Schaller, Micrometals, Inc., private communication.

[40] H. M. Schlicke, *Essentials of Dielectromagnetic Engineering*, John Wiley and Sons, Inc., New York (1961), pp. 72–73.

[41] J. E. Knowles, "The Origin of the Increase in Magnetic Loss Induced by Machining Ferrites," *IEEE Transactions on Magnetics*, **11**, 1 (1975).

[42] *Magnetic Recording*, vol. 1, C. D. Mee and E. D. Daniel, eds., McGraw-Hill Book Company, New York (1987), p. 280.

[43] Y. Sasaki, T. Matsuoka, and M. Yamaguchi, "Effect of Dimensions on Power Losses in Mn-Zn Ferrite Cores," *IEEE Translation Journal on Magnetics in Japan*, **1**, 9 (1985), pp. 1082–1084.

[44] Mee, p. 280.